The Dissertation Committee for Hyun Hwa Jo Certifies that this is the approved version of the following dissertation:

OPTICAL CHIRALITY SENSING ENSEMBLES: MECHANISTIC STUDIES AND APPLICATIONS IN SYNTHETIC METHODOLOGY DEVELOPMENT

Committee:

Eric V. Anslyn, Supervisor

Michael J. Krische

Hung-Wen Liu

Adrian T. Keatinge-Clay

David W. Hoffman

OPTICAL CHIRALITY SENSING ENSEMBLES: MECHANISTIC STUDIES AND APPLICATIONS IN SYNTHETIC METHODOLOGY DEVELOPMENT

by

Hyun Hwa Jo, B.S.

Dissertation

Presented to the Faculty of the Graduate School of

The University of Texas at Austin

in Partial Fulfillment

of the Requirements

for the Degree of

Doctor of Philosophy

The University of Texas at Austin

August 2015

Dedication

To my parents and my brother, for always being there for me.

Acknowledgements

First and foremost, my profoundest recognition goes to my advisor, Eric Anslyn, for his continuous support and tremendous advocacy during the last five years in the department. Although there were many discouraging moments, as it often goes in the nature of scientific research, Eric has always led me to overcome the frustration and to stay enthusiastic. It is his boundless passion in research and science that has defined for me the ideal mindset of a true scientist, and that is to always remain inquisitive even when something may appear to be straightforward at first glance. There can never be enough words to convey what I have learned from him over the years, but most of all, I am especially appreciative of his understanding. He could always find the positive in any situation, even when we encountered roadblocks in our work, and most importantly, manages to see the best in everyone. I feel extremely lucky to have someone like Eric as my advisor, from who I can confidently say that I have learned to live life confidently, both on a professional and personal level. I would also like to thank Dr. Lei You, who has led and advised me since I first began on this project, much of which has been inspired from his early work. I would also like to acknowledge Dr. Mike Krische, who has provided me with invaluable support and insight, and Xin Gao for his collaboration in assisting me with the synthetic procedures for my project.

Next, I would like to extend my deepest gratitude to the past and present members of the Anslyn group: Leo Joyce, Pedro Metola, Michelle Adams, Reid Long, Alex Gade, and Katharine Diehl for their interesting conversations, not only limited purely to research; Jiney Jose, Royota Saito, Kodi Beyeh, Ram Edupuganti, and Ye Zhong for the inspiration and motivation they provided; John Lin, Brette Chapin, Maggie Meadows,

Igor Kolesnichenko, Rogelio Escamilla, Logan Bachman, and Brenden Herrera for making the laboratory a fun and exciting place to be; Helen Seifert, Diana Zamora-Olivares, Adam Garland, Erik Hernandez and Jimmy Reuther for keeping the east side of the office from missing out on all of the fun.

In addition, I would also like to thank my dearest friends, whom I am unable see as often as I would like, but are never far from my thoughts. My warmest appreciation goes to Ulziimaa Ganzorig and Eunice An for the countless number of fond memories and colorful talks. A special thanks to Alicia An, for being my personal editor since freshman year and always providing a listening ear to my many musings.

Last but never least, I lend my most heartfelt gratitude to my family. I cannot imagine traversing my way through these years without their unrivaled love and support. It has truly been the most interesting journey yet.

OPTICAL CHIRALITY SENSING ENSEMBLES: MECHANISTIC STUDIES AND APPLICATIONS IN SYNTHETIC METHODOLOGY DEVELOPMENT

Hyun Hwa Jo, Ph.D.

The University of Texas at Austin, 2015

Supervisor: Eric V. Anslyn

In the pharmaceutical industry, the development of molecular or chemical sensors for an analyte of interest and the determination of the enantiomeric purity of chiral molecules is essential. Chirality sensors were developed for analytes, such as alcohols, carboxylic acids, ketones, etc., which are valuable building blocks for the synthesis of complex pharmaceuticals. As such, the development of protocols for enantiomeric excess (*ee*) analysis of alcohols is of significant interest. Furthermore, high-throughput *ee* screening (HTS) has become crucial due to advances in the methods of combinatorial chemistry and parallel synthesis. Chapter 1 presents the overview of optical detection methods for *ee* analysis, as they are more suitable for HTS, compared to chromatographic techniques.

The alcohols are important functional groups that are widely found in natural products such as terpenes, steroids and saccharides. Accordingly, the development of protocols involving multi-component dynamic assembly for *ee* analysis of alcohols has been extensively explored. Chapter 2 presents the *ee* screening method utilizing a reversible tetradentate ligand-based assembly that incorporates the chiral alcohols. The inclusion of alcohols into the ligand structure induces a twist which results in large

Cotton effects in the circular dichroism spectra; indicative of the handedness of the alcohol. The objective of the work has been applying this chiral alcohol sensing assay for a true HTS in combination with the parallel synthesis of chiral homo-allylic alcohol.

Chapter 3 reports on past studies performed to further gain kinetics and the mechanistic insight toward the multi-component assembly reaction. By elucidating the mechanism of the assembly reaction, we can further optimize the experimental conditions of the reaction in the development of a new assembly.

Finally, Chapter 4 presents an effort toward the advancement of a novel sensor for α-chiral ketones. Chiral ketones produced by α-arylation of α,α-difluorocarbonyl compounds has been of interest in medicinal chemistry. This is not only contributed by carbonyl functionality, but by the importance of aromatic compounds containing a fluorine atom or a trifluoromethyl group on an aromatic ring. Improving the original chiral ketone assay to achieve HTS will substantially aid developments in synthetic methodology.

Table of Contents

List of Tables

List of Figures

List of Schemes

Chapter 1: Methods for Rapid Determination of Enantiomeric Excess

1.1 Introduction

The synthesis of chiral compounds that are optically pure has been of growing interest in the modern pharmaceutical industry. The significance of this development is due to the chirality of the majority of synthetic drugs. For instance, the pharmaceutical's market share of single-enantiomer drugs increased from 27% in 1996 to 39 % in 2002.[1,2] The human body is effectively a chiral environment which reacts uniquely with different enantiomers. Enantiomers of a chiral drug can often exhibit variations in bioavailabilities, metabolism rate, potency, or toxicity.[3] A common example that highlights the necessity of single-enantiomer drugs is with the introduction of thalidomide. This drug was sold worldwide to pregnant women as a treatment for morning sickness in the early 1960s. It was later found that only one of the enantiomers of this compound was responsible in treating morning sickness while the rest were teratogenic, which resulted in birth defects during pregnancy. Even in less drastic cases, where the other enantiomer is neither toxic or harmful, quantitative differences between the bioactivity of the two molecules have to be taken into account. For instance, theenantiomer of citalopram, used to treat depression, is 30 times more potent than the *R*-enantiomer.

With these considerations in mind, the introduction and widespread use of asymmetric synthesis and chiral separation technologies have enabled pharmaceutical manufacturers to develop single-enantiomer drugs. The most commonly employed method to obtain enantiomerically enriched compounds is asymmetric synthesis using a chiral catalyst. This method has been shown to be a cost-effective method, saving money

and generations of waste via the avoidance of purification and discarding of the undesired enantiomer.

The optimization of asymmetric reaction to increase the yield of a preferential enantiomer and the enantiomeric purity of the reaction is another key part in methodology development. Conventionally, the creation and optimization of asymmetric catalysts are achieved through inordinately time-consuming methods, such as with trial and error. However, recent advances have allowed for the screening for asymmetric catalyst using combinatorial libraries with parallel synthesis and the subsequent analysis of a large number of chiral catalysts. Often, the analysis of the enantiomeric purity acted as the bottleneck in the discovery of high-throughput reactions.

Enantiomeric excess (*ee*), a measurement of enantiomeric composition of a chiral compound, is defined by **Equation 1.1**. A high value of *ee* represents a more successful asymmetric synthesis. *ee* ranges from -100% to +100% as shown in Equation 1.1, but is often reported as the absolute value in the literature.

$$ee = \left(\frac{[\mathrm{R}] - [\mathrm{S}]}{[\mathrm{R}] + [\mathrm{S}]}\right) \times 100$$

Equation 1.1

In order to determine *ee*, a chiral environment is needed, since enantiomers possess the same physical properties in an achiral environment. Traditionally, the degree of enantiopurity of a product is found using either high performance liquid chromatography (HPLC) or gas chromatography (GC). While these techniques are highly accurate, they are not amenable to studying a large number of samples in short periods of time. Attempts to develop rapid methods that expedite the screening processes have

been undertaken.[3] These methods are based on optical spectroscopy, such as circular dichroism (CD), fluorescence, and UV-visible. These alternate strategies have been well-adapted in high-throughput reactions due to the advantages of their simple and rapid analysis, as well as the ability to be used for real-time analysis.[3]

1.1.1 High-Throughput Approaches in Asymmetric Reaction Discovery and Optimization

The traditional approach in the discovery of reaction in asymmetric synthesis is first to design a reaction which accounts for the catalyst, auxiliary, and other components in the system. The reaction is then performed and its enantioselectivity subsequently analyzed. At this point, in order to optimize the reaction, the system is redesigned followed by synthesis and analysis. This cycle repeats until the desired *ee* is obtained. This trial and error-based reaction discovery system is a vastly time-consuming method.

High-throughput screening (HTS), which is the process of testing a large number of analytes simultaneously, has been essential for the synthesis development in combinatorial chemistry and parallel synthesis.

1.1.1.1 Combinatorial Chemistry

For the past two decades, combinatorial chemistry has proven to be a useful synthetic tool in peptide and small molecule synthesis, in addition to asymmetric synthesis. It is with a collection of methods that provides the means for the simultaneous chemical synthesis of a large number of compounds, which utilizes a variety of starting materials. The resulting compound library could contain all of the possible chemical structures that can be produced in this manner.[52] There are two major approaches in

combinatorial chemistry. The first approach is the “mix and split synthesis”, and the other is coined “parallel synthesis”.

1.1.1.2 The Split-and-Mix Synthesis

The mix and split synthesis involves attaching starting materials to the polymer beads. The polymer resin beads are then split into a number of equal portions (x) and each of these is then individually reacted with a single different reagent. After this reaction, and subsequent washing to remove excess reagents, all the beads are recombined and mixed together and split again into portions (x). This entire process may then be repeated (for a total of n times) by reacting with the next set of reagents. The number of compounds that are obtained from the geometric increase in potential products would be x^n. The completed beads can be screened in order to determine whether any produces the desired activity.[53] The library with the best performance can be identified and tested further. The screening of bead-based split and mix combinatorial chemistry libraries is a powerful high-throughput approach that aids in the discovery of new chemical compounds able to interact with and modulate the activities of targets of interest.

1.1.1.3 Parallel Synthesis

Parallel synthesis is a technique widely used by researchers for the discovery of new compounds and screening of optimal process conditions. In parallel synthesis, combinations with different reaction conditions are prepared separately, in parallel, using hundreds of reaction vessels.

In medicinal chemistry, parallel synthesis applications can be utilized for lead identification, lead optimization, and determination of optimal reaction conditions

(Figure 1.1). Lead generation, also known as hit to lead, describes an early stage in drug discovery where small molecule hits from a HTS are evaluated and undergo limited optimization in order to distinguish promising lead compounds. Lead optimization is the process by which a drug candidate is designed after an initial lead compound is identified. This complex and iterative process of synthesis and characterization of a potential drug collected together represent the bigger picture of how chemical structure and activity relate in terms of interactions with its targets and its metabolism. Screening for select conditions involves optimization of the processes through improved understanding of synthetic routes, solvent systems, optimal temperatures and concentrations, correct reagents, reaction times, and selection of catalysts.

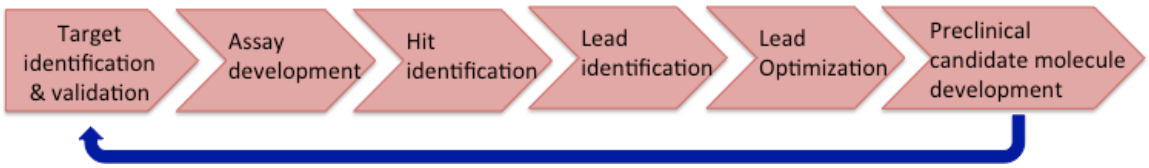

Figure 1.1: Stages of drug development

1.1.1.4 Tools for Parallel Synthesis

The widespread applications of parallel synthesis for the breakthrough of new drugs or methodology development is driving the evolution of novel technologies and tools, which enables the production of compounds at a greater rate than previously thought possible. For high-throughput parallel synthesis, multi-well reaction plates or reaction blocks can be utilized. The delivery of reagent can be accomplished using the multi-channel pipettor or robotic system. The purification process can also be done in parallel with a filter plate or purification tower. Also, an evaporator manifold for 24, 48

or 96 well blocks, which delivers equal amounts of gas to each well in order to gently speed solvent evaporation, is commercially available (Figure 1.2).

Figure 1.2: Tools for parallel synthesis. Clockwise from the top left: 96-well plate with sealing caps, Evaporator/manifold system in multi-well block, parallel synthesis reaction block, parallel purification tower.

Development of such tools for parallel synthesis led to the final step of reaction discovery, which is testing of the product of the desired activity. In asymmetric synthesis, the focus is the determination of *ee* of multiple reactions that were performed in parallel. Traditionally, the enantiomeric composition of the compound was quantified by using

chromatographic methods. However, optical methods have been more of an interest due to the advances in parallel synthesis, as they are more suitable for a HTS.

1.2 CHROMATOGRAPHIC METHODS

1.2.1. Introduction

The most common chromatographic methods that determine *ee* are chiral high-performance liquid chromatography (HPLC), chiral gas-chromatography (GC), or capillary electrophoresis (CE).

Chromatography is a well-known technique that has been used to separate, identify and determine the molecules of the analytes in a complex mixture and quantify the enantiomeric composition in a quick and relatively simple way. The adaptability of chromatography in a wide range of compounds, including biomolecules, makes this separation method very powerful.

Chromatographic separation is based on the different interactions of chemical compounds with a stationary phase and a mobile phase. The components of a mixture are carried through the stationary phase, which is fixed in the system, by the streaming of the mobile phase. The mobile phase is a liquid in liquid chromatography (LC), and it is a gas in gas chromatography (GC). The different migration velocities resulting from the different distribution of the analytes between mobile and stationary phase indicates that the stationary phase can be viewed as receptors in host-guest chemistry. For the determination of *ee*, chiral stationary phase would be used, which will interact uniquely with each individual enantiomer in a compound.

There are two approaches in chiral separation by chromatographic techniques; a direct and an indirect separation. The indirect approach involves derivatization of the

chiral compound with a chiral auxiliary to form diastereomeric complexes. These diastereomeric complexes can be separated by utilizing the achiral stationary phase. However, due to the extra derivatization step with prerequisites, such as absence of racemization during derivatization, absence of diastereomeric fractionation upon sample handling and injection, absence of diastereomeric bias upon detection, as well as the quantitative enantiomeric purity of the auxiliary, the direct chiral separation is more commonly used.[54] Typically in the direct approach, a chiral stationary phase is utilized as a selector, which forms transient diastereomers upon reversible interactions with analytes. This is advantageous, as it does not need to be further purified in order to separate enantiomers.

The packing materials of the column, the stationary phase, can be considered as a receptor. In liquid chromatography (LC) or gas chromatography (GC), commonly used in combination with mass spectrometry (MS), the analytes in the mixture interact differently with receptors (ligands) in the chiral chromatographic column. The speed of the different enantiomers varies upon the column selectivity and is controlled by the choice of the phase system. If a detector is coupled with the chromatographic system, the elution of the analytes can be observed as peaks. A chromatography based system is a great analytical tool that detects and isolates analytes in the mixture due to their sensitivity and functions even in exceedingly low concentrations.

Choosing the right chiral column to screen is a first crucial step in the identification and separation for each analyte in chromatographic methods. Therefore, researchers sought for the advancement of chiral stationary phases. The most popular classes of chiral stationary phases are based on polysaccharides, such as cellulose or

amylose. Also, a number of classes of chiral stationary phases are available; polymer-based carbohydrates, polysaccharide derivatives, macrocyclic glycopeptides, cyclodextrins, chiral synthetic polymer, and chiral ligand exchange.[54-57]

1.2.2 High Performance Liquid Chromatography

A chromatographic technique known as chiral high performance liquid chromatography (HPLC) is considered one of the power tools used in analytical chemistry. Chiral recognition can be achieved based on the ability of the chiral stationary phase to interact uniquely with each enantiomer to form transient-diastereomeric complexes. It requires a minimum of three interactions through hydrogen bonding, π-π interactions, dipole stacking, inclusion complexing, or steric bulk. To quantify *ee* using chiral HPLC requires a process of finding a suitable chiral column and ideal operating conditions that will separate the enantiomers.

Chiral HPLC has been widely used in *ee* analysis for its precise and accurate measurement. However, with the advances in parallel synthesis and combinatorial chemistry, HPLC technique suffers from several disadvantages. These include the reduction of resolving power of the column and the high cost of chiral columns, which are generally more expensive than comparable achiral stationary phases.[58] The primary drawback, however, is the prolonged analysis time that involves equilibration of the column. Although this instrument can be automated, analyzing samples one at a time is a time-consuming process, which can be cumbersome when trying to screen thousands of samples at a time. Even with a rapid chiral HPLC analysis, the minimum of ten minutes is required, which allows for about 144 samples to be analyzed in a day.[59] However, when factoring in the time used for re-equilibration of the solvent system and the

reloading of the solvent, much fewer than 144 samples will be analyzed by a chiral HPLC in a day.

Today, several parallel HPLC systems are available commercially and the multiplexing technology enabled parallel HPLC systems to synchronize to individual components, including the gradient pump, auto sampler, detection system and fraction collector. In the market, a HPLC system using up to 8 columns in parallel with flow control unit is the best-improved system available. Compared to standard HPLC, parallel HPLC systems possess the advantage in reduction of analysis time.

1.2.3 Gas Chromatography

There have been growing applications in the research fields of natural products, asymmetric synthesis, biological studies, etc. that utilize chiral gas chromatography (GC). The chiral separation using GC for *ee* determination works similarly to the HPLC technique, except that in GC, the mobile phase is a gas rather than a liquid. Like in the HPLC technique, direct chiral separation is commonly used where the separation of enantiomers is based upon the reversible interaction with chiral stationary phase in GC.

GC presents numerous advantages over HPLC for the separation of enantiomers. Since the mobile phase is gas, it is faster in the analysis and thereby more suitable for a HTS. Also, high efficiency and sensitivity are important merits of GC when separating volatile enantiomers. Other benefits include short column equilibration time, ease of coupling to mass spectrometry (MS), and ease of trace impurity quantitation.

However, the downside of this technique is that the injected samples need to be thermally stable and not racemized, since the high column temperatures can cause racemization of the chiral stationary phase and the analyte. Also, the high column

temperatures limit the analysis to be only suitable for compounds that are small and volatile. Most importantly, although GC is a high-speed analysis compared to HPLC, it remains to be in a serial method, which is not suitable for a true HTS.

1.2.4 Capillary Electrophoresis (CE)

Capillary electrophoresis (CE) is a technique which separates enantiomers upon the differential migration of analytes in an applied electric field. These separations are facilitated by the use of high voltages, and may generate electro-osmotic and electrophoretic flow of buffer solutions and ionic species, respectively, within the capillary.

The basic instrumentation for CE requires a capillary tube with a optical viewing window, a controllable high voltage power supply, two electrodes, two buffer reservoirs, and an ultraviolet (UV) detector (Figure 1.3). Chiral CE separation is achieved by adding a chiral selector to the buffer. Electrodes are located at the ends of the capillary, and are placed in the buffer reservoirs and the optical viewing window is aligned with the detector. After filling the capillary tube with buffer and a chiral selector, the sample can be introduced by dipping one end of the capillary into the sample solution and a high voltage is applied across the capillary tube. This causes the analytes in the sample to migrate along its length at different rates and to subsequently separate.[60]

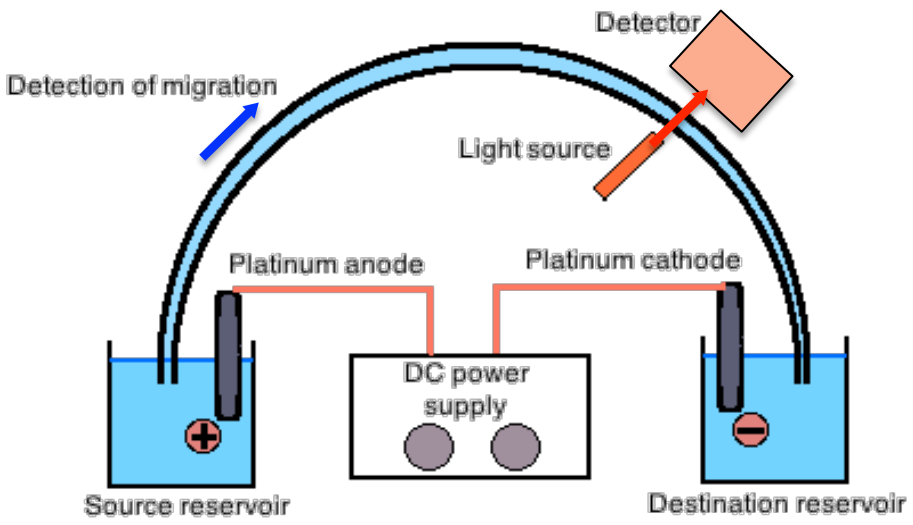

Figure 1.3: Basic configuration of the P/ACE capillary electrophoresis system.

One of the many advantages in utilizing chiral CE for *ee* analysis is that it requires a small sample size and chiral selector. More importantly, it is rapid and highly efficient, which results in higher resolution. Additionally, the apparatus itself is fairly low cost and easy to set up. Although chiral selector is generally expensive, since very little amount of chiral selector is required, it still proves more economical than HPLC. However, the primary disadvantage of CE is that it cannot be used for the isolation of enantiomers on a preparative scale and is limited to the analyte that can be ionizable in the analysis buffer.

1.3 Optical Spectroscopic Methods

1.3.1 Introduction

One method of chiral catalyst and auxiliary discovery is high-throughput screening (HTS), where rapid quantification of product enantiomeric excess (*ee*) and yield is required to achieve high efficiency.[4,5] Currently, the use of chiral chromatographic methods is the most common strategy in order to measure *ee* values, as previously discussed. However, these methods are associated with high cost (solvent, column replacement) and low duty cycle (equilibration time), and as a result, are not ideal for HTS. To achieve the speed required for true HTS, methods that avoid elution are most desirable.

Optical spectroscopy based *ee* determination is preferable due to the inherently short analysis time and lack of chromatographic separation as they use instrumentation, such as circular dichroism (CD) spectrometers, fluorimeters, UV-vis spectrophotometers, etc. The typical analysis time using these instruments would be within a minute, which is significantly faster compared to using chromatographic methods.

These methods, however, often require derivatization of the analyte, which add additional steps to the screening process.[5] Hence, host-guest systems that selectively target the asymmetric transformation products are ideal. Currently, our group has developed optical spectroscopy-based host-guest systems with the aim of rapid determination of enantiomeric excess. In this section, the group work that has been reported will be discussed.

This section begins with enantioselective indicator displacement assays (eIDAs) that target α-hydroxycarboxylates,[14-16] vicinal diols,[14-18] and α-amino acids.[19-22] This is followed by circular dichroism (CD) and exciton coupled circular dichroism (ECCD)

techniques for diamines, amines, carboxylic acids, amino acids, secondary alcohol, cyclohexanones, and aldehydes.

1.3.2 Enantioselective Indicator Displacement Assay (eIDA)

In an enantioselective indicator displacement assay (eIDA), the quantification of enantiomeric excess (*ee*) is based on displacement of an indicator by a chiral analyte.

1.3.2.1. eIDA for α-Hydroxycarboxylates and Vicinal Diols

One of our first eIDAs exploited the binding of boronic acids to α-hydroxyacids and vicinal diols.[14-16] The assay was developed with boronic acid receptors and catechol indicators. A representative example is shown in Figure 1.4. It was hypothesized that the presence of stereocenters neighboring the boron atom in the host would result in enantioselective association with chiral guests. In addition, *o*-aminomethyl functionality was utilized to aid the association equilibria.[15] In the initial study with boronic acid receptor (*S,S*)-**1.1** and various α-hydroxycarboxylates, using **PV** as the colorimetric indicator, an average of ±15% error was observed for the determined *ee* values.

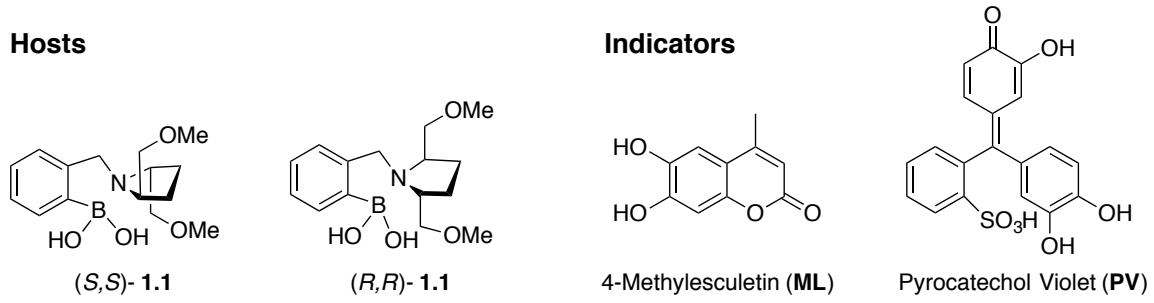

Figure 1.4: Examples of structures of the hosts and indicators used in the study.

In an effort to enhance the assay's sensitivity and improve the accuracy in *ee* measurements, fluorescent indicators were investigated.[15] 4-Methylesculetin **ML**, along with receptor (*S,S*)-**1.1**, were used to develop mathematical relationships that correlate optical signal to *ee* and concentration. It was found that iterative fitting the curve of fluorescence intensity *vs ee* using Origin® software yielded the best results. With this approach, the average error in *ee* was found to be ±7%. Further studies with a series of receptors, a series of indicators, and other guest substrates produced a protocol that may be employed to optimize indicator selection, concentration of the indicator, and the chiral receptor concentration.[16]

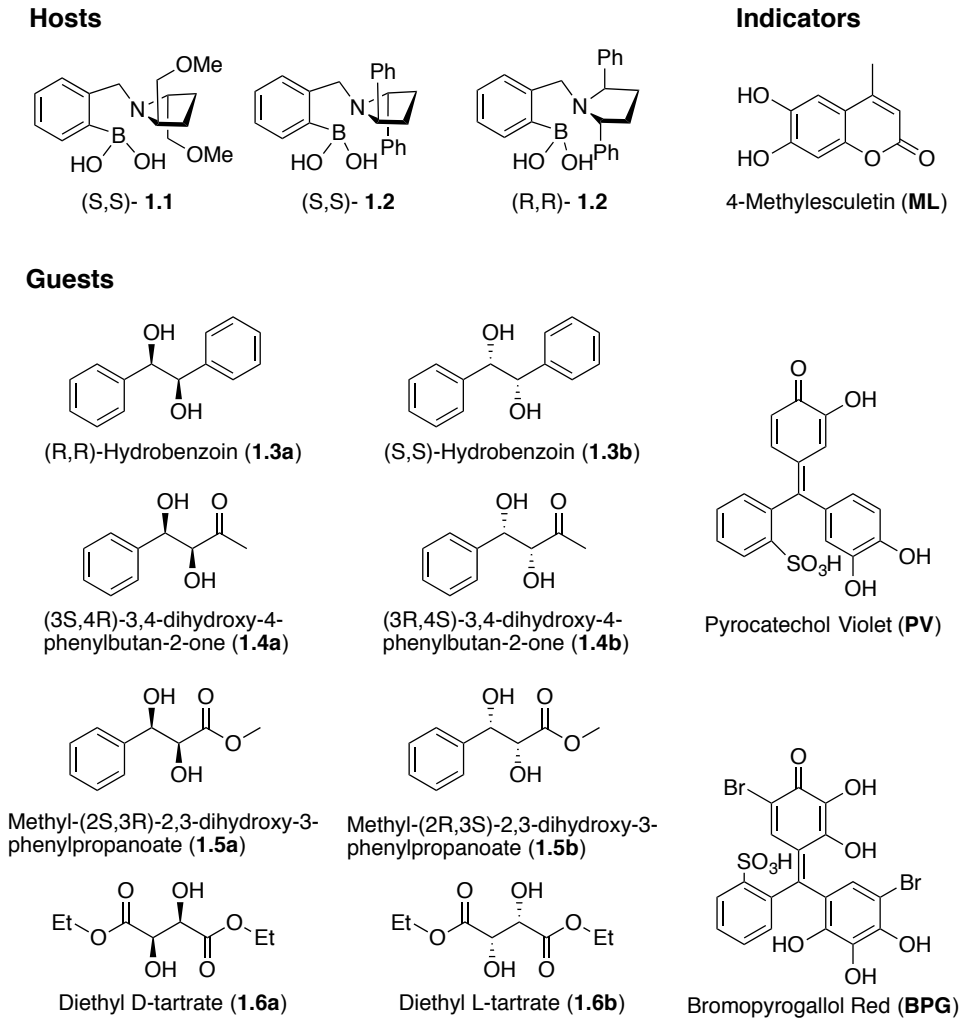

Figure 1.5: The hosts, guest enantiomers, and indicators used for developing HTS protocol.

The boronic acid and vicinal diol host-guest eIDA was further explored to extend the scope of detection and practicality.[17,18] In the reported study,[17] four pairs of syn-vicinal diol enantiomers were selected as guests along with three indicators (Figure 1.5). Two additional chiral hosts, (*S*,*S*)-**1.2** and (*R*,*R*)-**1.2**, were introduced to the system along with the previously reported host (*S*,*S*)-**1.1** to enhance the enantioselectivity. Using 96-

well plates and a UV-Vis plate reader, absorbance data was collected at different wavelengths with each host-indicator pair (3 for each pair, 9 total). The wavelengths were selected on the basis of the largest absorbance changes. Principal Component Analysis (PCA) on the absorbance data displayed excellent differentiation of both the identity of the diols and their enantiomers (Figure 1.6). Furthermore, the eIDA successfully differentiated samples with different guest concentration at various *ee* values on a PCA score plot (Figure 1.7). To demonstrate the predictive power of this system, artificial neural network (ANN) analysis with 14 absorbance inputs yielded an average absolute error of ±0.08 mM for sample concentration and ±7% for *ee*.

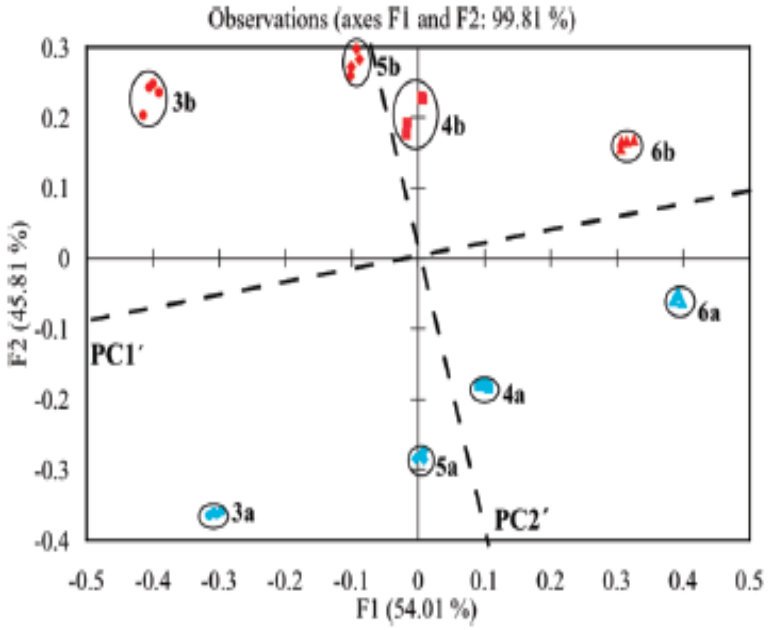

Figure 1.6: The PCA plot of the diol enantiomers discriminated with (*S*,*S*)-**1.1-**PV, (*R*,*R*)-1.2-ML, and (*S*,*S*)-**1.2**-PV receptor-indicator pair. The study was conducted in 10 mM p-toluenesulfonic acid/Hunig's base buffer (pH 7.4) in 100% MeOH at 25 °C.

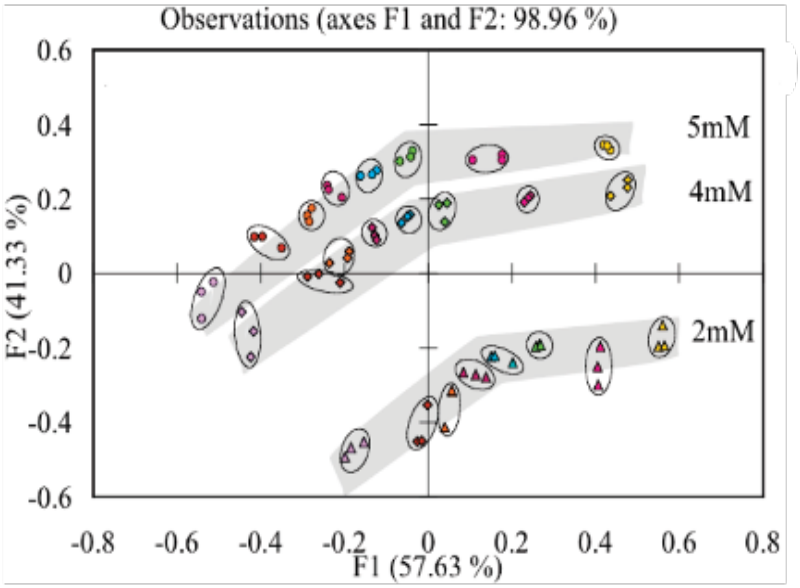

Figure 1.7: The PCA plot of diol **1.5** with varying *ee* and at three different concentrations discriminated by (*S,S*)-**1.1**-BPG, (*R,R*)-**1.2**-ML, and (*S,S*)-**1.2**-PV receptor-indicator pair. The study was conducted in 10 mM p-toluenesulfonic acid/Hunig's base buffer (pH 7.4) in 100% MeOH at 25 °C.

In an effort to perform HTS using this eIDA procedure, a stepwise process for a protocol development for concentration and *ee* determination was published.[18] The protocol described a 5 step process which includes optimization of the eIDA host and indicator concentration using UV-Vis titrations, screening for the best host-indicator combination to discriminate the enantiomers of interest, training of an ANN, analyzing unknown *ee* analytes, and, lastly, loading the absorbance results onto the trained ANN to determine *ee* and concentration. With the exception of the first step, which is only required to be done once per host-indicator pair, all the steps can be performed on a well-plate reader allowing for true HTS. The developed protocol was employed to analyze samples of hydrobenzoin with unknown *ee* and an average error of ±0.17 mM in the range of 3-8 mM concentration and ±2.4% for *ee*. When tested with samples synthesized

with established Sharpless asymmetric dihydroxylation reactions, the protocol was able to identify the best ligand as reported by literature.[17]

1.3.2.2. eIDA for α-Amino Acids

Another system of eIDAs was developed for *ee* determination of α-amino acids.[19-22] The system utilized Cu^{II} with chiral ligands **1.7** and **1.8** as hosts complexed to chromazurol *S* to form the receptor (Figure 1.8). Upon enantioselective coordination of chiral α-amino acids to form diastereomeric complexes, the selected colorimetric indicators were released, thus resulting in absorbance changes. Using X-ray crystallographic data, the enantioselectivity was postulated to have arisen from both the favored positioning of the dimethoxybenzylic rings on ligand **1.7** and the steric interactions of the phenyl groups on ligand 8 with the amino acid side chain. Using this eIDA, 13 out of the 17 examined amino acids were enantioselectively discriminated. Further study with *ee* calibration curves indicated approximately ±11.9% average error for *ee* determination. To further demonstrate its practicality, a high throughput screening protocol promoting this eIDA was developed with 96-well plates and four α-amino acids. (Figure 1.9).[22] The average absolute error of *ee* determination for all four of the amino acids was ±9.7% using only receptor $[Cu^{II}((R,R)\text{-}\mathbf{1.7})]^{2+}$; receptor $[Cu^{II}((R,R)\text{-}\mathbf{1.8})]^{2+}$ had unsatisfactory results. . In hopes of improving the eIDA's predictive power, ANN analysis was applied to the data collected. With ANN, the average absolute error of *ee* was found to be ±10.0%. An asymmetrically synthesized α-amino acid with unknown was subjected to the eIDA. The determined *ee*, from the reported eIDA, was found to be in satisfactory agreement with values measured with chiral HPLC and a ^1H NMR chiral shift agent.

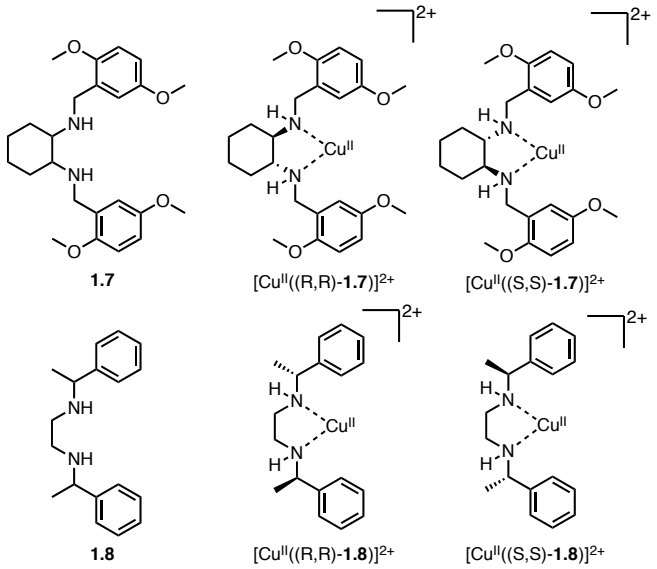

Figure 1.8: Structures of the chiral ligands (**1.7** and **1.8**) and the receptors formed with Cu^{II} and chiral ligand.

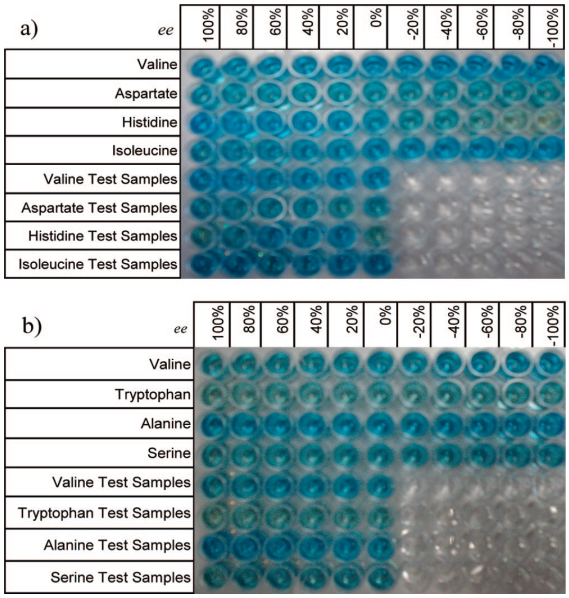

Figure 1.9: The 96-well plate used for making the *ee* calibration curves. Each plate had 4 rows of amino acids samples for producing the calibration curve with 6 test samples on the bottom. (a)$[Cu^{II}((R,R)\text{-}\mathbf{1.7})]^{2+}$ was used as the receptor. (b) $[Cu^{II}((R,R)\text{-}\mathbf{1.8})]^{2+}$ was the receptor.

In our research, the focus for *ee* determination switched from UV-Vis and fluorescence based systems to Circular Dichroism (CD) based methods. Accounting for this change was the signal dependence on the concentration of chiral analyte. Furthermore, with UV-Vis based systems, anything that can be absorbed in the region of detection could interfere with the signal of interest. This fact, in the context of HTS for chiral catalysts, would mean additional purification steps, which are not ideal for the process. A second reason for the change was simplification in host design. The hosts for eIDAs were often not commercially available and required synthesis, whereas most of our CD based hosts are formed with commercially available compounds or ligands that can be made with simple synthetic procedures. For the reasons given here, we moved the focus of our work to various forms of CD spectroscopy.

1.3.3 Circular Dichroism (CD)

Circular dichroism (CD) spectroscopy is an optical technique that is inherently sensitive to chirality. It enables one to analyze and differentiate analytes in a chiral host-guest system, and is applicable to high-throughput screening (HTS). Most chiral building blocks do not display strong Cotton effects in CD spectroscopy. However, intense Cotton effects can be produced when metal complexes carry MLCT bands, or when identical chromophores have a helical twist, leading to exciton-coupled circular dichroism (ECCD). The sign of the Cotton effect provides valuable information in determining the absolute configuration of the chiral analyte, and the CD signals can be directly correlated to the *ee* of the sample. For our CD based sensors, titration studies are typically performed to determine saturation point and the binding stoichiometry of the host-guest

interaction. The use of guest concentrations beyond the saturation point leads to concentration independent spectral responses.

In combination with statistical and chemometric techniques, such as linear discriminant analysis (LDA), artificial neural networks (ANNs), and principal component analysis (PCA), the CD spectral data can be further analyzed to find trends in the data as well as uncover characteristics of the data that best differentiate the chemo- and enantio-identity of the products. LDA is a technique used to determine linear combinations of features that maximize the separation between classes and minimizes the separation within classes.[23,24] Lastly, PCA is a tool that can classify and identify variance in the data.[25] These analysis techniques allow for highly accurate discrimination of chemoselectivity and enantioselectivity in sample reactions.

1.3.3.1. Metal-to-Ligand-Charge Transfer (MLCT) CD Assays

Our first CD-based assay for *ee* involved analysis of a metal complex that has CD-active metal-to-ligand-charge transfer (MLCT) bands.[26,27] The MLCT band in the visible region of the CD spectrum was particularly noteworthy, as most organic functional groups are CD-silent in this range, showing signals only in the 190-220 nm region. A simple inorganic coordination complex with *R*- or *S*- BINAP (2,2'-diphenylphosphino-1,1'-binaphthyl), a binaphthyl diphosphine ligand with axial chirality, was used as a host system to discriminate the chirality of diamines, primary amines, and cyclohexanones.[26-30] The axial chirality of BINAP arises from the limited rotation at room temperature of the bond linking the two sterically hindered two napthyl rings. The coordination complex with a transition metal, such as copper or palladium, introduces structural rigidity to the BINAP and its ligands derivatives.[28] Upon the addition of a chiral

guest, the MLCT bands were modulated, allowing for enantiomeric differentiation. BINAP was also selected because both of its enantiomerically pure forms are commercially available. The guest molecules can be directly used with the metal complex when the number of host binding sites and the number of functional handles of the guest are the same. Otherwise, the guests need to be derivatized in order to bind to the metal complex.

Racemic and Chiral Metal Complexes as Hosts for Diamines

Chiral metal complexes that have CD active MLCT bands, such as [CuI(BINAP)(MeCN)2]PF6 (**1.9**) or $[Pd^{II}(BINAP)(MeCN)_2]PF_6$ (1.10), were used to differentiate enantiomers of chiral vicinal 1,2-diamines (Figure 1.10).[26] Both enantiomers of **1.9** have MLCT bands around 340 nm in the CD spectrum, giving opposite Cotton effects for the *R* and *S* copper-coordinated complexes (Figure 1.11). Because there are no CD signals above 300 nm for the diamine analytes tested, or for the metal alone with diamines, the signals above 300 nm are indicative of the chemical identity, chirality, and concentration of the guests. Distinctive CD-active MLCT bands were observed for each diamine and its enantiomer when complexed with *R*- or *S*- **1.9**. Also, by comparing the intensity difference between CD signals of the complexes of diamine enantiomers with *R*-**1.9** or *S*-**1.9**, the *ee* for diamines was evaluated with an average error of ±3.8%.

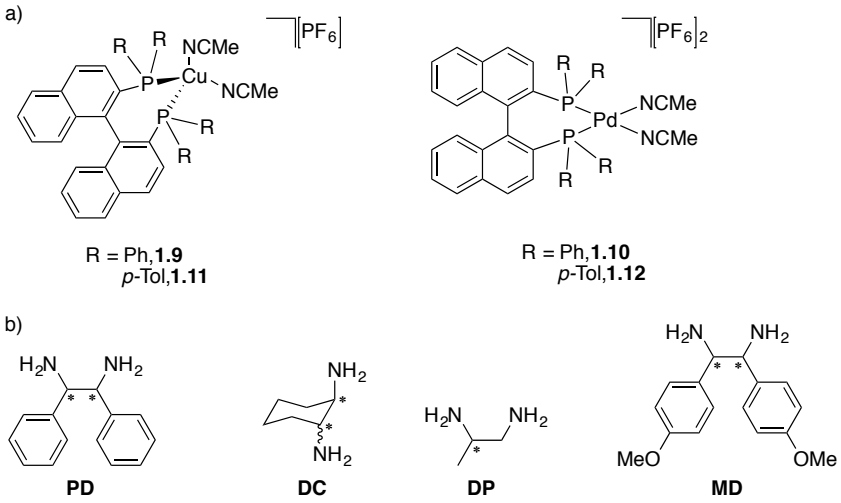

Figure 1.10: (a) Racemic-metal complexes employed. (b) Diamines employed: 1,2-phenylethylenediamine (**PD**), 1,2-diaminocyclohexane (**DC**), 1,2-diaminopropane (**DP**), bis(4-methoxyphenyl)-1,2-diaminoethane (**MD**).

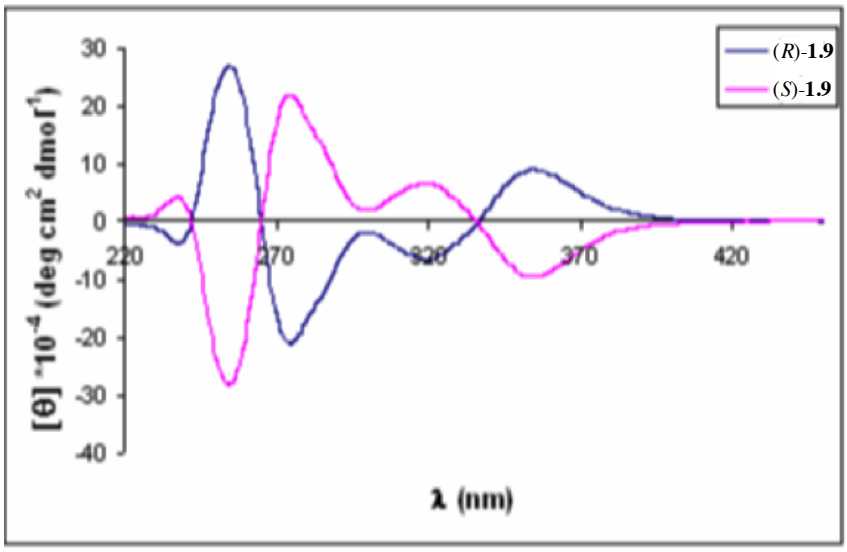

Figure 1.11: CD spectra of *R*-**1.9** [0.4mM] and *S*-**1.9** [0.4mM] between 220 nm and 450 nm.

The LDA plot in Figure 1.12, generated from the CD data of all receptors at chosen wavelengths, showed chemical identification and chiral discrimination of all of

the diamine analytes, which was determined by their individual clustering through the four quadrants. When the same data was analyzed with multilayer perceptron (MLP) ANNs, *ee* and concentration ($[G]_t$) were determined with average errors of ±3.8% and ±18.6%, respectively.

The racemic mixtures of **1.9** and **1.10** were also employed to discriminate enantiomers of chiral diamines.[27] Of course, the racemic mixture did not show any CD signals alone, but upon binding with enantiopure vicinal 1,2-diamines, CD active MLCT bands were observed. The LDA plot successfully classified the diamines and their handedness.

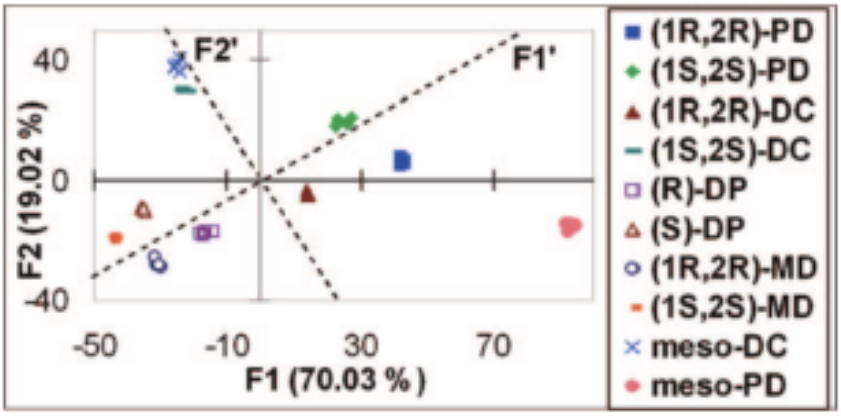

Figure 1.12: Response patterns for all the analytes using (*R*)-**1.9** receptor obtained by LDA.

Chiral Metal Complexes as a Host for α-Chiral Primary Amines

The same metal complex **1.9** was employed to discriminate α-chiral primary amines.[29] However, the addition of underivatized chiral amines to *R*-**1.9** did not exhibit any signal modulation by CD spectroscopy. Therefore, a simple derivatization of chiral amines to form imines that can coordinate with *R*-**1.9** was necessary. Chiral imines were formed from the condensation of chiral amines with 2-pyridinecarboxaldehyde in

situ (Scheme 1). The modulated MLCT signal, which is indicative of the coordination of the imines with *R*-**1.9**, was observed in the CD spectrum (Figure 1.13). The CD signals were characteristic to each analyte, and the data was further analyzed with LDA and PCA. In the PCA plot, F1 axis defines chirality with negative values for *R*-enantiomers and positive values for *S*-enantiomers, and F2 axis defines concentration. The average error for *ee* was ±17%, which led us to develop a method that could provide a more accurate enantiodiscrimination.[45]

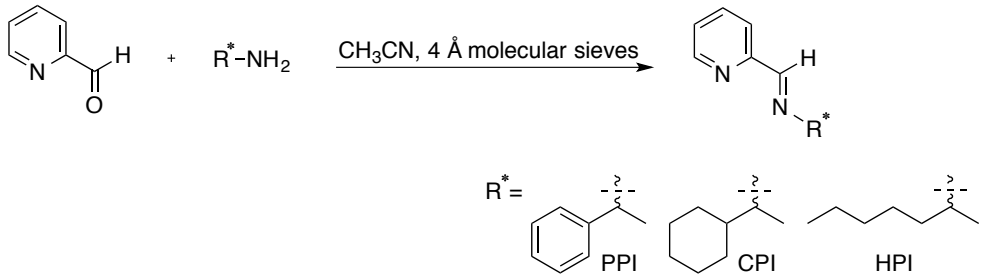

Scheme 1.1: Derivatization of the amines to form the corresponding Schiff bases.

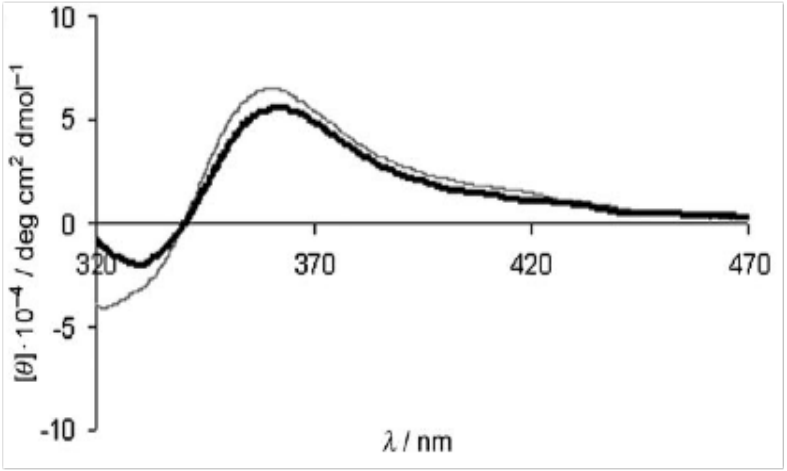

Figure 1.13: CD spectrum for (*R*)-**1.9** [0.4mm] and the enantiomers of CPI [0.8 mm](regular line=(*R*)-CPL, bold line=(*S*)-CPL).

Chiral Cu(I) Metal Complexes as Hosts for α-Chiral Cyclohexanones

Complex **1.9** was also applied to the enantiodiscrimination of α-chiral cyclohexanones.[30] In order to create bidentate ligands which produce a twist upon binding with *R*- or *S*-**1.9**, enantiomerically pure α-chiral cyclohexanones were derivatized with 1-methyl-1-(2-pyridyl) hydrazine to form hydrazones (Scheme 1.2). The nitrogen atoms in the pyridyl group and hydrazone moieties coordinate to a CuI, forming a metal complex. Upon the addition of hydrazone to enantiomerically pure **1.9**, diastereomers will be produced with different twist angles. Different twist angles between the naphthyl rings in BINAP were predicted based upon steric interactions between the phosphine ligand and the R group on the ketones. The degree of twist is reflected in the CD spectrum, allowing for discrimination between the two enantiomers. The *R*-enantiomers of hydrazones with *S*-**1.9**, compared to *S*-enantiomers, will cause a larger change in the twist, thus inducing a larger change in the CD signals from the original MLCT band of **1.9** (Figure 1.14). The enantiomeric host *R*-**1.9** produces a mirror image CD spectrum. Through the use of calibration curves, these studies allow *ee* determination of the chiral cyclohexanones to be performed with an absolute error of ± 7%.

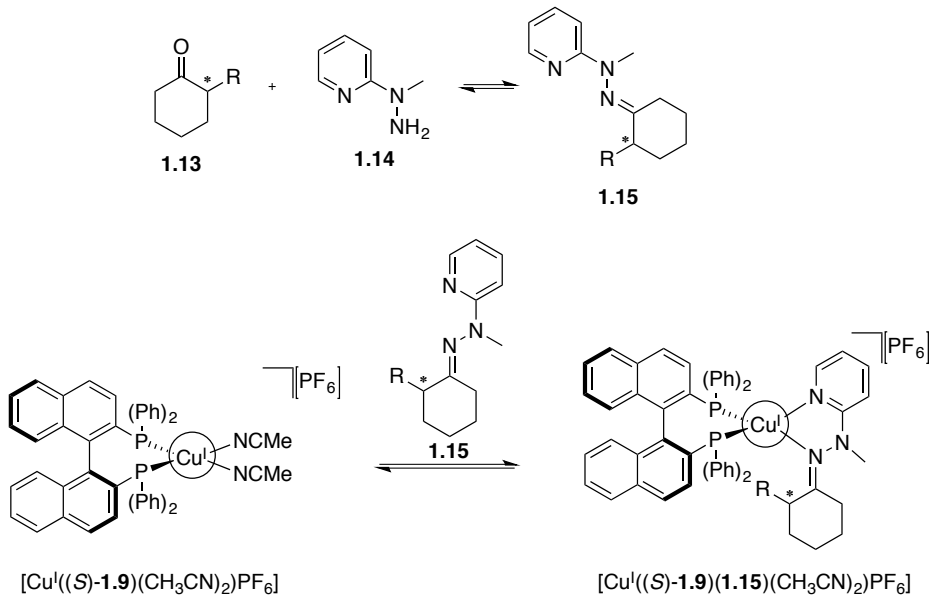

Scheme 1.2: Derivatization of *R*-chiral cyclohexanones (**1.13**) with 1-methyl-1-(2-pyridyl) hydrazine (**1.14**) to produce a bidentate analyte (**1.15**), followed by complexation to (**1.9**).

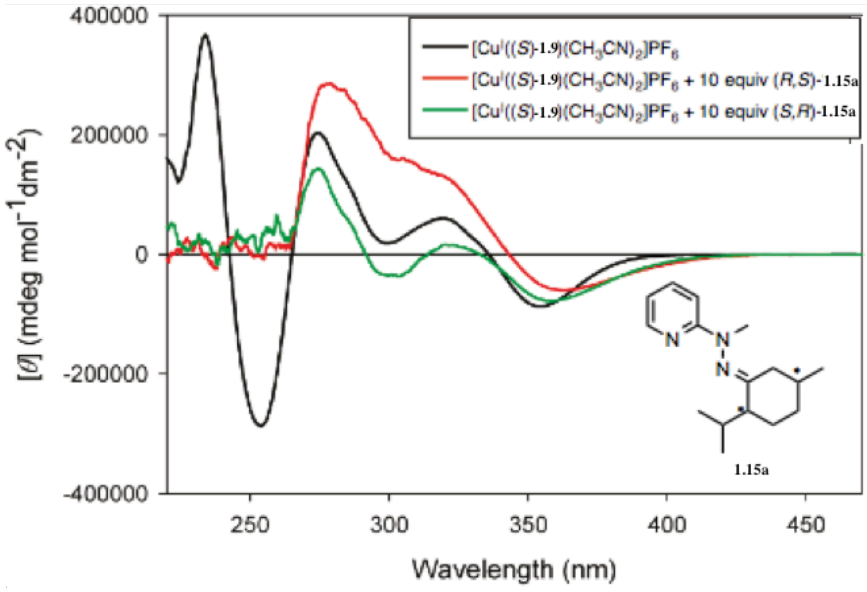

Figure 1.14: CD spectra of **1.9** (401 µM) in CH3CN (black), *S*-**1.9** (401 µM) mixed with (*R,S*)- **1.6** (4 mM) (red), and *S*-**1.9** (401 µM) mixed with (*S,R*)- **1.6** (4 mM) (green).

1.3.3.2. A Boronic Acid Receptor for Chiral Primary Amines

Another method for the analysis of chiral primary amines was created using an assembly from the Bull and James groups,[31,32] where enantiopure 1,1'-bi-2-naphthol (BINOL) assembles with o-formylphenyl boronic acid (FPBA) and α-chiral primary amines (Scheme 1.3). Enantiomerically pure a BINOL and BINOL-FPBA mixture both have a CD signal that is modulated upon addition of *R* or *S* guest amines.[33] The three-component assembly forms an imine coordinated boronate ester, and it was hypothesized that the absolute configuration of the amine would modify the torsional angles of *S* or *R*-BINOL, resulting in the modulation in CD. However, molecular modeling experiments using Spartan showed no evidence of distortion of the dihedral angle of BINOL in the product assembly. The change in CD occurs from extending the chromophore ability of the chiral amine through condensation with the aromatic boronic acid (Figure 1.15).

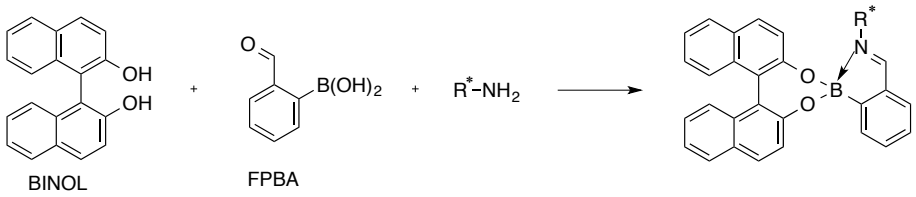

Scheme 1.3: Assembly developed by the Bull and James groups.

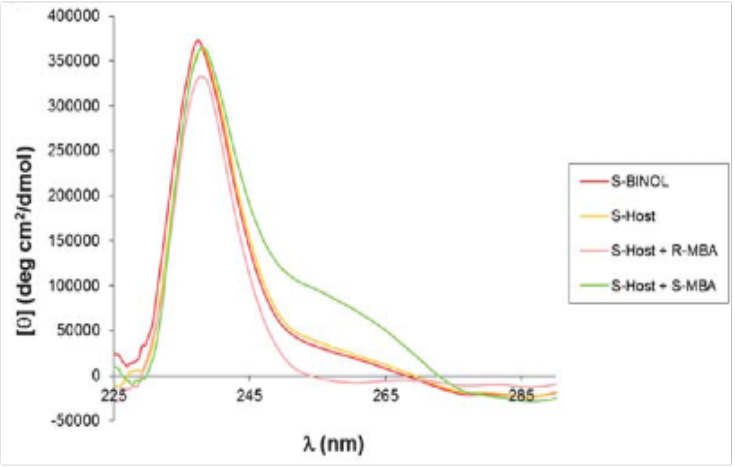

Figure 1.15: CD spectra of the assembly of MBA with (S)-BINOL-FPBA.

Various amine analytes were assembled with BINOL and analogues, and with FPBA (Figure 1.16). The CD spectra of the resulting complexes exhibited differences in intensity and shape, making it possible to discriminate their identities and chirality. With all of the data obtained from varying hosts and guests, PCA and LDA plots were generated to classify the amines. The *ee* analysis done was highly accurate, giving an average absolute error of ±5.8% using the calibration curves generated.

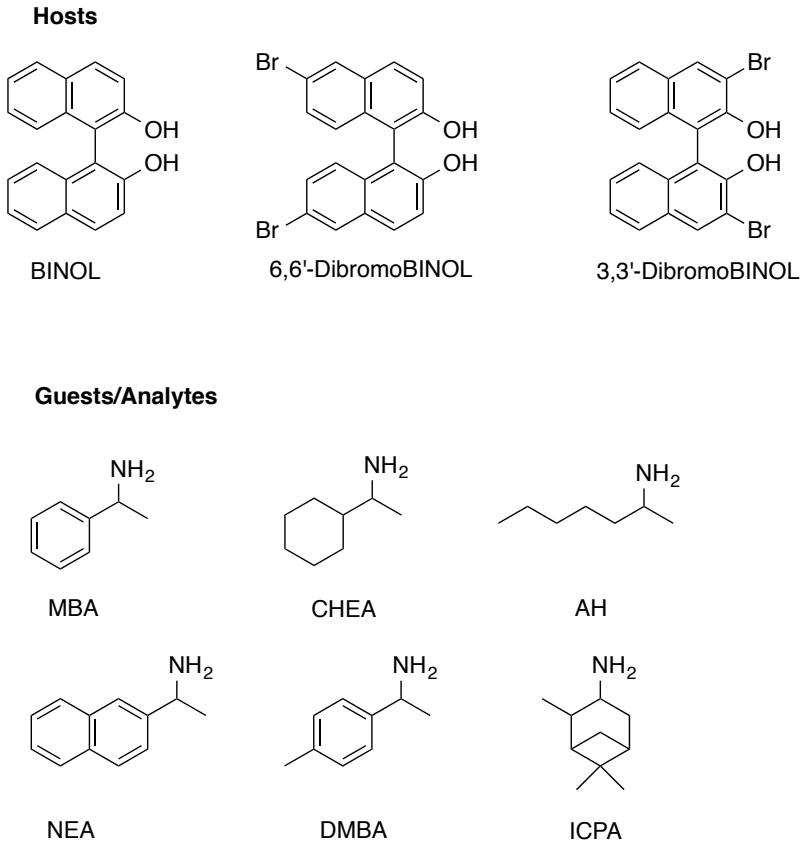

Figure 1.16: Structures of the compounds used as hosts and guests/analytes.

1.3.3.3. Exciton-Coupled Circular Dichroism (ECCD)

One form of CD, namely exciton-coupled circular dichroism (ECCD),[34] has been widely employed in chirality sensing for various analytes.[35-44] When a compound contains two or more chromophores that can be oriented in a helical fashion, ECCD signals are generated. This phenomenon leads to bisignate CD curves centered at the UV-Vis absorption maximum. Enantiomers have mirror image CD spectra, and the sign of the Cotton effect is used to determine the absolute configuration of the analyte. Practically, chiral analytes must be derivatized with chromophores or need to be bound to receptors containing chromophores through supramolecular interactions.

In Situ Generated Fe^{II} Complexes as a Host for Chiral Amines

The method described in section 3.1.2 for chiral monoamines[29] suffers from several drawbacks. First, the derivatization of 2-pyridinecarboxaldehyde to form bidentate imines takes two hours. Second, it gave a moderately high average error of ±17%. Lastly, the calibration curves are concentration dependent. In an effort to eliminate the need for the synthesis of a host and to create a simple and quick assay, our group has turned to self-assembly. In one example, Fe^{II} was used as a metal center to coordinate three equivalents of bidentate imines, which were created from the condensation between a chiral amine and aldehyde **1.16**.[45] In order to reduce derivatization time, 3-hydroxy-2-pyridinecarbaldehyde was allowed to react with the chiral primary amines to form chiral imines (Scheme 1.4). Followed by this in situ amine derivatization, Fe^{II} was added to form octahedral complexes that possess different helical twists. There are four possible stereoisomers for enantiomerically pure amines, and 24 possible stereoisomers for mixtures of *R* and *S* amines. These isomers result from helical isomerism (clockwise, counterclockwise), configurational isomerism (fac and mer), as well as *R* and *S* amines. However, this complexity does not interfere in *ee* determination and enantiomeric differentiation because the isomers interchange rapidly in equilibria. The three asymmetrically oriented ligands bonded to Fe^{II} generate ECCD signals, which correlate with the identity of the stereogenic center of the imines and the helicity of the complex (Figure 1.17). Imines with a *R* stereogenic center induce a counterclockwise twist and have a negative ECCD couplet, and vice versa.

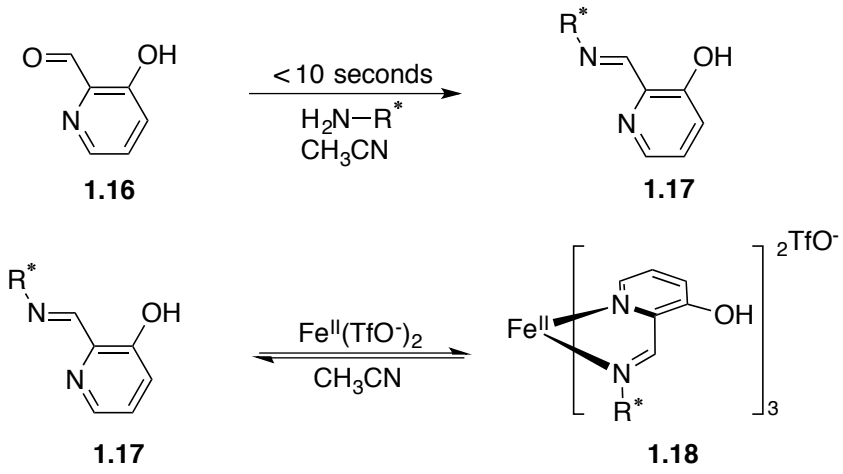

Scheme 1.4: Aldehyde **1.16** reacts rapidly with an amine to form imine **1.17**, followed by complexation with Fe^{II} to form **1.18**.

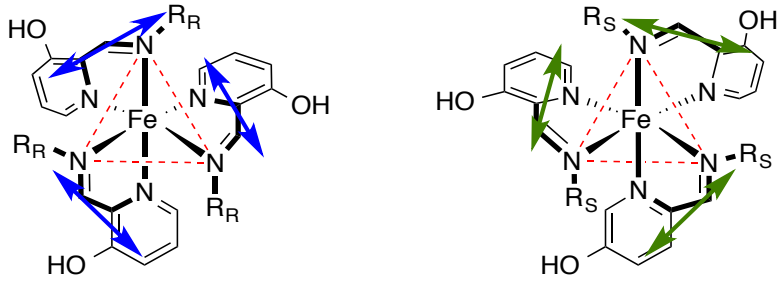

Figure 1.17: Helical arrangements of the transition dipoles that couple to give rise to the positive and negative ECCD couplets for the Δ-(*R*)- and Λ-(*S*)-fac isomers, respectively.

Amines with aromatic, cyclic, and acyclic functionality were differentiated by the CD signal intensity and shape (Figure 1.18). A concentration-independent calibration curve was generated to determine *ee* with a low average error of ±5%.

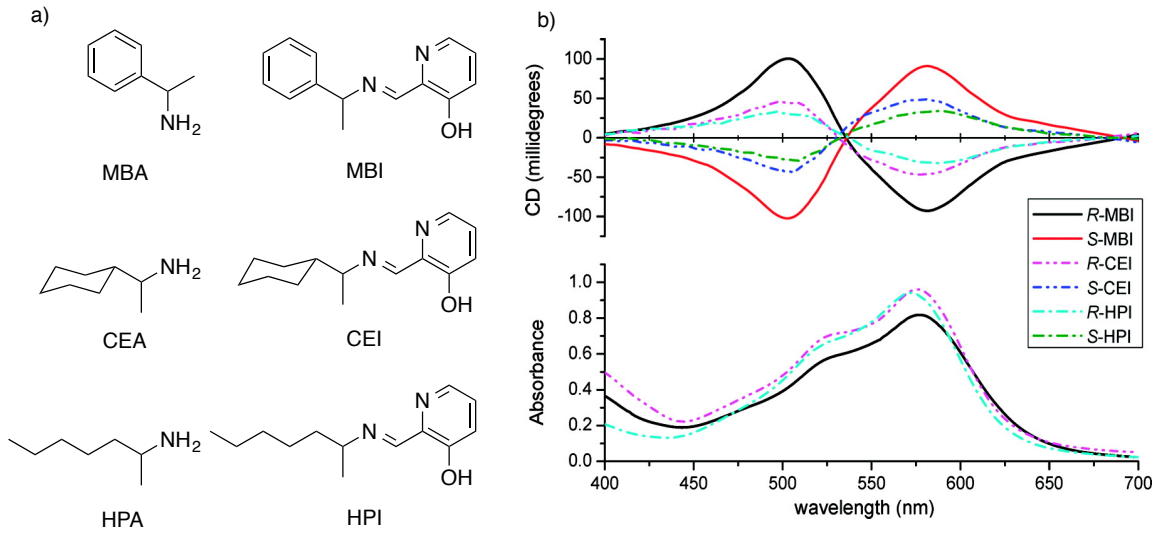

Figure 1.18: a) Structures of (left) MBA, CEA, and HPA, the three amines studied, and (right) MBI, CEI, and HPI, the three imines formed after reaction of the amines with aldehyde 1.16. b) UV–vis and CD spectra of the MLCT bands for the three different imines studied, MBI (3 mM), CEI (6 mM), and HPI (7 mM), at 100% and –100% *ee* in acetonitrile with 1 mM Fe^{II} in a 0.1 cm quartz cell from 400 to 700 nm.

Fe^{II} complexes as a host for α-chiral aldehydes

Adapting the two protocols previously discussed,[29,45] an assay for chiral aldehydes was created.[46] Imines generated from compound **1.14** with various chiral aldehydes coordinate with metal upon the addition of Fe^{II} triflate (Scheme 1.4 and Figure 1.19). Compared to our previous approach,[29] this assay was advantageous because the derivatization of the amine to form an imine was reduced from two hours to a half hour. The complexation of synthesized bidentate imines **1.19**-**1.21** with Fe^{II} led to large CD signals, which were used to determine *ee* of α-chiral aldehydes. The CD signal was used to discriminate absolute configuration of the α-chiral aldehydes, as well as their *ee* values with an absolute average error of ±5%.

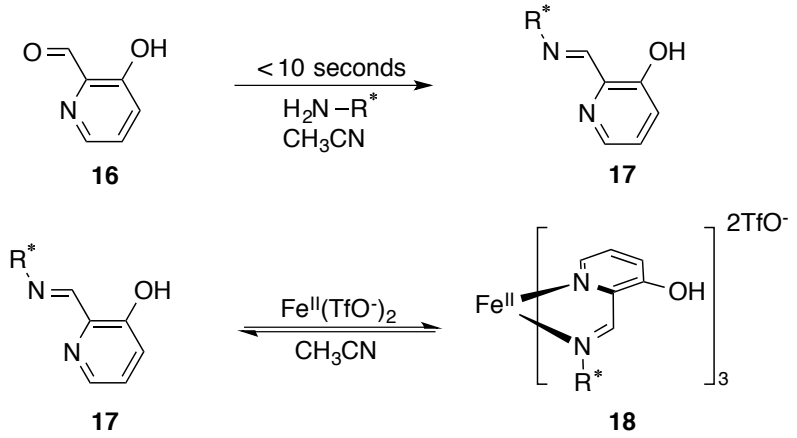

Scheme 1.4: Aldehyde **1.16** reacts rapidly with an amine to form imine **1.17**, followed by complexation with Fe^{II} to form **1.18**.

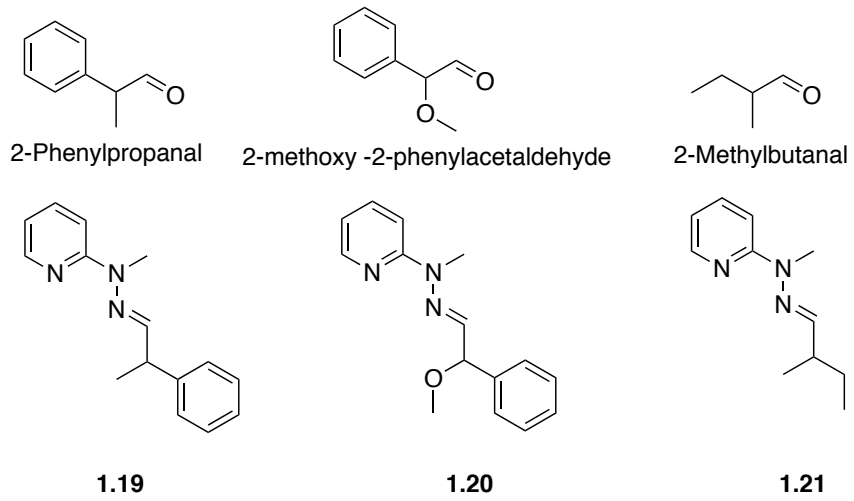

Figure 1.19: Structures of aldehyde studied, and **1.19**, **1.20**, and **1.21** created by reaction with **1.15**.

A Cu^{II} Complex as a Host for Chiral Carboxylates and α-Amino Acids

Our group has also exploited ECCD for the analysis of chiral carboxylates.[47] Achiral host $[(BQPA)Cu^{II}(ClO_4)]$ **1.22** is easy to synthesize and has an empty

coordination site for monodentate carboxylate binding (Scheme 1.5). Host complex **1.22** alone has two different helical isomers that exchange rapidly in equilibria, resulting in no CD signal. However, binding of a chiral guest causes one twist to dominate, and thereby generates the corresponding ECCD couplet (Figure 1.20). This method has the advantage of avoiding an analyte derivatization step. The guest forms a complex that has a minimum steric interaction with the groups on the stereocenter, thus dictating the helicity. *R*-enantiomers gave negative CD couplets, which are indicative of a P helical isomer with a counterclockwise twist, and vice versa. The difference in steric size of the groups attached to the stereocenter is directly correlated to the magnitude of the CD signal. Calibration curves for the determination of *ee* of carboxylates were generated, and gave an average absolute error of ±3%.

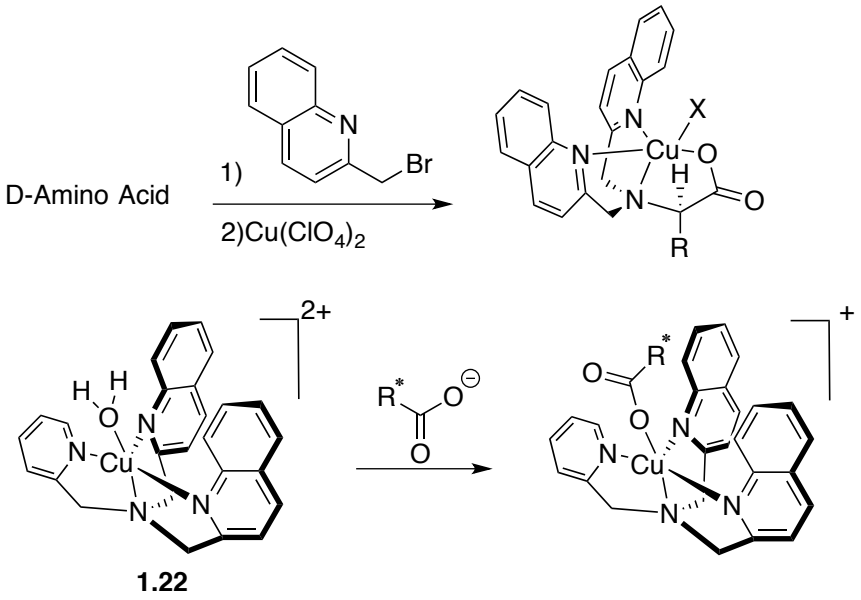

Scheme 1.5: Protocol to determine absolute configuration of chiral amino acids (Top) and proposed complex formation between [(BQPA)$Cu^{II}(ClO_4)_2$] host **1.22** and chiral carboxylate guest.

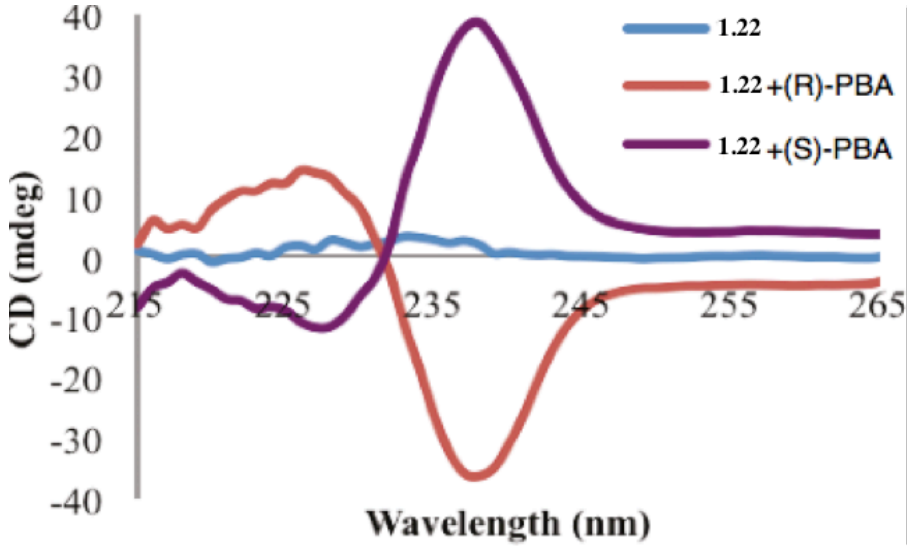

Figure 1.20: CD spectra of host **1.22** (0.5 mM) by itself and with each enantiomer of PBA (1.0 mM) in default buffer (75% MeCN/H2O with 20 mM HEPES buffer at pH 7.4).

Amino acids contain carboxylate groups, and hence host **1.22** was also used as a sensor for *α*-amino acids and *β*-homoamino acids.[48] Boc-protected α-amino acids and Boc-protected *β*-amino acids follow the same operating principles as the previously studied carboxylates. For both *α*-amino acids and *β*-homoamino acids, D-isomers led to a P-type helix, whereas L-isomers led to an M-type helix. However, due to the increase in the degrees of rotational freedom in *β*-homoamino acids, reduced CD signals were observed (Figure 1.21 and 1.22). ɣ-Amino acids were not suitable for this system.

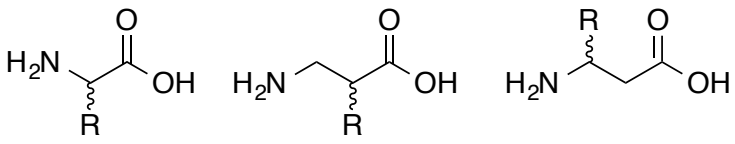

Figure 1.21: Types of amino acids.

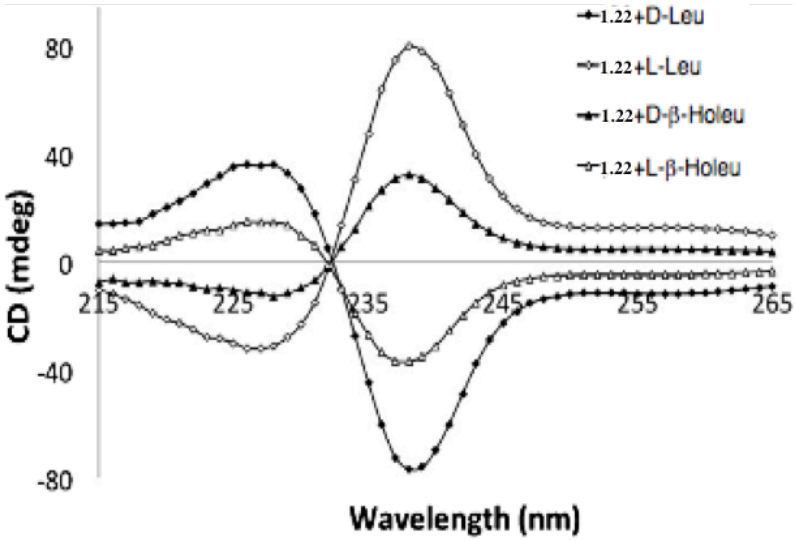

Figure 1.22: CD spectra for each indicated guest (1.0 mm) with host **1.22** (0.5 mm) in default buffer.

A Zn^{II} Mediated Multi-Component Assembly as a Host for Chiral Secondary Alcohols

Our most recent ECCD-based sensor targets chiral secondary alcohols and was formed via a dynamic multi-component assembly process.[49] Four components: 2-pyridinecarboxaldehyde, di-(2-picolyl)amine, $zinc^{II}$ triflate and the chiral alcohol were mixed together, and reversible covalent bonding formed assembly **1.23** (Scheme 1.6). The assembly possesses a helical twist of the pyridines that relies on the handedness of the stereocenter at the hemiaminal ether carbon. The stereocenter, in turn, is dictated by the handedness of the alcohol. The helical twist of the tris-pyridine complex induces a large Cotton effect in the CD spectrum resulting from ECCD. *R*-Alcohols lead to a preference of an *S*-stereocenter at the hemiaminal ether carbon, giving a preferential P twist of the tris(pyridine) ligand and a negative ECCD couplet, while the opposite is true for *S*-alcohols.[50] The sign of the Cotton effect is therefore indicative of the handedness of the alcohol stereocenter and the unique CD signals for each alcohol allow determination

of alcohol identity. This system has successfully been used to quantify *ee* values of chiral secondary alcohols with a ±3% error.

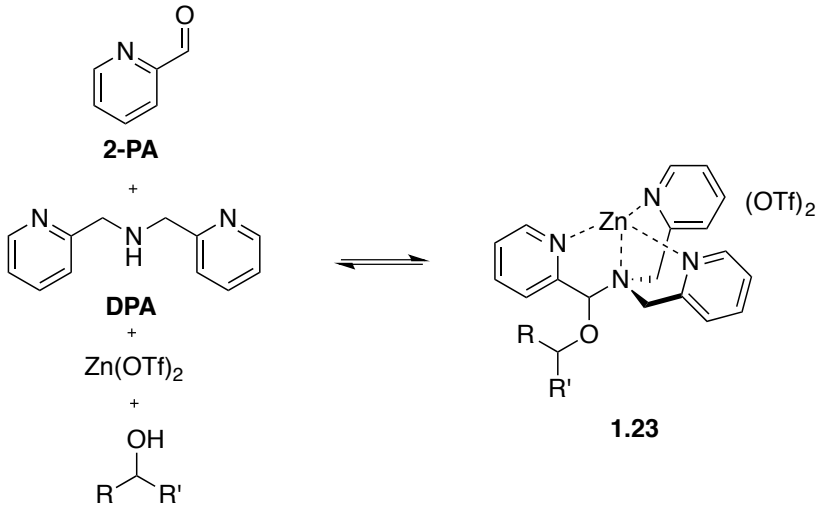

Scheme 1.6: Four-component reversible covalent assembly for secondary alcohol binding.

The diastereomeric ratio (dr) of the assembly with chiral alcohols was linearly correlated with the magnitude of the CD signal (Figure 1.23).[51] Furthermore, Charton steric parameters linearly correlate with the dr values and thereby also the ECCD intensity. From these correlations, the magnitude of CD values of various alcohols could be predicted with an average absolute error of ±9.5%.

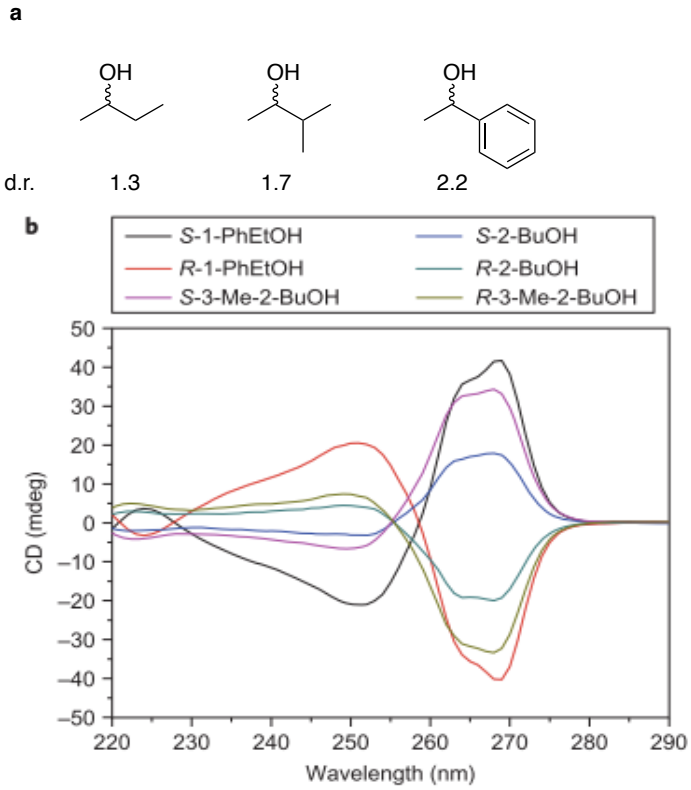

Figure 1.23: a) Dr values for assemblies with chiral mono-ols (*R* or *S*) obtained from ^{1}H NMR. b) CD spectra of assembly derived from three alcohols (0.175 mM 2-PA, 0.525 mM mono-ol).

1.3.3.4 Conclusions

The use of optical spectroscopy for the determination of enantiomeric excess values has the potential to revolutionize reaction and catalyst development. Many researchers, including our group, have pioneered this effort with a focus on either colorimetric or circular dichroism approaches. A series of assays targeting several chiral functional groups have been created: diols, diamines, amines, alcohols, carboxylic acids,

aldehydes and ketones. In addition, a series of strategies for optical modulations have been implemented: indicator-displacement assays, CD-active MLCT excitation, and exciton-coupled circular dichroism. While the absolute errors in the *ee* values are not yet as low as those traditionally associated with chiral HPLC analysis, advances in lowering the errors can be anticipated in the near future. Yet, even with errors of around 5% to 10%, one can quickly identify trends in data and find the "hits" within hundreds of samples. This ability to screen with errors that are relatively large in comparison to HPLC has been reiterated to our group numerous times by chemists in big-pharma. Thus, true high-throughput screening is right around the corner.

1.4 Summary and Outlook

In asymmetric synthesis, the introduction of automated systems and robotics has led to a direction focusing on combinatorial and parallel synthesis for chiral catalysts. In order to test with the primary objective of determining enantiomeric purity, the generated products high-throughput screening methods became indispensable. The analysis technique has been slowly shifting from the current chromatographic technique to an optical signal base technique. As thousands of compounds can be generated, the optical signaling based methods are more rapid in the measurement of *ee*. The user-friendly instrumentation and its compatibility with 96-well plates allow for one to screen hundreds of samples in a relatively short amount of time. Our group, amongst many other researchers in the field, is contributing in the development and optimization of an optical method based assay for a rapid determination of *ee* of various analytes.

1.5 REFERENCES

1. Jaroch, S.; Weinmann, H.; Zietler, K. Asymmetric Organocatalysis. *Chem. Med. Chem.* **2007**, *2*, 1261–1264.

2. Lin, G. Q.; Li, Y. M.; Chan, A. S. *Principles and Applications of Asymmetric Synthesis*; Wiley: New York, 2001.

3. Christmann, M.; Braese, S. *Asymmetric Synthesis: The Essentials, ed.*; Wiley: New York, 2008.

4. Tsukamoto, M.; Kagan, H. B. Recent Advances in the Measurement of Enantiomeric Excesses. *Adv. Synth. Catal.* **2002**, *344*, 453–463.

5. Finn, M. G. Emerging methods for the rapid determination of enantiomeric excess. *Chirality* **2002**, *14*, 534–540.

6. Welch, C. J.; Szczerba, T.; Perrin, S. R. Some recent high-performance liquid chromatography separations of the enantiomers of pharmaceuticals and other compounds using the Whelk-O 1 chiral stationary phase. *J. Chromatogr. A* **1997**, *758*, 93–98.

7. Welch, C. J.; Grau, B.; Moore, J.; Mathre, D. J. Use of Chiral HPLC-MS for Rapid Evaluation of the Yeast-Mediated Enantioselective Bioreduction of a Diaryl Ketone. *J. Org. Chem.* **2001**, *66*, 6836–6837.

8. Welch, C. J.; Fleitz, F.; Antia, F.; Yehl, P.; Waters, R.; Ikemoto, N.; Amstrong, I. J. D.; Mathre, D. Chromatography as an Enabling Technology in Pharmaceutical Process Development: Expedited Multikilogram Preparation of a Candidate HIV Protease Inhibitor. *Org. Process Res. Dev.* **2004**, *8*, 186– 191.

9. Sigman, M. S.; Jacobsen, E. N. Schiff Base Catalysts for the Asymmetric Strecker Reaction Identified and Optimized from Parallel Synthetic Libraries. *J. Am. Chem. Soc.* **1998**, *120*, 4901– 4902.

10. Wolf, C.; Hawes, P. A. A High-Throughput Screening Protocol for Fast Evaluation of Enantioselective Catalysts. *J. Org. Chem.* **2002**, *67*, 2727–2729.

11. Pu, L. Fluorescence of organic molecules in chiral recognition. *Chem. Rev.* **2004**, *104*,1687-1716.

12. Wolf, C.; Bentley, K. W. Chirality sensing using stereodynamic probes with distinct electronic circular dichroism output. *Chem. Soc. Rev.* **2013**, *42*, 5408-5424.

13. Bentley, K. W., Wolf, C. Stereodynamic Chemosensor with Selective Circular Dichroism and Fluorescence Readout for in Situ Determination of Absolute Configuration, Enantiomeric Excess, and Concentration of Chiral Compounds. *J. Am. Chem. Soc.* **2013**, *135*, 12200-12203

14. Zhu, L.; Anslyn, E. V. Facile Quantification of Enantiomeric Excess and Concentration with Indicator-Displacement Assays : An Example in the Analyses of α-Hydroxyacids. *J. Am. Chem. Soc.* **2004**, *126*, 3676.

15. Zhu, L.; Zhong, Z.; Anslyn, E. V. Guidelines in implementing enantioselective indicator-displacement assays for α-hydroxycarboxylates and diols. *J. Am. Chem. Soc.* **2005**, *127*, 4260.

16. Zhu, L.; Shabbir, S. H.; Anslyn, E. V. Two methods for the determination of enantiomeric excess and concentration of a chiral sample with a single spectroscopic measurement. *Chem. Eur. J.* **2007**, *13*, 99.

17. Shabbir, S. H.; Joyce, L. A.; da Cruz, G. M.; Lynch, V. M.; Sorey, S.; Anslyn, E. V. Pattern-based recognition for the rapid determination of identity, concentration, and enantiomeric excess of subtly different threo diols. *J. Am. Chem. Soc.* **2009**, *131*, 13125.

18. Shabbir, S. H.; Anslyn, E. V. A general protocol for creating high-throughput screening assays for reaction yield and enantiomeric excess applied to hydrobenzoin. *Proc. Nat. Acad. Sci.* **2009**, *106*, 10487.

19. Folmer-Andersen, J. F.; Lynch, V. M.; Anslyn, E. V. Colorimetric enantiodiscrimination of α-amino acids in protic media. *J. Am. Chem. Soc.* **2005**, *127*, 7986.

20. Folmer-Andersen, J. F.; Kitamura, M.; Anslyn, E. V. Pattern-based discrimination of enantiomeric and structurally similar amino acids: an optical mimic of the mammalian taste response. *J. Am. Chem. Soc.* **2006**, *128*, 5652.

21. Leung, D.; Folmer-Andersen, J. F.; Lynch, V. M.; Anslyn, E. V. Using Enantioselective Indicator Displacement Assays To Determine the Enantiomeric Excess of α-Amino Acids. *J. Am. Chem. Soc.* **2008**, *130*, 12318.

22. Leung, D.; Anslyn, E. V. Transitioning enantioselective indicator displacement assays for α-amino acids to protocols amenable to high-throughput screening. *J. Am. Chem. Soc.* **2008**, *130*, 12328.

23. Coommans, D.; Massart, D.L.; Kaufman, L. Optimization by statistical linear discriminant analysis in analytical chemistry. *Anal. Chim. Acta.* **1979**, *112*, 97-122.

24. Li, Y.; Jiang, J.-H.; Chen, Z.-P.; Xu, C.-J.; Yu, R.-Q. Robust Linear Discriminant Analysis for Pattern Recognition, *J. Chemom.* **1999**, *13*, 3-13.

25. Ringner, M. What is Principal Component Analysis? *Nat. Biotechnol.* **2008**, 26, 303-304.

26. Nieto, S.; Lynch, V.M.; Anslyn, E.V.; Kim, H.; Chin, J. High-throughput Screening of Identity, Enantiomeric Excess, and Concentration using MLCT Transitions in CD Spectroscopy. *J. Am. Chem. Soc.* **2008**, *130*, 9232-9233.

27. Nieto, S.; Lynch, V.M.; Anslyn, E.V.; Kim, H.; Chin, J. Rapid Identification, Enantiomeric Excess and Concentration Determination Using Simple Racemic Metal Complexes. *Org. Lett.* **2008**, *10*, 5167-5170.

28. Dezhahang, Z.; Merten, C.; Poopari, R.M.; Xu, Y. Vibrational Circular Dichroism Spectroscopy of Two Chiral Binaphthyl Diphosphine ligands and their Palladium Complexes in Solution. *Dalton Trans.* **2012**, *41*, 10817.

29. Nieto, S.; Dragna, J.M.; Anslyn, E.V. A Facile Circular Dichroism Protocol for Rapid Determination of Enantiomeric Excess and Concentration of Chiral Primary Amines. *Chem. Eur. J.* **2010**, *16*, 227-232.

30. Leung, D.; Anslyn, E.V. Rapid determination of enantiomeric excess of α-chiral cyclohexanones using circular dichroism spectroscopy. *Org. Lett.* **2011**, *13*, 2298-2301.

31. Perez-Fuertes, Y.; Kelly, A.M.; Arimori, S.; Bull, S.D.; James, T.D. Simple protocol for NMR analysis of the enantiomeric purity of diols. *Org. Lett.* **2006**, *8*, 1971-1974.

32. Perez-Fuertes, Y.; Kelly, A.M.; Fossey, J.S.; Powell, S.D.; Bull, S.D.; James, T.D. Simple protocols for NMR analysis of the enantiomeric purity of chiral primary amines. *Nat. Protoc.* **2008**, *3*, 210-214.

33. Metola, P.; Anslyn, E.V.; James, T.D.; Bull, S.D. Circular dichroism of multi-component assemblies for chiral amine recognition and rapid ee determination. *Chem. Sci.* **2012**, *3*, 156-161.

34. Berova, N.; Di Bari, L.; Pescitelli, G. Application of electronic circular dichroism in configurational and conformational analysis of organic compounds. *Chem. Soc. Rev.* **2007**, *36*, 914-931.

35. Zahn. S.; Canary, J.W. Absolute Configurations of Primary Amines from Exciton-Coupled Circular Dichroism Spectra of Cu(II) Complexes of their N,N-Bisquinaldyl Derivatives. *Org. Lett.* **1999**, *1*, 861-864.

36. Zhang, J.; Holmes, A.E.; Sharma, A.; Brooks, N.R.; Rarig, R.S.; Zubieta, J.; Canary, J.W. Derivatization, Complexation and Absolute Configurational Assignment of Chiral Primary Amines: Application of Exciton-Coupled Circular Dichroism. *Chirality*. **2003**, *15*, 180-189.

37. Huang, X.; Nakanishi, K.; Berova, N. Porphyrins and Metalloporphyrins: Versatile Circular Dichroic Reporter Groups for Structural Studies. *Chirality*, **2000**, *12*, 237-255

38. Balaz, M.; De Napoli, M.; Holmes, A.E.; Mammana, A.; Nakanishi, K.; Berova, N.; Purrello, R. A cationic zinc porphyrin as a chiroptical sensor for Z-DNA. *Angew. Chem. Int. Ed.* **2005**, *44*, 4006-4009.

39. Matile, S.; Berova, N.; Nakanishi, K.; Novakova, S.; Philipova, I. Blagoev, B. Porphyrins: Powerful Chromophores for Structural Studies by Exciton-Coupled Circular Dichroism. *J. Am. Chem. Soc.* **1995**, *117*, 7021-7022.

40. Furusho, Y.; Kimura, T.; Mizuno, Y.; Aida, T. Chirality-Memory Molecule: A D2-Symmetric Fully Substituted Porphyrin as a Conceptually New Chirality Sensor. *J. Am. Chem. Soc.* **1997**, *119*, 5267-5268.

41. Tanasova, M.; Yang, Q.; Olmsted, C.C.; Vasileiou, C.; Li, X.; Anyika, M.; Borhan, B. An Unusual Conformation of α-Haloamides Due to Cooperative Binding with Zincated Porphyrins. *Eur. J. Org. Chem.* **2009**, 4242-4253.

42. Borovkov, V.V.; Lintuluoto, J.M.; Inoue, Y. Supramolecular Chirogenesis in Zinc Porphyrins: Mechanism, Role of Guest Structure, and Application for the Absolute Configuration Determination. *J. Am. Chem. Soc.* **2001**, *123*, 2979-2989.

43. Li, X.; Borhan, B. Prompt determination of absolute configuration for epoxy alcohols via exciton chirality protocol. *J. Am. Chem. Soc.* **2008**, *130*, 16126-16127.

44. Li, X.; Burrell, C.E.; Staples, R.J.; Borhan, B. Absolute Configuration for 1,n-Glycols: A Nonempirical Approach to Long-Range Stereochemical Determination. *J. Am. Chem. Soc.* **2012**, *134*, 9026-9029.

45. Dragna, J.M.; Pescitelli, G.; Tran, L.; Lynch, V.M.; Anslyn, E.V. In situ assembly of octahedral Fe(II) complexes for the enantiomeric excess determination of chiral amines using circular dichroism spectroscopy. *J. Am. Chem. Soc.* **2012**, *134*, 4298-4407.

46. Barman, S.; Anslyn, E.V. Rapid determination of enantiomeric excess of α-chiral aldehydes using circular dichroism spectroscopy. *Tetrahedron*. **2014**, *70*, 1357-1362.

47. Joyce, L.A.; Maynor, M.S.; Dragna, J.M.; Cruz, G.M.; Lynch, V.M.; Canary, J.W.; Anslyn, E.V. A simple method for the determination of enantiomeric excess and identity of chiral carboxylic acids. *J. Am. Chem. Soc.* **2011**, *133*, 13764-13752.

48. Joyce, L.A.; Canary, J.W.; Anslyn, E.V. Enantio- and chemoselective differentiation of protected α-amino acids and β-homoamino acids with a single copper(II) host. *Chem. Eur. J.* **2012**, *18*, 8064-8069.

49. You, L.; Berman, J.S.; Anslyn, E.V. Dynamic multi-component covalent assembly for the reversible binding of secondary alcohols and chirality sensing. *Nature. Chem.* **2011**, *3*, 943–948.

50. You, L.; Pescitelli, G.; Anslyn, E.V.; Di Bari, L. An exciton-coupled circular dichroism protocol for the determination of identity, chirality, and enantiomeric excess of chiral secondary alcohols. *J. Am. Chem. Soc.* **2012**, *134*, 7117-7125.

51. You, L.; Berman, J.S.; Lcuksanawichien, A.; Anslyn, E.V. Correlating Sterics Parameters and Diastereomeric Ratio Values for a Multicomponent Assembly To Predict Exciton-Coupled Circular Dichroism Intensity and Thereby Enantiomeric Excess of Chiral Secondary Alcohols. *J. Am. Chem. Soc.* **2012**, *134*, 7126-7134.

52. Terrett, N.K.; Gardner, M.; Gordon, D.W.; Kobylecki, R. J.; Steele, J. Combinatorial synthesis-the design of compound libraries and their application to drug discovery. *Tetrahedron* **1995**, *51*, 8135.

53. Pescarmona, P. P.; Van der Waal, J. C.; Maxwell, I. E.; Maschmeyer, T. Combinatorial chemistry, high-speed screening and catalysis. *Catal. Lett.* **1999**, *63*, 1.

54. Guebitz, G.; Schmid, M. G. Chiral separation principles in chromatographic and electromigration techniques. *Mol. Biotechnol.* **2006**, *32*, 159.

55. Thompson, R. A practical guide to HPLC enantioseparations for pharmaceutical compounds. *J. Liq. Chromatogr. Relat. Technol.* **2005**, *28*, 1215

56. Zhang, Y.; Wu, D.-R.; Wang-Iverson, D. B.; Tymiak, A. A. Enantioselective chromatography in drug discovery. *Drug Discovery Today* **2005**, *10*, 571

57. Ahuja, S. A strategy for developing HPLC methods for chiral drugs. *LCGC North Am.* **2008**, 70.

58. Chen, L.; Zhao, Y.; Gao, F.; Garland, M. Determination of enantiomeric excess using the ultraviolet-circular dichroism and the high-performance liquid chromatography-circular dichroism methods. *Appl. Spectrosc.* **2003**, *57*, 797.

59. Traverse, J. F.; Snapper, M. L. High-throughput methods for the development of new catalytic asymmetric reactions. *Drug Discovery Today* **2002**, *7*, 1002.

60. Kuhr, W. G.; Monnig, C. A. Capillary electrophoresis. *Anal. Chem.* **1992**, *64*, 389.

Chapter 2: Application of High Throughput Enantiomeric Excess Optical Assay involving a Dynamic Covalent Assembly for Sensing of Homo-allylic Alcohols

2.1 INTRODUCTION

The asymmetric synthesis of enantiomerically enriched organic compounds is crucial in the pharmaceutical industry.[1,2] For example, the asymmetric reduction of a ketone to an alcohol was used by Lilly to create Cymbalta, which is a prescription medication used to treat a certain type of depression called Major Depressive Disorder (MDD). It is also known to treat or manage generalized anxiety disorder, diabetic peripheral neuropathic pain, fibromyalgia, and chronic musculoskeletal pain. Another example is an asymmetric enamine hydrogenation used by Merck to generate Januvia, which is a type of prescription diabetes medicine that helps you control your blood sugar levels.

Enantioselective metal catalysis ranks among the foremost methods used in the manufacture of chiral pharmaceutical ingredients.[3-6] Asymmetric hydrogenation encompasses the majority of enantioselective metal catalyzed processes employed on scale.[5,6] Indeed, the largest volume application of enantioselective metal catalysis is the asymmetric iridium catalyzed imine hydrogenation used to generate the agrochemical metolachlor, which delivers over 10,000 metric tons of chiral product annually.[7,8] Inspired by the importance of asymmetric hydrogenation to the manufacture of chiral pharmaceutical and agrochemical products, the Krische group has developed a broad, new family of catalytic enantioselective C-C bond forming hydrogenations and transfer hydrogenations.[9,10] Among these processes, the iridium catalyzed C-C coupling of primary alcohols and allyl acetate to furnish enantiomerically enriched homoallylic

alcohols figures prominently,[11-15] as it has been widely adopted in natural product synthesis.[16-24]

In any asymmetric reaction, the goal is to achieve as high enantiomeric excess (ee) as possible, which commonly involves testing numerous experimental conditions, reagents, and/or catalysts, to optimize the *ee*. This has led to the use of parallel synthesis and high-throughput screening (HTS) for reaction discovery.[25] Due to utilization of micro-well plates, mini-block reactors and automated liquid handlers, these methods enable a series of reactions to be performed, varying any number of experimental parameters and reagents in a short amount of time. Conventionally for *ee* determination, chiral HPLC and GC are used. However, they are not suitable for HTS of *ee* when hundreds to even thousands of reactions are to be analyzed. For this reason, optical assays for *ee* determination using colorimetric,[26-28] fluorescence,[29,30] or circular dichroism (CD) spectroscopy,[25,31-32] are being created for the interrogation of chiral organic compounds.

Our group has reported several CD methods using dynamic assemblies for various chiral functional groups: amines, alcohols, carboxylic acids, and aldehydes/ketones.[33-36] Each assay was validated with a limited number of commercially available chiral examples. The assays are not as accurate as conventional chromatographic techniques, having errors ranging between 3 and 7%. However, such errors are deemed sufficient for a pre-screening of asymmetric reactions to discover trends or uncover hits. These errors are acceptable primarily due to the ease of use of the assays and their speed. For example, in each assay the chiral analyte is simply mixed with the assembly components, the solutions are allowed to reach equilibrium, and a robot transfers the samples from a 96-well plate to a CD spectrometer for the determination of 96 *ee* values in under two hours.[37] Alternatively, when using a laser table with four photo-elastic modulators, such a plate can be read in less than five minutes.[38] While the Anslyn amine and alcohol assays

have been used by Zhang[39] and Miller[40], respectively, to measure a few dozen *ee* values each,[41] we have yet to truly put the assays to the test measuring hundreds of values.

In this chapter, we describe our first successful combination of parallel reactions with rapid CD analysis. We describe how the Krische methodology for generating homo-allylic alcohols can be combined with our HTS *ee* assay for chiral alcohols.[34] Furthermore, we also have developed a quantitative Thin Layer Chromatography (TLC) analysis in order to avoid analyzing reactions with low yields, regardless of their *ee* values. In total, approximately 400 reactions were analyzed, with nearly 200 *ee* values being determined. Once the assays were considered functional, the total analysis time for the combined TLC and *ee* screening could be accomplished in under a day. The *ee* screening alone was easily performed in under four hours. The study validates that the assays are functional in a real-life setting.

2.2 Results and Discussions

Asymmetric Ir-catalyzed C-C coupling of primary alcohols with allyl-acetates, as described by Krische, to form chiral secondary homo-allylic alcohols were performed in parallel as a means to optimize the *ee* values thereof. Specifically, approximately 400 examples of this reaction were performed by varying the catalyst, adding acids and bases, and starting reactants to form 4-phenyl-1-butene-4-ol (**2.3**). The *ee* values for the transformations were determined in a high-throughput fashion using a 4-component assembly that creates a circular dichroism signal indicative of the extent of asymmetric induction. Further, a parallel and rapid quantitative TLC method measures the yield of each reaction, revealing which reactions give reliable *ee* values in the CD-based assay. Overall, the nearly 200 reactions whose *ee* values were determined could be quantitated

in under two hours. Using a combination of the TLC method to measure yield with the CD-assay to measure *ee* values, several trends in reaction conditions were revealed.

2.2.1 Iridium Catalyzed Carbonyl Allylation Reactions in 96-Well Mini-block.

Previously, the iridium catalyzed enantioselective carbonyl allylation protocol, based upon allyl acetate-alcohol transfer hydrogenative coupling, was developed by the Krische group.[11] This disclosed catalytic system for transfer hydrogenative carbonyl allylation employed allyl acetate and alcohol in the presence of an iridium catalyst generated in situ from $[Ir(cod)Cl]_2$ and a chelating triarylphosphine ligand. Allyl acetate was chosen as the allyl donor due to the low cost and its tractability. They reported that under optimal conditions, which employ the commercially available iridium complex $[Ir(cod)Cl]_2$ (2.5 mol %) in combination with (R)-BINAP (5 mol %) as ligand in THF at 100 °C in a sealed tube, along with Cs_2CO_3 (20 mol %) and *m*-NO_2BzOH (10 mol %) as additives, primary alcohols studied converted to corresponding homoallylc alcohols in good yield with excellent levels of enantioselectivity (Figure 2.1).[11]

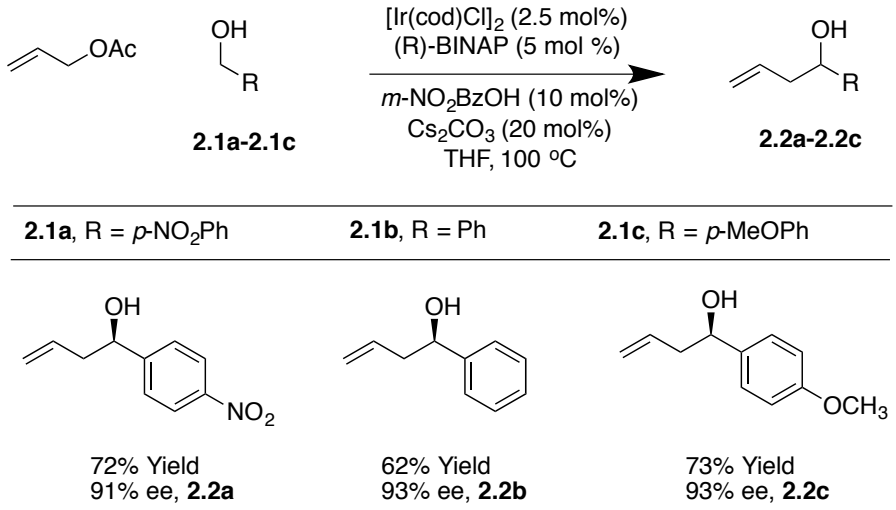

Figure 2.1: Carbonyl allylation from alcohol oxidation level via iridium-catalyzed coupling of allyl acetate to alcohols **2.1a- 2.1c**.

In their later work, they reported that employing chromatographically purified iridium catalysts, referred to as "preformed catalyst", allows alcohol-mediated carbonyl allylations and crotylations to be conducted at a significantly lower temperatures, resulting in enhanced levels of anti-diastereoselectivity and enantioselectivity. Using the preformed catalysts was advantageous in terms of yield and could be applied under milder conditions. Thus, in our studies we adopted the use of preformed catalysts (Equation 2.1).

Equation 2.1

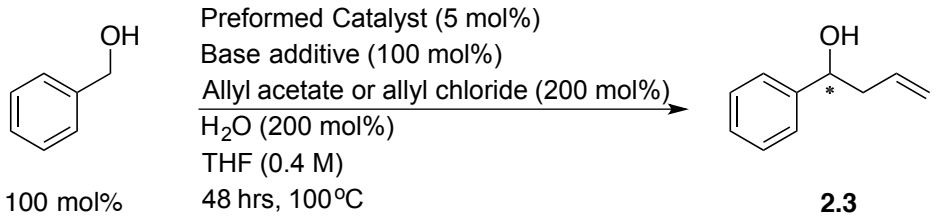

In the present study, 18 preformed catalysts were generated by varying the acid and the chiral phosphine ligands as shown in Equation 2.2 and Figure 2.2 (Table 2.1). Cesium carbonate as a base and allyl acetate were used for all preformed catalysts. Based upon previous results from the Krische group, the chiral phosphine SEGPHOS generally gives the highest *ee* values in the carbonyl allylation. But, due to the fact that BINAP is much less expensive, a major focus of this project was to screen reactions in an attempt to reveal conditions where BINAP would rival SEGPHOS. Previous studies also give the highest production yield of catalyst when a meta-substituted carboxylate was used. Thereby, we set out to explore *m*-nitrobenzoic acids with various electron-withdrawing and electron-donating groups on the para position.

Equation 2.2

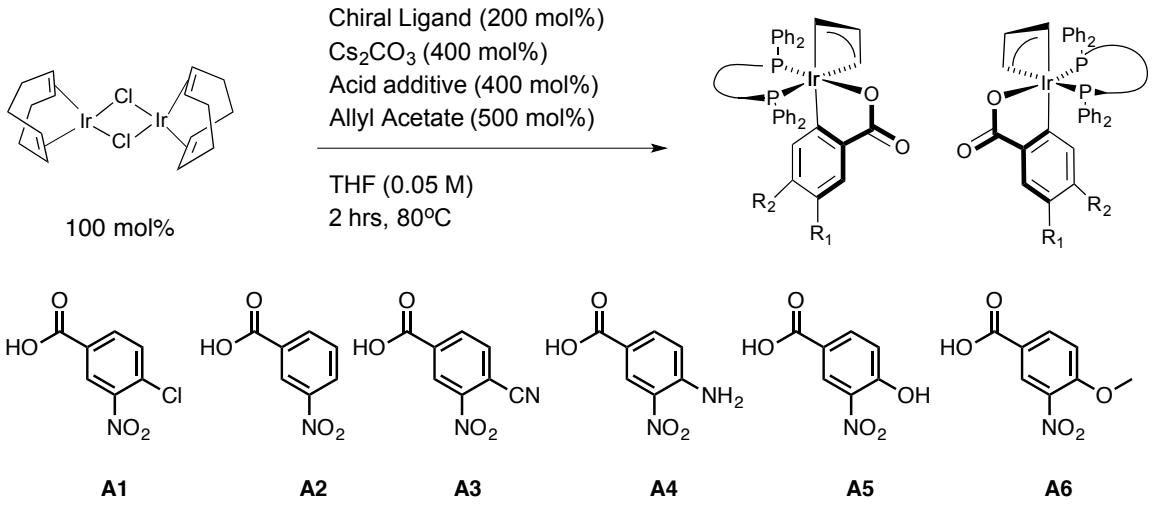

Figure 2.2: List of various carboxylic acids that were used to generate the preformed catalyst.

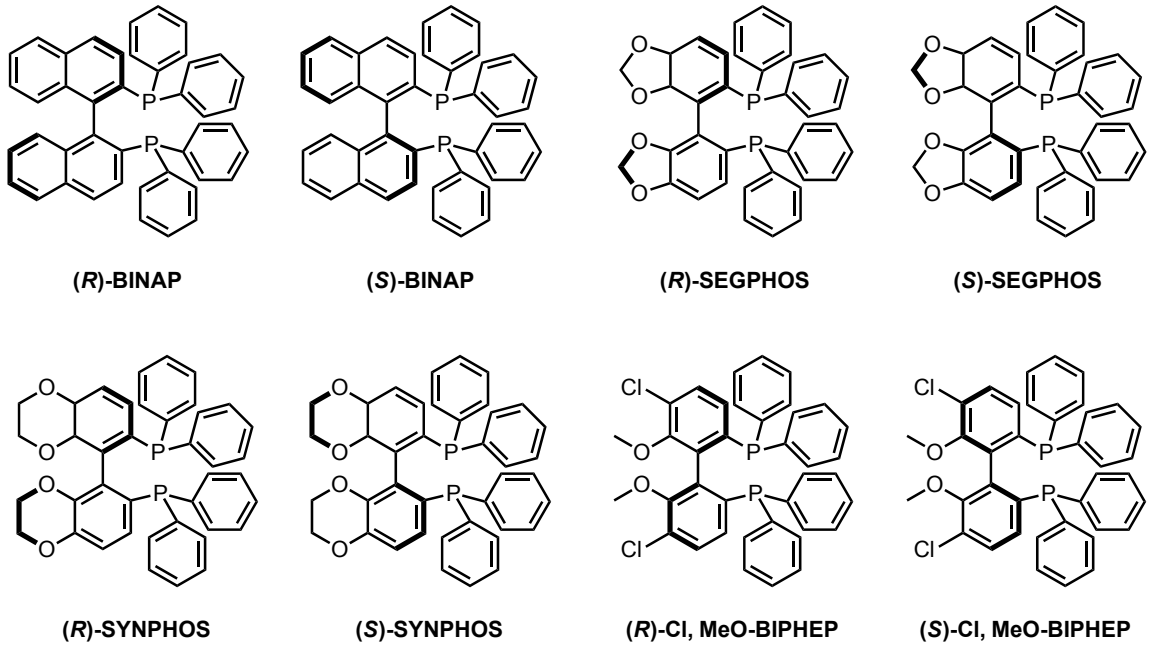

Figure 2.3: List of various triarylphosphine ligands that were used to generate the preformed catalyst.

Entry	Ligands	Acids	Preformed Catalysts
1	(*R*)-BINAP	A1	(*R*)-C1
2	(*R*)-BINAP	A3	(*R*)-C2
3	(*R*)-BINAP	A5	(*R*)-C3
4	(*R*)-SEGPHOS	A1	(*R*)-C4
5	(*R*)-SEGPHOS	A3	(*R*)-C5
6	(*R*)-SYNPHOS	A1	(*R*)-C6
7	(*R*)-SYNPHOS	A3	(*R*)-C7
8	(*R*)-Cl,MeO-BIPHEP	A1	(*R*)-C8
9	(*R*)-Cl,MeO-BIPHEP	A3	(*R*)-C9
10	(*S*)-BINAP	A1	(*S*)-C1
11	(*S*)-BINAP	A3	(*S*)-C2
12	(*S*)-BINAP	A5	(*S*)-C3
13	(*S*)-SEGPHOS	A1	(*S*)-C4
14	(*S*)-SEGPHOS	A3	(*S*)-C5
15	(*S*)-SYNPHOS	A1	(*S*)-C6
16	(*S*)-SYNPHOS	A3	(*S*)-C7
17	(*S*)-Cl,MeO-BIPHEP	A1	(*S*)-C8
18	(*S*)-Cl,MeO-BIPHEP	A3	(*S*)-C9

Table 2.1: Various conditions creating 18 combinations of catalysts, as shown in Equation 2.2.

Using the 18 catalysts described, as well as a series of other experimental conditions (described below), we performed nearly 400 carbonyl allylations that create 4-phenyl-1-butene-4-ol (Equation 2.1). For this parallel synthesis, a series of preformed

catalysts, bases and solvents were screened in 96-well reaction-blocks, sometimes loaded with only 48 reactions or at other times fully loaded, each well being a different reaction condition associated with its position on the plate. Often, when double-checking results, the plates were loaded with only 20 reactions. The reactions were stirred for two days, heated with two different procedures. In some cases the reaction-block was sealed, buried in a sand bath, and heated at 100 °C with a flea stir-bar in each well. Alternatively, the reaction-blocks could be placed directly on a heat plate with a temperature controller embedded in the reaction block. Both procedures gave consistent results. After two days the blocks were opened, and purification was performed using a parallel procedure involving various 96-well filter and collection plates. First, a small spatula of silica was added to each well (approximately 200 mgs), followed by simultaneous removal of the solvent from all wells using a Genevac (dry loading method). Second, each well of a 96-well filter plate was loaded with approximately 1 cm of silica. Each crude reaction mixture was loaded into this filter plate using the same positions as in the reaction plate. Approximately 2 mls of 2% EtOAc in hexanes, followed by about 2 mls of 5% EtOAc, was flushed through each well in the filter-plate and collected in deep-well plates. The first wash removes the excess benzyl alcohol, while the second wash elutes the product. The benzyl alcohol must be removed, because it can compete with the chiral secondary alcohol in the assay that reports the *ee* values (vida infra). The allyl moiety, either acetate or chloride, can co-elute with the product alcohol, since we found it has no influence on the *ee* determination. The solvent of the product-containing fractions from the second wash was removed again using a Genevac. By the end, homo-allylic alcohol **2.3** was the only compound that remained in the 96-well plate which responds in our *ee* assay.

2.2.2 Dynamic Covalent Muti-component Assembly for Enantiomeric Excess Sensing

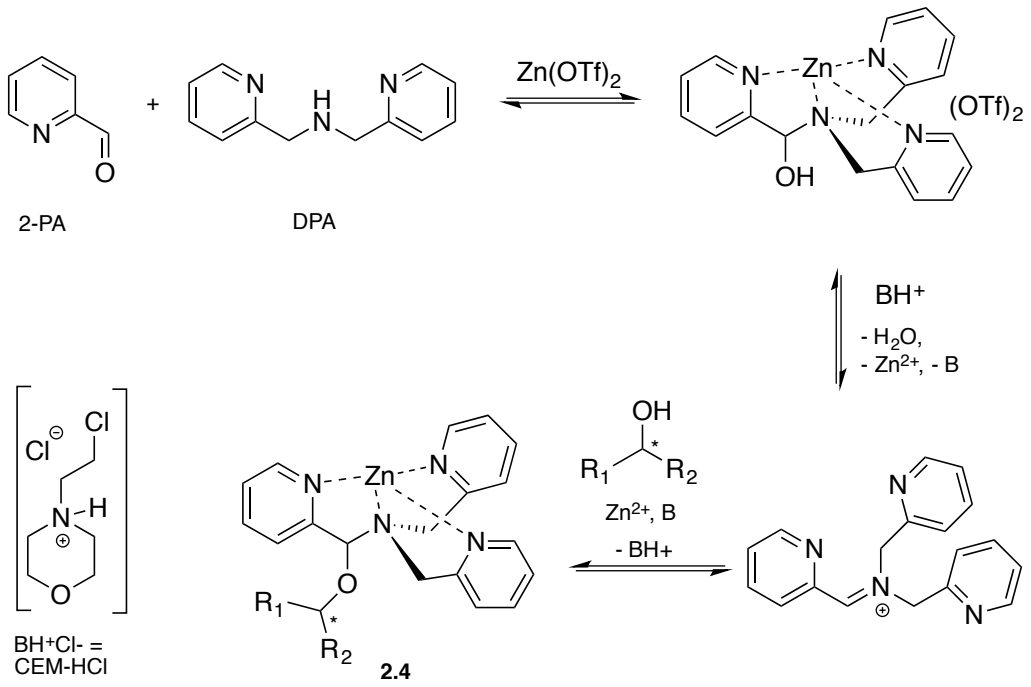

Figure 2.4. Four-component assembly that reports the *ee* values of chiral secondary alcohols via examination of the resulting CD spectra.

Our group previously reported an assay to measure the *ee* values of chiral secondary alcohols using a four-component assembly. The assembly arises from a combination of 2-picolinaldehyde (2-PA), di-(2-pyridylmethyl)amine (DPA), an alcohol and a zinc salt, creating a tris-pyridine inorganic coordination complex **2.4** (Figure 2.4.).[34,45] In the tris-pyridine complex, a hemi-aminal ether functional group exists, which induces a helical twist in the pyridine ligands, thereby inducing a large Cotton effect in the CD spectrum. Most chiral homo-allylic alcohols exhibit very weak or no signals in the CD spectrum. Thus, because our dynamic multi-component assembly creates large CD signals at wavelengths where the products do not absorb, we are in essence

amplifying the signal. Although this system has been successfully used to quantify the *ee* values of a variety of commercially available chiral secondary alcohols, the assay had yet to be used in a true high-throughput manner.

We first analyzed a series of homo-allylic alcohols to verify that our assay would function with such structures (Figure 2.5). The four-component assembly using each alcohol was studied by ^{1}H NMR and ESI-Mass spectroscopy. The presence of diastereomers of **2.4** formed from the homo-allylic alcohols was confirmed by ^{1}H NMR spectroscopy. Diastereomeric ratios (d.r.) were measured by integrating the hydrogen resonances of the chiral alcohols within the assembly (Figure 2.5). In the past, we have been able to create effective *ee* assays for alcohols with d.r. values as small as 1.2, and therefore every analyte examined would be useful in our assay.[46]

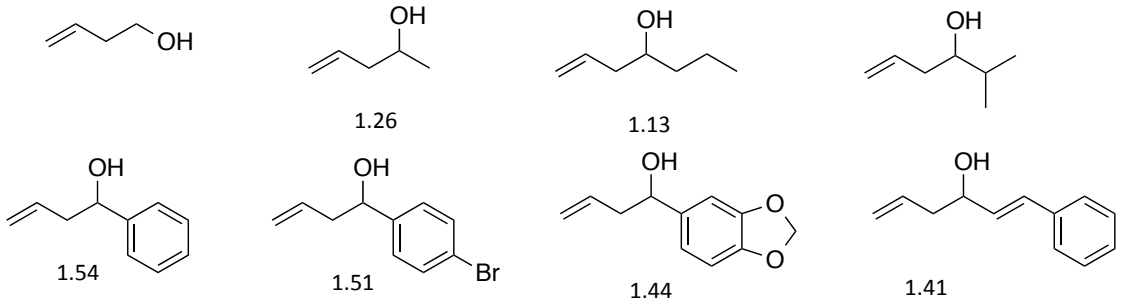

Figure 2.5: Various homoallylic alcohols studied and their d.r. values.

A titration was performed with **2.3** to find the minimum concentration required to reach signal saturation (Figure 2.6). Three equivalents were sufficient, thus removing concentration dependence at this or higher equivalents. Therefore, to create calibration curves that relate CD ellipticities to *ee*, 3 equivalents of **2.3** relative to the assembly was used. It is important to note that during the parallel reaction screening, if the yield of the alcohol was such that it had been lower than 3 equivalents, then the *ee* values

determined would be incorrect. Therefore, in many cases (as described below), we determined the reaction yield prior to measuring the *ee* values simply to verify that we could trust the *ee* values from our assay.

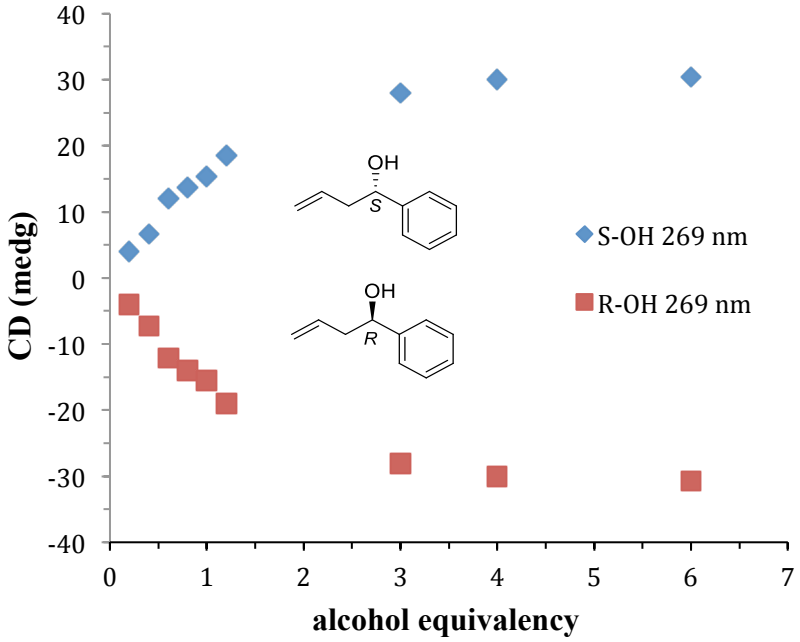

Figure 2.6: Titration of alcohol **2.3** into 2-PA, DPA, and Zn(II) triflate (all at 269 nm) in acetonitrile.

Prior to the anticipated parallel screening, a calibration curve for 4-phenyl-1-butene-4-ol (**2.3**) was generated using the CD spectra of the multi-component assembly reaction (Figure 2.7.). The calibration curve (Figure 2.8.) showed a correlation coefficient of 0.99.

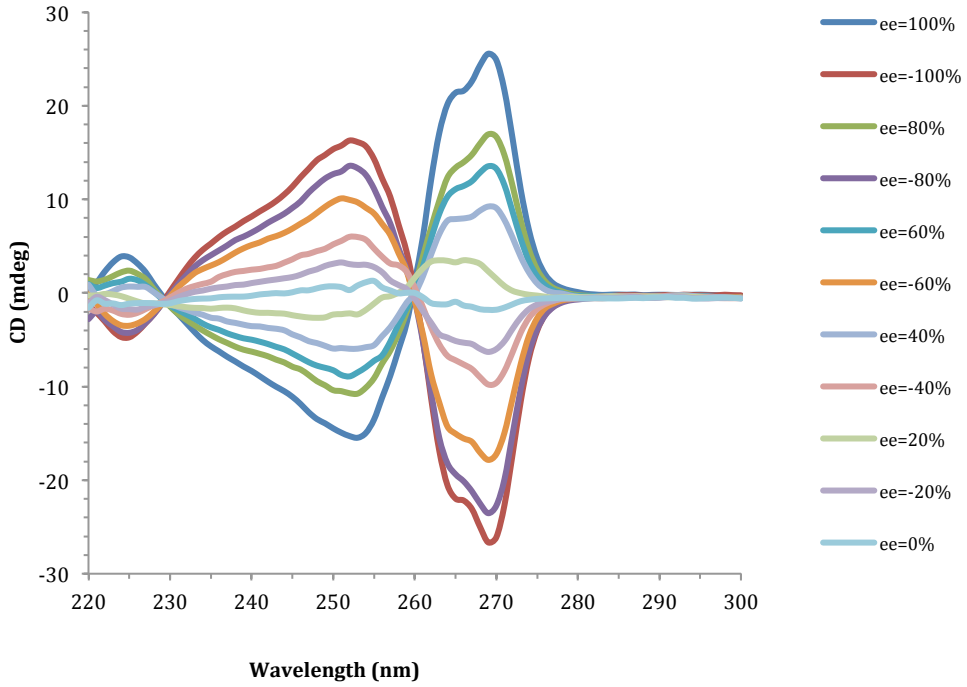

Figure 2.7: CD spectra of 4-phenyl-1-butene-4-ol derived assembly with different *ee* of alcohol (0.175 mM 2-PA, 0.525 mM alcohol).

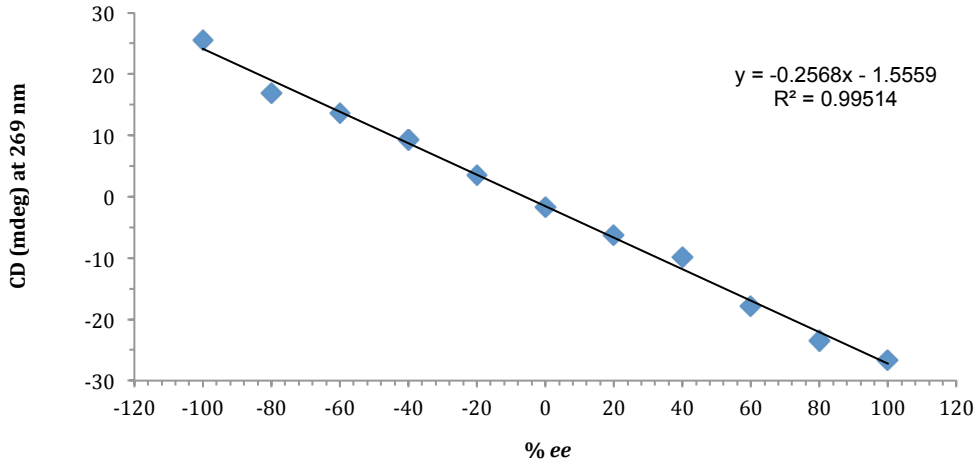

Figure 2.8: Linear *ee* calibration curve lines at 269 nm.

The approximately 400 samples of **2.3**, created using the parallel synthesis routine described above, were analyzed in numerous 96-well plates employing the multi-component assembly of 2PA, $Zn(OTf)_2$, DPA and CEM-HCl (Figure 2.4.). The analyses were performed in situ, in parallel, in acetonitrile, and in the presence of molecular sieves. The well plates were sealed with 96-well strip plates, and the mixtures were stirred at room temperature for ~ 18 hr, allowing the assembly equilibria to be achieved. A CD spectrum of each well was taken and the *ee* was determined using the calibration curve generated for **2.3**. Using a robot, the plate could be read in 2 hours, but using a newly developed CD laser system, each plate can be read in 5 minutes.[38]

2.2.3 Quantitative TLC Method in the Yield Determination to Pre-screen Allylation Reactions

As described above, a caveat for this parallel synthesis and the HTS *ee* assay is that a minimum of 3 equiv. of alcohol is needed to ensure saturation of the CD signal. If the reaction gives a low yield, then even if the reaction results in high enantioselectivity, the CD reported *ee* values will not be accurate. In order to circumvent this issue, we devised a rapid and parallel TLC method to roughly quantify the yield of each reaction.[47-50] The experiment was set up such that if 100% yield of **2.3** (Equation 2.1) were achieved, that would represent 6 equivalents to be used in the assembly whch measures *ee* values, hence far beyond the 3-4 equivalents needed to saturate the CD signal. Therefore, even around a 60 to 65 % yield would still give saturation of the CD signal and an accurate *ee* value. Hence, the assay created to measure yields needed to have a threshold of detection of 60% with a ±10% error. The yield can be calculated if we quantify the ratio between the starting precursor, benzyl alcohol and the product alcohol, 4-phenyl-1-butene-4-ol. If the yield was below 60%, further detection of the *ee* was not performed.

Benzyl alcohol and 4-phenyl-1-butene-4-ol are both luminant under a UV lamp when spotted on a silica gel plate. Microcaps were used to spot the reactions on the TLC plates. A box was constructed that held an iPhone with a hole for the camera, and a UV lamp was set to uniformly illuminate the TLC plate from one side of the box. The camera was placed the same distance from TLC plate as the lamp, because we found this was best at making the image not too bright or too dim.

To generate calibration curves in order to quantify the yield of the reactions, images of empty TLC plates were taken (Figure 2.9a). These are needed for subtracting the background when analyzing with computer software. Next, 11 samples that contain different ratios of starting and product alcohols, all at the same total concentration identical to that used in the parallel reactions, were spotted on the plates. The plates were allowed to dry and eluted in 20% ethyl acetate in hexane. The developed TLC plate was placed in the same location where the empty TLC plate was placed before, and the image was taken (Figure 2.9b).

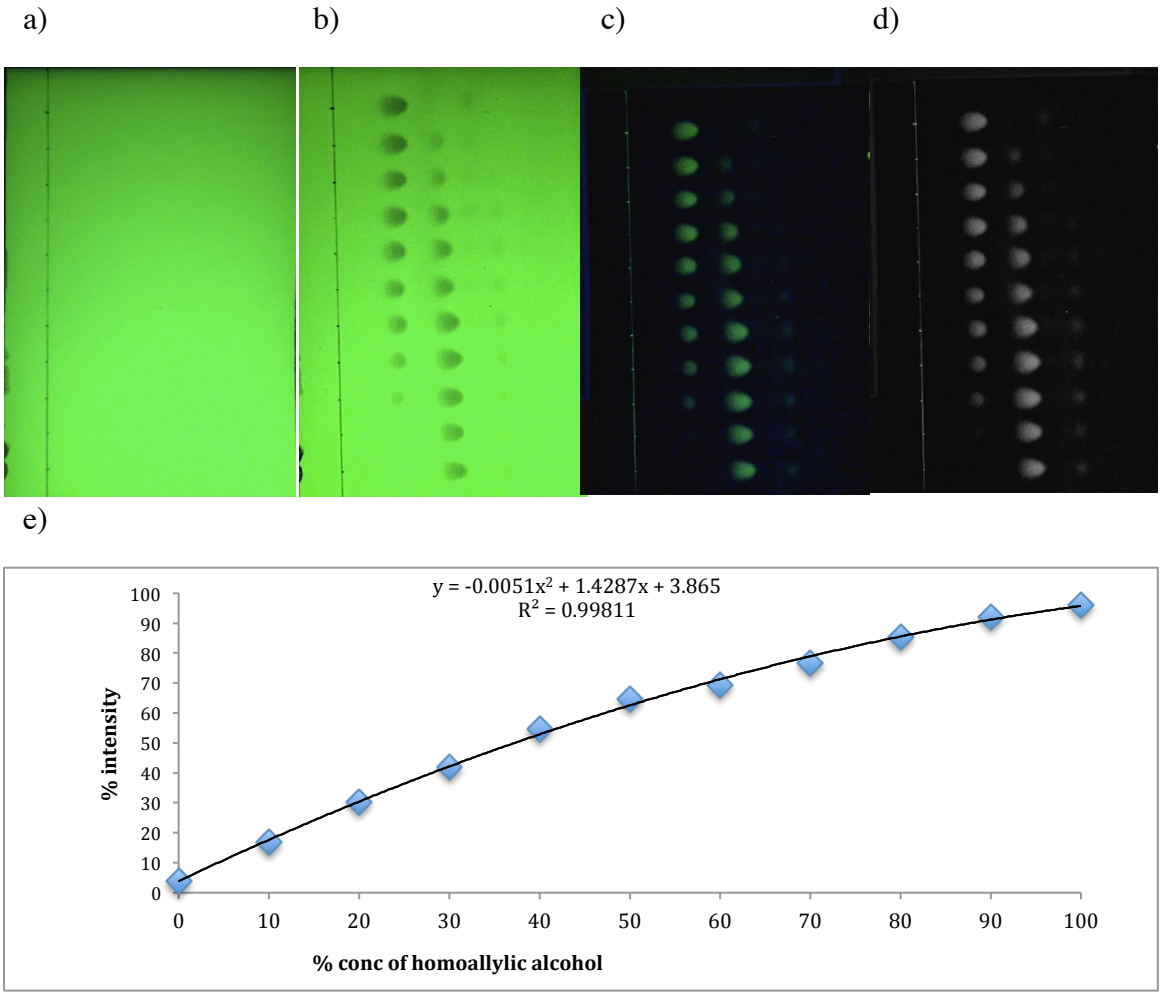

Figure 2.9: a) Raw image of blank TLC plate under UV lamp b) Raw image of TLC plate spotted with different ratios of starting and product alcohol under UV lamp c) Image of TLC plate when background is subtracted d) Background subtracted image of TLC plate in grey scale e) Calibration generated from % concentration of product alcohol to starting alcohol *vs* % product alcohol intensity counts for each development.

Entry	Base	Acid	% Yield	% Yield (calcd)
1	Cs_2CO_3	A1	85	80
2	Cs_2CO_3	BzOH	44	48
3	Na_2CO_3	A1	16	23
4	K_2CO_3	A1	24	27
5	Cy_2NMe	A1	-	-
6	Strychnine	A1	22	43
7	Brucine	A1	-	-

Table 2.2: Isolated yield and TLC method based yield varying base and acid additives to generate **2.3**.

The software Igor pro was used to analyze the images. By subtracting the background image, only benzyl alcohol and 4-phenyl-1-butene-4-ol spots appear (Figure 2.9c). After converting color to black and white (Figure 2.9d), the program counts the pixels of each spot and takes ratios of counted pixels, thereby generating a calibration curve (Figure 2.8, Table 2.2). The graph is slightly curved, due to the fact that at the low end the program picks up some signal for 1, even though there should be none (note that the graph does not start at zero on the y-axis). At the high end, the program detects some signal for benzyl alcohol although there is none (note that the values are less than 100% on the y-axis). Because the same issues will exist when analyzing hundreds of parallel reactions, we used a curve to fit the calibration data. This screening step, using simple TLC techniques, proved extremely useful. It was used either to eliminate some reactions before *ee* determination, or for checking the yields of reactions after *ee* determination when the CD signals were very low, implying either a low yield or poor enantioselectivity.

2.2.4 *Ee* Determination of Homo-allylic Alcohols

Combinations of 9 different pre-catalysts, their enantiomers, 4 different bases, 3 different solvents, and 2 different allyl moieties generated more than 400 reactions that were ran in parallel. Their yield and *ee* was checked rapidly using our CD method (see section 2.4). For randomly selected reactions, HPLC determined *ee* and CD determined *ee* was compared and gave average errors of ±7% for examples that give a yield of 1 above 60% (Table 2.3). For the pre-catalyst, using BINAP as a chiral ligand, along with *m*-NO_2-*p*-CN-BzOH, showed the highest *ee* of the product alcohol **2.3** (94%). Using SEGPHOS as a chiral ligand also gave comparable yield as well as an *ee* of 91%. The sample using BINAP with a 94% CD-determined *ee* value was checked via HPLC, revealing an *ee* of 98%. This is above the 94% *ee* found for catalysts incorporating SEGPHOS, determined using HPLC (Table 2.3, and section 2.4). Thus, our screening revealed conditions of which the less expensive ligand could rival SEGPHOS. Among the acids (A1- A6) that were used to generate preformed catalysts, having more electron-withdrawing groups para to the benzoic acid gave the best yield. Among inorganic bases, changing bases in the reaction resulted in differences in yield, but did not significantly change the *ee*. But there was a decrease in *ee* with the chiral base. Change in allyl moiety did not influence the yield or *ee* of **2.3**. A sample with a reasonably high yield that was confirmed by TLC, the *ee* determined by CD was in a small error range with the *ee* determined by HPLC.

It is important to note that when a low yield of alcohol was observed via the TLC assay, the CD determined and HPLC *ee* values showed quite a discrepancy (Table 2.3). Thus, one limitation of our rapid CD-based assays is that highly asymmetric transformations that are low yielding will be missed due to the fact that they would be inaccurately reported. Yet, we feel that the advances reported here using a simple and

quantitative TLC-approach will help to rule out miss-interpretations because the low-yielding reactions can be identified before CD-analysis.

Table 2.3: HPLC and CD determined *ee* and isolated and TLC method determined yield of **2.3** under various combinations of preformed catalysts, acids, bases and solvents.

Pre-catalyst	Allyl Moiety	Base	Solvent	CD *ee*	HPLC *ee*	TLC yield (%)	Isolated yield (%)
(R)-C1	1a	Cs_2CO_3	THF	90	92	80	85
			MeCN	8	54	25	18
			Dioxane	88	90	68	52
		K_2CO_3	THF	45	77	48	58
			MeCN	11	47	15	12
			Dioxane	65	68	32	25
		K_3PO_4	THF	85	90	80	80
			MeCN	12	48	25	23
			Dioxane	88	89	83	78
		strycine	THF	18	51	22	43
			MeCN	7	42	16	12
			Dioxane	12	38	33	48
(R)-C2	1a	Cs_2CO_3	THF	94	98	85	84
	1b	Cs_2CO_3	THF	90	94	85	-
	1a	K_3PO_4	THF	90	84	80	-
(R)-C4	1a	Cs_2CO_3	THF	88	93	75	80
	1b	Cs_2CO_3	THF	87	93	78	76
(R)-C5	1a	Cs_2CO_3	THF	89	94	80	78
	1b	Cs_2CO_3	THF	90	94	75	80
	1a	K_3PO_4	THF	91	96	70	-
(R)-C6	1a	Cs_2CO_3	THF	86	84	82	77

Table 2.3 (continued)

	1b	Cs_2CO_3	THF	85	84	77	-
(R)-C8	1a	Cs_2CO_3	THF	84	86	80	75
(R)-C8	1b	Cs_2CO_3	THF	84	85	75	-

2.3 CONCLUSIONS

We successfully demonstrated parallel enantioselective carbonyl allylation reactions using multi-well mini-blocks, followed by *ee* determination using a dynamic multi-component CD assay. By performing the synthesis of the analytes as well as sensing assemblies in multi-well plates, we have achieved true HTS. The overall result shows that when the reaction gives a reasonable yield (>60%), the CD based *ee* assay gives acceptable errors. However, when the yield of **2.3** is low, because saturation is not reached in the multi-component assembly, the *ee* values are inaccurate. Our screen revealed conditions for the specific analyte **2.3** that allowed the less expensive BINAP ligand to rival SEGPHOS, a ligand that is found to generally give high *ee* for other similar carbonyl allylations.[42,43] Similarly, each of our group's HTS assays should allow chemists to analyze hundreds of reactions that create the same chiral structure using the same calibration curve for CD versus *ee* values.

2.4 EXPERIMENTAL DETAILS

2.4.1. Materials and Methods

NMR spectra were recorded on Agilent MR 400 at The University of Texas at Austin NMR facility. ESI-mass spectra were obtained on Agilent 6100 at The University of Texas at Austin mass spectrometry facility. Circular dichroism (CD) spectra were recorded on a Jasco J-815 spectropolarimeter at The University of Texas facility. High

performance liquid chromatography (HPLC) analysis was performed with OD-H column from Chiralcel.

2.4.2. Synthesis of Pre-catalysts

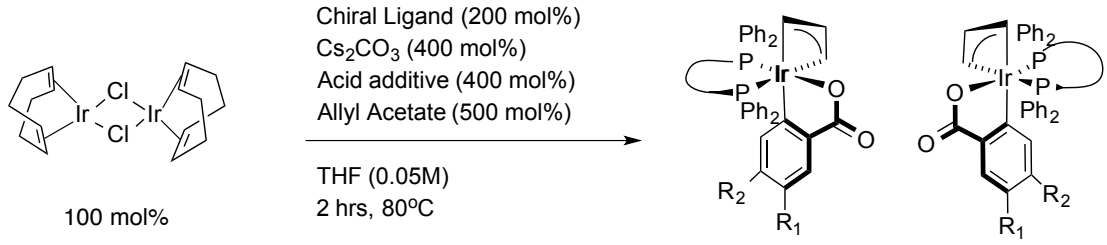

Figure 2.10: Synthesis of pre-catalysts with various phospho ligands.

A pressure tube equipped with a magnetic stirbar was charged with $[Ir(cod)Cl]_2$ (161.9 mg, 0.24 mmol, 100 mol%), phospho ligand (0.48 mmol, 200mol%), Cs2CO3 (312.9 mg, 0.96 mmol, 400 mol%) and 4-Cl-3-NO_2BzOH (192.5 mg, 0.96 mmol, 400 mol%). The tube was purged with argon and an outlet for 5 minutes, followed by the addition of allyl acetate (142μL, 1.2 mmol, 500 mol%) in THF (5.2 mL, 0.05 M). The mixture was stirred for 30 min at room temperature under argon. The reaction mixture was then stirred for 90 min at 80 °C. Upon cooling to ambient temperature, the reaction mixture was diluted and rinsed with CH_2Cl_2 and concentrated in vacuo at ambient temperature. The compound was purified by flash chromatography (SiO_2, 20% Et_2OAc/CH_2Cl_2) and concentrated in vacuo at ambient temperature. The light brown gum was dissolved in a small amount of THF and precipitated upon rapid addition of HPLC grade hexanes. Gravity filtration, followed by removal of trace solvents with flushing N_2 gives a yellow powder.

Pre-catalyst	Phospho ligand	Acid	Yield (%)
(R)-C1	(R)-BINAP	4-Cl-3-NO_2BzOH	80
(R)-C2	(R)-BINAP	4-CN-3-NO_2BzOH	78
(R)-C3	(R)-BINAP	4-OH-3-NO_2BzOH	66
(R)-C4	(R)-SEGPHOS	4-Cl-3-NO_2BzOH	76
(R)-C5	(R)-SEGPHOS	4-CN-3-NO_2BzOH	83
(R)-C6	(R)-SYNPHOS	4-Cl-3-NO_2BzOH	76
(R)-C7	(R)-SYNPHOS	4-CN-3-NO_2BzOH	79
(R)-C8	(R)-Cl, MeO-BIPHEP	4-Cl-3-NO_2BzOH	79
(R)-C9	(R)-Cl, MeO-BIPHEP	4-CN-3-NO_2BzOH	81
(S)-C1	(S)-BINAP	4-Cl-3-NO_2BzOH	81
(S)-C2	(S)-BINAP	4-CN-3-NO_2BzOH	80
(S)-C3	(S)-BINAP	4-OH-3-NO_2BzOH	65
(S)-C4	(S)-SEGPHOS	4-Cl-3-NO_2BzOH	76
(S)-C5	(S)-SEGPHOS	4-CN-3-NO_2BzOH	80
(S)-C6	(S)-SYNPHOS	4-Cl-3-NO_2BzOH	78
(S)-C7	(S)-SYNPHOS	4-CN-3-NO_2BzOH	78
(S)-C8	(S)-Cl, MeO-BIPHEP	4-Cl-3-NO_2BzOH	80
(S)-C9	(S)-Cl, MeO-BIPHEP	4-CN-3-NO_2BzOH	82

Table 2.4: List of pre-catalysts generated and the isolated yield

2.4.3. General Procedures for Synthesis of 1-Phenylbut-3-en-1-ol (2.3)

To a vial in the mini-block, pre-catalyst (8.75 µmol, 5 mol%) and stock solutions of benzyl alcohol (17.5 µmol, 100 mol%), base (10.5 µmol, 6 mol%) in THF (0.4 M) and H_2O (0.35 mmol, 200 mol%) were placed. The stock solution of allyl acetate (0.35 mmol, 200 mol%) in THF was added to the mixture and was left to stir at 100 ºC for 48 hours, at which point the reaction mixture was evaporated onto silica gel using Genevac.

Purification of the product by mini-plug silica column chromatography on 96-well filter plate (SiO_2: ethyl acetate:hexanes, 1:50 to 1:20) provided **2.3** as a colorless oil. Spectroscopic properties matched those in the literature **2.3**.

HPLC: (Chiralcel OD-H column, hexanes:i-PrOH = 95:5, 0.5 mL/min, 254 nm), (*R*)-1-Phenylbut-3-en-1-ol: 17.2 min, (*S*)-1-Phenylbut-3-en-1-ol: 15.2 min.

Instrumentation

Initially, we have attempted to create a 96-well plate sandwiched between two metal blocks by sealing the plate with screws. Typically, multi-well microplates are employed in biolab, such as with PCR experiments, polystyrene plates are widely used. However, in our study, we employed organic solvent (THF) by heating it to reflux at 100 ºC. Thereby, polypropylene multi-well plates were utilized, which has a high temperature tolerance and resistance to most organic solvents. The main technical problem that we encountered stems from the sealing of the well plate in order to ensure that the solvent will not evaporate or counter contaminate to neighboring wells. Sealing tapes, films, mats and strips for well plates, as well as molded rubber mats, were used to prevent the solvent from escaping. However, the metal plates, which were utilized to ensure proper sealing as well as to conduct heat, did not hold securely to the well plate to further perform the reactions.

Next, we sought after a commercially available parallel synthesis plate purchased from Analytical Sales and Services, Inc. The parallel synthesis/optimization plates were composed of four different components. The optimization 96-well block holds 96 glass vials that can contain 250µL. Replacement films and replacement mats cover the vials, and finally, the metal block is subsequently sealed at the vials' top with numerous screws. The silicone rubber mats provide compression sealing. These assembled 96-well reaction

plates are validated to have less than 5% solvent loss with prolonged heating above boiling point, which proves suitable for our study.

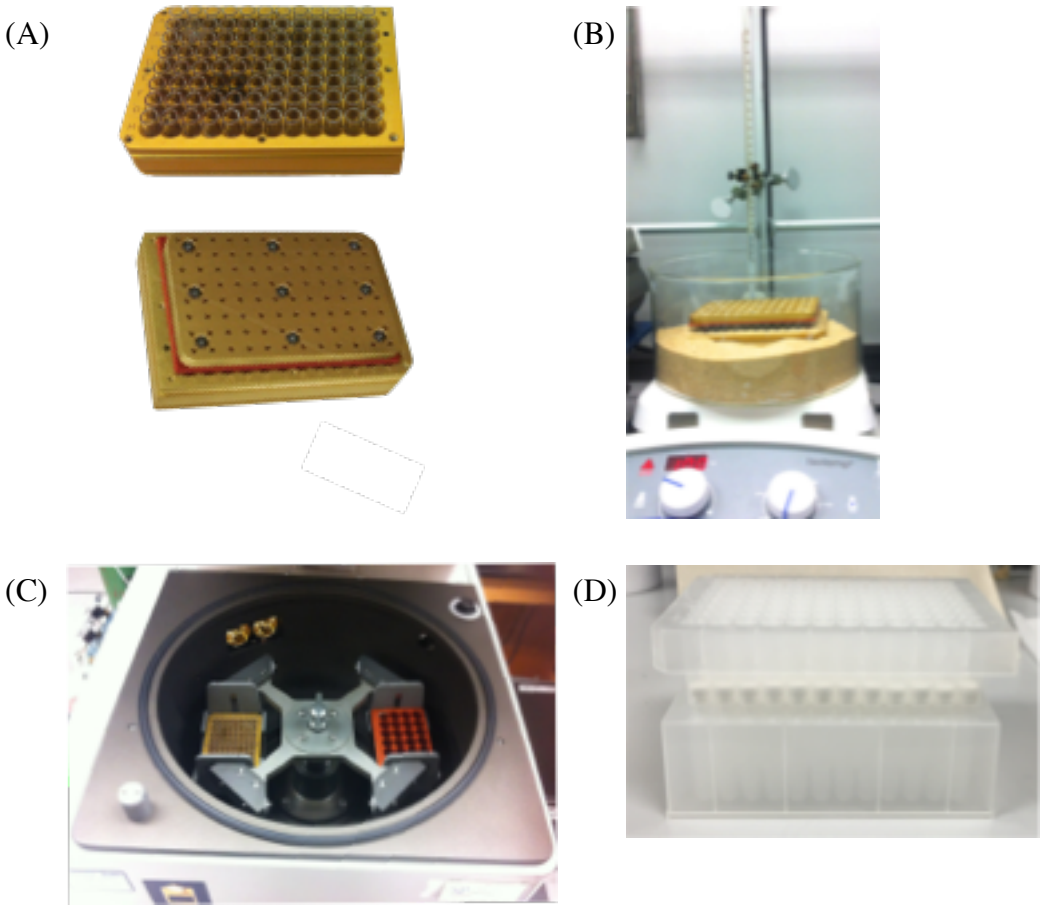

Figure 2.11: Instrumentation for parallel synthesis and purification of alcohol **2.3**. (A) 96-parallel mini-block. (B) Reaction at 100 °C for 48 hrs in either a sand bath or directly up on the hot plate. (C) Removal of the solvent by centrifugal evaporator (Genevac). (D) Short chromatography column using silica loaded 96-well filter plate.

2.4.4. Diastereomeric Ratio Determination of Alcohols using Multi-component Assembly

Synthesis of Chiral Homo-allylic Alcohols

(*R*)- 4-phenyl-1-buten-4-ol

In an oven-dried microwave tube, benzalcohol (108.1 mg, 1.0 mmol, 100 mol%), (*R*)-I (53 mg, 0.05 mmol, 5 mol%), Cs_2CO_3(195.5 mg, 0.60 mmol, 60 mol%), 4-chloro-3-nitrobenzoic acid (20.2 mg, 0.1 mmol, 10 mol%), and THF (2.5 mL, 0.4 M) were mixed and stirred. Freshly ditilled allyl acetate (200.2 mg, 2.0 mmol, 200 mol%), via Hickman distillation apparatus, was added to the mixture and followed by the addition of H_2O (36 µL, 2.0 mmol, 200 mol%). The mixture was allowed to stir at room temperature for 30 minutes. The reaction vessel was placed in a microwave reactor, and the temperature was set at 90 C under Power Max mode at medium stir for 6 hrs. The reaction mixture was diluted in CH_2Cl_2 and in order to do a dry packing, small amounts of SiO_2 were added to the diluted solution and concentrated in vacuo. Purification was performed by column chromatography (SiO_2). First, the mixture was flashed with hexanes, followed by 1:20 ethyl acetate: hexanes. After the removal of starting aldehyde precursors (UV-active), 1:10 ethyl acetate: hexanes collected product containing fractions. The solvent was removed in vacuo, and colorless oil of (*R*)- 4-phenyl-1-buten-4-ol in 76 % yield (96 % e.e.). After collecting the alcohol product, the column was flashed with 1:1 ethyl acetate: hexanes to remove any other organic impurities, followed by changing the eluent system to 20% CH_2Cl_2 in THF. The yellow band was collected and concentrated in vacuo. (*R*)-C1 (42 mg, 0.040 mmol) was recovered as a yellowish brown gum in 77% yield.

^{1}H NMR (400 MHz, CD_3Cl): δ7.29 (m, 5H), 5.8 (m, 1H), 5.1 (m, 2H), 4.6 (dd, J = 7.6, 5.4 Hz, 1H), 2.4 (m, 2H), 1.9 (s, 1H)

HPLC (Chiralcel OD-H column, hexanes: *i*-PrOH = 95:5, 0.5 mL/min, 254 nm): t_{major} = 12.8 min, t_{minor} = 16.2 min, *ee* = 96%

(*S*)- 4-phenyl-1-buten-4-ol

The procedure is the same as the preparation for (*R*)- 4-phenyl-1-buten-4-ol. The only change in the procedure is using (*S*)-C1 (53 mg, 0.05 mmol, 5 mol%), in place of (*R*)-C1. The yield was 75 %. (*S*)-C1 was recovered in 77 % yield.

^{1}H NMR (400 MHz, CD_3Cl): δ7.29 (m, 5H), 5.8 (m, 1H), 5.1 (m, 2H), 4.6 (dd, J = 7.6, 5.4 Hz, 1H), 2.4 (m, 2H), 1.9 (s, 1H)

HPLC (Chiralcel OD-H column, hexanes: *i*-PrOH = 95:5, 0.5 mL/min, 254 nm): t_{major} = 17.2 min, t_{minor} = 13.8 min, *ee* = 94%

(*R*)-4-(4-Bromophenyl)-1-buten-4-ol

The procedure is the same as the preparation for (*R*)- 4-phenyl-1-buten-4-ol. The only change in the procedure is using 4-bromo-benzalcohol instead of using benzalcohol.

^{1}H NMR (400 MHz, CD3Cl): δ7.49 (d, J = 8.4 Hz, 2H), 7.25 (d, J = 8.4 Hz, 2H), 5.8 (m, 1H), 5.1 (m, 2H), 4.7 (dd, J = 7.6, 5.4 Hz, 1H), 2.4 (m, 2H), 2.1 (s, 1H)

HPLC (Chiralcel OD-H column, hexanes: *i*-PrOH = 95:5, 0.5 mL/min, 254 nm): t_{major} = 20.4 min, t_{minor} = 23.1 min, *ee* = 96%

(*S*)-4-(4-Bromophenyl)-1-buten-4-ol

The procedure is the same as the preparation for (*R*)-4-(4-Bromophenyl)-1-buten-4-ol. The only change in the procedure is using (*S*)-C1 (53 mg, 0.05 mmol, 5 mol%), in place of (*R*)-C1.

^{1}H NMR (400 MHz, CD3Cl): δ7.49 (d, J = 8.4 Hz, 2H), 7.25 (d, J = 8.4 Hz, 2H), 5.8 (m, 1H), 5.1 (m, 2H), 4.7 (dd, J = 7.6, 5.4 Hz, 1H), 2.4 (m, 2H), 2.1 (s, 1H)

HPLC (Chiralcel OD-H column, hexanes: *i*-PrOH = 95:5, 0.5 mL/min, 254 nm): t_{major} = 22.9 min, t_{minor} = 20.4 min, *ee* = 93%

(*R*)-1-(benzo[d][1,3]dioxol-5-yl)but-3-en-1-ol

The procedure is the same as the preparation for (*R*)- 4-phenyl-1-buten-4-ol. The only change in the procedure is the starting aldehyde. Piperonly alcohol was used in this reaction.

^{1}H NMR (400 MHz, CD3Cl): δ6.93 (s, 1H), 6.8 (m, 2H), 5.92 (s, 2H), 5.8 (m, 1H), 5.14 (m, 2H), 4.65 (d, J = 6.8 Hz, 1H), 2.46 (t, J = 6.5 Hz, 2H), 2.1 (s, 1H)

HPLC (Chiralcel OD-H column, hexanes: *i*-PrOH = 95:5, 0.5 mL/min, 254 nm): t_{major} = 15.4 min, t_{minor} = 19.2 min, *ee* = 93%

(*S*)-1-(benzo[d][1,3]dioxol-5-yl)but-3-en-1-ol

The procedure is the same as the preparation for (*R*)-1-(benzo[d][1,3]dioxol-5-yl)but-3-en-1-ol. The only change in the procedure is using (*S*)-C1 (53 mg, 0.05 mmol, 5 mol%), in place of (*R*)-C1.

^{1}H NMR (400 MHz, CD3Cl): δ6.93 (s, 1H), 6.8 (m, 2H), 5.92 (s, 2H), 5.8 (m, 1H), 5.14 (m, 2H), 4.65 (d, J = 6.8 Hz, 1H), 2.46 (t, J = 6.5 Hz, 2H), 2.1 (s, 1H)

HPLC (Chiralcel OD-H column, hexanes: *i*-PrOH = 95:5, 0.5 mL/min, 254 nm): t_{major} = 19.3 min, t_{minor} = 15.4 min, *ee* = 92%

Diastereomeric Ratio for Various Alcohols using NMR Method

The binding of enantiomerically pure alcohols was also investigated, and the presence of diastereomers was determined by ^{1}H NMR spectra. The faces of the iminium ion intermediate are enantiotopic in the assembly reactions. Therefore, the complex formed by adding chiral alcohols will have two stereocenters. The consequence here is the formation of two sets of enantiomers. In ^{1}H NMR spectra, we cannot differentiate enantiomers; however, we confirmed the creation of diastereomers. Diastereomeric ratios (d.r.) were measured by integrating hydrogen peak areas of chiral alcohols within

the assembly. The d.r. values are consistent with the relative sizes of two groups on the stereocenters of alcohols.

All assembly reactions were performed in situ in acetonitrile without isolation and purification. To a stirred solution of pyridine-2-carboxyaldehyde (35 mM, 1 equiv.), zinc triflate (1 equiv.) in acetonitrile, 3 Å molecular sieves (4-8 mesh), di-(2-picolyl)amine (1.2 equiv.), and a target alcohol (5 equiv.) and 4-(2-chloroethyl)morpholine hydrochloride (1 equiv.) were added in the order. The mixture was stirred at room temperature overnight. The assembly solution was characterized by ^{1}H NMR and ESI-MS. For alcohols that possess stereocenters, diastereomers were generated, and the diastereomeric ratios (d.r.) were calculated using integrals in the ^{1}H NMR spectra.

Name of alcohols	**% yield**	**d.r.**
3-buten-1-ol	95.1	-
3-buten-2-ol	88.34	1.21
1-penten-3-ol	88	1.25
2-butyn-1-ol	86.12	-
3-butyn-2-ol	76.7	1.71
4-penten-2-ol	80	1.26
1-hepten-4-ol	77.8	1.13
2-methyl-5-hexen-3-ol	81.1	-
4-phenyl-1-buten-4-ol	88.8	1.54
4-(4-Bromophenyl)-1-buten-4-ol	81.3	1.51
1-(benzo[d][1,3]dioxol-5-yl)but-3-en-1-ol	82.8	1.44
(E)-1-phenylhexa-1,5-dien-3-ol	71.5	1.41

Table 2.5: Percent yield and d.r. of various alcohols in the assembly reactions calculated by integrals in ^{1}H NMR spectra.

2.4.5 Spectrometry and Spectroscopy

^{1}H NMR of 4-penten-2-ol in Multi-component Assembly

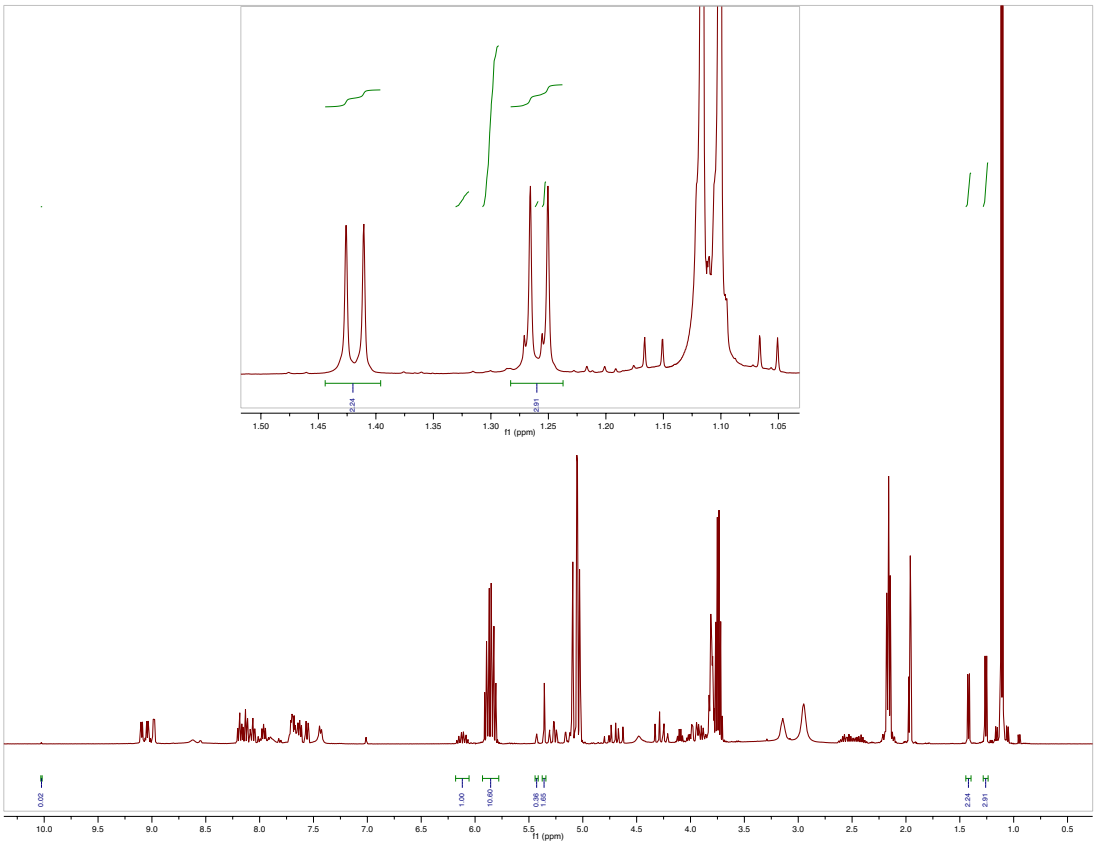

Diastereomeric ratio: 1.26, % alcohol incorporation: 80%

^{1}H NMR of 1-phenylethanol in Multi-component Assembly

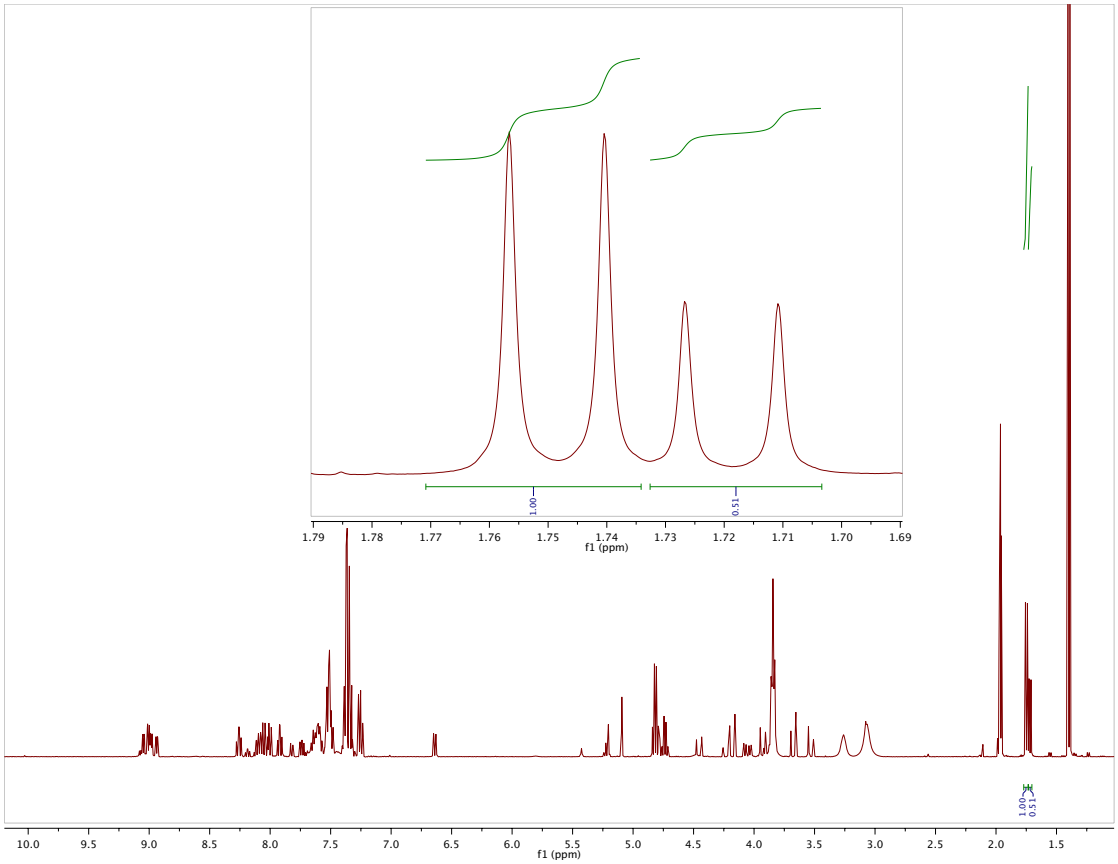

Diastereomeric ratio: 1.96, % alcohol incorporation: 86%

^{1}H NMR of 4-(4-Bromophenyl)-1-buten-4-ol in Multi-component Assembly

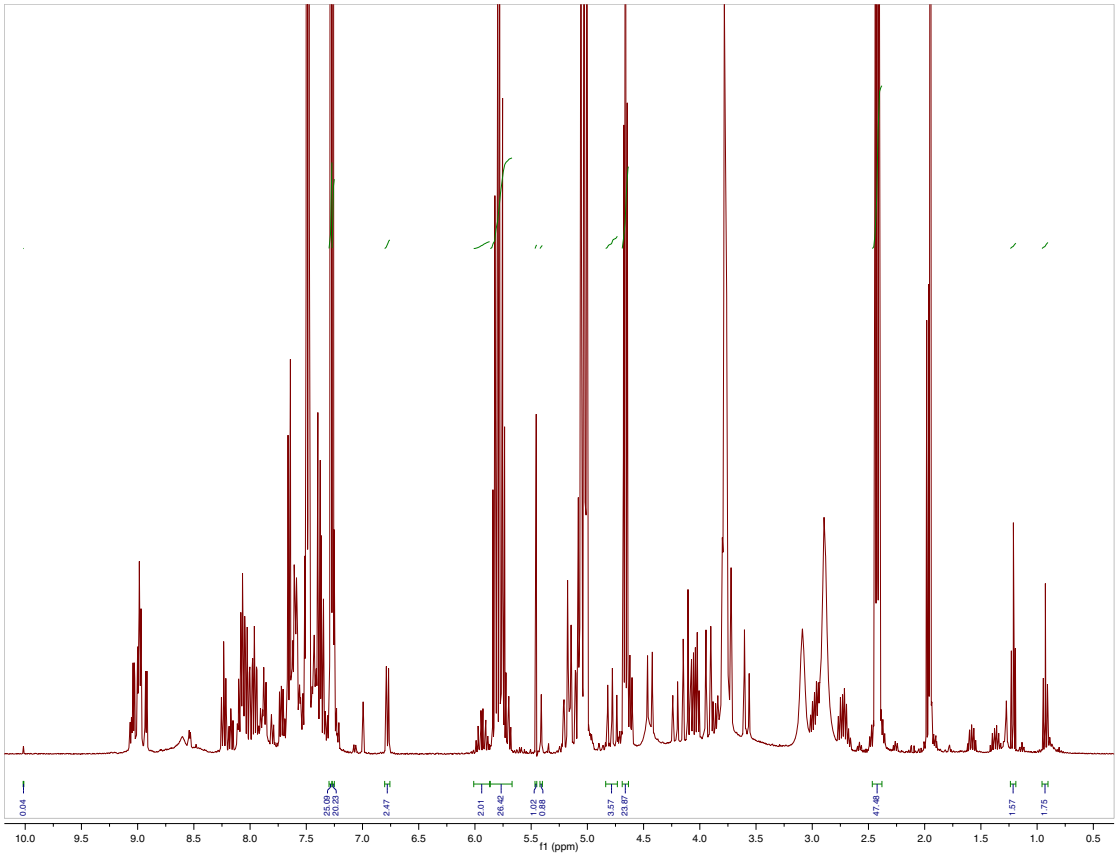

Diastereomeric ratio: 1.51, % alcohol incorporation: 81%

^{1}H NMR of 4-phenyl-1-buten-4-ol in Multi-component Assembly

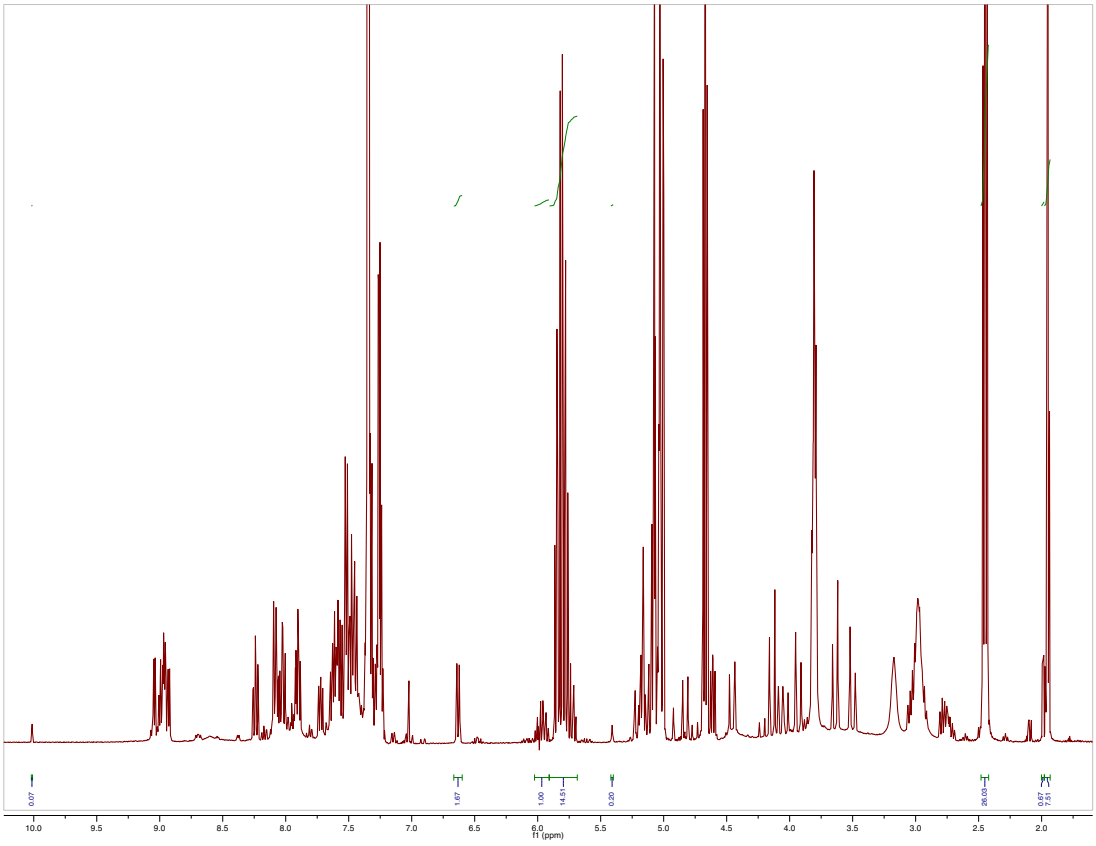

Diastereomeric ratio: 1.54, % alcohol incorporation: 88%

^{1}H NMR of 1-Hepten-4-ol in Multi-component Assembly

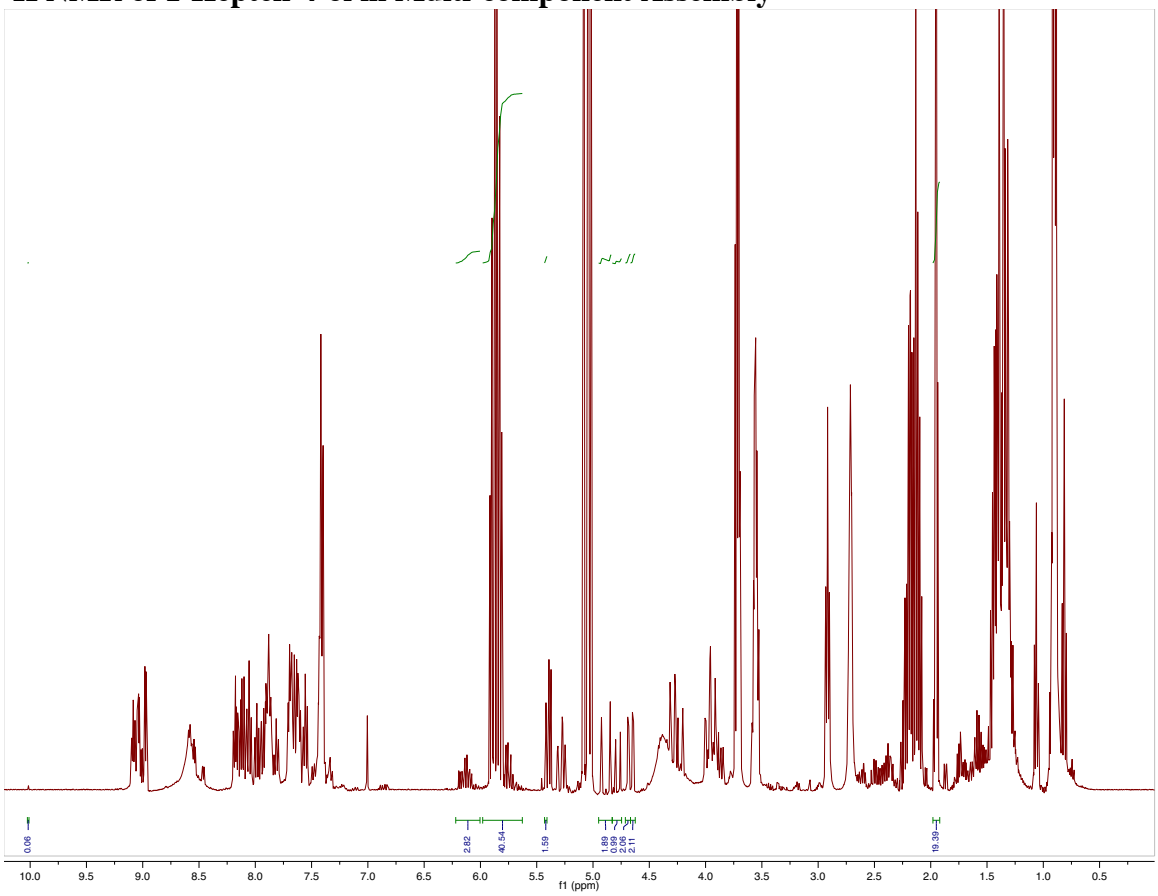

Diastereomeric ratio: 1.13, % alcohol incorporation: 78%

^{1}H NMR of 2-Methyl-5-hexen-3-ol in Multi-component Assembly

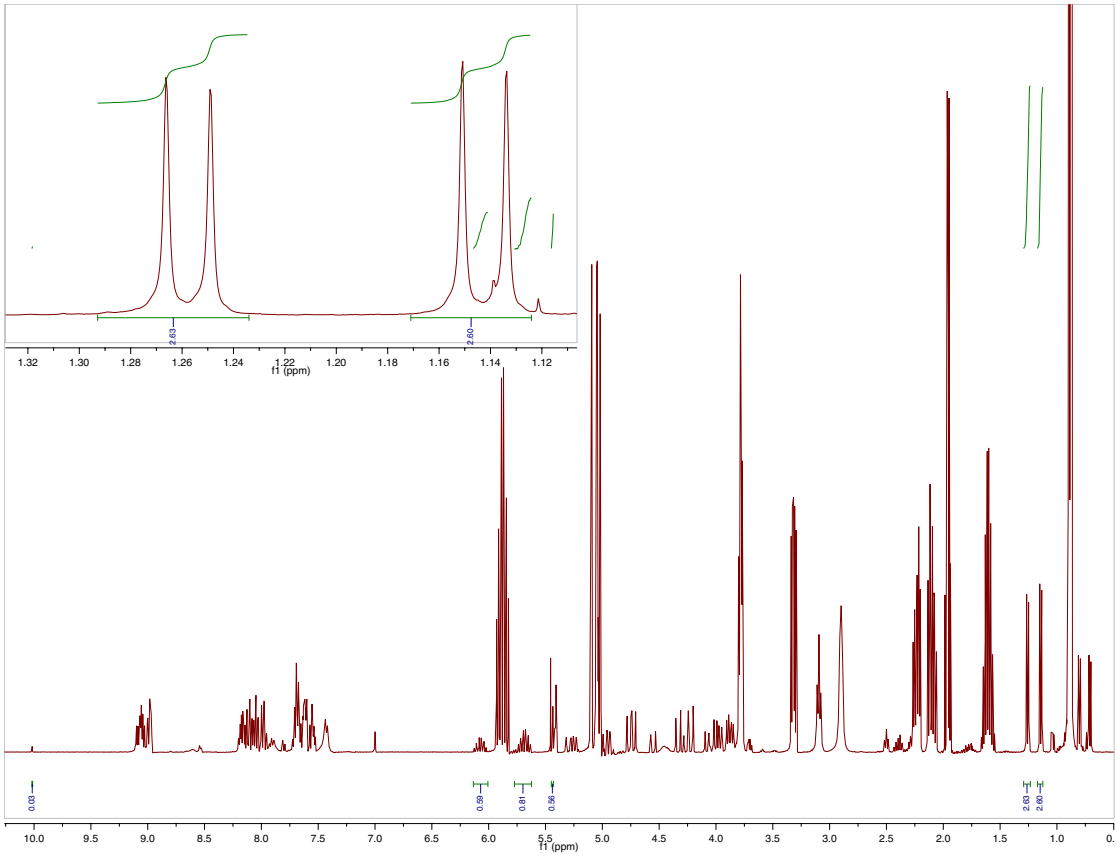

Diastereomeric ratio 1.06, % alcohol incorporation: 81%

^{1}H NMR of 3-Butyn-2-ol in Multi-component Assembly

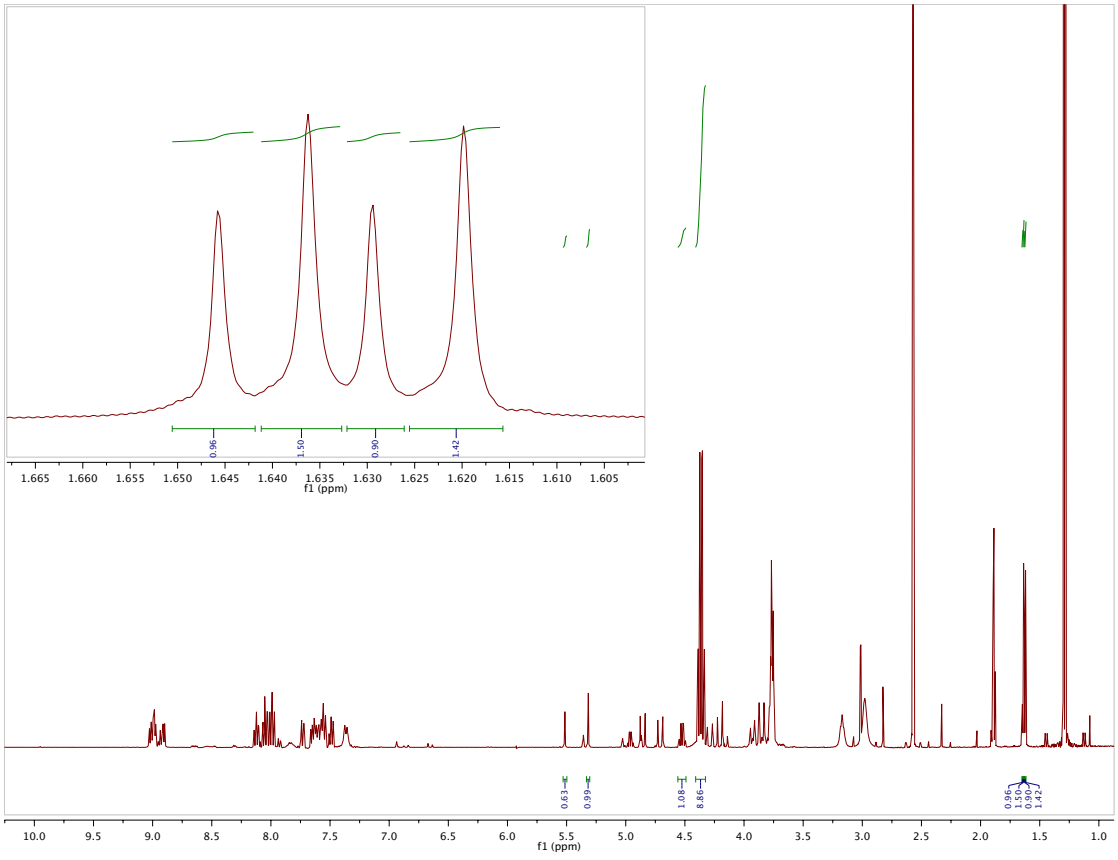

Diastereomeric ratio: 1.71, % alcohol incorporation: 77%

^{1}H NMR of 5-Hexyn-3-ol in Multi-component Assembly

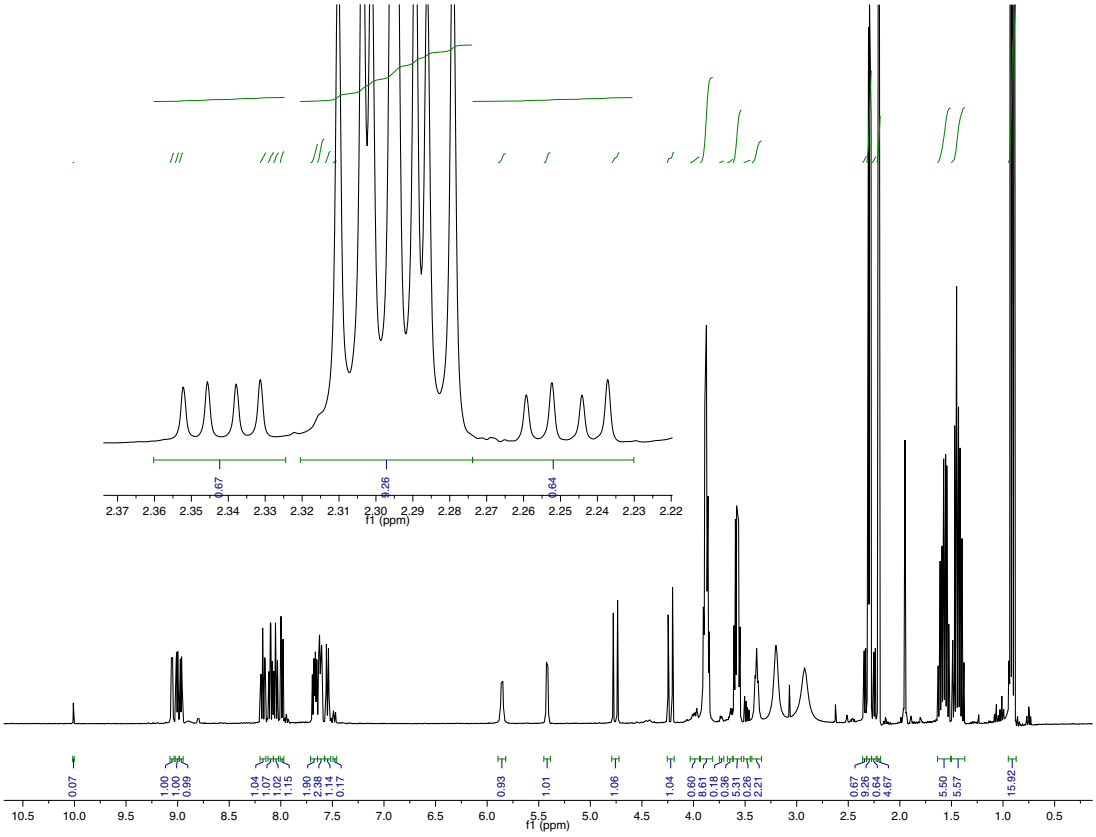

Diastereomeric ratio: 1.25, % alcohol incorporation: 14%

^{1}H NMR of 3-Buten-2-ol in Multi-component Assembly

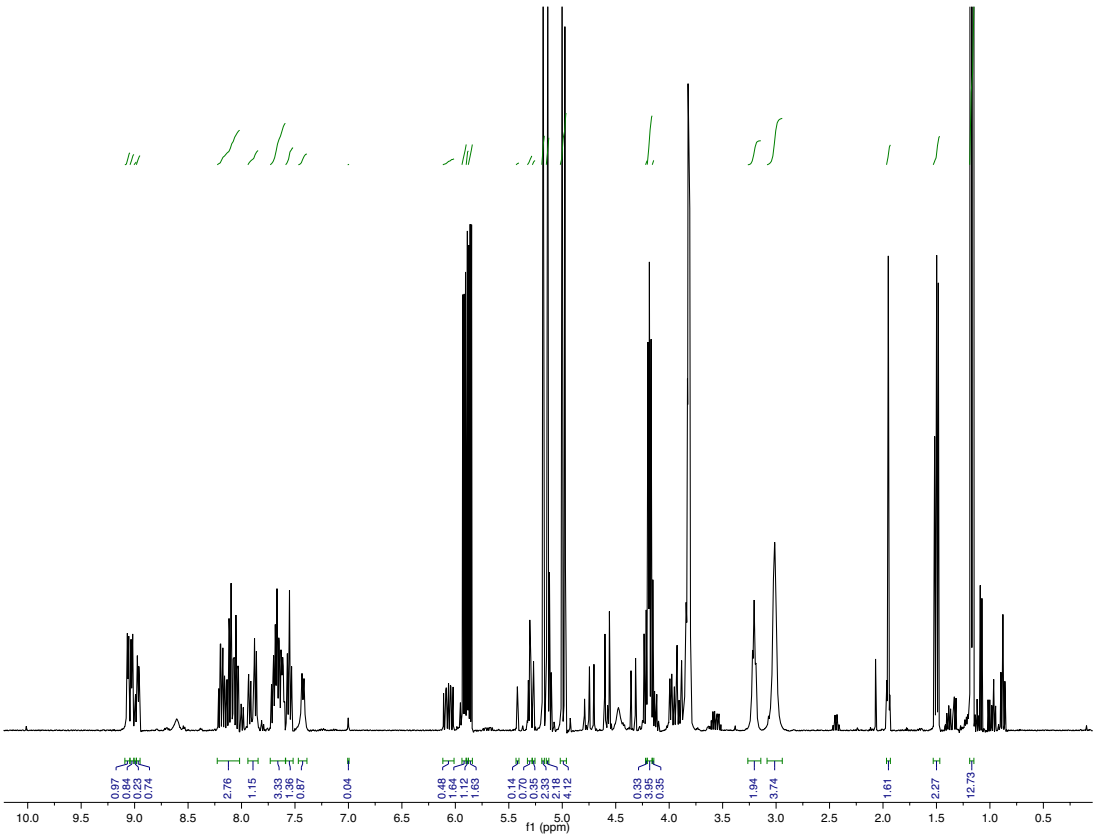

Diastereomeric ratio: 1.21, % alcohol incorporation: 88%

^{1}H NMR of 1-Penten-3-ol in Multi-component Assembly

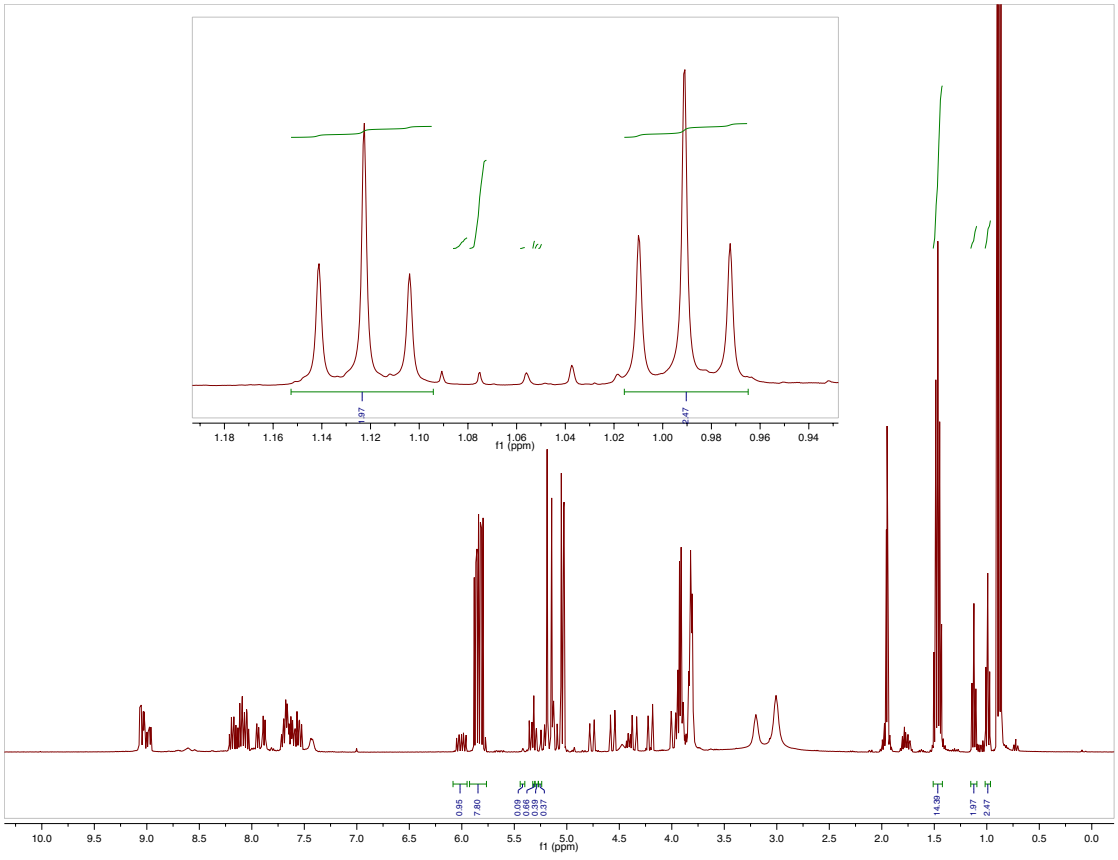

Diastereomeric ratio: 1.25, % alcohol incorporation: 88%

^{1}H NMR of 4-[3,4-(Methylenedioxy)phenyl]-1-buten-4-ol in Multi-component Assembly

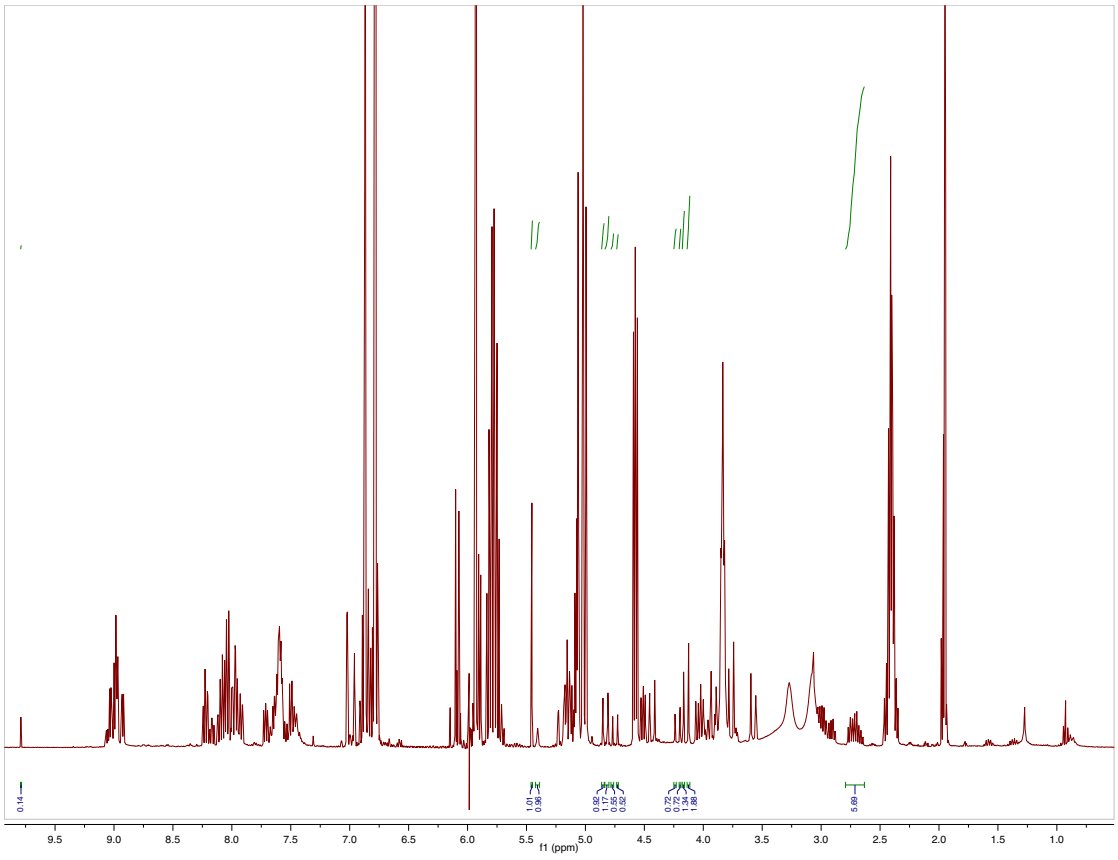

Diastereomeric ratio: 1.44, % alcohol incorporation: 83%

CD Spectroscopy of Free Alcohols and Alcohol Incorporated Assemblies

1-Phenylbut-3-en-1-ol (2.3)

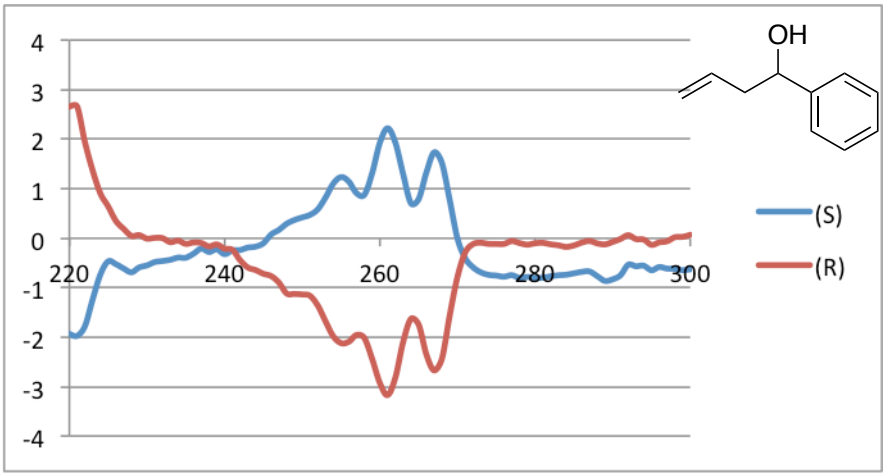

Figure 2.13: CD spectra of *R*-and *S*-1-Phenylbut-3-en-1-ol.

4-Penten-2-ol

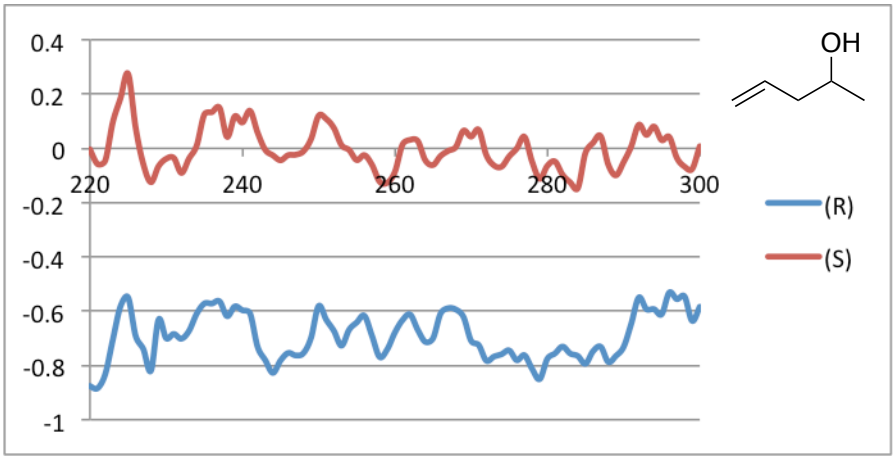

Figure 2.14: CD spectra of *R*-and *S*-4-penten-2-ol.

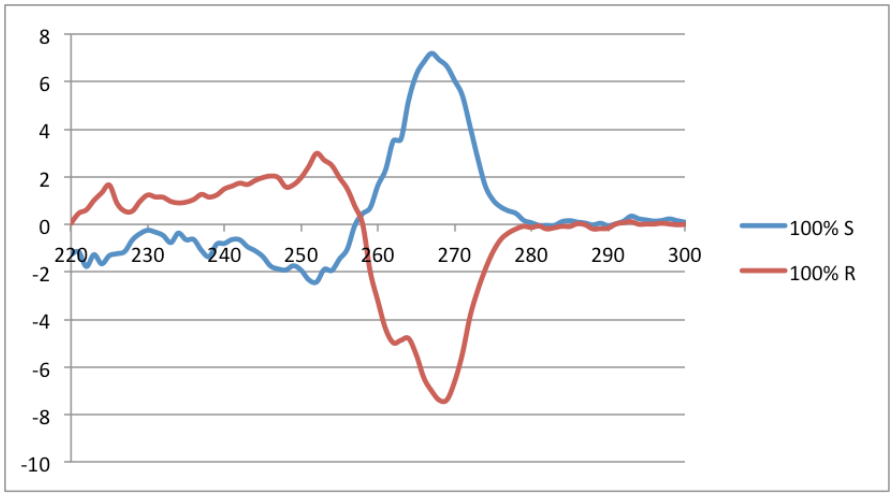

Figure 2.15: CD spectra of *R*-and *S*-4-penten-2-ol incorporated multi-component assemblies. The max CD value is 7 mdeg at 269 nm.

4-[3,4-(Methylenedioxy)phenyl]-1-buten-4-ol

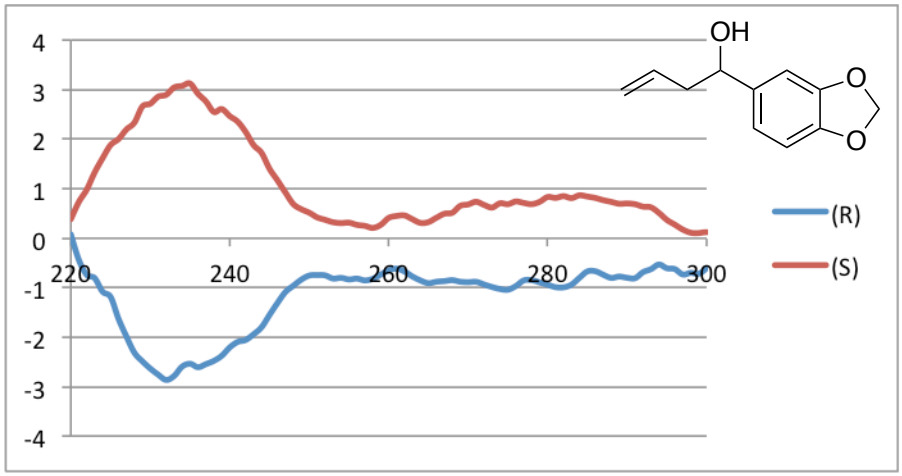

Figure 2.16: CD spectra of *R*-and *S*-4-[3,4-(Methylenedioxy)phenyl]-1-buten-4-ol.

4-[3,4-(Methylenedioxy)phenyl]-1-buten-4-ol in Multi-component Assembly

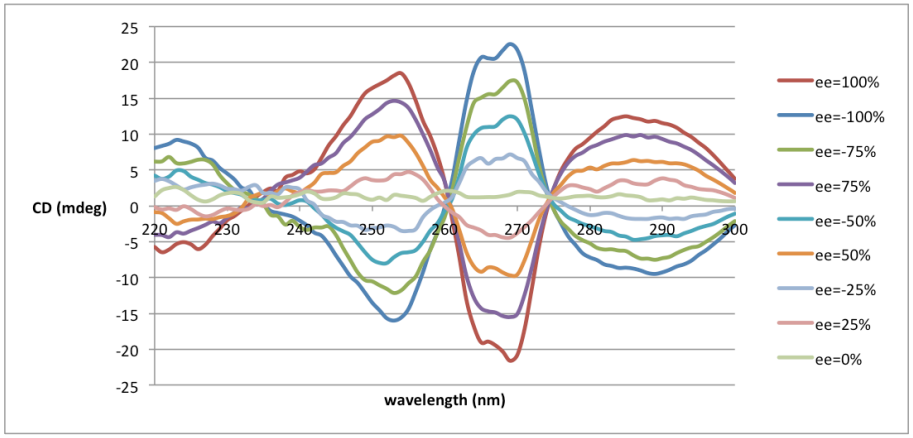

Figure 2.17: CD spectra of 4-[3,4-(methylenedioxy)phenyl]-1-buten-4-ol incorporated multi-component assembly varying enantiomeric composition.

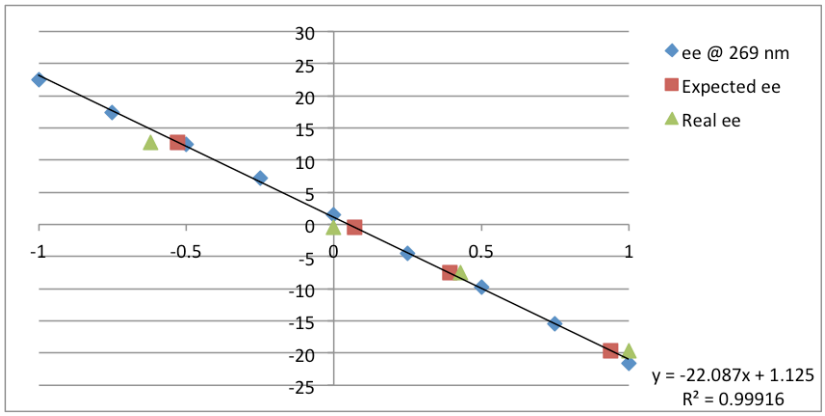

ee	CD at 269 nm
-1	22.5753
1	-21.5798
-0.75	17.4222
0.75	-15.4873
-0.5	12.505
0.5	-9.66873
-0.25	7.18924
0.25	-4.41307

Figure 2.18:Calibration curve generated from CD at 269 nm.

3-butyn-2-ol

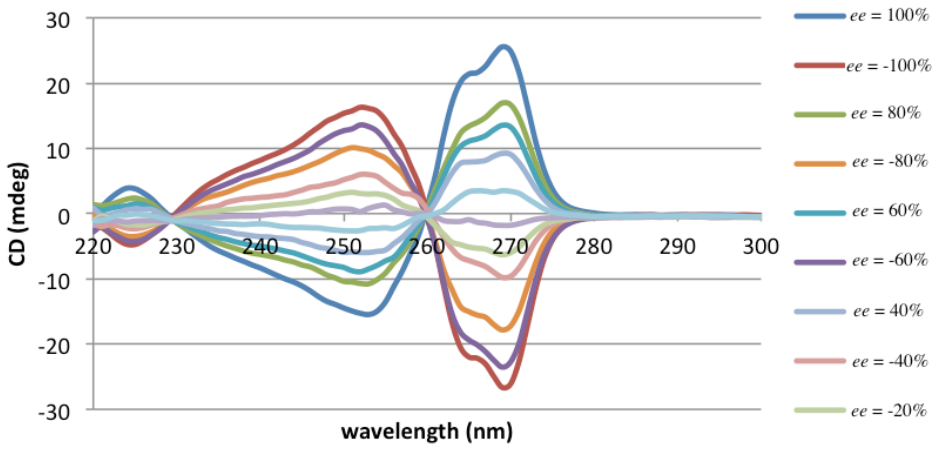

Figure 2.19: CD spectra of 3-butyn-2-ol incorporated multi-component assemblies varying the enantiomeric composition.

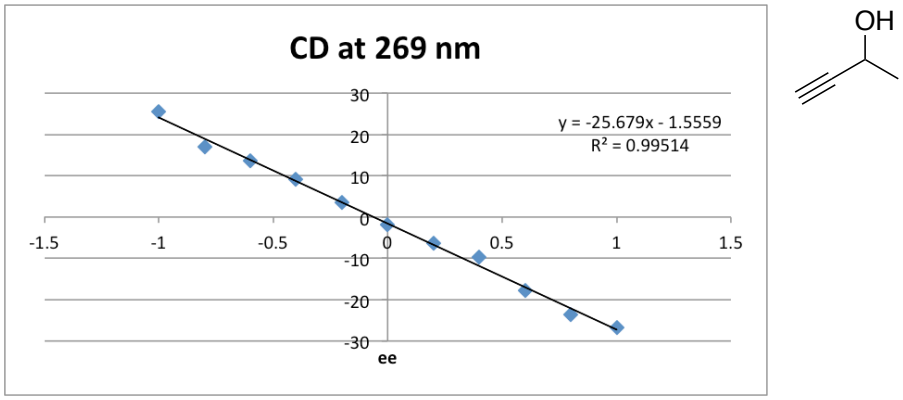

Figure 2.20: Calibration curve for 3-butyn-2-ol from CD at 269 nm.

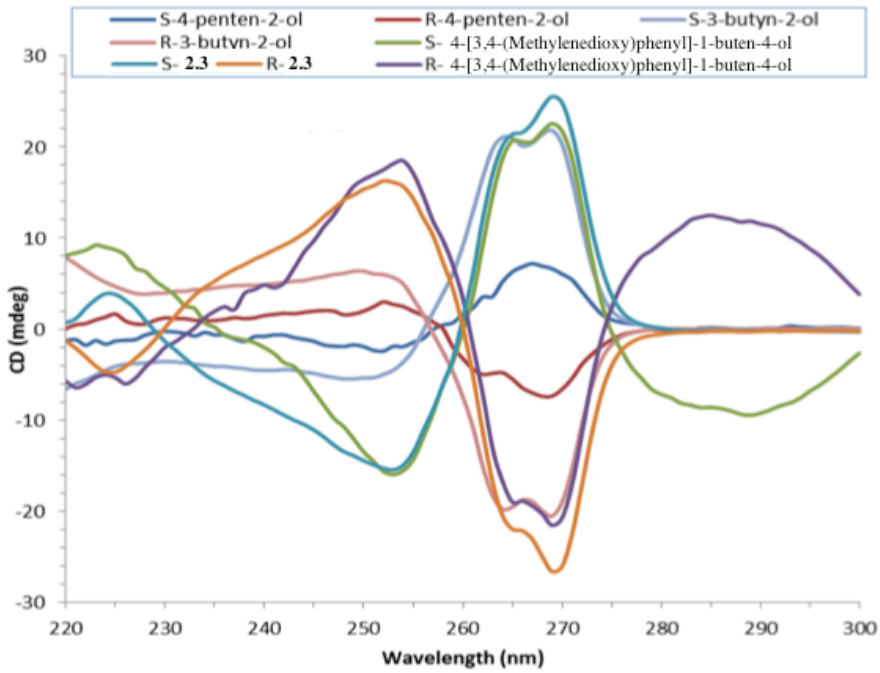

Figure 2.21: CD spectra of various enantiopure chiral alcohols.

2.4.6. Procedures for Multi-component Assembly

All reactions were performed using stock solution of each component in situ in acetonitrile without isolation and purification. Pyridine-2-carboxyaldehyde (2-PA, 35 mM, 0.0175 mmol, 1 equiv.), zinc triflate ($Zn(OTf)_2$, 35 mM, 0.0175 mmol, 1 equiv.), di-(2-picolyl)amine (DPA, 42mM, 0.021 mmol, 1.2 equiv.), 1-phenylbut-3-en-1-ol (1, equivalents varies within allylation reactions performed.), and 4-(2-chloroethyl)morpholine hydrochloride (CEM-HCl, 35 mM, 0.0175 mmol, 1 equiv.) were stirred together in acetonitrile in the presence of 3Å activated molecular sieves. The mixture was stirred at room temperature.

2.4.7. General Procedures for TLC Analysis

Each reaction was spotted onto TLC silica plate and developed with 10% ethylacetate in hexane. The TLC plate was placed inside the box that has the UV lamp

attached and the photo was taken using an iPhone. It is important that each time, the TLC plate was placed at the same position and that a picture of the blank TLC plate was taken before the development. The pictures were converted to grey-scale using any generic of photo management software, then using a software Igor pro, the intensity for each spot was counted and the ratio between the starting alcohol and the product alcohol was calculated as percentile.

Figure 2.12: Instrumentation set-up for TLC imaging technique.

2.4.8. Tables of CD determined *ee* and TLC method based % yield of 2.3 for each reaction

Allylation was performed for each pre-catalyst varying allyl moiety, base and solvent to give product alcohol **2.3**, followed by multi-component assembly. The *ee* obtained from a CD based calibration curve and yield estimated using the TLC method for each condition are shown below. Some of the reactions were randomly selected to compare with HPLC *ee* and isolated yield. When using enantiomers of the pre-catalysts, essentially the opposite *ee* were obtained with slight fluctuations in yield.

Pre-catalyst	Allyl Moiety	Base	Solvent	CD *ee*	TLC yield (%)
(*R*)-C1	1a	Cs_2CO_3	THF	90	80
			MeCN	8	25
			Dioxane	88	68
		K_2CO_3	THF	45	48
			MeCN	11	15
			Dioxane	65	32
		K_3PO_4	THF	85	80
			MeCN	12	25
			Dioxane	88	83
		strycine	THF	18	22
			MeCN	7	16
			Dioxane	12	33
	1b	Cs_2CO_3	THF	93	68
			MeCN	14	20
			Dioxane	90	65
		K_2CO_3	THF	58	52
			MeCN	18	24
			Dioxane	35	28
		K_3PO_4	THF	92	80
			MeCN	20	28
			Dioxane	88	64
		strycine	THF	19	24
			MeCN	11	25
			Dioxane	16	24

Table 2.6: CD determined *ee* and TLC determined yield with preformed catalyst (*R*)-C1.

Pre-catalyst	Allyl Moiety	Base	Solvent	CD *ee*	TLC yield (%)
(R)-C2	1a	Cs_2CO_3	THF	94	85
			MeCN	12	20
			Dioxane	86	65
		K_2CO_3	THF	52	61
			MeCN	14	10
			Dioxane	68	52
		K_3PO_4	THF	90	80
			MeCN	21	28
			Dioxane	92	77
		strycine	THF	20	25
			MeCN	12	14
			Dioxane	12	18
	1b	Cs_2CO_3	THF	90	85
			MeCN	7	12
			Dioxane	90	72
		K_2CO_3	THF	33	43
			MeCN	7	12
			Dioxane	68	48
		K_3PO_4	THF	88	87
			MeCN	15	22
			Dioxane	88	75
		strycine	THF	18	14
			MeCN	10	12
			Dioxane	21	34

Table 2.7: CD determined *ee* and TLC determined yield with preformed catalyst (*R*)-C2.

Pre-catalyst	Allyl Moiety	Base	Solvent	CD *ee*	TLC yield (%)
(R)-C3	1a	Cs_2CO_3	THF	85	74
			MeCN	15	22
			Dioxane	78	70
		K_2CO_3	THF	65	51
			MeCN	14	22
			Dioxane	64	52
		K_3PO_4	THF	70	80
			MeCN	14	28
			Dioxane	67	58
		strycine	THF	15	22
			MeCN	8	12
			Dioxane	12	12
	1b	Cs_2CO_3	THF	87	80
			MeCN	12	19
			Dioxane	87	70
		K_2CO_3	THF	49	44
			MeCN	10	18
			Dioxane	69	52
		K_3PO_4	THF	80	70
			MeCN	14	22
			Dioxane	78	68
		strycine	THF	11	28
			MeCN	6	10
			Dioxane	10	23

Table 2.8: CD determined *ee* and TLC determined yield with preformed catalyst (*R*)-C3.

Pre-catalyst	Allyl Moiety	Base	Solvent	CD *ee*	TLC yield (%)
(R)-C4	1a	Cs_2CO_3	THF	88	75
			MeCN	12	28
			Dioxane	81	61
		K_2CO_3	THF	66	52
			MeCN	14	20
			Dioxane	61	44
		K_3PO_4	THF	88	80
			MeCN	12	22
			Dioxane	75	68
		strycine	THF	8	20
			MeCN	11	15
			Dioxane	21	28
	1b	Cs_2CO_3	THF	87	78
			MeCN	10	14
			Dioxane	82	70
		K_2CO_3	THF	45	50
			MeCN	13	22
			Dioxane	78	41
		K_3PO_4	THF	87	80
			MeCN	12	10
			Dioxane	85	70
		strycine	THF	22	20
			MeCN	12	20
			Dioxane	8	24

Table 2.9: CD determined *ee* and TLC determined yield with preformed catalyst (*R*)-C4.

Pre-catalyst	Allyl Moiety	Base	Solvent	CD *ee*	TLC yield (%)
(R)-C5	1a	Cs_2CO_3	THF	89	80
			MeCN	17	12
			Dioxane	86	64
		K_2CO_3	THF	52	48
			MeCN	12	20
			Dioxane	60	42
		K_3PO_4	THF	91	70
			MeCN	15	28
			Dioxane	90	65
		strycine	THF	25	24
			MeCN	14	16
			Dioxane	20	28
	1b	Cs_2CO_3	THF	90	75
			MeCN	15	32
			Dioxane	89	64
		K_2CO_3	THF	45	49
			MeCN	14	22
			Dioxane	65	38
		K_3PO_4	THF	88	72
			MeCN	18	25
			Dioxane	87	68
		strycine	THF	21	34
			MeCN	14	21
			Dioxane	16	28

Table 2.10: CD determined *ee* and TLC determined yield with preformed catalyst (*R*)-C5.

Pre-catalyst	Allyl Moiety	Base	Solvent	CD *ee*	TLC yield (%)
(R)-C6	1a	Cs_2CO_3	THF	86	82
			MeCN	18	30
			Dioxane	75	62
		K_2CO_3	THF	44	51
			MeCN	14	12
			Dioxane	60	28
		K_3PO_4	THF	85	66
			MeCN	10	28
			Dioxane	70	57
		strycine	THF	18	11
			MeCN	12	18
			Dioxane	18	21
	1b	Cs_2CO_3	THF	85	77
			MeCN	18	12
			Dioxane	70	58
		K_2CO_3	THF	42	52
			MeCN	10	18
			Dioxane	55	42
		K_3PO_4	THF	84	80
			MeCN	8	16
			Dioxane	48	55
		strycine	THF	15	20
			MeCN	15	21
			Dioxane	18	31

Table 2.11: CD determined *ee* and TLC determined yield with preformed catalyst (*R*)-C6.

Pre-catalyst	Allyl Moiety	Base	Solvent	CD *ee*	TLC yield (%)
(R)-C7	1a	Cs_2CO_3	THF	82	78
			MeCN	12	22
			Dioxane	75	64
		K_2CO_3	THF	37	61
			MeCN	18	15
			Dioxane	55	22
		K_3PO_4	THF	74	58
			MeCN	15	22
			Dioxane	77	62
		strycine	THF	20	14
			MeCN	16	14
			Dioxane	18	25
	1b	Cs_2CO_3	THF	87	80
			MeCN	9	14
			Dioxane	68	60
		K_2CO_3	THF	44	54
			MeCN	11	16
			Dioxane	59	52
		K_3PO_4	THF	76	72
			MeCN	12	24
			Dioxane	51	58
		strycine	THF	18	21
			MeCN	6	10
			Dioxane	12	27

Table 2.12: CD determined *ee* and TLC determined yield with preformed catalyst (*R*)-C7.

Pre-catalyst	Allyl Moiety	Base	Solvent	CD *ee*	TLC yield (%)
(R)-C8	1a	Cs_2CO_3	THF	84	80
			MeCN	9	11
			Dioxane	61	58
		K_2CO_3	THF	46	54
			MeCN	17	15
			Dioxane	61	42
		K_3PO_4	THF	84	71
			MeCN	10	8
			Dioxane	77	59
		strycine	THF	15	16
			MeCN	7	10
			Dioxane	10	12
	1b	Cs_2CO_3	THF	84	75
			MeCN	11	16
			Dioxane	66	55
		K_2CO_3	THF	40	43
			MeCN	12	14
			Dioxane	53	52
		K_3PO_4	THF	80	71
			MeCN	14	18
			Dioxane	55	52
		strycine	THF	12	22
			MeCN	10	14
			Dioxane	12	14

Table 2.13: CD determined *ee* and TLC determined yield with preformed catalyst (*R*)-C8.

Pre-catalyst	Allyl Moiety	Base	Solvent	CD *ee*	TLC yield (%)
(R)-C9	1a	Cs_2CO_3	THF	85	82
			MeCN	11	8
			Dioxane	62	56
		K_2CO_3	THF	40	36
			MeCN	16	18
			Dioxane	61	52
		K_3PO_4	THF	86	78
			MeCN	14	14
			Dioxane	52	55
		strycine	THF	10	12
			MeCN	15	6
			Dioxane	17	15
	1b	Cs_2CO_3	THF	83	78
			MeCN	13	12
			Dioxane	76	55
		K_2CO_3	THF	66	48
			MeCN	14	12
			Dioxane	63	38
		K_3PO_4	THF	84	75
			MeCN	12	12
			Dioxane	55	40
		strycine	THF	18	27
			MeCN	6	9
			Dioxane	11	18

Table 2.14: CD determined *ee* and TLC determined yield with preformed catalyst (*R*)-C9.

Pre-catalyst	Allyl Moiety	Base	Solvent	CD *ee*	TLC yield (%)
(*S*)-C1	1a	Cs_2CO_3	THF	88	82
			MeCN	12	23
			Dioxane	86	65
		K_2CO_3	THF	43	52
			MeCN	8	22
			Dioxane	66	35
		K_3PO_4	THF	87	79
			MeCN	14	29
			Dioxane	85	80
		strycine	THF	20	24
			MeCN	13	17
			Dioxane	15	33
	1b	Cs_2CO_3	THF	93	67
			MeCN	10	25
			Dioxane	88	69
		K_2CO_3	THF	61	50
			MeCN	22	26
			Dioxane	39	32
		K_3PO_4	THF	90	79
			MeCN	22	30
			Dioxane	90	65
		strycine	THF	17	28
			MeCN	12	25
			Dioxane	12	24

Table 2.15: CD determined *ee* and TLC determined yield with preformed catalyst (*S*)-C1.

Pre-catalyst	Allyl Moiety	Base	Solvent	CD *ee*	TLC yield (%)
(*S*)-C2	1a	Cs_2CO_3	THF	95	80
			MeCN	15	14
			Dioxane	87	62
		K_2CO_3	THF	52	69
			MeCN	15	22
			Dioxane	70	48
		K_3PO_4	THF	88	80
			MeCN	20	29
			Dioxane	91	80
		strycine	THF	22	27
			MeCN	14	12
			Dioxane	19	22
	1b	Cs_2CO_3	THF	92	81
			MeCN	8	14
			Dioxane	90	70
		K_2CO_3	THF	34	43
			MeCN	12	13
			Dioxane	71	48
		K_3PO_4	THF	89	88
			MeCN	14	24
			Dioxane	92	80
		strycine	THF	22	15
			MeCN	18	12
			Dioxane	25	36

Table 2.16: CD determined *ee* and TLC determined yield with preformed catalyst (*S*)-C2.

Pre-catalyst	Allyl Moiety	Base	Solvent	CD *ee*	TLC yield (%)
(*S*)-C3	1a	Cs_2CO_3	THF	81	71
			MeCN	11	20
			Dioxane	77	68
		K_2CO_3	THF	65	54
			MeCN	19	22
			Dioxane	62	51
		K_3PO_4	THF	72	80
			MeCN	12	28
			Dioxane	68	59
		strycine	THF	12	22
			MeCN	10	11
			Dioxane	16	15
	1b	Cs_2CO_3	THF	88	75
			MeCN	14	22
			Dioxane	85	72
		K_2CO_3	THF	50	46
			MeCN	12	20
			Dioxane	71	53
		K_3PO_4	THF	80	70
			MeCN	16	24
			Dioxane	80	72
		strycine	THF	15	22
			MeCN	4	20
			Dioxane	6	17

Table 2.17: CD determined *ee* and TLC determined yield with preformed catalyst (*S*)-C3.

Pre-catalyst	Allyl Moiety	Base	Solvent	CD *ee*	TLC yield (%)
(*S*)-C4	1a	Cs_2CO_3	THF	87	68
			MeCN	12	32
			Dioxane	80	62
		K_2CO_3	THF	68	58
			MeCN	17	40
			Dioxane	58	42
		K_3PO_4	THF	88	77
			MeCN	15	18
			Dioxane	73	72
		strycine	THF	10	20
			MeCN	14	15
			Dioxane	22	29
	1b	Cs_2CO_3	THF	86	74
			MeCN	15	18
			Dioxane	80	80
		K_2CO_3	THF	46	54
			MeCN	15	26
			Dioxane	80	44
		K_3PO_4	THF	88	80
			MeCN	14	15
			Dioxane	83	72
		strycine	THF	12	24
			MeCN	8	22
			Dioxane	12	22

Table 2.18: CD determined *ee* and TLC determined yield with preformed catalyst (*S*)-C4.

Pre-catalyst	Allyl Moiety	Base	Solvent	CD *ee*	TLC yield (%)
(*S*)-C5	1a	Cs_2CO_3	THF	90	77
			MeCN	22	16
			Dioxane	86	62
		K_2CO_3	THF	54	48
			MeCN	18	24
			Dioxane	62	44
		K_3PO_4	THF	91	72
			MeCN	15	14
			Dioxane	89	65
		strycine	THF	24	22
			MeCN	18	18
			Dioxane	22	27
	1b	Cs_2CO_3	THF	90	72
			MeCN	19	31
			Dioxane	90	67
		K_2CO_3	THF	46	47
			MeCN	12	27
			Dioxane	66	37
		K_3PO_4	THF	89	71
			MeCN	22	23
			Dioxane	87	67
		strycine	THF	24	36
			MeCN	14	27
			Dioxane	19	31

Table 2.19: CD determined *ee* and TLC determined yield with preformed catalyst (*S*)-C5.

Pre-catalyst	Allyl Moiety	Base	Solvent	CD *ee*	TLC yield (%)
(*S*)-C6	1a	Cs_2CO_3	THF	86	78
			MeCN	12	32
			Dioxane	77	57
		K_2CO_3	THF	46	56
			MeCN	19	14
			Dioxane	62	24
		K_3PO_4	THF	87	64
			MeCN	12	32
			Dioxane	72	58
		strycine	THF	22	13
			MeCN	14	19
			Dioxane	18	22
	1b	Cs_2CO_3	THF	86	67
			MeCN	19	14
			Dioxane	72	62
		K_2CO_3	THF	41	60
			MeCN	12	22
			Dioxane	54	40
		K_3PO_4	THF	83	78
			MeCN	13	14
			Dioxane	46	55
		strycine	THF	17	22
			MeCN	12	14
			Dioxane	14	22

Table 2.20: CD determined *ee* and TLC determined yield with preformed catalyst (*S*)-C6.

Pre-catalyst	Allyl Moiety	Base	Solvent	CD *ee*	TLC yield (%)
(*S*)-C7	1a	Cs_2CO_3	THF	83	74
			MeCN	14	14
			Dioxane	77	58
		K_2CO_3	THF	39	63
			MeCN	22	22
			Dioxane	54	28
		K_3PO_4	THF	72	48
			MeCN	13	34
			Dioxane	77	64
		strycine	THF	22	17
			MeCN	13	21
			Dioxane	20	28
	1b	Cs_2CO_3	THF	87	67
			MeCN	13	16
			Dioxane	70	65
		K_2CO_3	THF	46	51
			MeCN	13	22
			Dioxane	62	49
		K_3PO_4	THF	80	71
			MeCN	14	28
			Dioxane	47	61
		strycine	THF	17	24
			MeCN	4	11
			Dioxane	14	14

Table 2.21: CD determined *ee* and TLC determined yield with preformed catalyst (*S*)-C7.

Pre-catalyst	Allyl Moiety	Base	Solvent	CD *ee*	TLC yield (%)
(*S*)-C8	1a	Cs_2CO_3	THF	81	77
			MeCN	12	15
			Dioxane	58	62
		K_2CO_3	THF	49	61
			MeCN	13	19
			Dioxane	60	43
		K_3PO_4	THF	84	68
			MeCN	11	12
			Dioxane	78	51
		strycine	THF	22	14
			MeCN	10	20
			Dioxane	12	14
	1b	Cs_2CO_3	THF	82	66
			MeCN	13	21
			Dioxane	69	54
		K_2CO_3	THF	43	59
			MeCN	17	18
			Dioxane	55	49
		K_3PO_4	THF	81	68
			MeCN	19	2
			Dioxane	54	50
		strycine	THF	14	34
			MeCN	12	10
			Dioxane	15	14

Table 2.22: CD determined *ee* and TLC determined yield with preformed catalyst (*S*)-C8.

Pre-catalyst	Allyl Moiety	Base	Solvent	CD *ee*	TLC yield (%)
(*S*)-C9	1a	Cs_2CO_3	THF	85	80
			MeCN	11	12
			Dioxane	60	54
		K_2CO_3	THF	44	39
			MeCN	19	22
			Dioxane	62	54
		K_3PO_4	THF	86	77
			MeCN	19	19
			Dioxane	54	50
		strycine	THF	14	21
			MeCN	11	10
			Dioxane	13	21
	1b	Cs_2CO_3	THF	82	70
			MeCN	19	14
			Dioxane	77	51
		K_2CO_3	THF	69	50
			MeCN	18	15
			Dioxane	67	43
		K_3PO_4	THF	86	72
			MeCN	14	10
			Dioxane	59	30
		strycine	THF	14	33
			MeCN	10	11
			Dioxane	12	18

Table 2.23: CD determined *ee* and TLC determined yield with preformed catalyst (*S*)-C9.

2.5 REFERENCES

1. Aitken A.; Kilényi, S. N. Asymmetric Synthesis. 1992.

2. Hadik, P.; Szabó, L.-P.; Nagy, E. D,L-lactic acid and D,L-alanine enantioseparation by membrane process. *Desalination*, 2002, **148**, 193–198.

3. Farina, V.; Reeves, J. T.; Senanayake, C. H.; Song, J. J. Asymmetric synthesis of active pharmaceutical ingredients. *Chem. Rev.*, 2006, **106**, 2734–2793.

4. C. A. Busacca, D. R. Fandrick, J. J. Song, and C. H. Senanayake, *Adv. Synth. Catal.*, 2011, **353**, 1825–1864.

5. Etayo, P.; Vidal-Ferran, A. Rhodium-catalysed asymmetric hydrogenation as a valuable synthetic tool for the preparation of chiral drugs. *Chem. Soc. Rev.*, 2013, **42**, 728–754.

6. Ager, D. J.; de Vries, A. H. M.; de Vries, J. G. Asymmetric homogeneous hydrogenations at scale. *Chem. Soc. Rev.*, 2012, **41**, 3340–3380.

7. Blaser, H.-U. The Chiral Switch of (S)-Metolachlor: A Personal Account of an Industrial Odyssey in Asymmetric Catalysis. *Adv. Synth. Catal.*, 2002, **344**, 17–31.

8. Blaser, H.-U.; Pugin, B.; Spindler, F.; Thommen, M. From a chiral switch to a ligand portfolio for asymmetric catalysis. *Acc. Chem. Res.*, 2007, **40**, 1240–1250.

9. Ketcham, J. M.; Shin, I.; Montgomery, T. P.; Krische, M. J. Catalytic enantioselective C-H functionalization of alcohols by redox-triggered carbonyl addition: borrowing hydrogen, returning carbon. *Angew. Chem. Int. Ed. Eng.*, 2014, **53**, 9142–9150.

10. Hassan A.; Krische, M. J. Unlocking Hydrogenation for C-C Bond Formation: A Brief Overview of Enantioselective Methods. *Org. Proc. Res. Dev.*, 2011, **15**, 1236–1242.

11. Kim, I. S.; Ngai, M.-Y.; Krische, M. J. Enantioselective iridium-catalyzed carbonyl allylation from the alcohol or aldehyde oxidation level using allyl acetate as an allyl metal surrogate. *J. Am. Chem. Soc.*, 2008, **130**, 6340–6341.

12. Kim, I. S.; Ngai, M.-Y.; Krische, M. J. Enantioselective iridium-catalyzed carbonyl allylation from the alcohol or aldehyde oxidation level via transfer hydrogenative coupling of allyl acetate: departure from chirally modified allyl metal reagents in carbonyl addition. *J. Am. Chem. Soc.*, 2008, **130**, 14891–14899.

13. Lu, Y.; Kim, I. S.; Hassan, A.; Del Valle, D. J.; Krische, M. J. 1,n-glycols as dialdehyde equivalents in iridium-catalyzed enantioselective carbonyl allylation and iterative two-directional assembly of 1,3-polyols. *Angew. Chem. Int. Ed. Eng.*, 2009, **48**, 5018–5021.

14. Schmitt, D. C.; Dechert-Schmitt, A.-M. R.; Krische, M. J. Iridium-catalyzed allylation of chiral β-stereogenic alcohols: bypassing discrete formation of epimerizable aldehydes. *Org Lett*, 2012, **14**, 6302–6305.

15. Dechert-Schmitt, A.-M. R.; Schmitt, D. C.; Krische, M. J. Protecting-group-free diastereoselective C-C coupling of 1,3-glycols and allyl acetate through site-selective primary alcohol dehydrogenation. *Angew. Chem. Int. Ed.*, 2013, **52**, 3195–3198.

16. Dechert-Schmitt, A.-M. R.; Schmitt, D. C.; Gao, X.; Itoh, T.; Krische, M. J. Polyketide construction via hydrohydroxyalkylation and related alcohol C-H functionalizations: reinventing the chemistry of carbonyl addition. *Nat Prod Rep*, 2014, **31**, 504–513.

17. Han, S. B.; Hassan, A.; Kim, I. S.; Krische, M. J. Total synthesis of (+)-roxaticin via C-C bond forming transfer hydrogenation: a departure from stoichiometric chiral reagents, auxiliaries, and premetalated nucleophiles in polyketide construction. *J. Am. Chem. Soc.*, 2010, **132**, 15559–15561.

18. Gao, X.; Woo, S. K.; Krische, M. J. Total synthesis of 6-deoxyerythronolide B via C-C bond-forming transfer hydrogenation. *J. Am. Chem. Soc.*, 2013, **135**, 4223–4226.

19. Lu, Y.; Woo, S. K.; Krische, M. J. Total synthesis of bryostatin 7 via C-C bond-forming hydrogenation. *J. Am. Chem. Soc.*, 2011, **133**, 13876–13879.

20. Willwacher J.; Fürstner, A. Catalysis-based total synthesis of putative mandelalide A. *Angew. Chem. Int. Ed. Eng.*, 2014, **53**, 4217–4221.

21. Feng, Y.; Jiang, X.; De Brabander, J. K. Studies toward the unique pederin family member psymberin: full structure elucidation, two alternative total syntheses, and analogs. *J. Am. Chem. Soc.*, 2012, **134**, 17083–17093.

22. Wan, S.; Wu, F.; Rech, J. C.; Green, M. E.; Balachandran, R.; Horne, W. S.; Day, B. W.; Floreancig, P. E. Total synthesis and biological evaluation of pederin, psymberin, and highly potent analogs. *J. Am. Chem. Soc.*, 2011, **133**, 16668–16679.

23. Kretschmer, M.; Dieckmann, M.; Li, P.; Rudolph, S.; Herkommer, D.; Troendlin, J. Menche, D. *Chem. Eur. J.*, 2013, **19**, 15993–16018.

24. Prévost, S.; Thai, K.; Schützenmeister, N.; Coulthard, G.; Erb, W.; Aggarwal, V. K. Synthesis of Prostaglandin Analogues, Latanoprost and Bimatoprost, Using Organocatalysis via a Key Bicyclic Enal Intermediate. *Org. Lett.*, 2015, **17**, 504–507.

25. Jo, H. H.; Lin, C.-Y.; Anslyn, E. V. Rapid optical methods for enantiomeric excess analysis: from enantioselective indicator displacement assays to exciton-coupled circular dichroism. *Acc. Chem. Res.*, 2014, **47**, 2212–2221.

26. Zhu, L.; Zhong, Z.; Anslyn, E. V. Guidelines in implementing enantioselective indicator-displacement assays for alpha-hydroxycarboxylates and diols. *J. Am. Chem. Soc*., 2005, **127**, 4260–4269.

27. Leung, D.; Folmer-Andersen, J. F.; Lynch, V. M.; Anslyn, E. V. Using enantioselective indicator displacement assays to determine the enantiomeric excess of alpha-amino acids. *J. Am. Chem. Soc*., 2008, **130**, 12318–12327.

28. Shabbir, S. H. ; Joyce, L. A.; da Cruz, G. M.; Lynch, V. M.; Sorey, S.; Anslyn, E. V. Pattern-based recognition for the rapid determination of identity, concentration, and enantiomeric excess of subtly different threo diols. *J. Am. Chem. Soc*., 2009, **131**, 13125–13131.

29. Pu, L. Fluorescence of organic molecules in chiral recognition. *Chem. Rev*., 2004, **104**, 1687–1716.

30. Hembury, G. A.; Borovkov, V. V.; Inoue, Y. Chirality-sensing supramolecular systems. *Chem. Rev*., 2008, **108**, 1–73.

31. Berova, N.; Di Bari, L.; Pescitelli, G. Application of electronic circular dichroism in configurational and conformational analysis of organic compounds. *Chem. Soc. Rev*., 2007, **36**, 914–931.

32. Wolf C.; Bentley, K. W. Chirality sensing using stereodynamic probes with distinct electronic circular dichroism output. *Chem. Soc. Rev*., 2013, **42**, 5408–5424.

33. Nieto, S.; Dragna, J. M.; Anslyn, E. V. A facile circular dichroism protocol for rapid determination of enantiomeric excess and concentration of chiral primary amines. *Chem. Eur. J*., 2010, **16**, 227–232.

34. You, L.; Berman, J. S; Anslyn, E. V. Dynamic multi-component covalent assembly for the reversible binding of secondary alcohols and chirality sensing *Nat. Chem*., 2011, **3**, 943–948.

35. Joyce, L. A.; Maynor, M. S.; Dragna, J. M.; da Cruz, G. M.; Lynch, V. M.; Canary, J. W.; Anslyn, E. V. A simple method for the determination of enantiomeric excess and identity of chiral carboxylic acids. *J. Am. Chem. Soc*., 2011, **133**, 13746–13752.

36. Leung D.; Anslyn, E. V. Rapid determination of enantiomeric excess of α-chiral cyclohexanones using circular dichroism spectroscopy. *Org. Lett*., 2011, **13**, 2298–2301.

37. Fiedler, S.; Cole, L.; Keller, S. Automated Circular Dichroism Spectroscopy for Medium-Throughput Quantification of Protein Conformation. *Biophy. J*., 2013, **104**, 20a.

38. Metola, P.; Nichols, S. M.; Kahr, B.; Anslyn, E. V. Well Plate Circular Dichroism Reader for the Rapid Determination of Enantiomeric Excess. *Chem. Sci*., 2014, **5**, 4278–4282.

39. Zhao, Q.; Wen, J.; Tan, R.; Huang, K.; Metola, P.; Wang, R.; Anslyn, E. V.; Zhang X., Rhodium-catalyzed asymmetric hydrogenation of unprotected NH imines assisted by a thiourea. *Angew. Chem. Int. Ed.*, 2014, **53**, 8467–8470.

40. Giuliano, M. W.; Lin, C.-Y.;Romney, D. K.; Miller, S. J.; Anslyn, E. V. *Adv. Synth. Catal.* **2015**, *357*, *In Press*. DOI: 10.1002/adsc.201500230.

41. Yoon, H.; Lee, C.-H.; Jang, W.-D. Absolute stereochemical determination of chiral carboxylates using an achiral molecular tweezer. *Chem. Eur. J.*, 2012, **18**, 12479–12486.

42. Han, S. B.; Gao, X.; Krische, M. J. Iridium-catalyzed anti-diastereo- and enantioselective carbonyl (trimethylsilyl)allylation from the alcohol or aldehyde oxidation level. *J. Am. Chem. Soc.*, 2010, **132**, 9153–9156.

43. Han, S. B.; Han, H.; Krische, M. J. Diastereo- and enantioselective anti-alkoxyallylation employing allylic gem-dicarboxylates as allyl donors via iridium-catalyzed transfer hydrogenation. *J. Am. Chem. Soc.*, 2010, **132**, 1760–1761.

44. Gao, X.; Zhang, Y. J.; Krische, M. J. Iridium-catalyzed anti-diastereo- and enantioselective carbonyl (α-trifluoromethyl)allylation from the alcohol or aldehyde oxidation level. *Angew. Chem. Int. Ed.*, 2011, **50**, 4173–4175.

45. Jo, H. H.; Edupuganti, R.; You, L.; Dalby, K. N.; Anslyn, E. V. Mechanistic studies on covalent assemblies of metal-mediated hemi-aminal ethers. *Chem. Sci.*, 2015, **6**, 158–164.

46. You, L.; Berman, J. S.; Lucksanawichien, A.; Anslyn, E. V. *J. Am. Chem. Soc.*, 2012, **134**, 7126–7134.

47. Khedr A.; Sheha, M. Quantitative Thin-Layer Chromatographic Method of Analysis of Azithromycin in Pure and Capsule Forms *J. Chromatogr. Sci.*, 2003, **41**, 10–16.

48. Hess, A. V. I. Digitally Enhanced Thin-Layer Chromatography: An Inexpensive, New Technique for Qualitative and Quantitative Analysis. *J. Chem. Educ.*, 2007, **84**, 842.

49. Askal, H. F.; Khedr, A. S.; Darwish, I. A.; Mahmoud, R. M. Quantitative Thin-Layer Chromatographic Method for Determination of Amantadine Hydrochloride. *Int. J. Biomed. Sci.,* 2008, **4**, 155–160.

50. Hoeltz, M.; Welke, J. E.; Noll, I. B.; Dottori, H. A. Photometric procedure for quantitative analysis of Aflatoxin B1 in peanuts by thin-layer chromatography using charge coupled device detector *Quím. Nova.*, 2010, **33**, 43–47.

Chapter 3: Mechanistic Studies on Covalent Assemblies of Metal-Mediated Hemi-Aminal Ethers

3.1 INTRODUCTION

Dynamic Covalent Bonding (DCB) can be used to exchange molecular components in order to reach the thermodynamic minima of a system.[1-6] In recent decades, DCB has been explored due to its far-reaching applicability in supramolecular chemistry.[7-10] For instance, DCB is useful in creating new molecular receptors, protein ligands, and sensors.[11-15] It is quite common to combine metal-coordination or donor-acceptor interactions with dynamic covalent bonds. [13,16]

One application to which DCB has been applied is the determination of chirality. The discrimination of chiral compounds is essential in the pharmaceutical industry, where enantiomeric purity of chiral drugs can greatly influence therapeutic and biological properties.[17] Much effort has been devoted to creating methods that report the enantiomeric excess (*ee*) of target chiral building blocks using supramolecular and dynamic covalent bond chemistry.[18-20]

Our group reported a one-pot protocol involving multiple dynamic covalent bonds that target chiral alcohols.[21] This system forms a hemi-aminal (**3.1**) from three components which subsequently forms a hemi-aminal ether (**3.3**) from a fourth component (alcohol) upon dehydration (Figure 3.1). The reversibility of the covalent bonds in this assembly enables the exchange of all four components.[22] The use of the assembly to measure *ee* values of alcohols has been covered in-depth.[21,23,24] In this paper, a mechanistic investigation of this multi-component assembly is reported. Understanding the mechanism of this assembly should enable further exploration of dynamic hemi-aminal ether formation in a variety of contexts.[25-27]

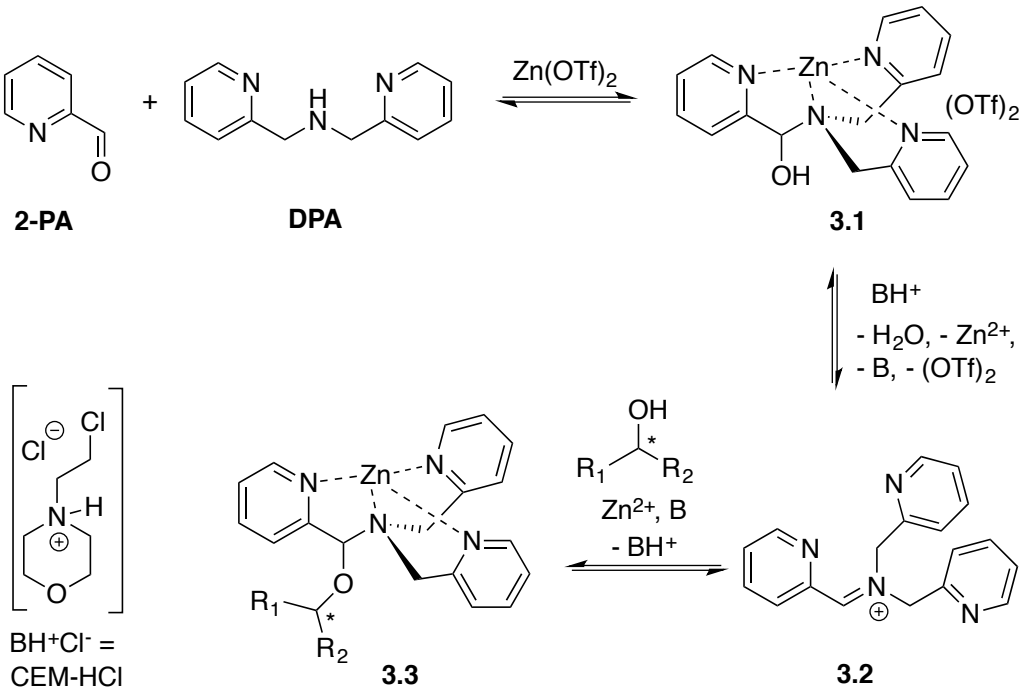

Figure 3.1: Reversible multicomponent-assembly for the binding of chiral secondary alcohols.

3.2 Results and Discussion

The use of reversible covalent-bonding in a four-component assembly incorporating chiral alcohols was recently reported to give a method for determining the enantiomeric excess of the alcohols via CD spectroscopy. Experiments that probe the mechanism of this assembly, which consists of 2-formylpyridine (2-PA), dipicolylamine (DPA), Zn(II), and alcohols, to yield zinc-complexes of tren-like ligands, are presented. The studies focus upon the mechanism of conversion of a hemi-aminal (**3.1**) to a hemi-aminal ether (**3.3**), thereby incorporating the fourth component. It was found that molecular sieves along with 3 to 4 equivalents of alcohol are required to drive the conversion of **3.1** to **3.3**. Attempts to isolate an intermediate in this reaction via the addition of strong Lewis-acids led to the discovery of a five-membered ring pyridinium salt (**3.5**), but upon exposure to Zn(II) and alcohols gave different products than the assembly. This was interpreted to support the intermediacy of an iminium species. Kinetic studies reveal that the conversion of **3.1** to **3.3** is zero-order in alcohol with large excesses of alcohol, supporting rate-determining formation of an intermediate prior to reaction with alcohol.

Further, the magnitude of the rate constant for interconversion of **3.1** and **3.3** are similar, supporting the notion that there are similar rate-determining steps (rds's) for the forward and reverse reactions. Hammett plots show that the rds involves creation of a negative charge (interpreted as the loss of positive charge), supporting the notion that decomplexation of Zn(II) from the assemblies to generate apo-forms of **3.1** and **3.3** is rate-determining. The individual mechanistic conclusions are combined to create a qualitative reaction coordinate diagram for the interconversion of **3.1** and **3.3**.

3.2.1 Extent of Alcohol Incorporation in Multi Component Assembly

In our previous work, which described the use of the four-component assembly given in Figure 3.1, we postulated that the reaction proceeded via iminium ion **3.2**, which would then add alcohols to create hemi-aminal ethers that are thermodynamically stabilized via binding of Zn(II) to the tren-like ligand.[21] Molecular sieves play a major role in the assembly process by scavenging water to drive the equilibrium, which involves alcohol incorporation. Depending on the absence or presence of molecular sieves in the solution, the alcohol incorporation jumps from 40% to 90%, respectively (Table 3.1). Further, the Brønsted acid (CEM-HCl), used as a catalyst, is critical to the assembly. Without a Brønsted acid, no hemi-aminal ether is formed (Table 3.1). It was found that CEM-HCl is the most effective acid catalyst, and led to the best yield of the hemi-aminal ether complex when Brønsted acids were screened.[21] CEM-HCl forms 3,12-dioxa-6,9-diazoniadispiro[5.2.5.2]hexadecane in the presence of DPA by slowly releasing hydrochloric acid (Figure 3.2).[28]

# of sieves	Brønsted acid	% Alcohol incorporation
0	N	0
0	Y	40
2	N	0
2	Y	88
4	N	0
4	Y	90

Table 3.1: Percent yield of hemi-aminal ether complex when number of molecular sieves (3Å) and presence of Brønsted acid were varied. (Concentration of 2-PA: 35 mM, DPA: 42 mM, alcohol: 175 mM and Zn(II) : 35 mM in acetonitrile).

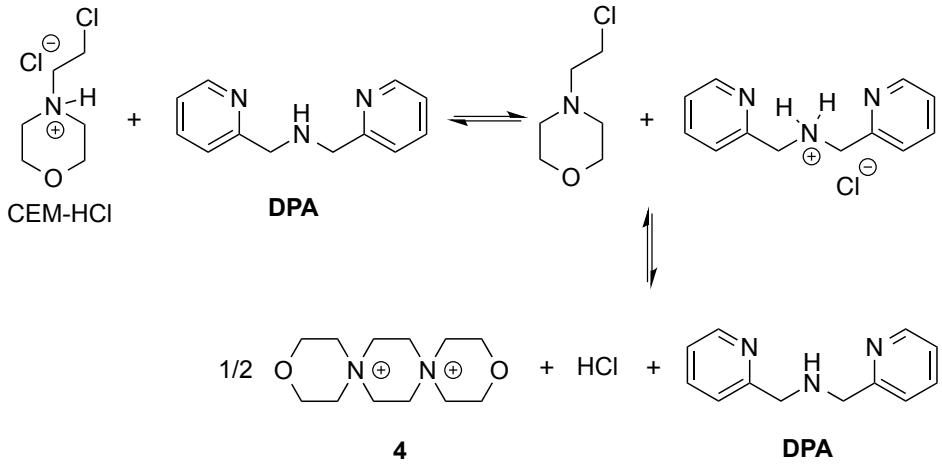

Figure 3.2: Pathway of CEM-HCl to form 3,12-dioxa-6,9-diazoniadispiro[5.2.5.2]-hexadecane releasing HCl.

In addition to the necessity of molecular sieves, one needs an excess of alcohol to drive the assembly to completion. Figure 3.3A shows the yield of the assembly as a function of the number of equivalents of an alcohol (4-penten-2-ol). As previously reported, the assembly with chiral alcohols results in circular dichroism (CD) signals. Figure 3.3B displays the CD intensity as a function of alcohol concentration, which shows that an excess of the alcohol is required to

ensure complete assembly. To ensure saturation in the assembly reactions, all experiments for *ee* determination are conducted using 3 equiv. or more of alcohol.

$$K_{eq} = \frac{[\mathbf{3.3}][H_2O]}{[\mathbf{3.1}][ROH]} \qquad \text{(Equation 3.1)}$$

Because molecular sieves and excess alcohol are required to drive the reaction to completion, it was anticipated that the value of the equilibrium constant (K_{eq}) between **3.1** and **3.3** must be less than 1. The ^{1}H-NMR chemical shifts of **3.1** and **3.3** are distinct, and thus it is a simple matter of integration of the respective resonances to measure a K_{eq} value, along with knowledge of the starting concentrations of all reactants: **3.1** and alcohol, and a controlled amount of water (Equation 3.1). Thus, with an initial concentration of **3.1** being 35 mM, water at 35 mM, and alcohol at 175 mM, Equation 3.1 yielded a K_{eq} value of 0.042.

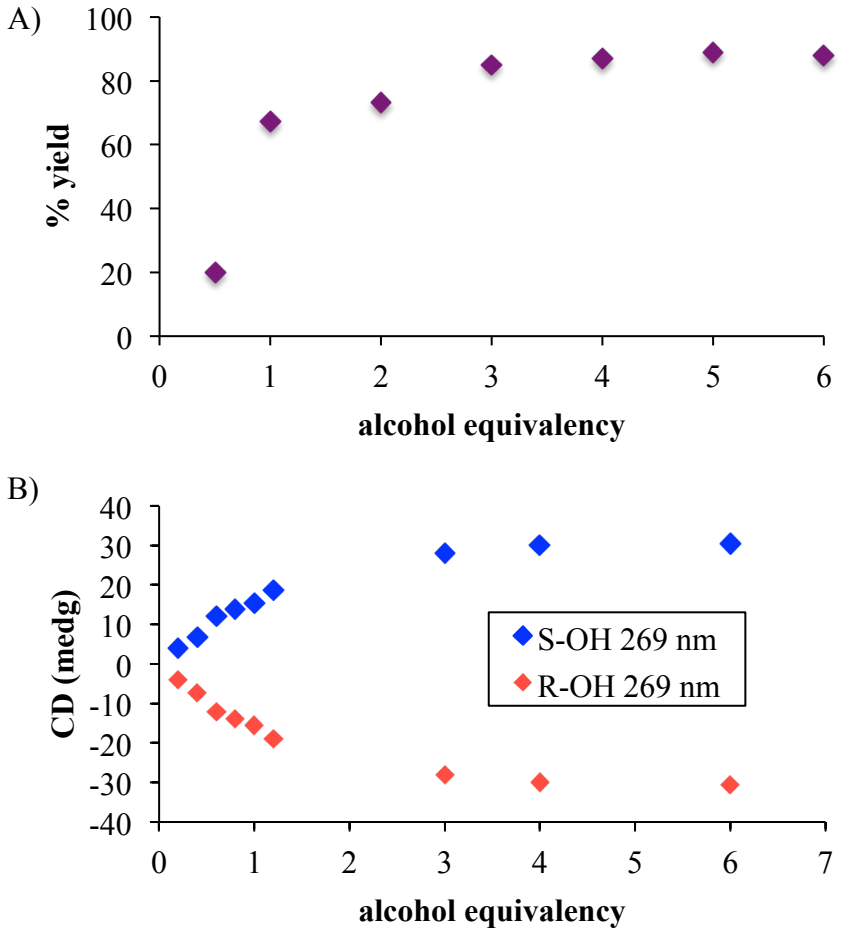

Figure 3.3: A) The percent yields and B) CD intensities of hemi-aminal ether formation when the equivalency of alcohol was varied. (Concentration of 2-PA: 35 mM, DPA: 42 mM and Zn(II) : 35 mM in acetonitrile).

3.2.2 Isolation and Characterization of the Intermediate

Although not commonly isolated, iminium salts have been characterized previously.[29] With this precedent in mind, we set out to create iminium **3.2** as a means to test its validity as the intermediate in the assembly process shown in Figure 3.1. To isolate salt **3.2**, we used powerful Lewis acids such as TMS-OTf and BF_3-OEt_2 to facilitate DPA in addition to 2-PA (Figure 3.4).

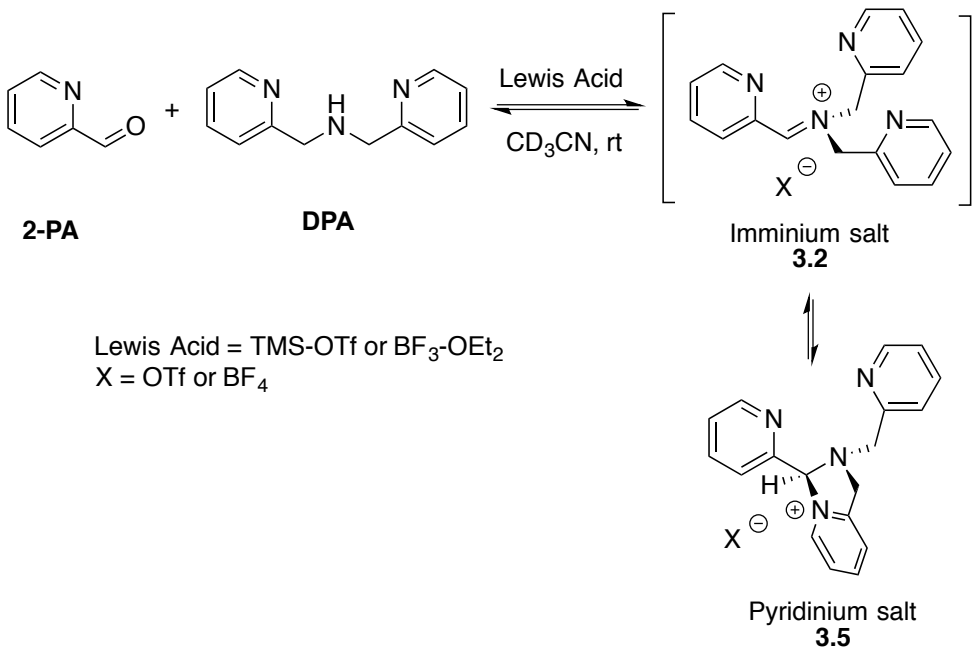

Figure 3.4: Lewis acid assisted condensation and formation of a pyridinium salt. The cyclization of **3.2** to **3.5** is 5-endo-trig, and thus not strictly allowed by Baldwin's rules.

In an NMR tube, upon the addition of one equivalent of TMS-OTf or BF_3-OEt_2 to a mixture of 2-PA and DPA in CD_3CN (60 mM), resonances for a new product along with unreacted 2-PA were observed. The ^1H NMR spectrum was not consistent with **3.2** as the product, because two inequivalent CH_2-groups were formed and the hydrogens on each CH_2 were diastereotopic (see section 3.4). When excess BF_3-OEt_2 (more than 2 equiv.) was used to push the addition of DPA to completion in acetonitrile, a yellow precipitate was isolated at 0 °C. The precipitate was separated and crystals were grown by slow diffusion of diethyl ether into a solution of the yellow solid in acetonitrile at 0 °C. X-ray diffraction analysis revealed pyridinium salt **3.5**.

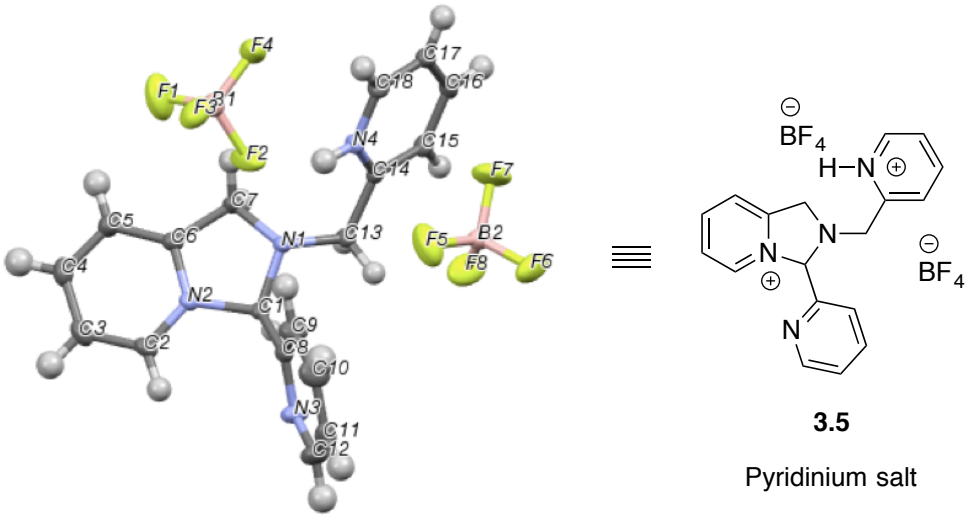

Figure 3.5: X-ray structure of pyridinium salt **3.5** created from 2-picolinaldehyde, dipicolylamine and excess BF_3-OEt_2.

However, the addition of water or alcohol and $Zn(OTf)_2$ to the pyridium salt **3.5** did not produce good yields of the hemi-aminal **3.1** or hemi-aminal ether **3.3**, respectively. Instead, a myriad of additional un-isolable products were created. Therefore, although while pyridinium salt **3.5** can be isolated, it must not in actuality be the correct intermediate formed in the assembly. We interpret this evidence as supporting iminium **3.2** as the true intermediate that reacts with water or an alcohol to create **3.1** or **3.3**, respectively. One rationalization for these results stem from Baldwin's rules.[30,31] The cyclization of **3.2** to **3.5** is 5-endo-trig, which is forbidden by these rules. A second rationalization comes from the expected lifetime of an iminum in the presence of water. For example, in water as the solvent, iminium ions have lifetimes on the order of only picoseconds.[32-35] Hence, irrespective of the intramolecularity of the pyridine, only in the absence of an external water or alcohol nucleophile does the cyclization occur. Apparently, in the presence of these nucleophiles, their intermolecular addition outcompetes the intramolecular addition of pyridine.

3.2.3 Kinetics

As described above, the three-component assembly readily forms the hemi-aminal complex **3.1**, and with the assistance of a Brønsted acid catalyst, it will create the hemi-aminal ether **3.3** in the presence of an alcohol. Therefore, to explore the mechanism of formation of **3.3**, it was most convenient to start with preformed **3.1**. A plausible mechanism for the creation of **3.3** is given in Figure 3.6. It starts with loss of Zn(II) from the tren-like ligand, followed by acid catalyzed elimination of water to create **3.2**. Given that **3.2** is the highest energy species along the sequence, either of the two steps prior to formation of **3.2** could be rate-determining. Thus, we set out to determine if loss of metal or elimination of water is the slow step leading to **3.2**.

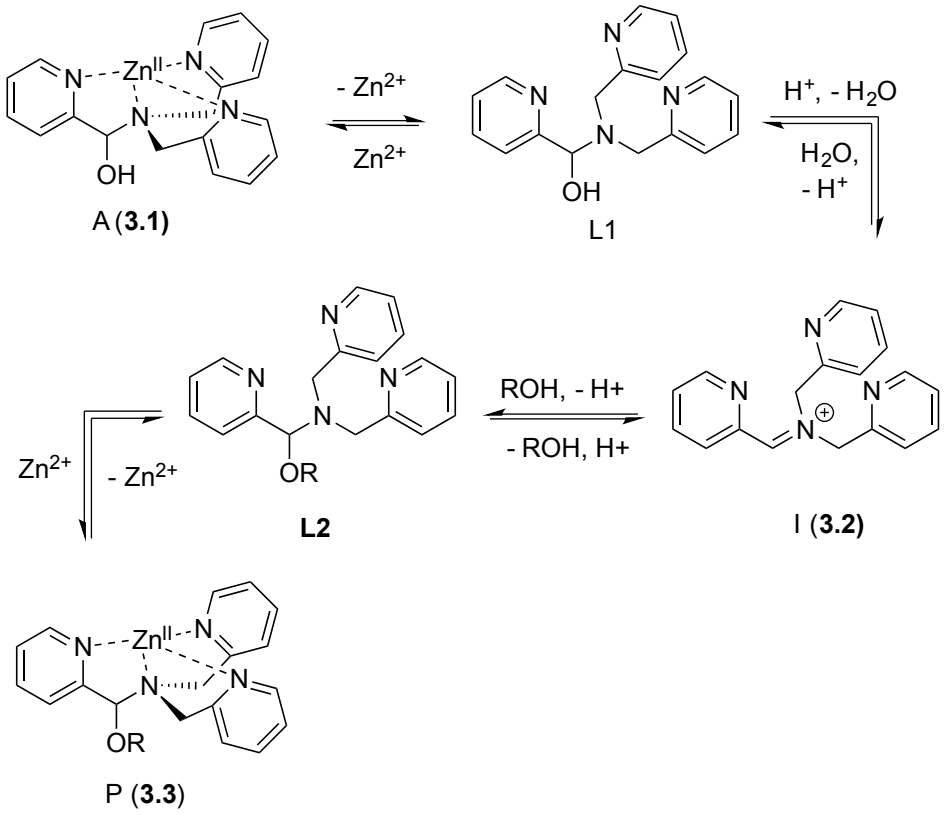

Figure 3.6: Proposed pathway for interconverion of **3.1** and **3.3**.

As shown in Figure 3.7, the two steps leading to the intermediate can be combined to simplify the mathematical analysis, although either of the two steps could be rate limiting. The

form of the rate expression predicts a second order reaction at low concentrations of alcohol (first order in **3.1** and alcohol). To test this dependence, we analyzed the reaction as first order in **3.1** and zero-order in alcohol using three equivalents of alcohol (and no molecular sieves). The standard plot of ($\ln\{[A]_o / ([A]_o - [P])\}$) versus time exhibited a trend with significant curvature (Figure 3.8), therefore not conforming to first order kinetics. However, the rate expression predicts that the reaction should become increasingly first order in **3.1** and zero-order in alcohol as the alcohol concentration increases. The mechanism is analogous to an S_N1 reaction, where at high concentrations of nucleophile, a zero order dependence of nucleophile is the norm. As seen in Figure 3.8, the kinetic plot becomes increasingly linear, and at 18 or more equivalents of alcohol, the plot conforms nicely to pseudo-first order kinetics. Under these conditions the concentration of alcohol is large enough to compete with any residual water or water released during the reaction. The rate constant k_{-1} is predicted to be larger than k_2 due to a larger nucleophilicity of water relative to alcohols, accounted by water's smaller size.[36] Thus, it takes an excess of alcohol to cause the rate expression to simplify to first order in **3.1** only. When 2 equivalents of water were added at this high concentration of alcohol, the rate drops drastically and the reaction loses first order behaviour, analogous to the common ion effect in an S_N1 reaction.[37]

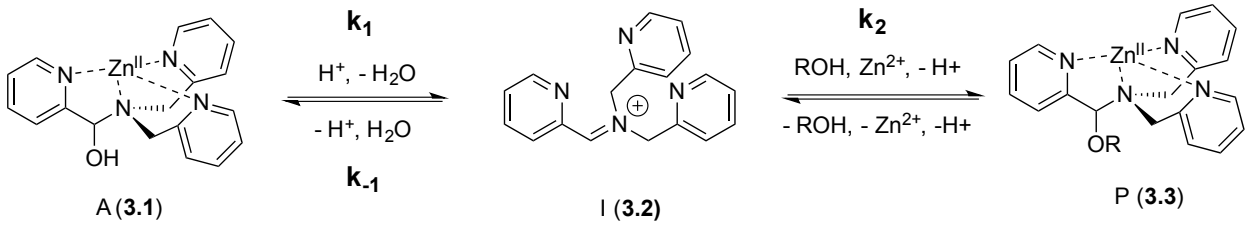

$$\frac{d[P]}{dt} = \frac{k_1 k_2 [\mathrm{A}][\mathrm{ROH}]}{k_{-1}[\mathrm{H_2O}] + k_2[\mathrm{ROH}]}$$

Figure 3.7: Simplified mechanism and associated rate equation.

This kind of kinetics is referred to as saturation kinetics, and it is indicative of a pre-equilibrium prior to the formation of a high energy intermediate that then reacts with the alcohol. Taking the values of the initial slopes in Figure 3.8, where the concentration of alcohol was the only variable, leads to the graph shown in Figure 3.9. Zero order dependence of alcohol in the reaction was verified as a plateau in this plot. The experiments given above, however, do not distinguish as to whether the loss of Zn(II) or the loss of water is the slow step leading to the intermediate.

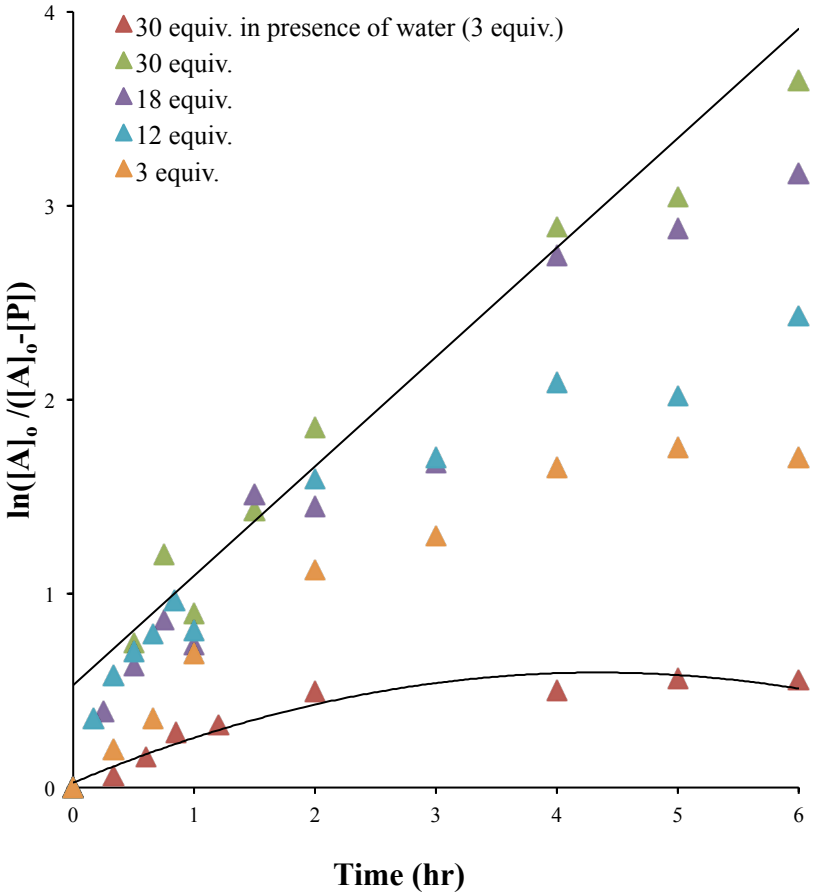

Figure 3.8: A plot of $\ln([A]_o/([A]_o-[P])$ versus time as a function of the equivalents of alcohol. **A** is hemi-aminal **3.1** and **P** is **3.3**. (All experiments: 35 mM of 2-PA and Zn(II) were used for the assembly reaction).

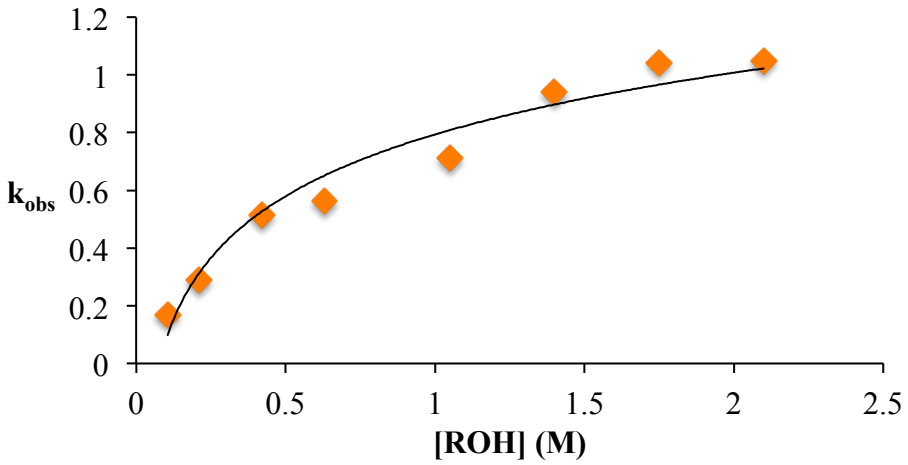

Figure 3.9: The variation in k_{obs} as a function of the starting concentration of alcohol. Concentration of 2-PA was 35 mM for all experiments.

The mechanism given in Figure 3.6 has analogous steps leading to the intermediate, either starting from reactant **3.1** or product **3.3**. The difference is the departure of water or departure of alcohol directly before formation of intermediate **3.2**. The rate of departure of water is predicted to be slower than that of alcohol departure due to the increased stability of the hemi-aminal over the hemi-aminal ether, as revealed from the equilibrium constant measured (see above). However, the difference in the rate of loss of Zn(II) from either the hemi-aminal **3.1** or the hemi-aminal either **3.3** is likely minimal. Thus, in order to reveal whether metal loss or leaving group departure is the slow step in formation of the intermediate(s), we followed the time course for the forward and reverse reactions during the initial period of the transformations. The reactions involve the addition of alcohol to **3.1** or water to **3.3**. All experiments were performed with the concentration of 2-PA being 0.035 M, and alcohol or water fixed at 0.175 M. By fitting a linear line to the first 10% of reaction, we were able to estimate rate constants of the two reactions. We find rate constants that are approximately the same (0.30 hr^{-1} *vs* 0.35 hr^{-1}). This was the first experiment that indicated that the rate-determining step in hemi-aminal to hemi-aminal ether is loss of the metal.

Although the forward and reverse rate constants are approximately the same, thereby indicating that the rate-determining steps for the forward and reverse reactions are both likely

due to the loss of Zn(II), it is true that the rate from hemi-aminal ether back to hemi-aminal is slightly faster. This is to be predicted because an ROH is anticipated to be a better leaving group. Thus, we sought even stronger evidence that the loss of Zn(II) is rate-determining, and therefore we performed a Hammett linear free energy analysis.

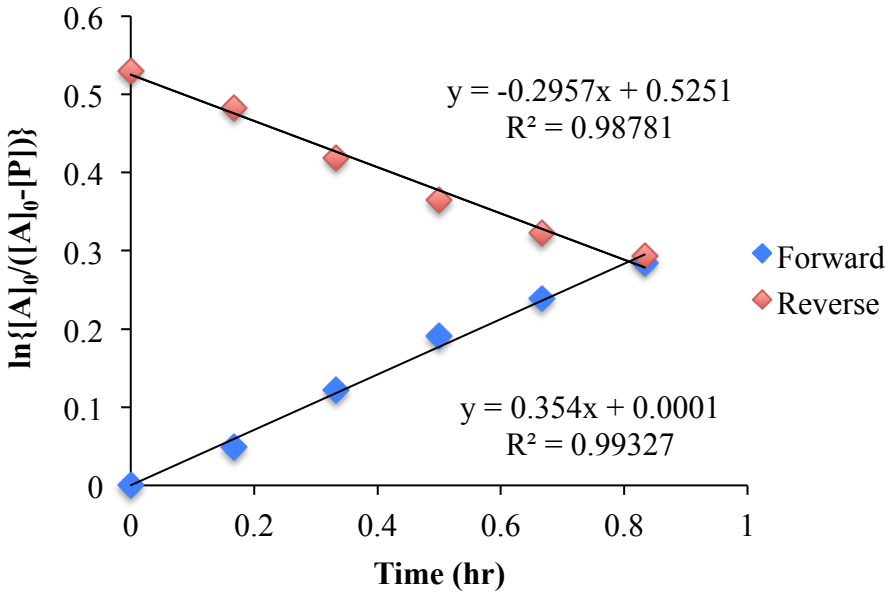

Figure 3.10: A plot of *ln* $[A]_o/[A]$ *vs* time in forward and reverse reactions only over the first 10% of reaction.

3.2.4 Hammett Analysis

To further explore the reaction mechanism a Hammett plot was generated. By plotting the $\log(k_X/k_H)$ values for various substituted 2-PA's versus the sigma (σ) electronic substituent constant, we constructed a Hammett plot. Hammett plots are informative because they show how reaction mechanisms vary as a function of the electronic changes induced by substituents.[38]

A series of 2-pyridinecarboxaldehyde derivatives bearing electron-donating or electron-withdrawing substituents that are para to the aldehyde were investigated for the reaction of **3.1** to **3.3** using 4-penten-2-ol as the alcohol (Figure 3.11 and 3.12). From the Hammett plot (log (k_X/k_H) versus sigma[39]), rho was obtained as the slope. Rho describes the sensitivity of the reaction to substituent effects. The calculated rho value from the graph is positive. This leads to

the conclusion that negative charge is building during the rds of the assembly, or alternatively, there is a loss of positive charge.

A)

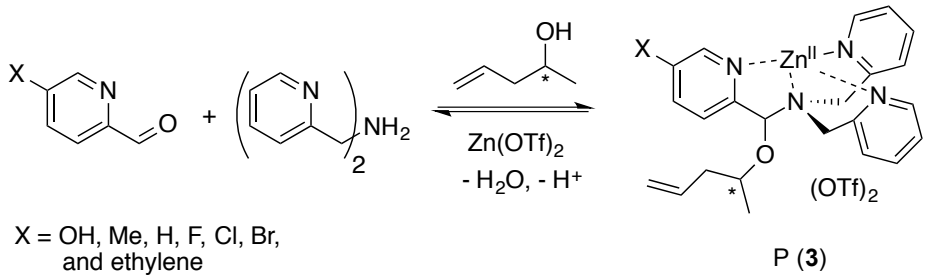

X = OH, Me, H, F, Cl, Br, and ethylene

P (**3**)

B)

X	σ_{para}	log (k_X/k_H)
OH	-0.38	-0.21
Me	-0.14	-0.062
H	0	0
F	0.15	0.15
ethylene	0.23	0.13
Cl	0.24	0.17
Br	0.26	0.16

Figure 3.11: A) Four-component covalent assembly reactions with various R-X structures. B) σpara values[38,39] and corresponding log (k_X/k_H) values for encountered substituents.

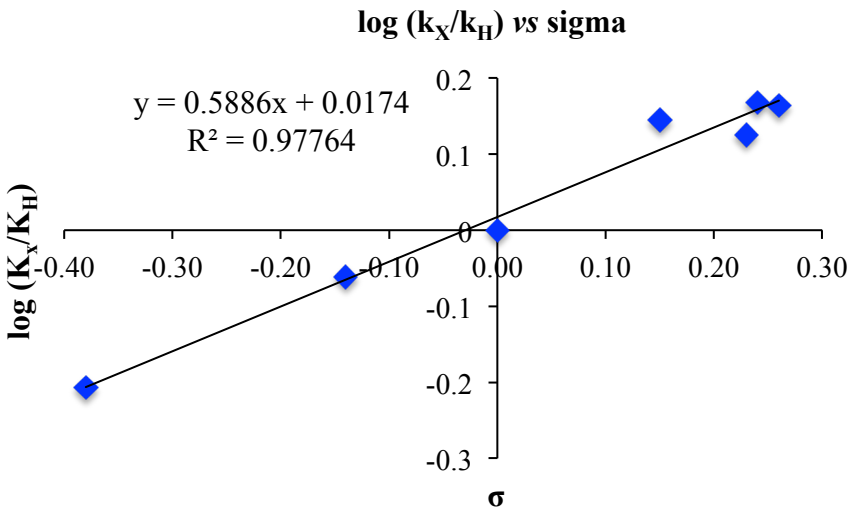

Figure 3. 12: Hammett plot for four-components assembly with para substituted 2-picolinaldehyde.

The two possible rate-determining steps for the formation of intermediate **3.2** either involve loss of the Zn(II) cation or formation of a positive iminium, respectively. Loss of a cation is analogous to increased negative charge, whereas formation of an iminium involves creation of a positive charge. Because a positive rho value was found, this supports loss of Zn(II) as the rds in the conversion of **3.1** to **3.3**, as was also supported by the fact that the forward and reverse reaction rate constants of Figure 3.7 are basically the same.

A Hammett plot using σ+ was also generated (see section 2.4). Such a Hammett plot includes resonance, whereas σ primarily reflects induction. The plot using σ^+ contained significantly more scatter, with a R^2 value of 0.84 compared to the normal Hammett plot (R^2 of 0.977). This is in further accordance with our conclusion that the rds is the loss of Zn(II). If the rds was the loss of water, instead, we would predict a better Hammett plot with σ^+, because **3.2** is stabilized via direct resonance with the substituents. However, the substituents primarily affect metal chelation via induction.

3.2.5 Proposed Mechanism

The experiments described above allow one to create a qualitative reaction coordinate diagram (Figure 3.13) for the interconversion of **3.1** (**A**) and **3.3** (**P**). First, because the

equilibrium constant for the reaction is less than 1, the energy of **A** and alcohol is placed lower than **P** and water (ΔG^o). Second, because the loss of Zn(II) from **A** and **P** was found to have similar rate constants, the barriers leading from **A** and **P** to **L1** and **L2**, respectively, are placed the highest on the diagram and their activation energies are comparable ($\Delta G_1^{\ddagger} = \Delta G_2^{\ddagger}$). Next, we place intermediate **I** in the center of the diagram, which our results support as being **3.2** rather than **3.5**. Third, because water is a better nucleophile than an alcohol, the barrier from **I** to **L1** ($\Delta G_{L1}^{\ddagger}$) is drawn lower than the barrier of **I** to **L2** ($\Delta G_{L2}^{\ddagger}$). The remaining question involves the relative energies of **L1** and **L2**, and whether their energy difference is similar to the difference in their activation energies to achieve **I**. However, we postulated above that the bond strengths between OH and OR in **A** and **P** likely do not change significantly whether or not Zn(II) is bound. Thus, as a fourth point, the energy difference between **L1** and **L2** should be similar to that between **A** and **P**. This reasoning led to the qualitative placement of **L1** and **L2** on the diagram. The third and fourth insights used here to generate the reaction coordinate diagram also led to the conclusion that the activation energy used to create **I** from **L1** is higher than from **L2** to **I**. This is consistent with the notion that an alcohol is a better leaving group than water.

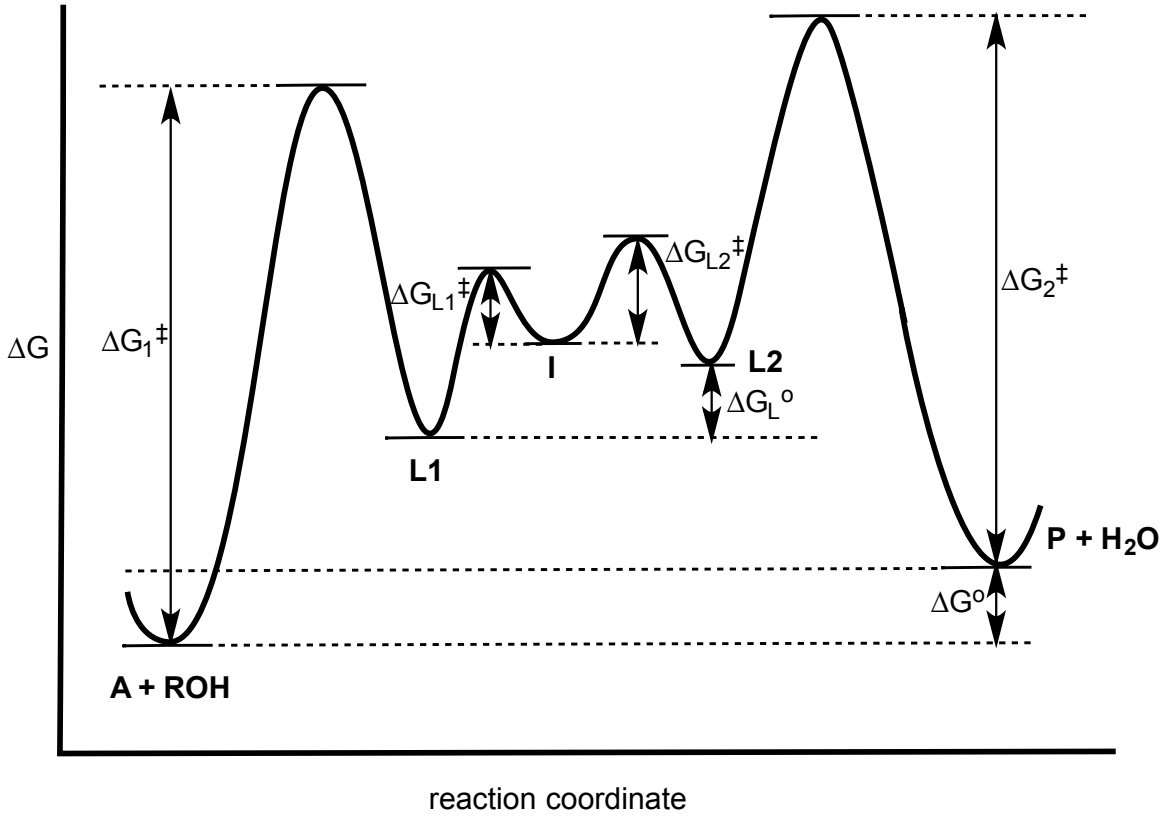

Figure 3.13: Hypothesized reaction coordinate diagram for the multi-component assembly reaction. See Figure 3.6 for identities of **A**, **L1**, **L2**, **I** and **P**.

3.3 Concluding Remarks

Mechanistic studies of the four-component assembly involving 2-PA, DPA, Zn(II), a secondary alcohol, and catalytic acid revealed several insights. First, the equilibrium lies toward hemi-aminal **3.1**, and thus the creation of a high yield of **3.3** requires molecular sieves. Further, the reaction can be driven toward **3.3** via the use of excess alcohol. Attempts to isolate the previously postulated iminium **3.2** instead led to the isolation of a pyridinium salt **3.5**. Yet, **3.5** does not produce the correct products and its formation is not allowed via Baldwin's rules, and thus **3.5** must form slower than the reaction of **3.2** with water or alcohols. The transformation of **3.1** to **3.3** is first order in **3.1** and zero order in alcohol only at high alcohol concentration, thus showing saturation kinetics in alcohol, analogous to an S_N1 reaction. This supports the creation of a high-energy intermediate that reacts in a fast step with alcohol. The rate-determining step in the formation of this intermediate is not the acid-catalyzed expulsion of

water, but rather the decomplexation of Zn(II) from the assembly. This conclusion is supported both by the fact that the forward and reverse rate constants for interconversion of **3.1** and **3.3** are essentially the same, and by a positive Hammett rho value that supports loss of positive charge in the rds. The mechanistic insights given herein should be informative for other dynamic reactions involving interconversions of hemi-aminals to hemi-aminal ethers.

3.4 Additional and Experimental Information

3.4.1 General Information

NMR spectra were recorded on Agilent MR 400 at The University of Texas at Austin NMR facility. ESI-mass spectra were obtained on Agilent 6100 at The University of Texas at Austin mass spectrometry facility. Circular dichroism (CD) spectra were recorded on a Jasco J-815 spectropolarimeter at The University of Texas facility.

3.4.2 General Procedures for Multi-component Assembly

All assembly reactions for kinetics and LEFR studies were performed *in situ* in acetonitrile without isolation and purification. Pyridine-2-carboxyaldehyde (**2-PA**, 35 mM, 1 equiv.), zinc triflate ($Zn(OTf)_2$, 35 mM, 1 equiv.), di-(2-picolyl)amine (**DPA**, 42mM, 1.2 equiv.), 4-penten-2-ol (ROH, 175 mM, 5 equiv. except for the alcohol dependence studies), and 4-(2-chloroethyl)morpholine hydrochloride (CEM-HCl, 35 mM, 1 equiv.) were stirred together in acetonitrile in the presence of 3Å activated molecular sieves. The mixture was stirred at room temperature.

3.4.3 Synthesis of Pyridinium Salt (3.5)

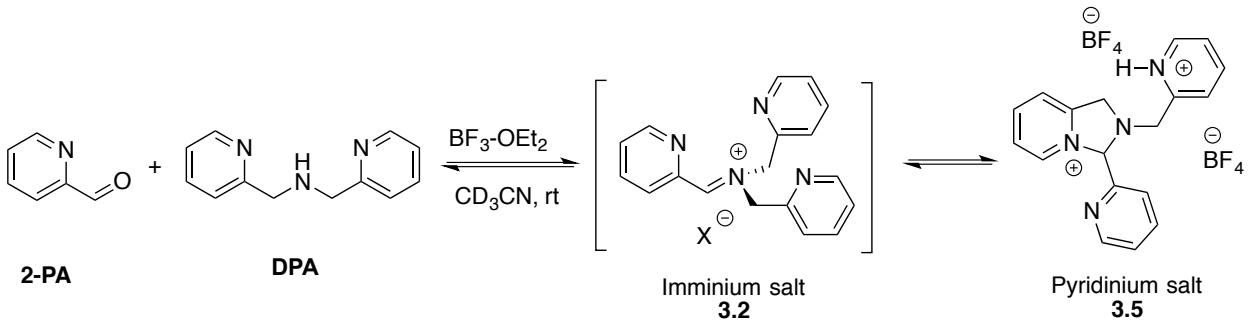

To pyridine-2-carboxaldehyde (**2-PA**, 3.21 mg, 0.03 mmol) in dry CD_3CN solution (60 mM), dipicolylamine (**DPA**, 7.17 mg, 0.036 mmol) was added. Then, BF_3-OEt_2 (5.11 µL, 0.036 mmol) was added dropwise. The reaction mixture was shaken for 3–5 min and then ^1H NMR, ^{13}C NMR, and mass spectrum were recorded.

3.4.4 Hammett Plot using σ^+

X	K_{eq}	σ^+	log (k_X/k_H)
OH	16.9	-0.92	-0.21
Me	23.6	-0.31	-0.062
H	27.2	0	0
F	38.0	-0.07	0.14
alkyne	36.3	-	0.13
Cl	40.1	0.11	0.17
Br	39.7	0.15	0.16

Table 3.2: σ^+ values and corresponding log (k_X/k_H) values for encountered substituents.

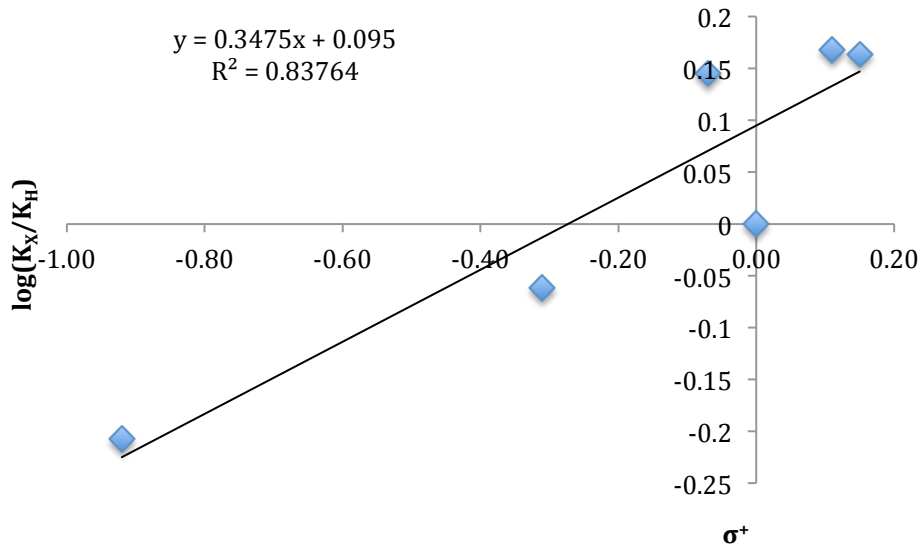

Figure 3.14: Hammett plot (σ^+) for four-component assembly with para substituted **2-PA**.

3.4.5 Spectrometry and Spectroscopy

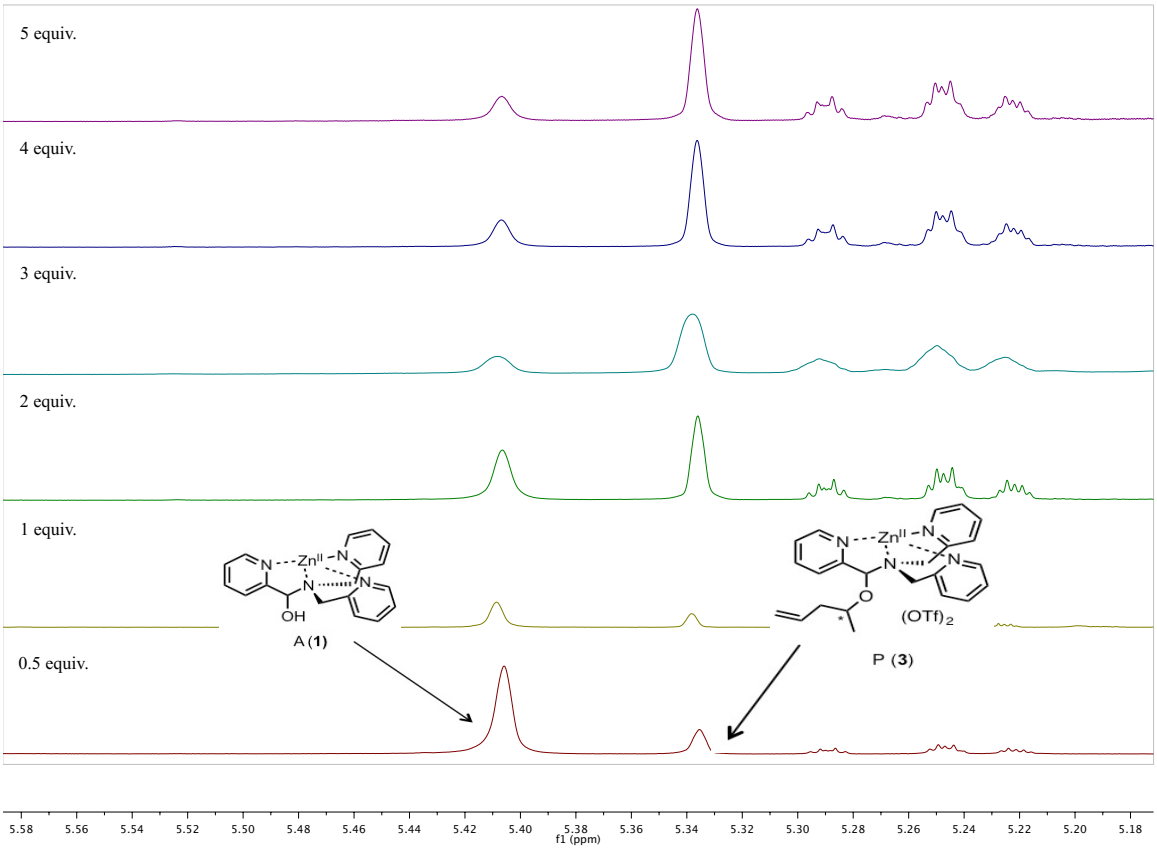

Figure 3.15: ^{1}H NMR of multi-component assembly varying the concentration of alcohol from 17.5 mM (0.5 equiv.) to 210 mM (6 equiv.). For alcohol, 4-penten-2-ol was chosen for all kinetic studies.

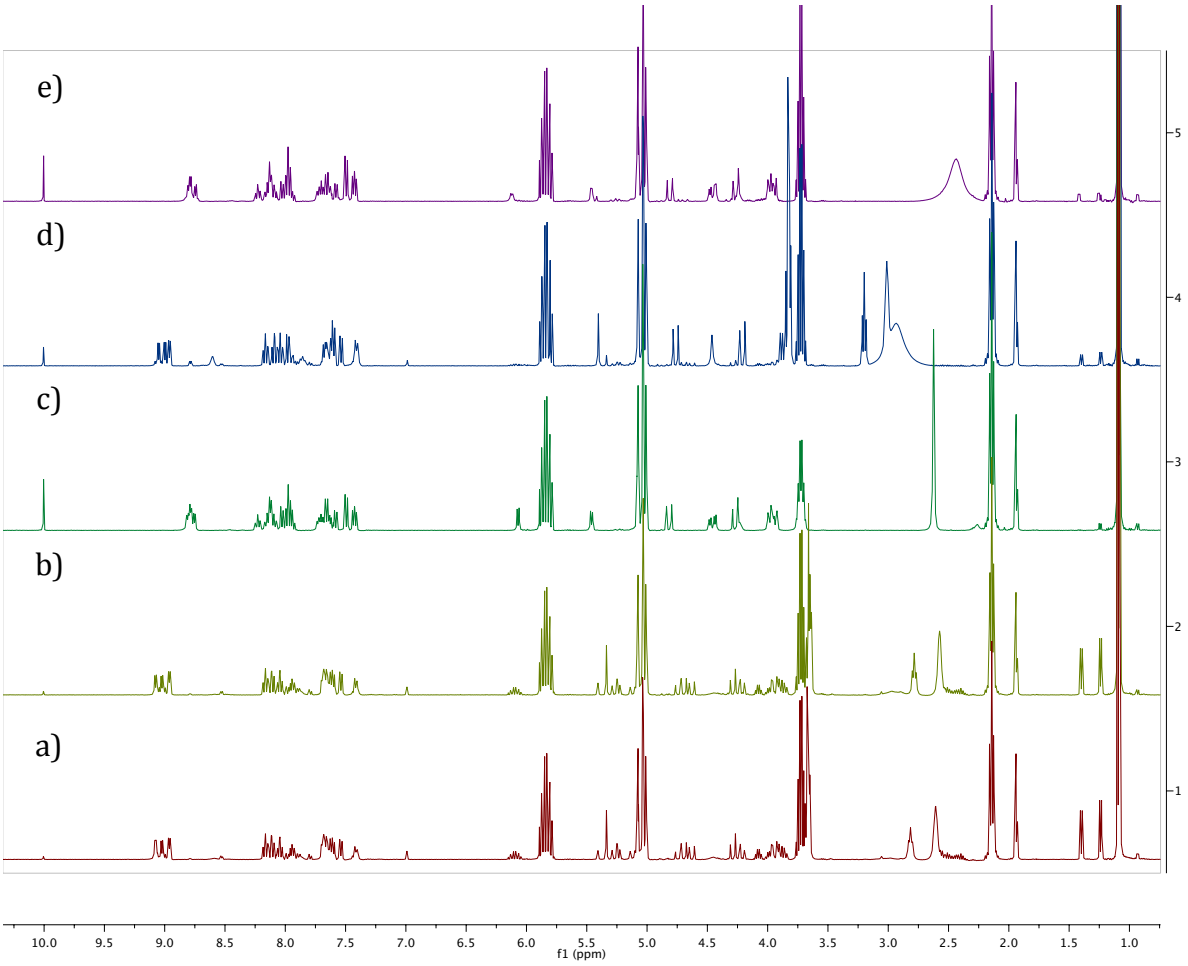

Figure 3.16: ^{1}H NMR of multi-component assembly varying the presence of molecular sieves and Brønsted acid (CEM-HCl). Concentration of alcohol (4-penten-2-ol) in CD_3CN is 175 mM (5 equiv.), 2PA is 35 mM (1 equiv.), DPA is 42 mM, and CEM-HCl is 35 mM. a) With the presence of two molecular sieves and brønsted acid b) With the presence of four molecular sieves and brønsted acid c) With the presence of four molecular sieves and without brønsted acid d) Without any molecular sieves but with the presence of brønsted acid e) Without either molecular sieves or brønsted acid.

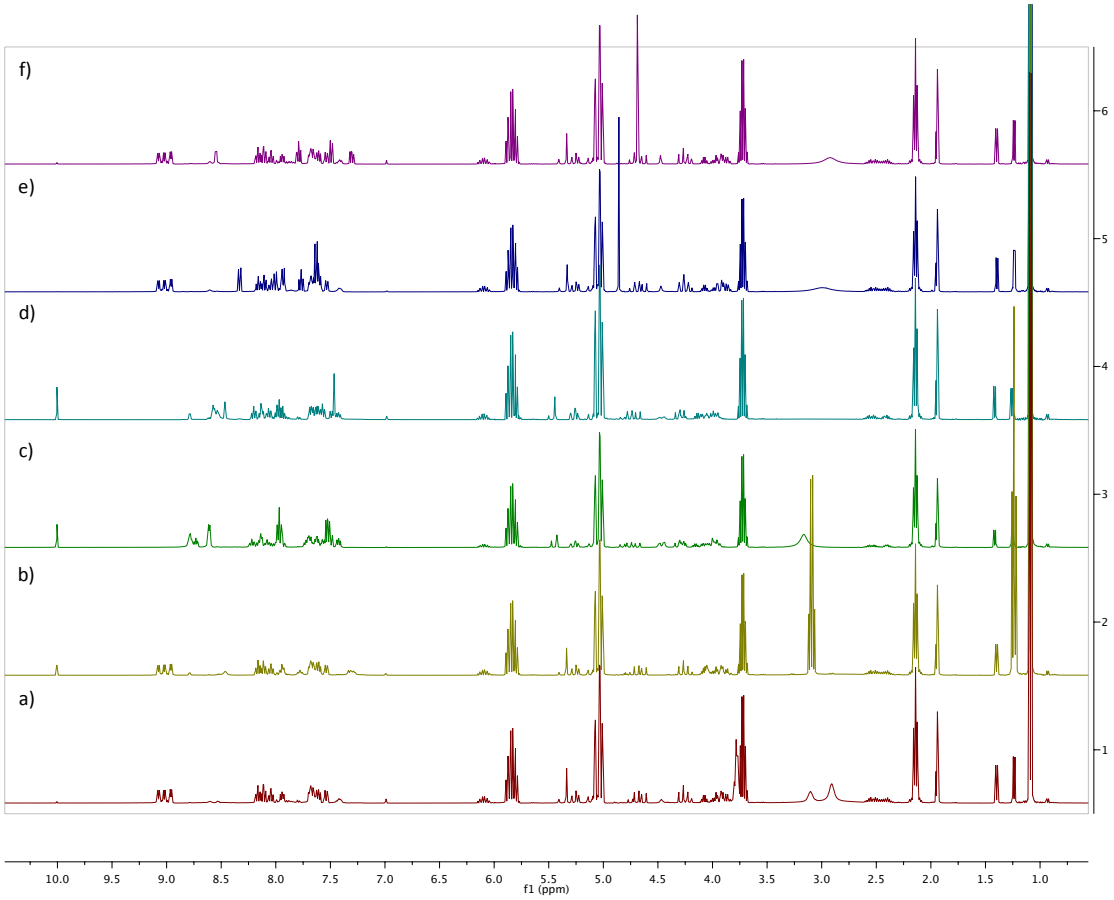

Figure 3.17: ^{1}H NMR of multi-component assembly varying Brønsted acids. Concentration of alcohol (4-penten-2-ol) in CD_3CN is 175 mM (5 equiv.), 2PA is 35 mM (1 equiv.), DPA is 42 mM, and brønsted acid is 35 mM. a) CEM-HCl (84.1% alcohol incorporation) b) tri-ethylammonium hydrochloride (75.0%) c) pyridinium triflate (46.8%) d) imidazolium triflate (60.7%) e) 2-chloromethylquinole hydrochloride (83.8%) e) 2-picolyl chloride hydride (80.1%) f) 4-picolyl chloride hydrochloride (80.5%).

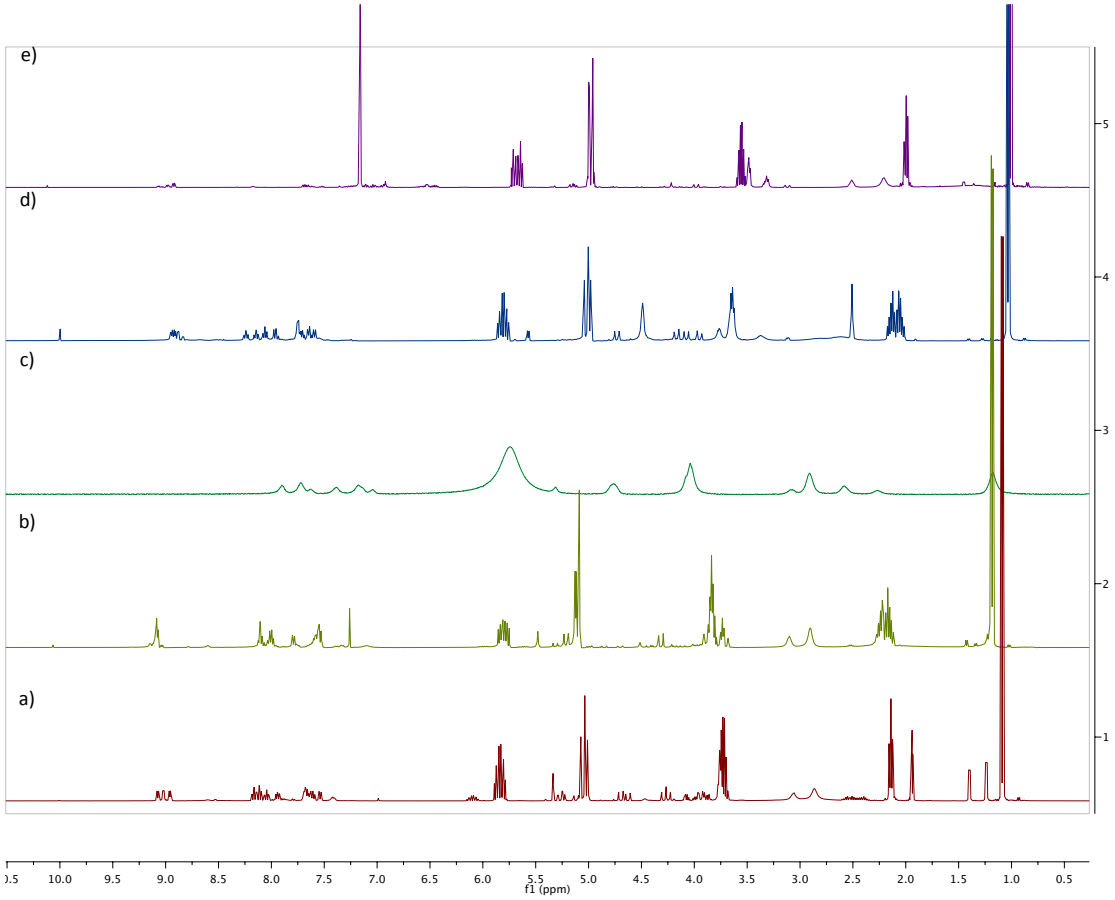

Figure 3.18: ^{1}H NMR of multi-component assembly varying solvents. Concentration of alcohol (4-penten-2-ol) in corresponding deuterated solvent is 175 mM (5 equiv.), 2PA is 35 mM (1 equiv.), DPA is 42 mM, and brønsted acid is 35 mM. a) CD_3CN (84.5% alcohol incorporation), and no alcohol incorporation observed in b) $CDCl_3$, c) CD_2Cl_2, d) *d*-DMSO and e) C_6D_6.

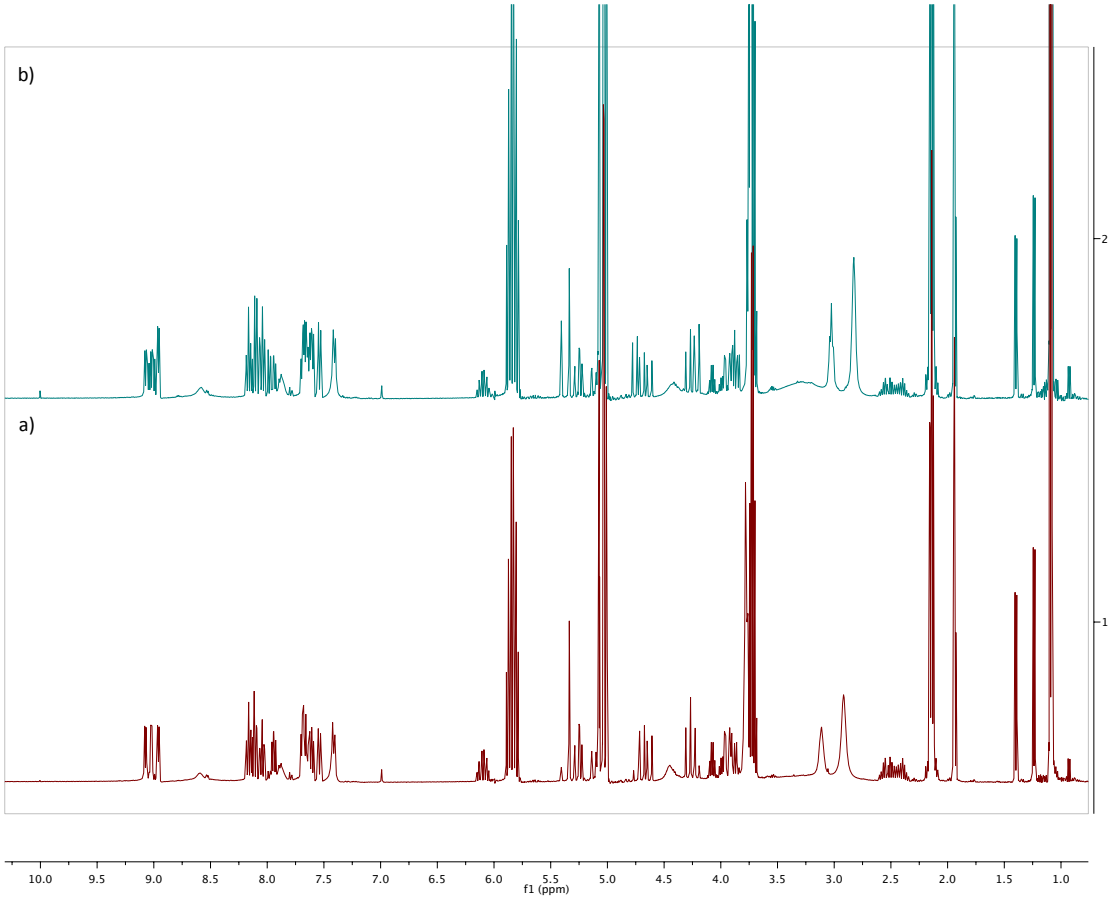

Figure 3.19: ^{1}H NMR of multi-component assembly to see the reversibility within the system in presence of molecular sieves. Concentration of alcohol (4-penten-2-ol) in CD_3CN is 175 mM (5 equiv.), 2PA is 35 mM (1 equiv.), DPA is 42 mM, and brønsted acid is 35 mM. a) after 22 hrs at r.t (89.2% alcohol incorporation) b) the addition of water (2.52uL, 5 equiv.) to a) and stirred overnight (alcohol incorporation decreased to 57.2%).

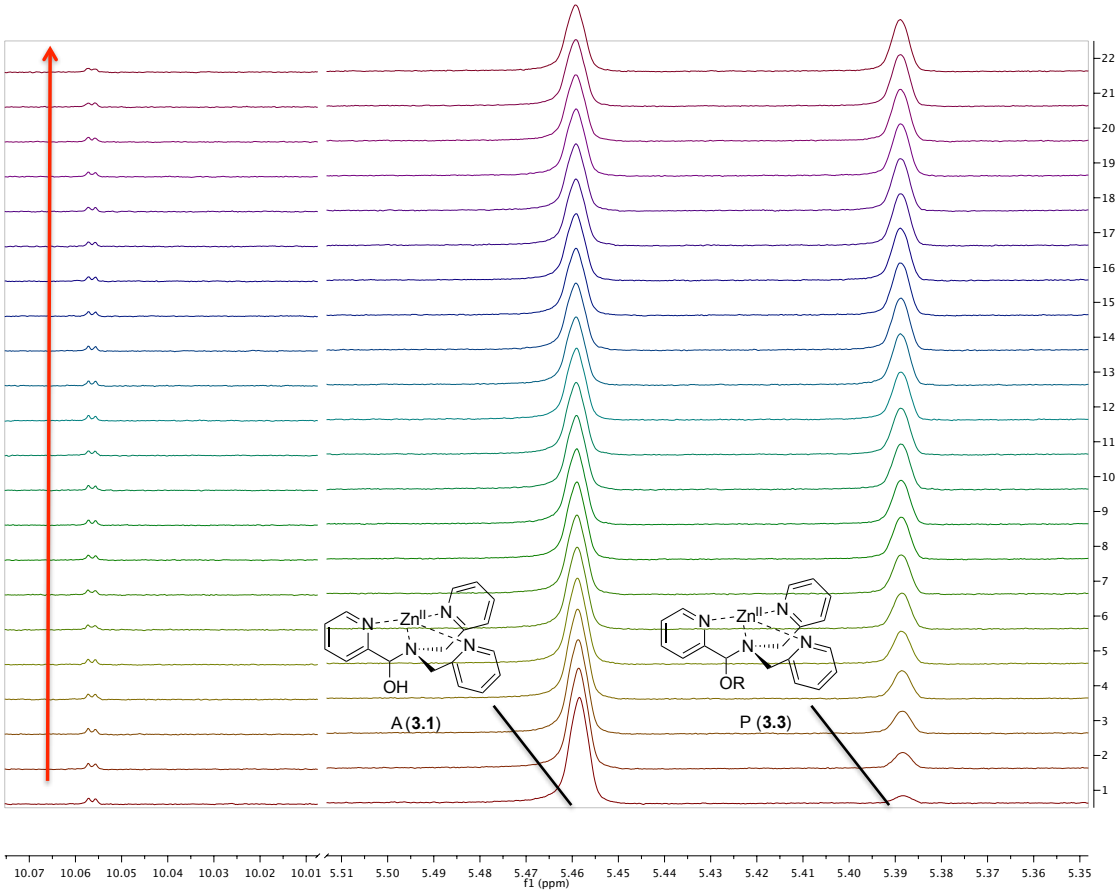

Figure 3.20: ^{1}H NMR spectra of multi-component assembly taken every 10 minutes for the first two hours (12 spectra) and then every hour for the next 10 hours in absence of the molecular sieves. Concentration of alcohol (4-penten-2-ol) in CD_3CN is 175 mM (5 equiv.), 2PA is 35 mM (1 equiv.), DPA is 42 mM, and Brønsted acid is 35 mM. The arrow indicates the direction of increasing reaction time. The alcohol incorporation is 4.7% after 10 mins (the bottom spectrum) and increased in yield up to 41.2% after 12 hours (the top spectrum).

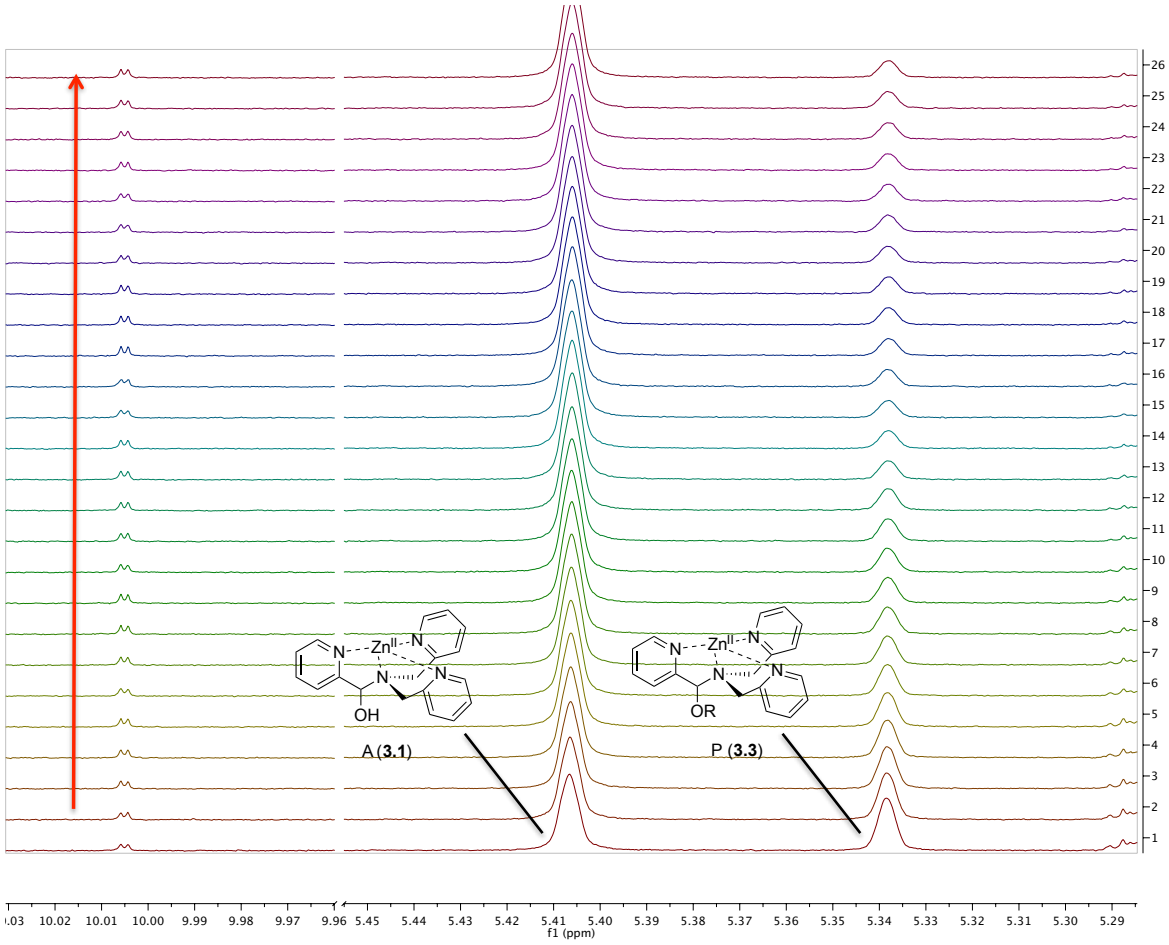

Figure 3.21: ^{1}H NMR spectra of multi-component assembly taken every 10 minutes for the first two hours (12 spectra), then every hour for the next 10 hours after the addition of H_2O into the assembly in the absence of the molecular sieves. Concentration of alcohol (4-penten-2-ol) in CD_3CN is 175 mM (5 equiv.), 2PA is 35 mM (1 equiv.), DPA is 42 mM, and Brønsted acid is 35 mM. The arrow indicates the direction of increasing reaction time. The alcohol incorporation is 38.2% after 10 mins (the bottom spectrum) and decreased in yield down to 13.0% after 16 hours (the top spectrum).

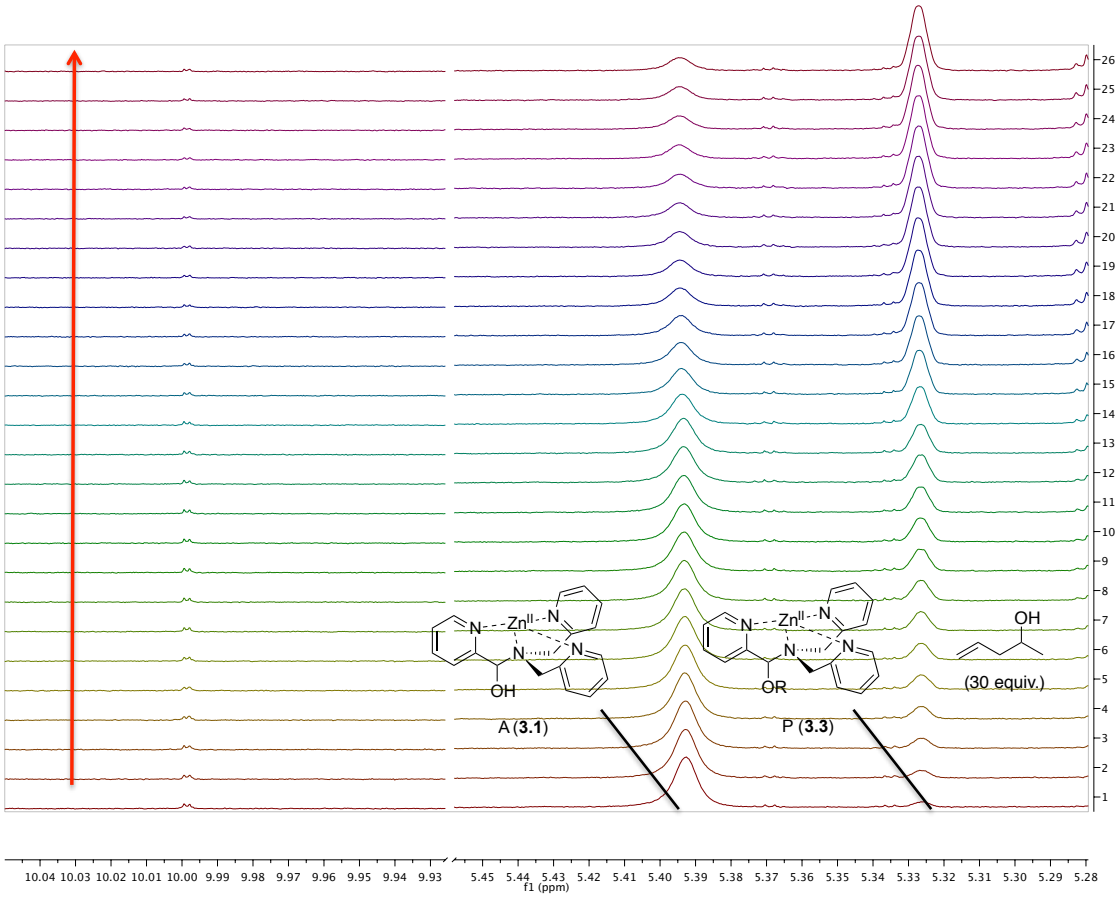

Figure 3.22: ^{1}H NMR spectra of multi-component assembly taken every 10 minutes for the first two hours (12 spectra), then every hour for the next 10 hours in the absence of the molecular sieves. Concentration of alcohol (4-penten-2-ol) in CD_3CN is 1050 mM (30 equiv.), 2PA is 35 mM (1 equiv.), DPA is 42 mM, and Brønsted acid is 35 mM. The arrow indicates the direction of increasing reaction time. The alcohol incorporation is 9.0% after 10 mins (the bottom spectrum) and increased in yield up to 72.6% after 12 hours (the top spectrum).

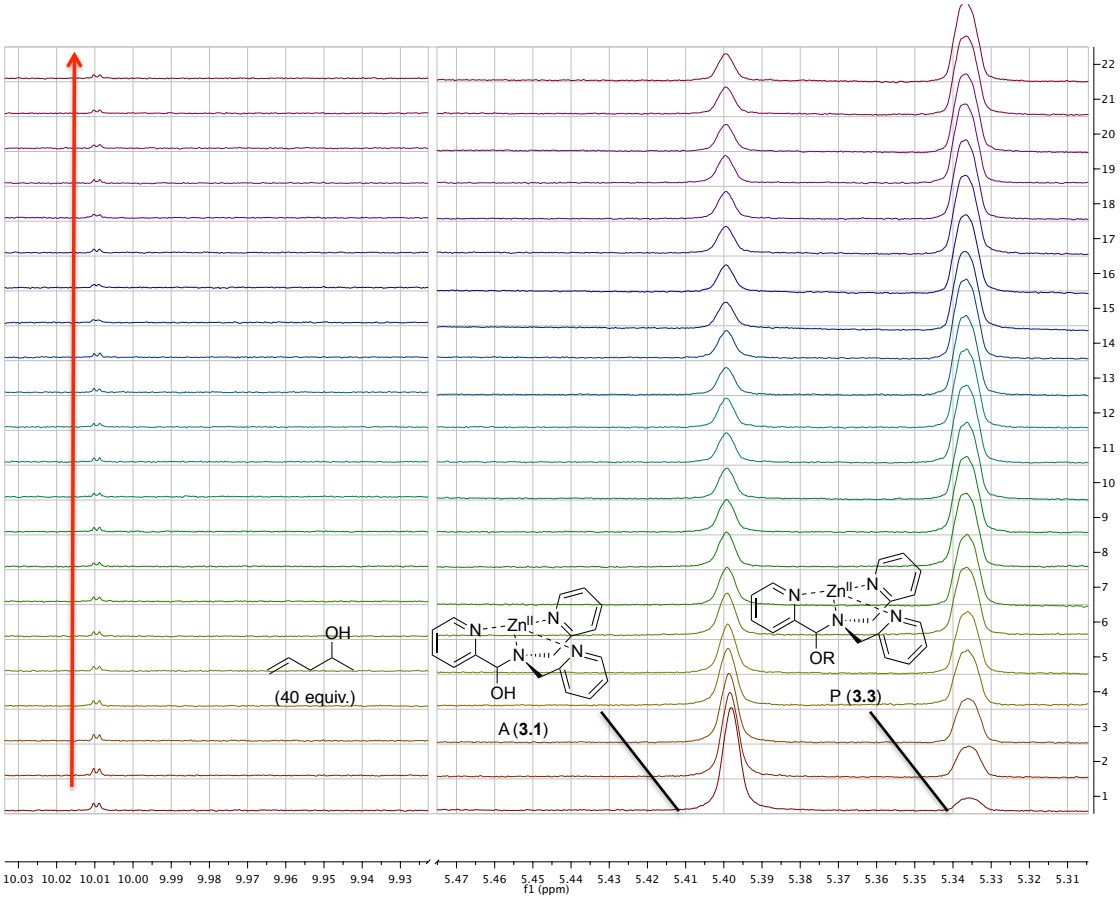

Figure 3.23: ^{1}H NMR spectra of multi-component assembly taken every 10 minutes for the first two hours (12 spectra), then every hour for the next 10 hours in the absence of the molecular sieves. Concentration of alcohol (4-penten-2-ol) in CD_3CN is 1400 mM (40 equiv.), 2PA is 35 mM (1 equiv.), DPA is 42 mM, and Brønsted acid is 35 mM. The arrow indicates the direction of increasing reaction time. The alcohol incorporation is 13.7% after 10 mins (the bottom spectrum) and increased in yield up to 79.6% after 12 hours (the top spectrum).

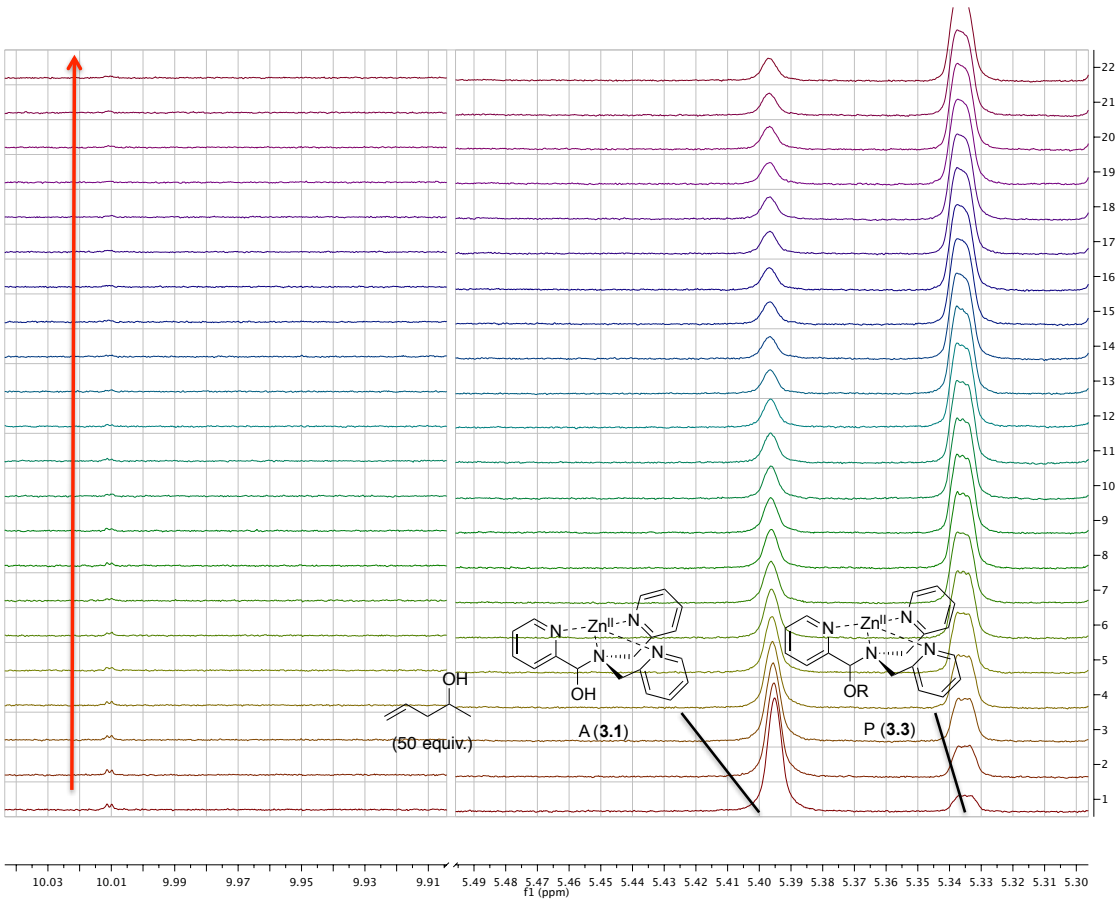

Figure 3.24: ^{1}H NMR spectra of multi-component assembly taken every 10 minutes for the first two hours (12 spectra) and then every hour for the next 10 hours in absence of the molecular sieves. Concentration of alcohol (4-penten-2-ol) in CD_3CN is 1750 mM (50 equiv.), 2PA is 35 mM (1 equiv.), DPA is 42 mM, and Brønsted acid is 35 mM. The arrow indicates the direction of increasing reaction time. The alcohol incorporation is 13.4% after 10 mins (the bottom spectrum) and increased in yield up to 87.2% after 12 hours (the top spectrum).

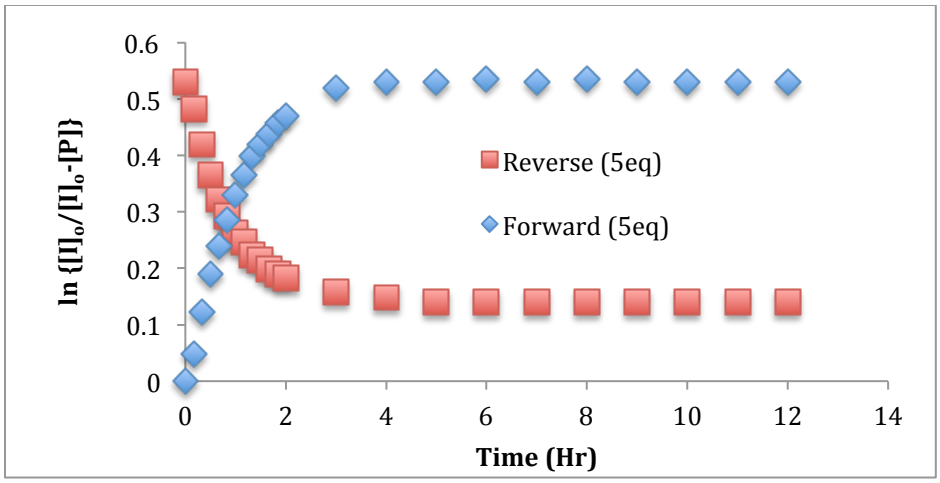

Figure 3.25: A plot of ln $[A]_o/[A]$ *vs* time in forward and reverse reactions until the reaction reach equilibria. Data points obtained from integrals in ^{1}H NMR spectra.

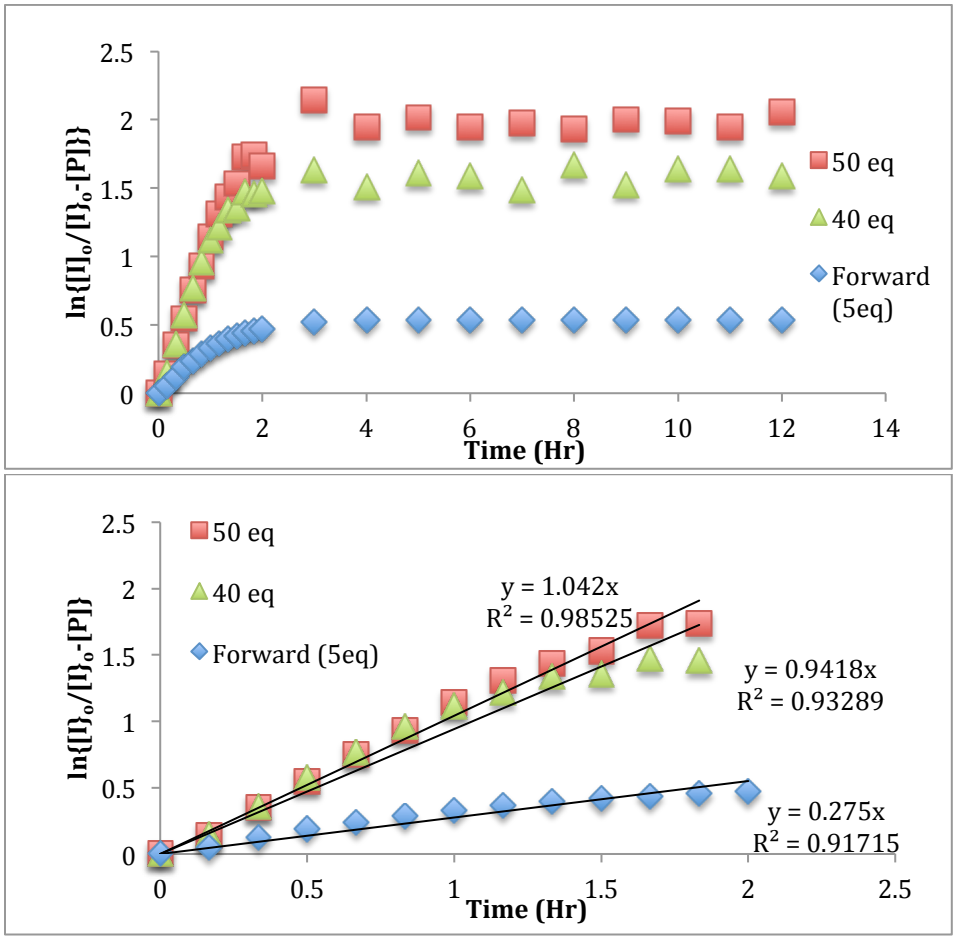

Figure 3.26: Top: A plot of ln $[A]_o/[A]$ *vs* time varying concentration of alcohol in the assembly. Bottom: Same only over the first 10% of reaction. Data points obtained from integrals in ^{1}H NMR spectra.

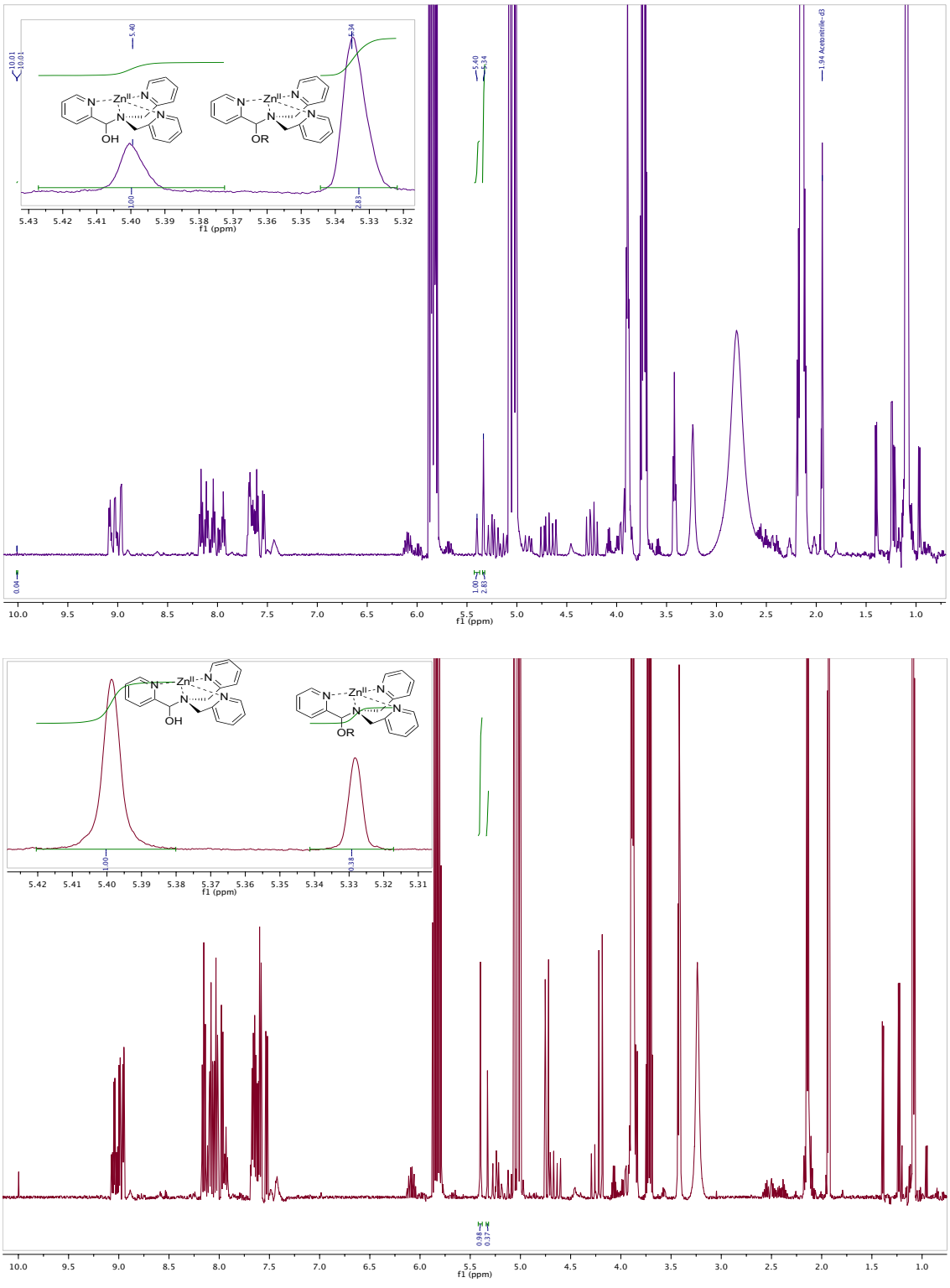

Figure 3.27: ^{1}H NMR spectra of multi-component assembly in equilibrium with 30 equiv. of alcohol (top) and 3 equiv. of alcohol (bottom). 2-PA is the aldehyde component and molecular sieves were not added to the reaction.

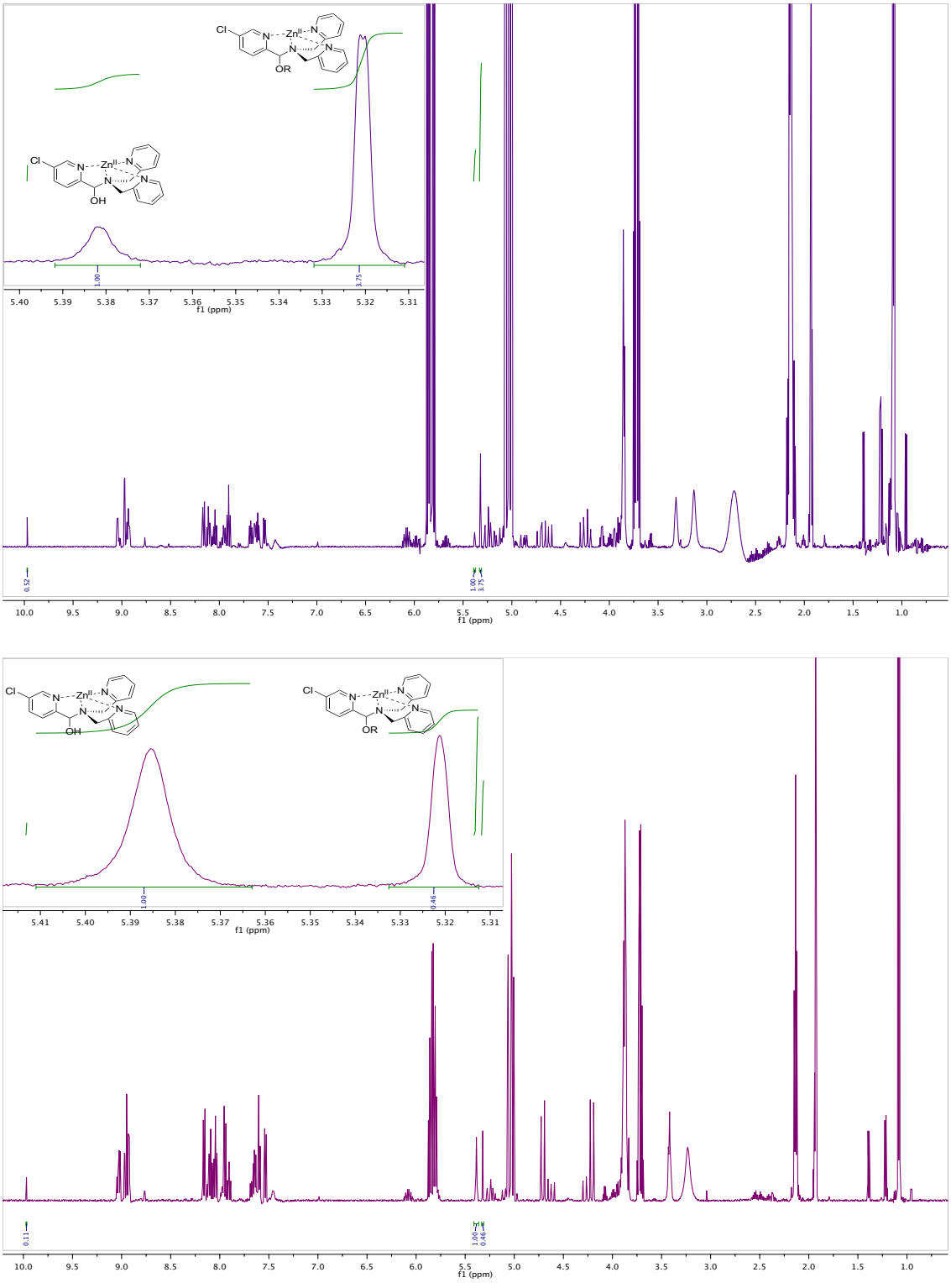

Figure 3.28: ^{1}H NMR spectra of multi-component assembly in equilibrium with 30 equiv. of alcohol (top) and 3 equiv. of alcohol (bottom). 5-Chloro-2-pyridinecarbaldehyde is the aldehyde component and molecular sieves were not added to the reaction.

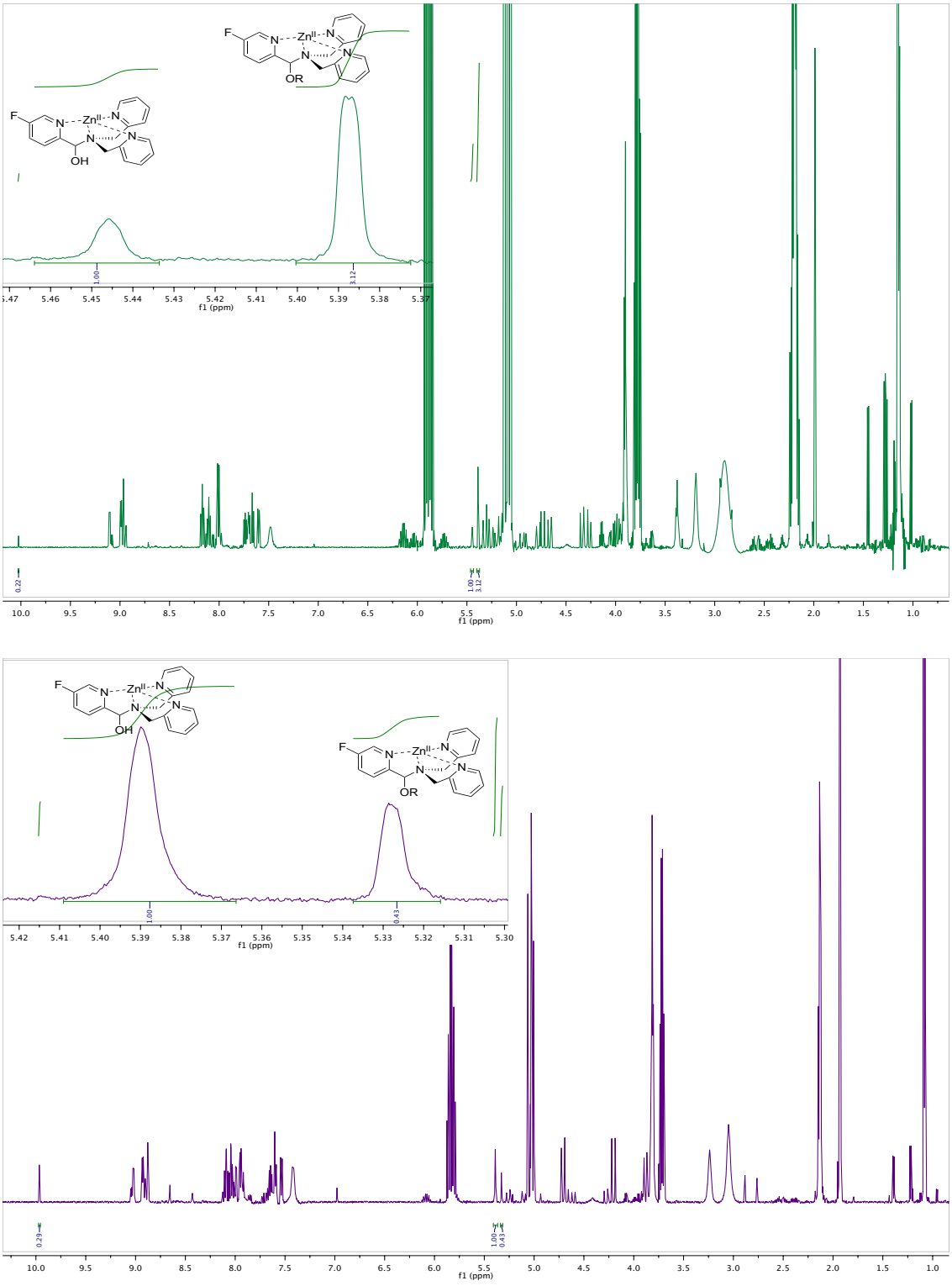

Figure 3.29: ^{1}H NMR spectra of multi-component assembly in equilibrium with 30 equiv. of alcohol (top) and 3 equiv. of alcohol (bottom). 5-Fluoro-2-pyridinecarbaldehyde is the aldehyde component and molecular sieves were not added to the reaction.

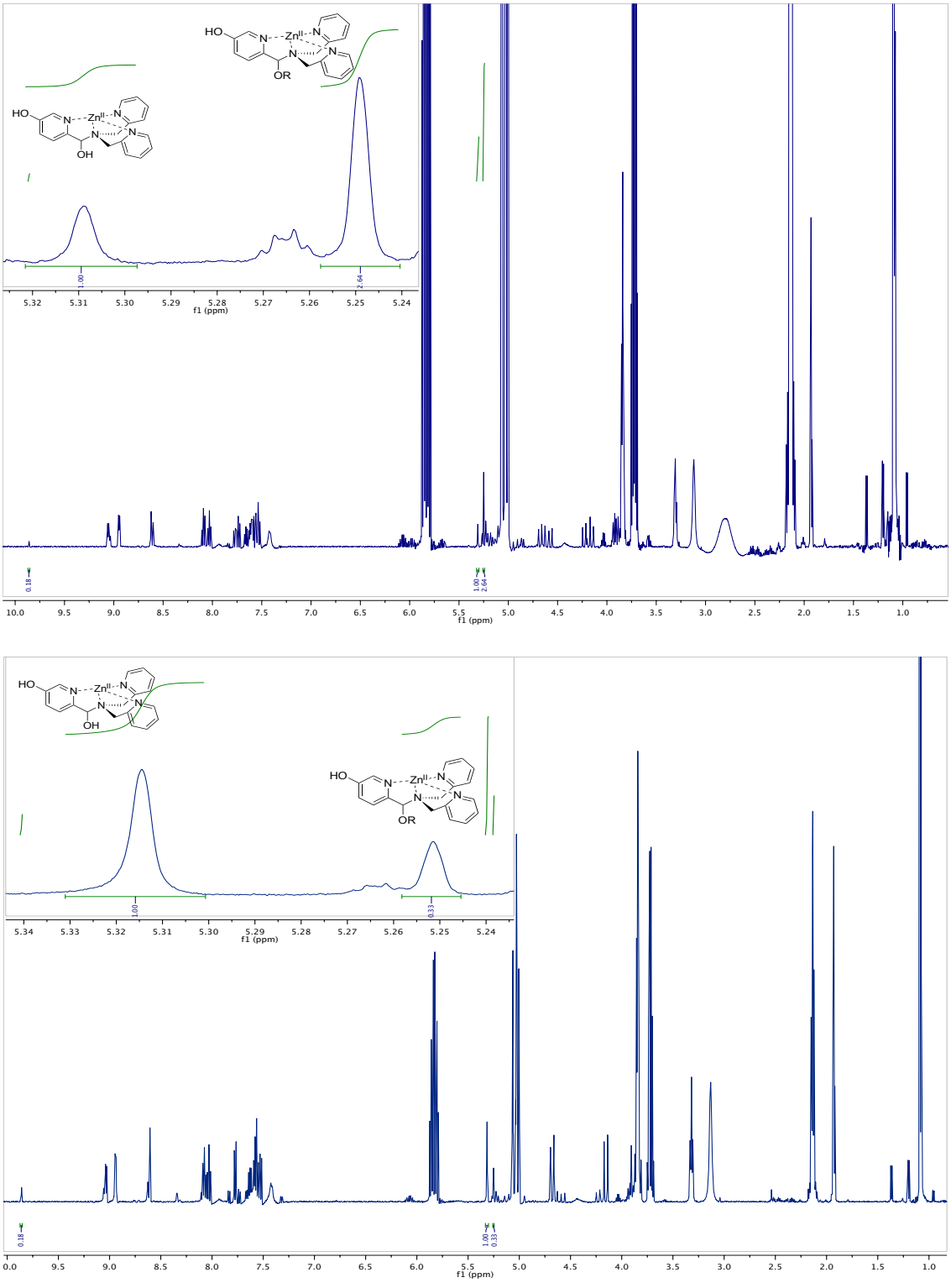

Figure 3.30: ^{1}H NMR spectra of multi-component assembly in equilibrium with 30 equiv. of alcohol (top) and 3 equiv. of alcohol (bottom). 5-Hydroxy-2-pyridinecarbaldehyde is the aldehyde component and molecular sieves were not added to the reaction.

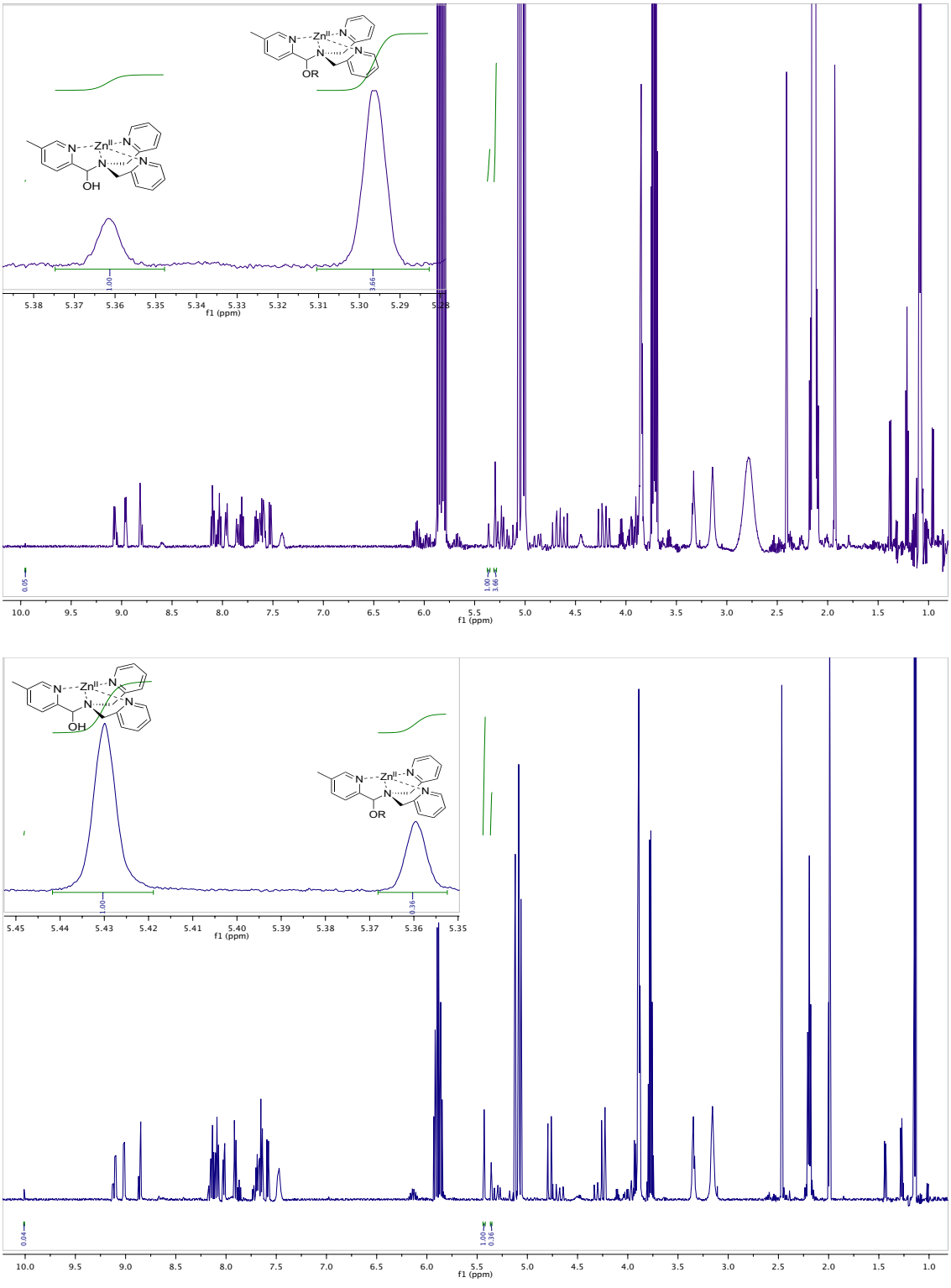

Figure 3.31: ^{1}H NMR spectra of multi-component assembly in equilibrium with 30 equiv. of alcohol (top) and 3 equiv. of alcohol (bottom). 5-Methyl-2-pyridinecarbaldehyde is the aldehyde component and molecular sieves were not added to the reaction.

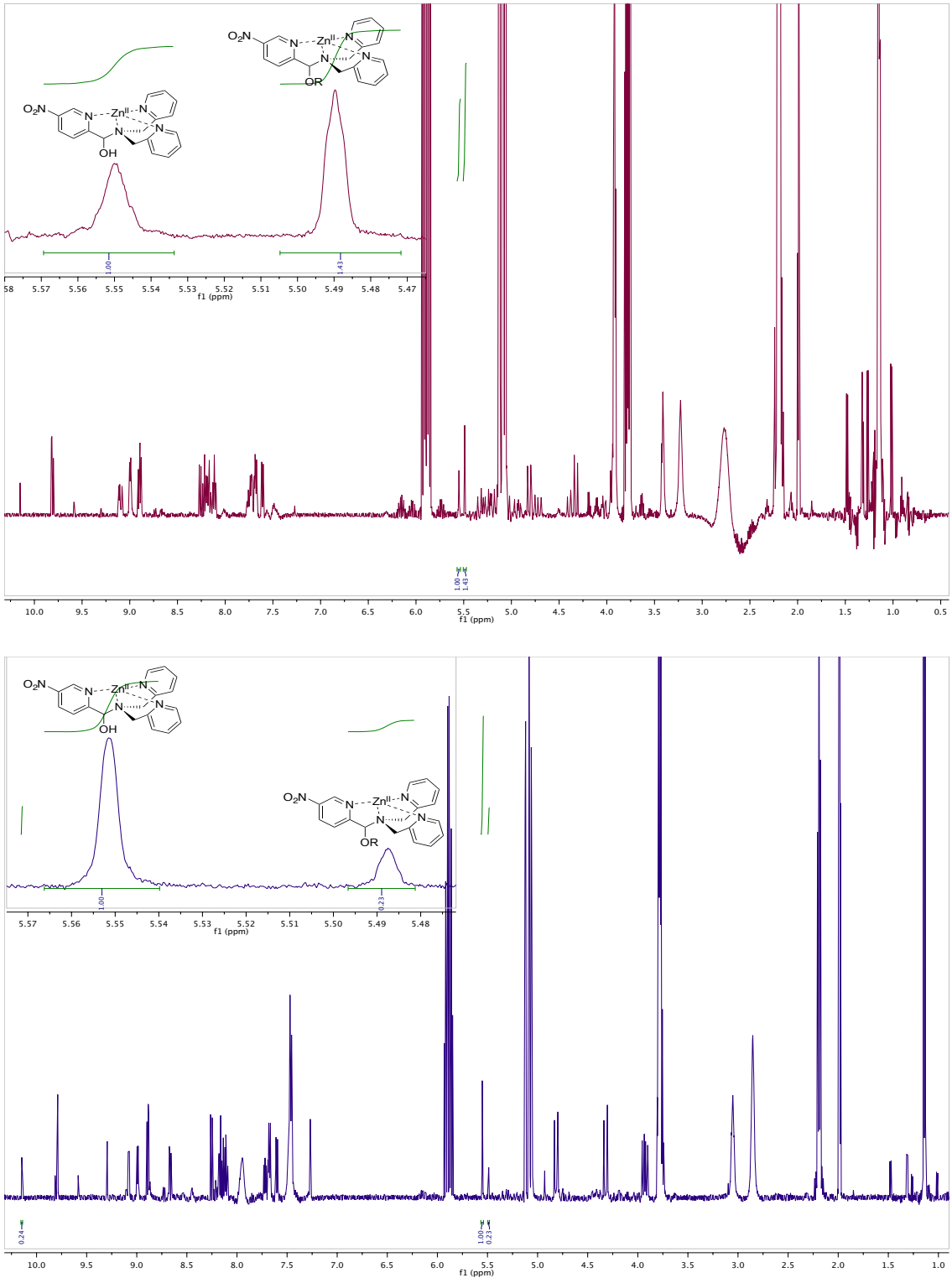

Figure 3.32: ^{1}H NMR spectra of multi-component assembly in equilibrium with 30 equiv. of alcohol (top) and 3 equiv. of alcohol (bottom). 5-Nitro-2-pyridinecarbaldehyde is the aldehyde component and molecular sieves were not added to the reaction.

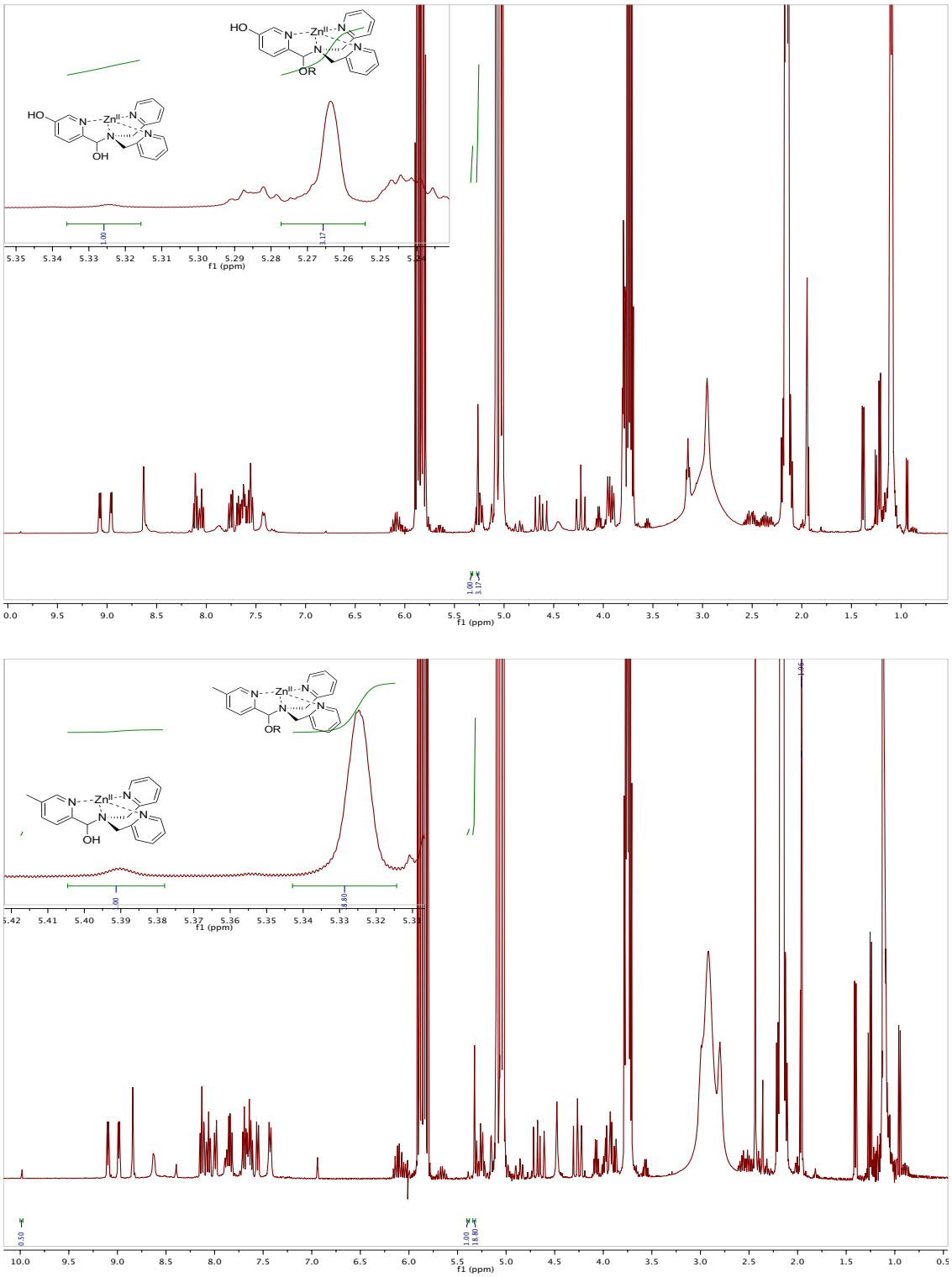

Figure 3.33: ^{1}H NMR spectra of multi-component assembly in equilibrium with 5-Hydroxy-2-pyridinecarbaldehyde (top) and 5-Methyl-2-pyridinecarbaldehyde (bottom). 30 equiv. of alcohols were used in the presence of molecular sieves.

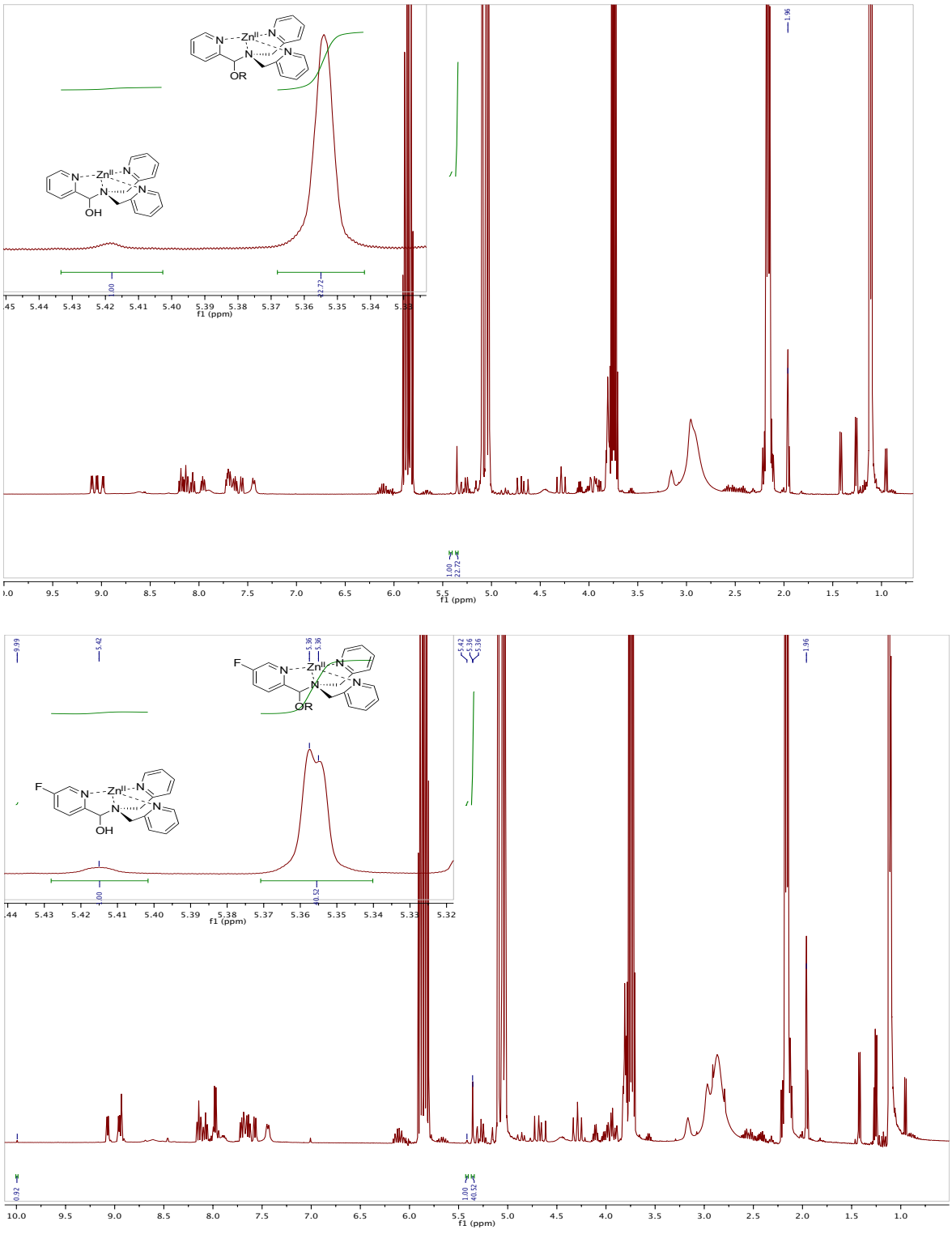

Figure 3.34: ^{1}H NMR spectra of multi-component assembly in equilibrium with 2-pyridinecarbaldehyde (top) and 5-fluoro-2-pyridinecarbaldehyde (bottom). 30 equiv. of alcohols were used in the presence of molecular sieves.

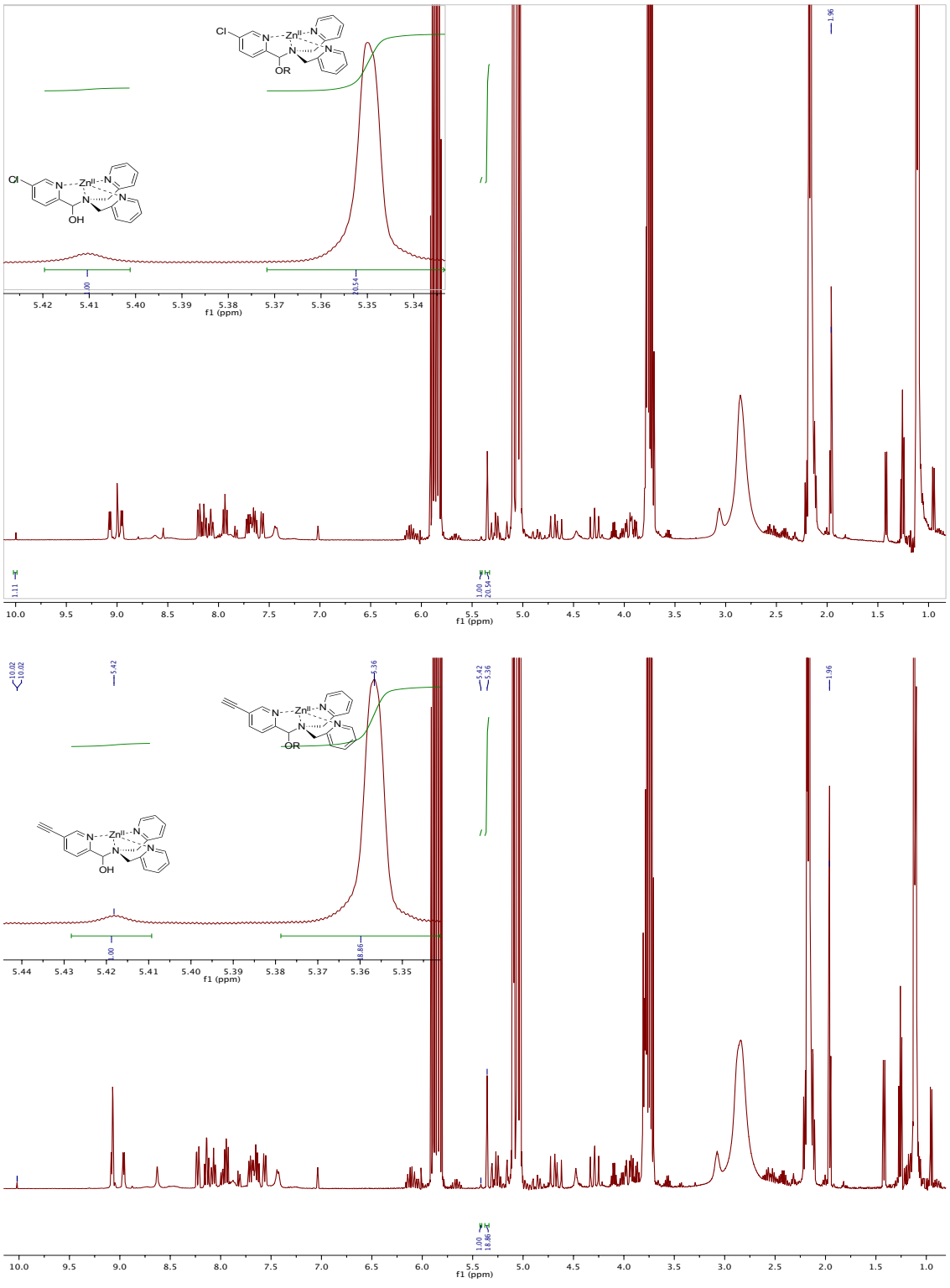

Figure 3.35: ^{1}H NMR spectra of multi-component assembly in equilibrium with 5-chloro 2-pyridinecarbaldehyde (top) and 5-ethynyl-2-pyridinecarbaldehyde (bottom). 30 equiv. of alcohols were used in the presence of molecular sieves.

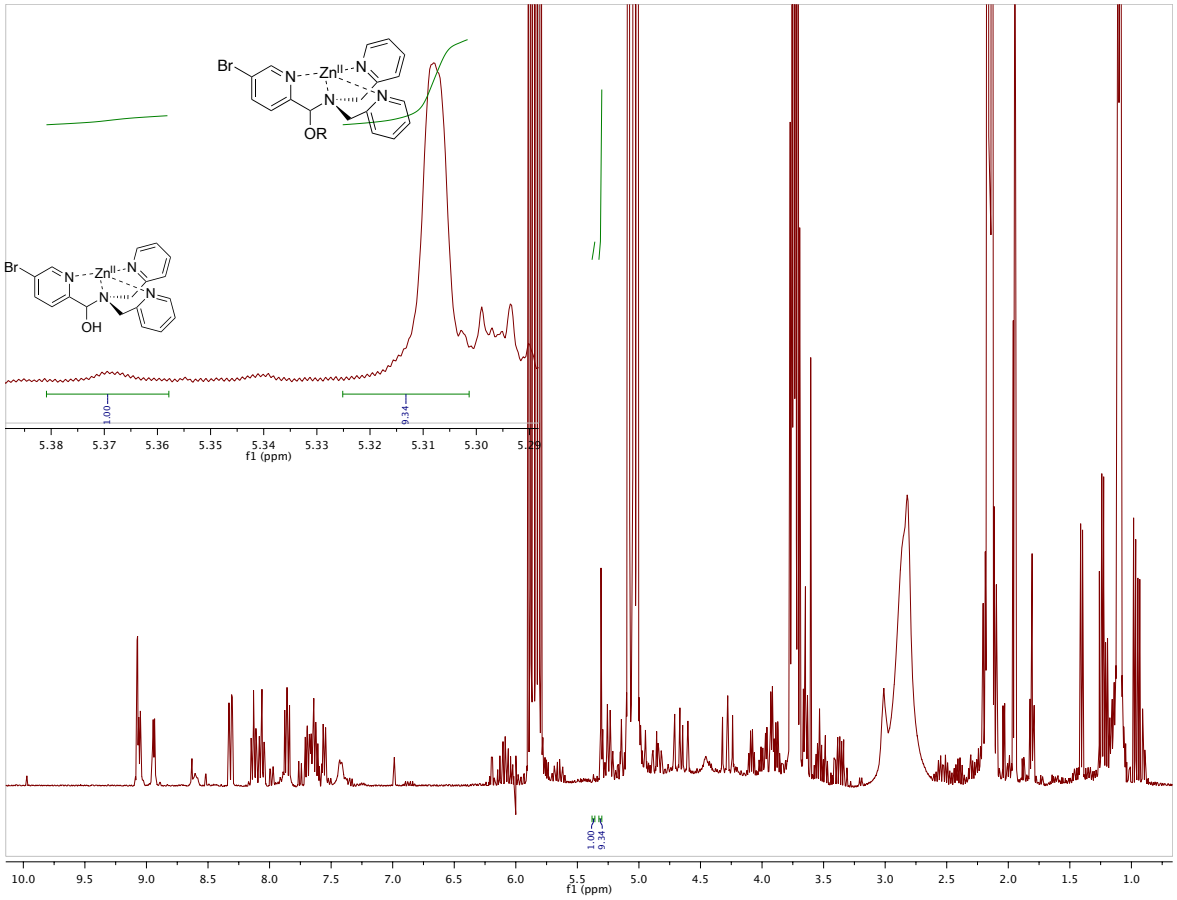

Figure 3.36: ^{1}H NMR spectra of multi-component assembly in equilibrium with 5-bromo 2-pyridinecarbaldehyde 30 equiv. of alcohols were used in the presence of molecular sieves.

para-	K_{eq}	sigma	log (K_x/K_H)
OH	16.91	-0.38	-0.21
Me	23.62	-0.14	-0.06
H	27.24	0	0.00
F	38.03	0.15	0.14
alkyne	40.13	0.23	0.13
Cl	36.34	0.24	0.17
Br	39.74	0.26	0.16

Table 3.3: K_{eq} calculated using integral values in ^{1}H NMR spectroscopy.

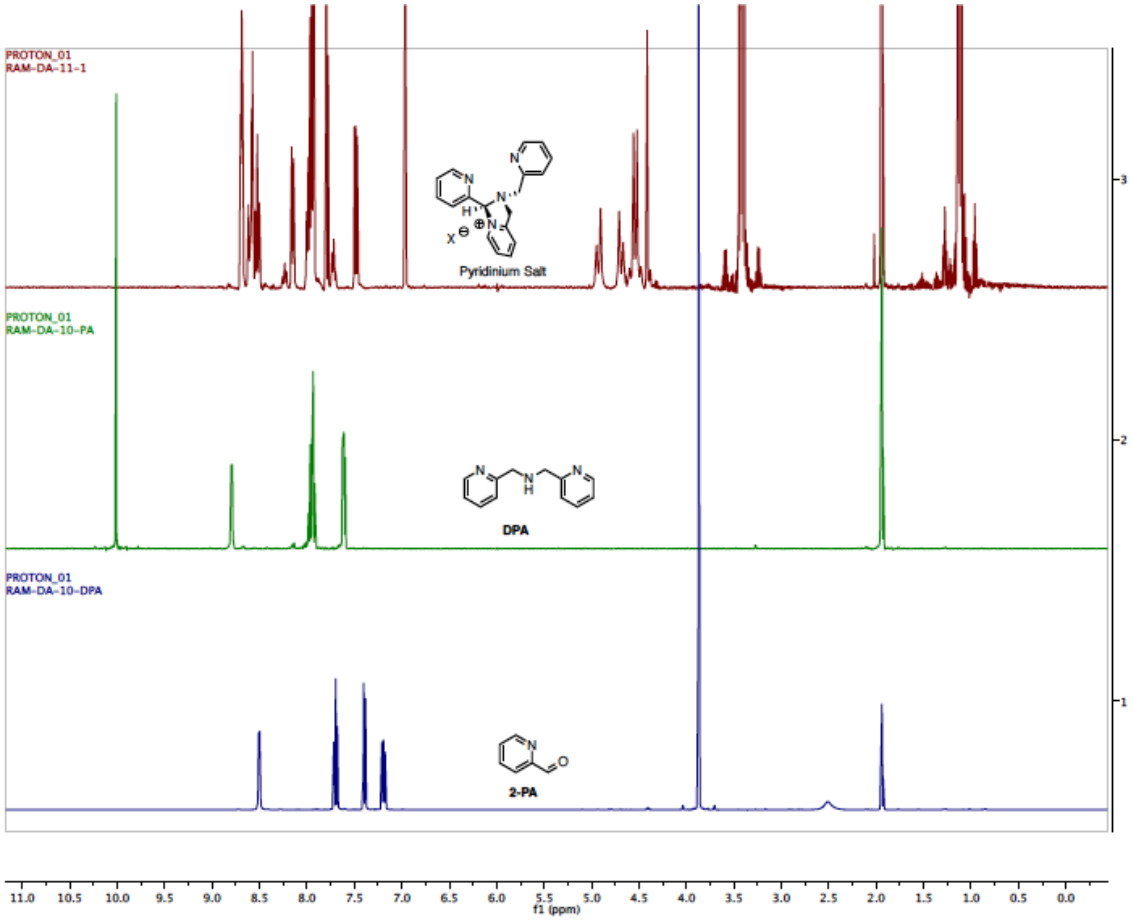

Figure 3.37: ^{1}H NMR of pyridinium salt (**3.5**) formed from **2-PA**(1.0 equiv.), **DPA** (1.2 equiv.), and BF_3-OEt_2 (1.2 equiv.) (top), ^{1}H NMR of **DPA** (middle) and ^{1}H NMR of **2-PA** (bottom). All nmrs recorded in CD_3CN.

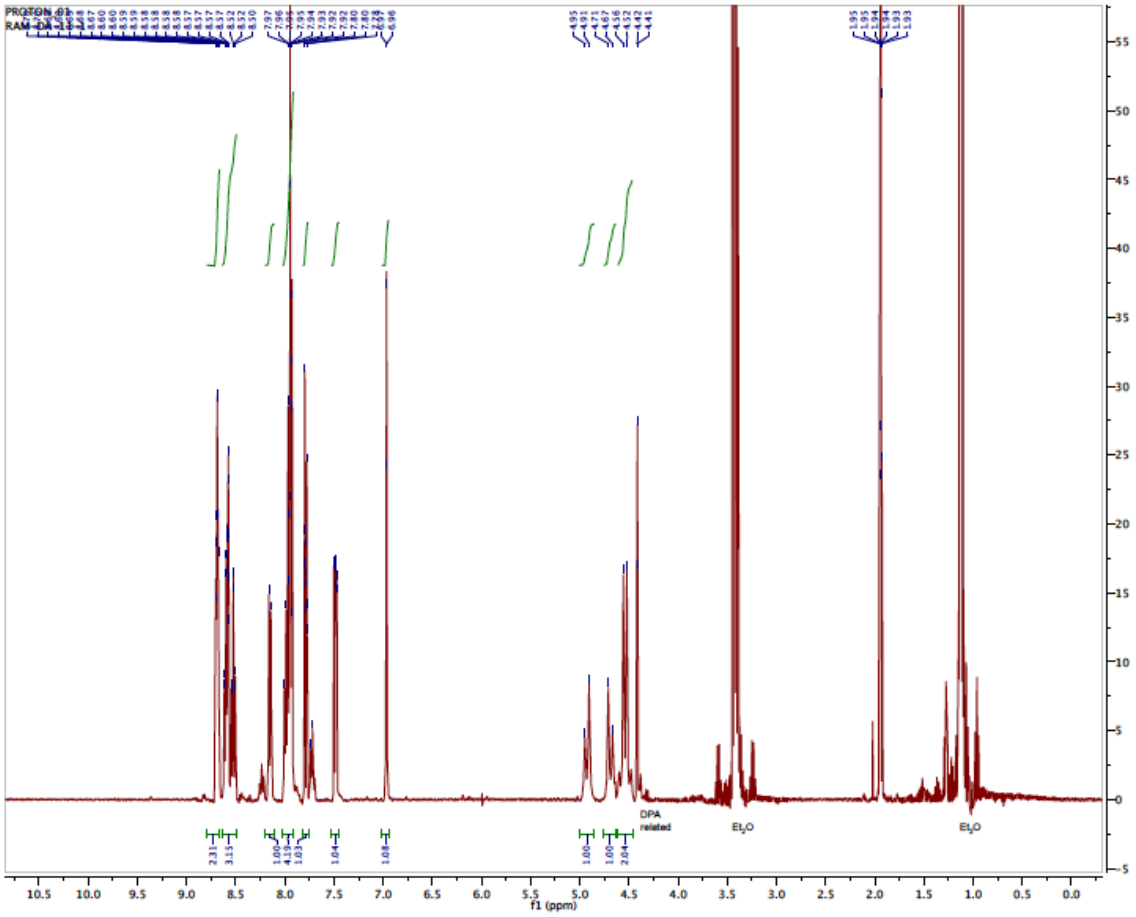

Figure 3.38: ^{1}H NMR of pyridinium salt (**3.5**) formed from **2-PA**(1.0 equiv.), **DPA** (1.2 equiv.), and BF_3-OEt_2 (1.2 equiv.) in CD_3CN.

Peaks corresponding to pyridinium salt (**3.5**): ^{1}H NMR (400 MHz, CD_3CN) δ 8.72–8.66 (m, 2H), 8.62–8.50 (m, 3H), 8.15 (d, *J* = 8.0 Hz, 1H), 8.00–7.91 (m, 4H), 7.79 (d, *J* = 8.0 Hz, 1H), 7.48 (m, 1H), 6.97 (s, 1H), 4.93 (d, *J* = 16.8 Hz, 1H), 4.69 (d, *J* = 16.8 Hz, 1H), 4.58 (d, *J* = 16.8 Hz, 1H), 4.50 (d, *J* = 16.8 Hz, 1H).

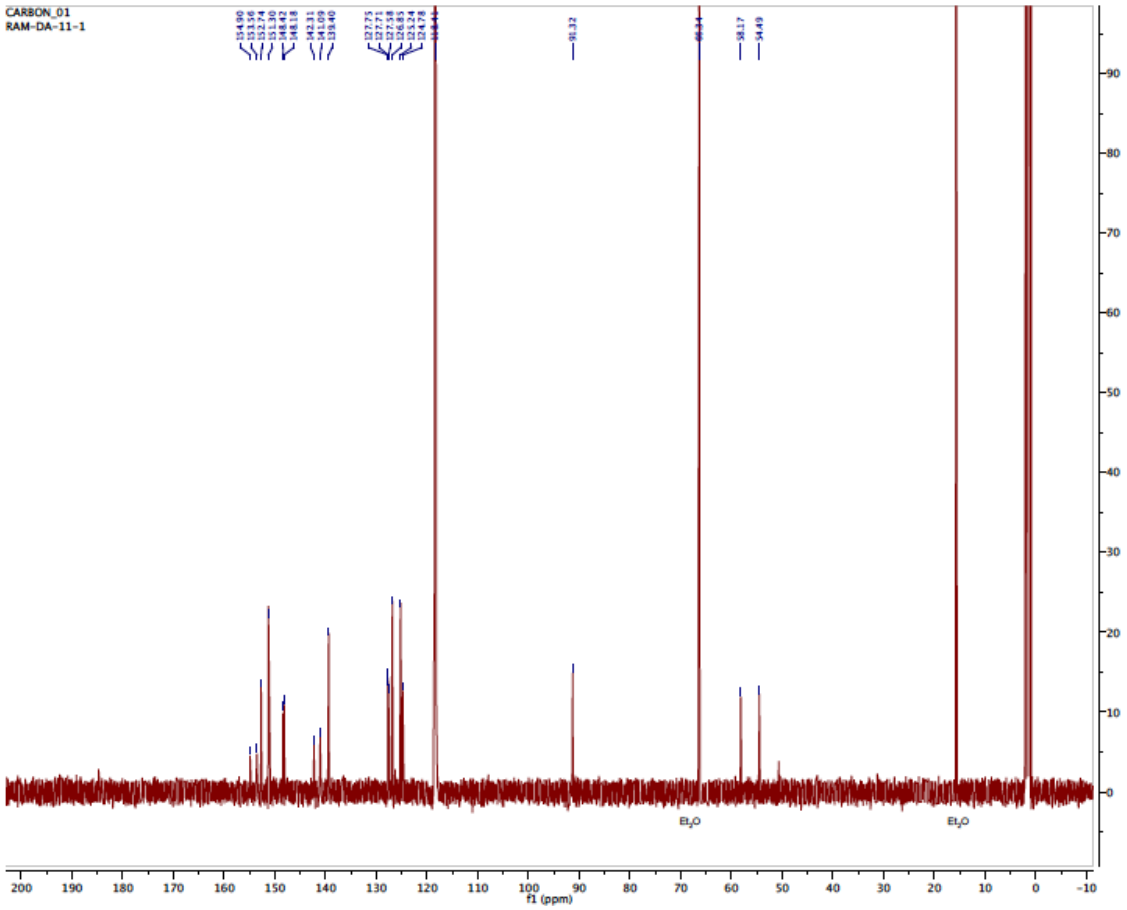

Figure 3.39: ^{13}C NMR of pyridinium salt (**3.5**) formed from **2-PA**(1.0 equiv.), **DPA** (1.2 equiv.), and BF_3-OEt_2 (1.2 equiv.) in CD_3CN.

Peaks corresponding to pyridinium salt (**3.5**): ^{13}C NMR (100 MHz, CD_3CN) δ 154.9, 153.6, 152.7, 151.3, 148.4, 148.2, 142.3, 141.1, 139.4, 127.8, 127.7, 127.6, 126.9, 125.2, 124.5, 91.3, 58.2, 54.5.

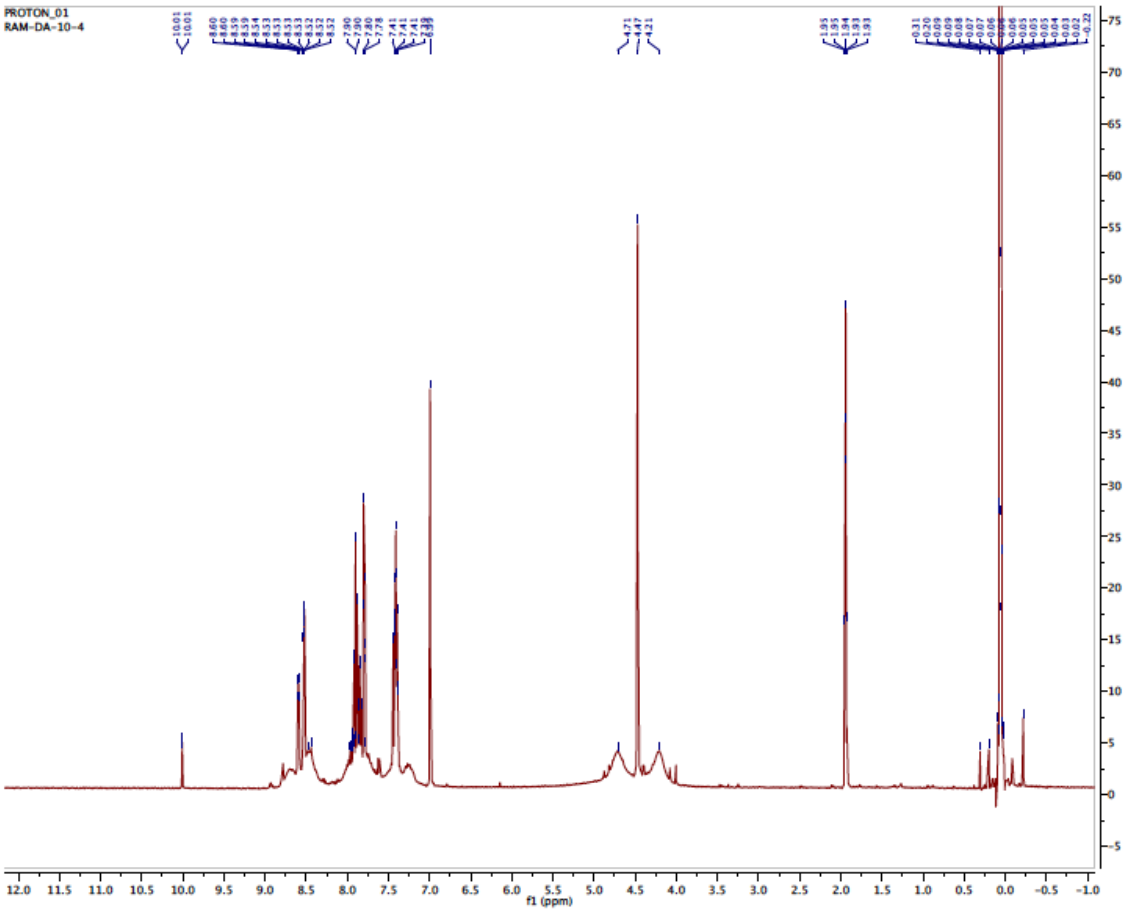

Figure 3.40: ^{1}H NMR of pyridinium salt (**3.5**) formed from **2-PA** (1.0 equiv.), **DPA** (1.2 equiv.) and TMS-OTf (1.2 equiv.) in CD_3CN.

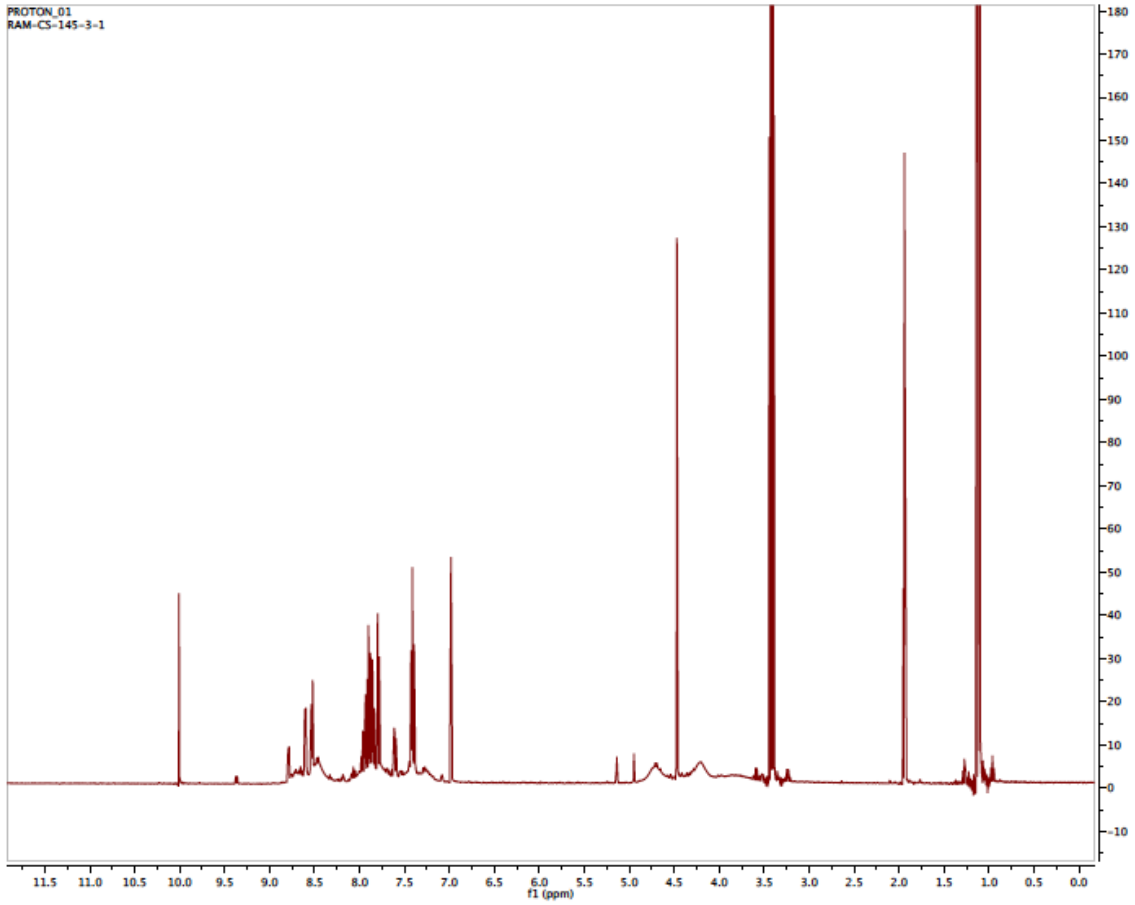

Figure 3.41: ^{1}H NMR of pyridinium salt (**3.5**) formed from **2-PA** (1.0 equiv.), **DPA** (1.0 equiv.) and BF_3-OEt_2 (1.0 equiv.) in CD_3CN.

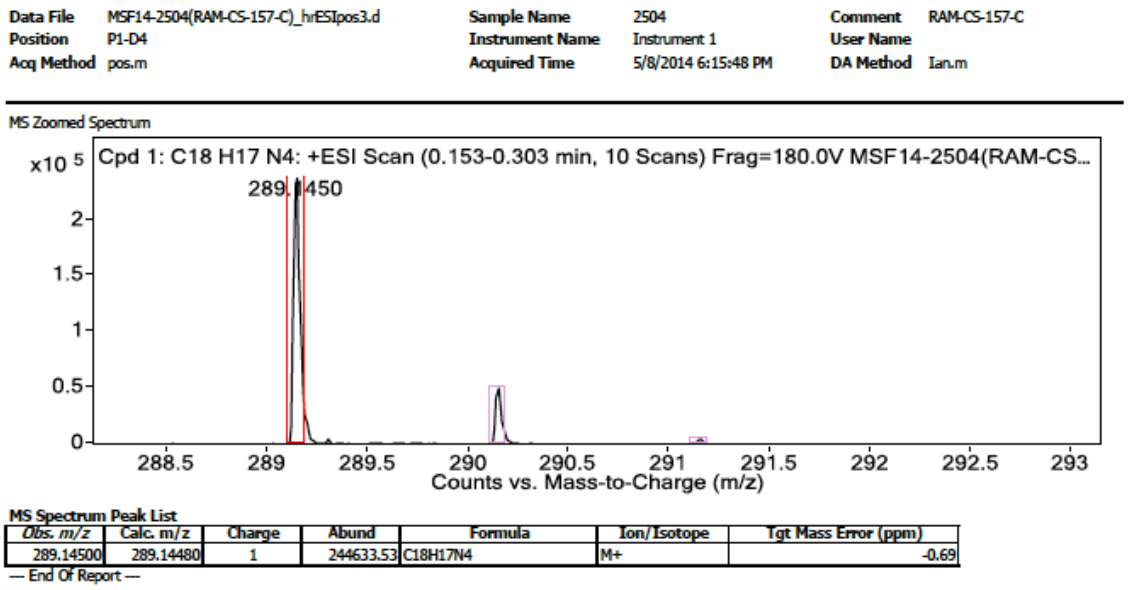

Figure 3.42: Mass spectrum of pyridinium salt (**3.5**) generated from **2-PA**, **DPA** and BF_3-OEt_2. HRMS calcd for $C_{18}H_{17}N_4^+$ (M^+) 289.1448. Found 289.1450.

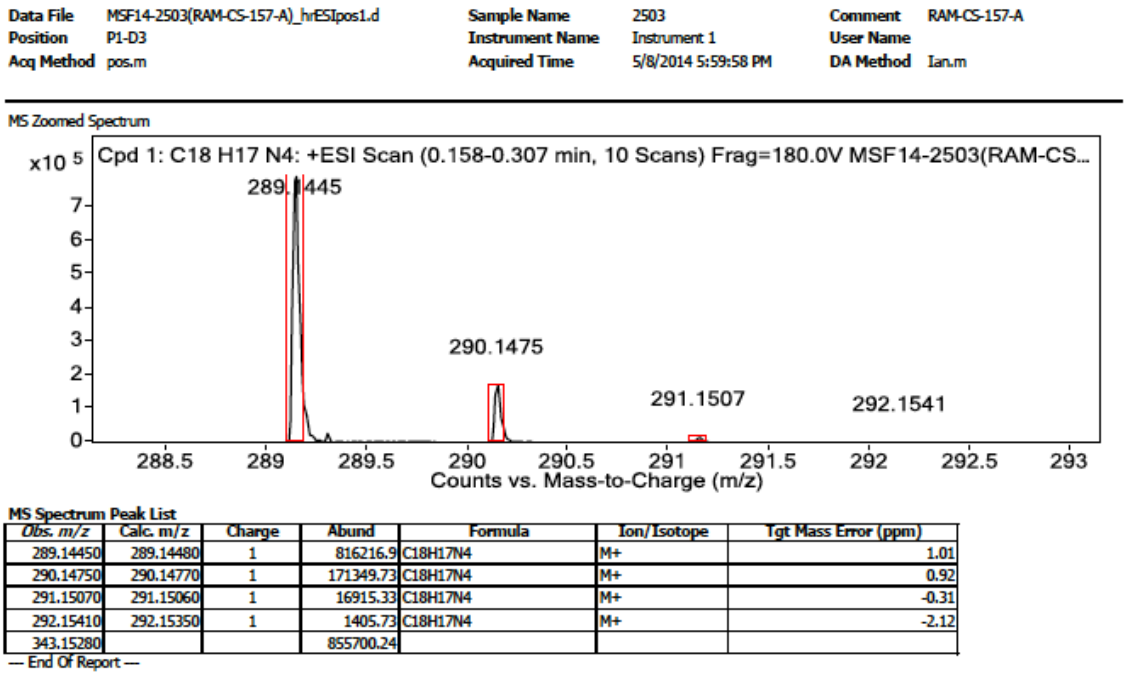

Figure 3.43: Mass spectrum of pyridinium salt generated from **2-PA**, **DPA** and TMS-OTf. HRMS calcd for $C_{18}H_{17}N_4^+$ (M^+) 289.1448. Found 289.1445.

3.4.6 Crystal Data and X-ray Experimental Procedures

X-ray Experimental for $(C_{18}H_{18}N_4)^{2+}$ - $2BF_4$: The data crystal was cut from a larger crystal and had the approximate dimensions; 0.22 x 0.20 x 0.10 mm. The data was collected at -120 °C on a Nonius Kappa CCD diffractometer using a Bruker AXS Apex II detector and a graphite monochromator with MoKa radiation (l = 0.71073Å). Reduced temperatures were maintained by use of an Oxford Cryosystems 600 low-temperature device. A total of 1117 frames of data were collected using w and ϕ-scans with a scan range of 1.1° and a counting time of 44 seconds per frame. Details of crystal data, data collection and structure refinement are listed in Table 3.4. Data reduction was performed using SAINT V8.27B.[40] The structure was solved by direct methods using SUPERFLIP[41] and refined by full-matrix least-squares on F^2 with anisotropic displacement parameters for the non-H atoms using SHELXL-2013.[42] Structure analysis was aided by use of the programs PLATON98[43] and WinGX.[44] Most of the hydrogen atoms were calculated in idealized positions. The hydrogen atom bound to N4 was observed in a ΔF map and refined with an isotropic displacement parameter.

The function, $\Sigma w(|F_O|^2 - |F_C|^2)^2$, was minimized, where $w = 1/[(s(F_O))^2 + (0.0508*P)^2 + (2.0034*P)]$ and $P = (|F_O|^2 + 2|F_C|^2)/3$. $R_W(F^2)$ refined to 0.128, with R(F) equal to 0.0482 and a goodness of fit, S, = 1.01. Definitions used for calculating R(F),$R_W(F^2)$ and the goodness of fit, S, are given below.[45] The data was checked for secondary extinction, but no correction was necessary. Neutral atom scattering factors and values used to calculate the linear absorption coefficient are from the International Tables for X-ray Crystallography (1992).[46] All figures were generated using SHELXTL/PC.[47] Tables of positional and thermal parameters, bond lengths and angles, torsion angles and figures are found elsewhere.

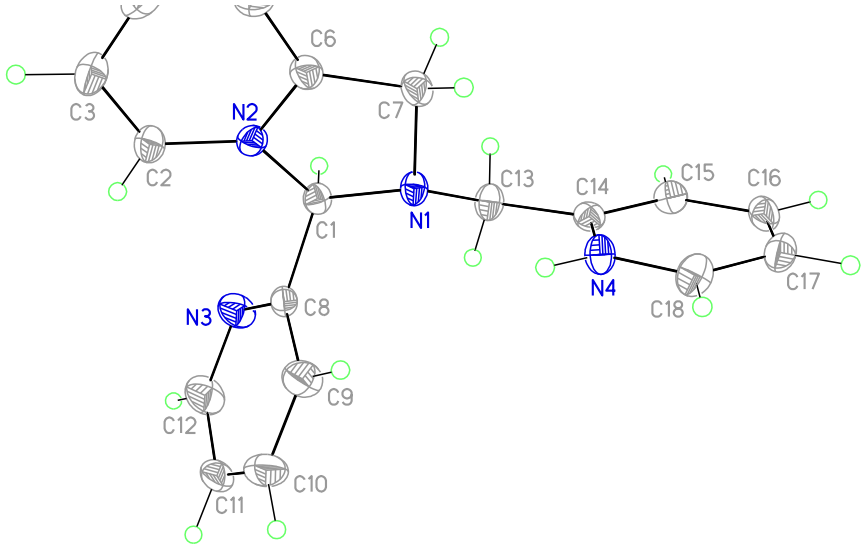

Figure 3.44: View the cation in **3.5** showing the atom labeling scheme. Displacement ellipsoids are scaled to the 50% probability level.

Table 3.4: Crystal data and structure refinement for pyridinium salt (**3.5**).

Empirical formula	C18 H18 B2 F8 N4	
Formula weight	463.98	
Temperature	153(2) K	
Wavelength	0.71073 Å	
Crystal system	monoclinic	
Space group	P 21/n	
Unit cell dimensions	a = 7.9704(6) Å	a= 90°.
	b = 9.6387(7) Å	b= 98.556(4)°.
	c = 26.395(2) Å	g = 90°.
Volume	2005.2(3) $Å^3$	
Z	4	
Density (calculated)	1.537 Mg/m^3	
Absorption coefficient	0.144 mm^{-1}	
F(000)	944	
Crystal size	0.220 x 0.200 x 0.100 mm	
Theta range for data collection	1.560 to 27.499°.	
Index ranges	-10<=h<=10, -12<=k<=12, -34<=l<=34	
Reflections collected	52310	
Independent reflections	4615 [R(int) = 0.0659]	
Completeness to theta = 25.242°	100.0 %	
Absorption correction	Semi-empirical from equivalents	
Max. and min. transmission	1.00 and 0.875	
Refinement method	Full-matrix least-squares on F^2	
Data / restraints / parameters	4615 / 0 / 293	
Goodness-of-fit on F^2	1.012	
Final R indices [I>2sigma(I)]	R1 = 0.0482, wR2 = 0.1119	
R indices (all data)	R1 = 0.0746, wR2 = 0.1281	
Extinction coefficient	n/a	
Largest diff. peak and hole	0.693 and -0.446 $e.Å^{-3}$	

Table 3.5: Atomic coordinates (x 10^4) and equivalent isotropic displacement parameters ($Å^2$x 10^3) for **3.5**. U(eq) is defined as one third of the trace of the orthogonalized U^{ij} tensor.

	x	y	z	U(eq)
C1	21(2)	8107(2)	6827(1)	17(1)
C2	-1418(3)	10189(2)	7143(1)	24(1)
C3	-2515(3)	11277(2)	7021(1)	30(1)
C4	-3155(3)	11542(2)	6513(1)	32(1)
C5	-2688(3)	10717(2)	6129(1)	28(1)
C6	-1592(2)	9632(2)	6263(1)	21(1)
C7	-920(3)	8533(2)	5950(1)	22(1)
C8	1508(2)	8213(2)	7251(1)	18(1)
C9	2998(3)	8877(2)	7188(1)	28(1)
C10	4268(3)	8944(3)	7602(1)	35(1)
C11	4012(3)	8351(2)	8058(1)	30(1)
C12	2481(3)	7714(2)	8087(1)	32(1)
C13	880(3)	6504(2)	6214(1)	21(1)
C14	1745(2)	6382(2)	5750(1)	18(1)
C15	1743(2)	5185(2)	5465(1)	21(1)
C16	2592(3)	5154(2)	5046(1)	23(1)
C17	3453(3)	6314(2)	4917(1)	24(1)
C18	3457(3)	7483(2)	5211(1)	24(1)
N1	480(2)	7944(2)	6315(1)	17(1)
N2	-997(2)	9407(2)	6759(1)	18(1)
N3	1226(2)	7631(2)	7689(1)	27(1)
N4	2601(2)	7487(2)	5613(1)	20(1)
B1	2599(3)	11281(2)	5493(1)	26(1)
B2	6047(3)	5942(3)	6481(1)	23(1)
F1	986(2)	11795(2)	5362(1)	63(1)
F2	2668(2)	10282(1)	5877(1)	50(1)
F3	3683(2)	12348(1)	5667(1)	41(1)
F4	3150(2)	10689(2)	5065(1)	45(1)
F5	6127(2)	7336(2)	6603(1)	59(1)
F6	7448(2)	5298(2)	6754(1)	48(1)

Table 3.5 (continued)

F7	6089(2)	5809(2)	5967(1)	56(1)
F8	4593(2)	5380(2)	6614(1)	51(1)

Table 3.6: Bond lengths [Å] and angles [°] for **3.5**.

C1-N1	1.461(2)	C12-N3	1.341(3)
C1-N2	1.489(2)	C12-H12	0.95
C1-C8	1.507(3)	C13-N1	1.458(2)
C1-H1	1.00	C13-C14	1.499(3)
C2-N2	1.345(2)	C13-H13A	0.99
C2-C3	1.373(3)	C13-H13B	0.99
C2-H2	0.95	C14-N4	1.343(2)
C3-C4	1.385(3)	C14-C15	1.376(3)
C3-H3	0.95	C15-C16	1.381(3)
C4-C5	1.384(3)	C15-H15	0.95
C4-H4	0.95	C16-C17	1.381(3)
C5-C6	1.375(3)	C16-H16	0.95
C5-H5	0.95	C17-C18	1.369(3)
C6-N2	1.342(2)	C17-H17	0.95
C6-C7	1.491(3)	C18-N4	1.344(3)
C7-N1	1.476(2)	C18-H18	0.95
C7-H7A	0.99	N4-H4N	0.86(3)
C7-H7B	0.99	B1-F1	1.373(3)
C8-N3	1.334(2)	B1-F3	1.378(3)
C8-C9	1.381(3)	B1-F4	1.393(3)
C9-C10	1.378(3)	B1-F2	1.394(3)
C9-H9	0.95	B2-F7	1.368(3)
C10-C11	1.373(3)	B2-F8	1.371(3)
C10-H10	0.95	B2-F5	1.381(3)
C11-C12	1.379(3)	B2-F6	1.382(3)
C11-H11	0.95		
N1-C1-N2	100.62(14)	C3-C2-H2	120.9
N1-C1-C8	114.61(15)	C2-C3-C4	119.8(2)
N2-C1-C8	112.80(15)	C2-C3-H3	120.1
N1-C1-H1	109.5	C4-C3-H3	120.1
N2-C1-H1	109.5	C5-C4-C3	120.2(2)
C8-C1-H1	109.5	C5-C4-H4	119.9
N2-C2-C3	118.28(19)	C3-C4-H4	119.9
N2-C2-H2	120.9	C6-C5-C4	118.6(2)

Table 3.6 (continued)

C6-C5-H5	120.7	C15-C14-C13	123.29(17)
C4-C5-H5	120.7	C14-C15-C16	119.62(18)
N2-C6-C5	119.51(18)	C14-C15-H15	120.2
N2-C6-C7	108.76(16)	C16-C15-H15	120.2
C5-C6-C7	131.68(18)	C17-C16-C15	120.12(18)
N1-C7-C6	102.10(15)	C17-C16-H16	119.9
N1-C7-H7A	111.3	C15-C16-H16	119.9
C6-C7-H7A	111.3	C18-C17-C16	119.01(18)
N1-C7-H7B	111.3	C18-C17-H17	120.5
C6-C7-H7B	111.3	C16-C17-H17	120.5
H7A-C7-H7B	109.2	N4-C18-C17	119.47(19)
N3-C8-C9	123.99(18)	N4-C18-H18	120.3
N3-C8-C1	113.52(16)	C17-C18-H18	120.3
C9-C8-C1	122.48(17)	C13-N1-C1	111.26(14)
C10-C9-C8	117.9(2)	C13-N1-C7	114.30(15)
C10-C9-H9	121.0	C1-N1-C7	107.15(14)
C8-C9-H9	121.0	C6-N2-C2	123.56(17)
C11-C10-C9	119.3(2)	C6-N2-C1	111.24(15)
C11-C10-H10	120.4	C2-N2-C1	124.89(16)
C9-C10-H10	120.4	C8-N3-C12	116.86(19)
C10-C11-C12	118.8(2)	C14-N4-C18	123.22(18)
C10-C11-H11	120.6	C14-N4-H4N	119.2(16)
C12-C11-H11	120.6	C18-N4-H4N	117.6(16)
N3-C12-C11	123.1(2)	F1-B1-F3	109.37(19)
N3-C12-H12	118.4	F1-B1-F4	109.88(19)
C11-C12-H12	118.4	F3-B1-F4	108.60(19)
N1-C13-C14	111.31(15)	F1-B1-F2	111.5(2)
N1-C13-H13A	109.4	F3-B1-F2	108.51(19)
C14-C13-H13A	109.4	F4-B1-F2	108.91(18)
N1-C13-H13B	109.4	F7-B2-F8	111.24(19)
C14-C13-H13B	109.4	F7-B2-F5	108.4(2)
H13A-C13-H13B	108.0	F8-B2-F5	109.7(2)
N4-C14-C15	118.55(17)	F7-B2-F6	109.66(19)
N4-C14-C13	118.14(17)	F8-B2-F6	109.74(19)

Table 3.7: Anisotropic displacement parameters ($Å^2 x\ 10^3$) for **3.5**. The anisotropic displacement factor exponent takes the form: $-2p^2[\ h^2\ a^{*2}U^{11} + ...\ + 2\ h\ k\ a^*\ b^*\ U^{12}\ ]$

	U^{11}	U^{22}	U^{33}	U^{23}	U^{13}	U^{12}
C1	18(1)	17(1)	15(1)	1(1)	5(1)	-2(1)
C2	23(1)	30(1)	19(1)	-4(1)	8(1)	0(1)
C3	28(1)	32(1)	31(1)	-7(1)	10(1)	5(1)
C4	26(1)	29(1)	40(1)	0(1)	6(1)	9(1)
C5	28(1)	32(1)	24(1)	3(1)	1(1)	7(1)
C6	21(1)	24(1)	17(1)	0(1)	3(1)	-1(1)
C7	27(1)	24(1)	15(1)	0(1)	1(1)	5(1)
C8	19(1)	18(1)	16(1)	-2(1)	3(1)	2(1)
C9	26(1)	36(1)	23(1)	1(1)	5(1)	-9(1)
C10	22(1)	48(1)	35(1)	-5(1)	2(1)	-9(1)
C11	26(1)	34(1)	26(1)	-10(1)	-9(1)	9(1)
C12	38(1)	40(1)	18(1)	4(1)	-1(1)	0(1)
C13	26(1)	18(1)	20(1)	1(1)	8(1)	1(1)
C14	18(1)	17(1)	16(1)	2(1)	0(1)	2(1)
C15	22(1)	17(1)	24(1)	1(1)	3(1)	-1(1)
C16	27(1)	21(1)	20(1)	-6(1)	0(1)	5(1)
C17	25(1)	28(1)	20(1)	3(1)	7(1)	7(1)
C18	28(1)	22(1)	26(1)	5(1)	10(1)	1(1)
N1	22(1)	17(1)	14(1)	1(1)	5(1)	2(1)
N2	16(1)	21(1)	17(1)	0(1)	4(1)	0(1)
N3	28(1)	34(1)	17(1)	4(1)	2(1)	-5(1)
N4	27(1)	15(1)	20(1)	-1(1)	7(1)	0(1)
B1	32(1)	20(1)	25(1)	-2(1)	5(1)	0(1)
B2	20(1)	30(1)	19(1)	0(1)	1(1)	-3(1)
F1	33(1)	57(1)	98(1)	-20(1)	5(1)	7(1)
F2	103(1)	20(1)	34(1)	-1(1)	28(1)	-14(1)
F3	47(1)	28(1)	46(1)	9(1)	-3(1)	-12(1)
F4	66(1)	42(1)	27(1)	0(1)	9(1)	17(1)
F5	50(1)	42(1)	88(1)	-21(1)	24(1)	-5(1)

Table 3.7 (continued)

F6	26(1)	69(1)	48(1)	25(1)	-1(1)	7(1)
F7	64(1)	83(1)	20(1)	-7(1)	5(1)	1(1)
F8	25(1)	72(1)	56(1)	17(1)	3(1)	-15(1)

Table 3.8: Hydrogen coordinates (x 10^4) and isotropic displacement parameters ($Å^2$x 10^3) for **3.5**.

	x	y	z	U(eq)
H1	-725	7319	6900	20
H2	-968	9993	7489	28
H3	-2834	11846	7285	36
H4	-3918	12293	6429	38
H5	-3115	10897	5779	34
H7A	-1795	7825	5835	26
H7B	-500	8932	5646	26
H9	3142	9276	6868	34
H10	5309	9396	7574	42
H11	4875	8380	8348	36
H12	2306	7315	8404	39
H13A	-180	5952	6163	25
H13B	1626	6120	6515	25
H15	1160	4385	5557	25
H16	2584	4334	4846	28
H17	4034	6301	4627	29
H18	4060	8286	5132	29
H4N	2590(30)	8250(30)	5786(9)	30(6)

Table 3.9: Torsion angles [°] for **3.5**.

N2-C2-C3-C4	0.0(3)	C14-C13-N1-C7	72.2(2)
C2-C3-C4-C5	-0.2(3)	N2-C1-N1-C13	-156.86(15)
C3-C4-C5-C6	0.5(3)	C8-C1-N1-C13	81.84(19)
C4-C5-C6-N2	-0.5(3)	N2-C1-N1-C7	-31.26(18)
C4-C5-C6-C7	176.7(2)	C8-C1-N1-C7	-152.56(16)
N2-C6-C7-N1	-15.9(2)	C6-C7-N1-C13	153.52(15)
C5-C6-C7-N1	166.7(2)	C6-C7-N1-C1	29.77(19)
N1-C1-C8-N3	-145.71(17)	C5-C6-N2-C2	0.3(3)
N2-C1-C8-N3	99.94(19)	C7-C6-N2-C2	-177.49(18)
N1-C1-C8-C9	35.5(3)	C5-C6-N2-C1	174.15(18)
N2-C1-C8-C9	-78.8(2)	C7-C6-N2-C1	-3.6(2)
N3-C8-C9-C10	-0.1(3)	C3-C2-N2-C6	0.0(3)
C1-C8-C9-C10	178.5(2)	C3-C2-N2-C1	-173.06(18)
C8-C9-C10-C11	0.2(4)	N1-C1-N2-C6	21.66(19)
C9-C10-C11-C12	-0.5(4)	C8-C1-N2-C6	144.23(16)
C10-C11-C12-N3	0.7(4)	N1-C1-N2-C2	-164.59(17)
N1-C13-C14-N4	25.0(2)	C8-C1-N2-C2	-42.0(2)
N1-C13-C14-C15	-156.79(18)	C9-C8-N3-C12	0.3(3)
N4-C14-C15-C16	-0.9(3)	C1-C8-N3-C12	-178.50(18)
C13-C14-C15-C16	-179.09(18)	C11-C12-N3-C8	-0.6(3)
C14-C15-C16-C17	0.7(3)	C15-C14-N4-C18	0.1(3)
C15-C16-C17-C18	0.4(3)	C13-C14-N4-C18	178.36(18)
C16-C17-C18-N4	-1.2(3)	C17-C18-N4-C14	1.0(3)
C14-C13-N1-C1	-166.27(15)		

Table 3.10: Hydrogen bonds for **3.5** [Å] and [°].

D-H...A	d(D-H)	d(H...A)	d(D...A)	<(DHA)
C1-H1...F5#1	1.00	2.51	3.160(2)	122
C1-H1...F6#1	1.00	2.43	3.384(2)	160
C2-H2...F6#2	0.95	2.49	3.144(2)	126
C2-H2...F8#2	0.95	2.48	3.391(3)	160
C7-H7A...F7#1	0.99	2.63	3.551(3)	155
C13-H13B...F8	0.99	2.45	3.181(3)	131
C15-H15...F1#3	0.95	2.55	3.327(3)	139
C17-H17...F3#4	0.95	2.46	3.207(2)	136
C17-H17...F7#5	0.95	2.56	3.165(3)	122
C18-H18...F4	0.95	2.43	3.119(3)	130
C18-H18...F4#4	0.95	2.56	3.396(3)	148
N4-H4N...F2	0.86(3)	1.98(3)	2.782(2)	155(2)

Symmetry transformations used to generate equivalent atoms:
#1 x-1,y,z #2 -x+1/2,y+1/2,-z+3/2 #3 x,y-1,z
#4 -x+1,-y+2,-z+1 #5 -x+1,-y+1,-z+1

3.5 REFERENCES

1. Jin, Y.; Yu, C.; Denman, R. J.; Zhang, W. Recent advances in dynamic covalent chemistry. *Chem. Soc. Rev.*, 2013, **42**, 6634-6654.

2. Gasparini, G.; Dal Molin, M.; Lovato A.; Prins, L. J. in *Supramolecular Chemistry*: *From Molecules to Nanomaterials*, ed. J. W. Steed and P. A. Gale, John Wiley & Sons, Ltd, 2012, DOI: 10.1002/9780470661345.

3. Miller, B. L. *Dynamic Combinatorial Chemistry*, John Wiley & Sons, 2009.

4. Corbett, P. T.; Leclaire, J.; Vial, L.; West, K. R.;. Wietor, J.-L; Sanders, J. K. M.; Otto, S. Dynamic combinatorial chemistry. *Chem. Rev.*, 2006, **106**, 3652–3711.

5. Lehn, J.-M. From supramolecular chemistry towards constitutional dynamic chemistry and adaptive chemistry. *Chem. Soc. Rev.*, 2007, **36**, 151–160.

6. Wojtecki, R. J.; Meador, M. A.; Rowan, S. J. Using the dynamic bond to access macroscopically responsive structurally dynamic polymers. *Nat. Mater.*, 2011, **10**, 14–27.

7. Wilson, A.; Gasparini, G.; Matile, S. *Chem. Soc. Rev.*, Functional systems with orthogonal dynamic covalent bonds. 2014, **43**, 1948–1962.

8. Jiang, X.; Lim, Y.-K.; Zhang, B. J.; Opsitnick, E. A.; Baik, M.-H.; Lee, D. Dendritic molecular switch: chiral folding and helicity inversion. *J. Am. Chem. Soc.*, 2008, **130**, 16812–16822.

9. Yang, Y.; Pei, X.-L.; Wang, Q.-M. Postclustering dynamic covalent modification for chirality control and chiral sensing. *J. Am. Chem. Soc.*, 2013, **135**, 16184–16191.

10. Vongvilai, P.; Ramström, O. Dynamic asymmetric multicomponent resolution: lipase-mediated amidation of a double dynamic covalent system. *J. Am. Chem. Soc.*, 2009, **131**, 14419–14425.

11. Rowan, S. J.; Cantrill, S. J.; Cousins, G. R. L.; Sanders, J. K. M.; Stoddart, J. F. Dynamic covalent chemistry. *Angew. Chem. Int. Ed. Engl.*, 2002, **41**, 898–952.

12. Herrmann, A. Dynamic combinatorial/covalent chemistry: a tool to read, generate and modulate the bioactivity of compounds and compound mixtures. *Chem. Soc. Rev.*, 2014, **43**, 1899–1933.

13. Lehn, J.-M. Constitutional dynamic chemistry: bridge from supramolecular chemistry to adaptive chemistry. *Top. Curr. Chem.*, 2012, **322**, 1–32.

14. Black, S. P.; Sanders, J. K. M.; Stefankiewicz, A. R. Disulfide exchange: exposing supramolecular reactivity through dynamic covalent chemistry. *Chem. Soc. Rev.*, 2014, **43**, 1861–1872.

15. Jin, Y.; Wang, Q.; Taynton, P.; Zhang, W. Dynamic covalent chemistry approaches toward macrocycles, molecular cages, and polymers. *Acc. Chem. Res.*, 2014, **47**, 1575–1586.

16. Aricó, F.; Chang, T.; Cantrill, S. J.; Khan, S. I.; Stoddart, J. F. Template-directed synthesis of multiply mechanically interlocked molecules under thermodynamic control. *Chem. Eur. J.*, 2005, **11**, 4655–4666.

17. Hadik, P.; Szabó, L.-P.; Nagy, E. D,L-lactic acid and D,L-alanine enantioseparation by membrane process. *Desalination*, 2002, **148**, 193–198.

18. Reetz, M. T.; Sell, T.; Meiswinkel, A.; MehlerK, G. A New Principle in Combinatorial Asymmetric Transition-Metal Catalysis: Mixtures of Chiral Monodentate P Ligands. *Angew. Chem. Int. Ed.,* 2003, **42**, 790-793.

19. Eelkema, R.; van Delden, R. A.; Feringa, B. L. Direct Visual Detection of the Stereoselectivity of a Catalytic Reaction. *Angew. Chem. Int. Ed.,* 2004, **43**, 5013-5016.

20. Long, J.; Hu, J.; Shen, X.; Ji, B.; Ding, K. Discovery of Exceptionally Efficient Catalysts for Solvent-Free Enantioselective Hetero-Diels–Alder Reaction*J. Am. Chem. Soc.*, 2002, **124**, 10-11.

21. You, L.; Berman, J. S.; Anslyn, E. V. Dynamic multi-component covalent assembly for the reversible binding of secondary alcohols and chirality sensing. *Nature. Chem.*, 2011, **3**, 943–948.

22. You, L.; Long, S. R.; Lynch, V. M.; Anslyn, E. V .Dynamic Multicomponent Hemiaminal Assembly. *Chem. Eur. J.*, 2011, **17**, 11017–11023.

23. You, L.; Pescitelli, G.; Anslyn, E. V.; Di Bari, L. An exciton-coupled circular dichroism protocol for the determination of identity, chirality, and enantiomeric excess of chiral secondary alcohols. *J. Am. Chem. Soc.*, 2012, **134**, 7117–7125.

24. You, L.; Berman, J. S.; Lucksanawichien, A.; Anslyn, E. V. Correlating sterics parameters and diastereomeric ratio values for a multicomponent assembly to predict exciton-coupled circular dichroism intensity and thereby enantiomeric excess of chiral secondary alcohols. *J. Am. Chem. Soc.*, 2012, **134**, 7126–7134.

25. Li, G.; Fronczek, F. R.; Antilla, J. C. Catalytic asymmetric addition of alcohols to imines: enantioselective preparation of chiral N,O-aminals. *J. Am. Chem. Soc.*, 2008, **130**, 12216–12217.

26. Star, A.; Goldberg, I.; Fuchs, B. Dioxadiazadecalin/Salen Tautomeric Macrocycles and Complexes: Prototypal Dynamic Combinatorial Virtual Libraries New Supramolecular Host Systems, Part 12. Part 11: ref. 1. We gratefully acknowledge support by a research grant from the Israel Science Foundation and by an Intel Scholarship (to A.S.), as well as the valuable assistance of Shimon Hauptman

with mass spectrometry and Yuri Paskover as an undergraduate research student. *Angew. Chem. Int. Ed. Engl.*, 2000, **39**, 2685–2689.

27. Fuchs, B.; Nelson, A.; Star, A.; Stoddart, J. F.; Vidal, S. Amplification of dynamic chiral crown ether complexes during cyclic acetal formation. *Angew. Chem. Int. Ed. Engl.*, 2003, **42**, 4220–4224.

28. Mason J. P.; Block, H. W. Preparation and Polymerization of β-4-Morpholinoethyl Chloride. *J. Am. Chem. Soc.*, 1940, **62**, 1443.

29. Lakhdar, S.; Tokuyasu, T.; Mayr, H. Electrophilic Reactivities of α,β-Unsaturated Iminium Ions. *Angew. Chem. Int. Ed. Engl.*, 2008, **47**, 8723–8726.

30. Baldwin, J. E. *J. Chem. Soc.,* Rules for ring closure. *Chem. Commun.* 1976, 734-736

31. Baldwin, J. E.; Thomas, R. C.; Kruse, L.I.; Silberman, L. Rules for ring closure: ring formation by conjugate addition of oxygen nucleophiles*J. Org. Chem.*, 1977, **42**, 3846–3852

32. Eldin, S.; Jencks, W. P. Lifetimes of Iminium Ions in Aqueous Solution*J. Am. Chem. Soc.*, 1995, **117**, 4851–4857.

33. Eldin, S.; Digits, J. A.; Huang, S-T.; Jencks, W. P. Lifetime of an Aliphatic Iminium Ion in Aqueous Solution. *J. Am. Chem. Soc.*, 1995, **117**, 6631–6632.

34. Eldin, S.; Jencks, W. P. Concerted Bimolecular Substitution Reactions of Anilino Thioethers. *J. Am. Chem. Soc.*, 1995, **117**, 9415–9418.

35. Dalby, K. N.; Jencks, W. P. Lifetimes of Imidinium Ions in Aqueous Solution*J. Am. Chem. Soc.*, 1997, **119**, 7271–7280.

36. Pearson, R. G.; Sobel, H. R.; Songstad, J. Nucleophilic reactivity constants toward methyl iodide and trans-dichlorodi(pyridine)platinum(II). *J. Am. Chem. Soc.*, 1968, **90**, 319–326.

37. Mendham, J.; Denney, R. C.; Barnes, J. D.; Thomas, M. J. K. *Vogel's Quantitative Chemical Analysis (6th Edition)*, Prentice Hall, 6th ed. 2000.

38. Ritchie C. D.; Sager, W. F. Progress in Physical Organic Chemistry. *Prog. Phys. Org. Chem.*, 1964, **2**, 323-400.

39. Chen, R.; Zhang, K.-C.; Liu, L.; Li, X.-S.; Guo, Q.-X. Substituent effects in X-C≡C-H···NH3 (or OH2, FH) hydrogen bonding. *Chem. Phy. Lett.*, 2001, **338**, 61–66.

Chapter 4: Sensing Protocols for a-Chiral Ketones

4.1 INTRODUCTION

Fluorinated compounds have demonstrated novel and exciting advancements in the biological arena, and the recent studies incorporating fluorine atoms to other small molecules have proven to be a booming industry in chemistry research. For development of drugs, the significance of fluorine cannot be overlooked as 20-25% of drugs in the pharmaceutical industry contains at least one fluorine atom.[1,2] Among many fluorine containing small molecule based drugs, aromatic compounds containing a fluorine atom or trifluoromethyl group on an aromatic ring are more commonly found. A drug molecule is considered to be efficient if it is able to pass through a cell membrane and into the lipid core, but not become trapped in it; in other words, it requires just the right amount of lipophilicity. Fluorine and trifluoromethyl substituents on an aryl group are known to control the lipophilicity and metabolic stability of organic compounds. The stereocontrolled and enantioselective synthesis of novel chiral fluorine compounds, especially compounds containing one or more -CHF- units, are of great interest in many fields. The compounds containing fluorine atoms at the benzyl position are more complex and difficult to prepare, and are thereby less widely investigated.

Also, the carbonyl group is a profoundly functional area of focus in organic chemistry, as it is easily transformed into many other functional groups, including alcohols, aldehydes, ketones, carboxylic acids, esters, amides, acyl (acid) chlorides, and acid anhydrides. Carbonyl compounds containing fluorine atoms would be especially interesting to study.

Recently, the Hartwig group has developed a simple method to convert aryl halides and ketones, esters and related compounds to *a*-aryl carbonyl compounds in the

presence of a base and a palladium catalyst. The direct arylation of *α,α*-difluoroacetophenone with bromobenzene is shown in Scheme 4.1 and 4.2.[3]

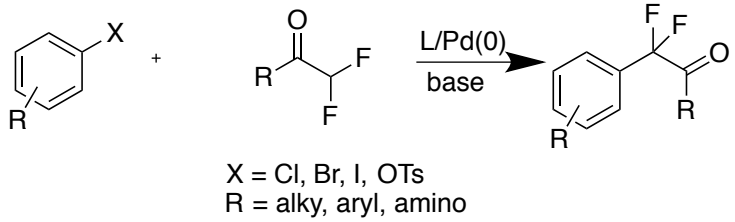

Scheme 4.1: α-Arylation of ketone with Pd catalyst.

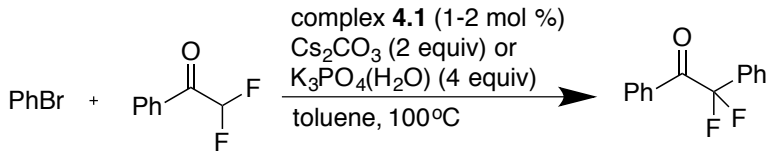

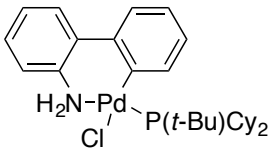

4.1

Scheme 4.2: α-Arylation of α,α-difluoroacetophenone with PhBr catalyzed by complex **4.1**.

Additionally, another protocol for α-arylation of ketones has been reported by the Hartwig group.[4] In order to generate chiral fluorine carbonyl compounds, the α-arylation of ketones with aryl and hetero-aryl chlorides were catalyzed by the combination of $Ni(COD)_2$ and (*R*)-BINAP or (*R*)-DIFLUORPHOS. It resulted in high enantioselectivity with various aryl halides substrates ranging from 90 to 99% *ee* (Scheme 4.3).

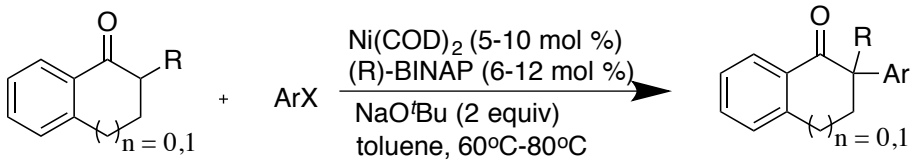

Scheme 4.3: Asymmetric α-arylation of indanones and tetralones with chloroarenes catalyzed by $Ni(COD)_2$/(*R*)-BINAP

As discussed in previous chapters, to be a HTS, in collaboration with various methodology groups, our goal is to build a CD based chiral sensing system for the *ee* determination of α-chiral ketones.

4.2 Previous Developed Assay for Alpha-chiral Ketone Sensing

Previously, our group developed a chiral sensing assay for α-chiral ketones.[5] This assay involves a simple derivatization step. A bidentate analyte (**4.4**) is produced from the condensation of α-chiral ketones with 1-methyl-1-(2—pyridyl) hydrazine (**4.3**) (Scheme 4.4). This derivatization step is required in order to complex with [Cu^1((*S*)-BINAP)($CH_3CN)_2$]PF_6, which would produce [Cu^1((*S*)-BINAP)(**4.4**)]PF_6.

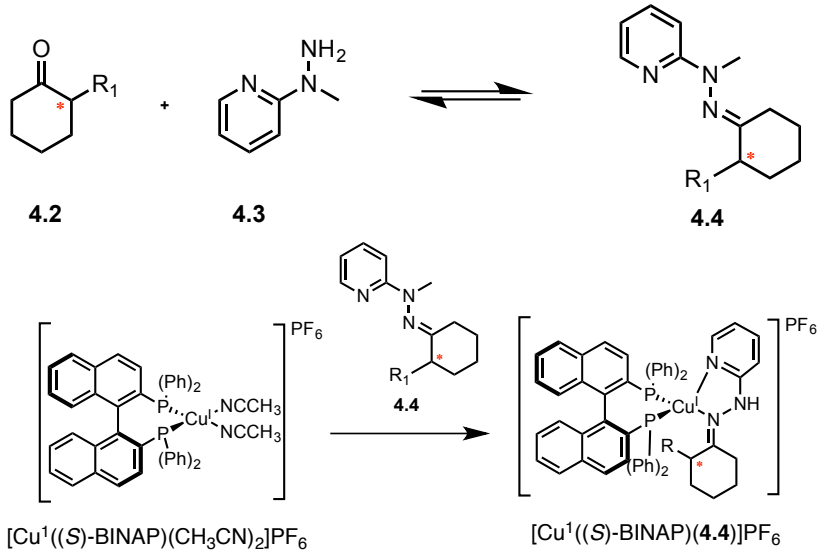

Scheme 4.4: Derivatization of α-chiral cyclohexanone followed by complexation to [Cu^1((*S*)-BINAP)($CH_3CN)_2$]PF_6.

The enantioselective discrimination of **4.4** comes from the complexation with $[Cu^{I}((S)\text{-BINAP})(CH_3CN)_2]PF_6$, which results in varying twist angles. In this assay, the two enantiomers of **4.4** will interact differently, primarily due to the sterics. The *R*-enantiomer of **4.4**, which has more steric clash with phosphine ligands, induces a larger twist to prevent such interaction, and *R*-enantiomer of **4.4** will have smaller twist. These twists can be directly correlated in CD measurement. The more steric interaction with the BINAP moiety, the larger twist is expected to arise from the napthyl rings, which in turn induces a larger change in the MLCT band.

Similarly, our group has employed assembly of octahedral Fe(II) complexes for *ee* determination of chiral amines.[6] Although the starting enantiomers are chiral amines, through a fast *in situ* derivatization step with aldehydes, chiral imines are produced. The chiral imine will be the analyte that would complex with $Fe^{II}(TfO^{-})_2$. This complexation generates numerous stereoisomers, where some would dominate over the others, resulting in ECCD. Although this assembly was developed for the sensing of chiral amines, in combining the previous two assays together, we attempted to construct a novel sensing assembly for α-chiral ketones.

4.3 KETONES OF INTEREST

α-Chiral ketones produced by Pd-catalyzed enantioselective α-arylation of α-fluorinated ketones are our target analytes. The work done by the Hartwig group demonstrates that reactions of α-fluorinated indanones with aryl bromides afford the corresponding α- arlylated products with high enantioselectivities in the presence of chiral monophosphine ligand (Scheme 4.5, where n=0). The enantioselectivities for tetralones (Scheme 4.5, n=1) were lower than those of indanones. Therefore, in order to

generate more enantioselective α-arylation for tetralones, development of a catalyst using novel chiral monophosphine ligands would be beneficial.

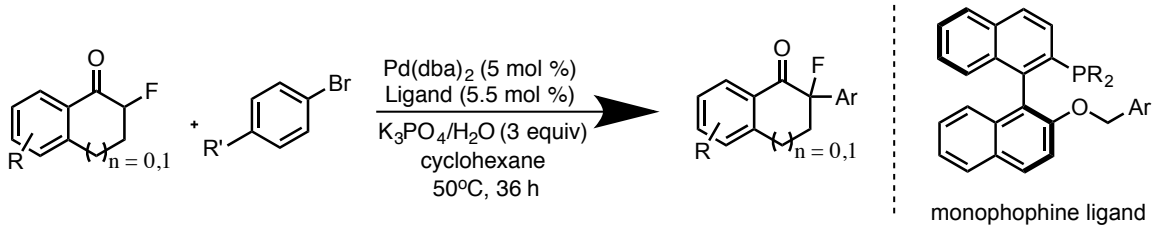

Scheme 4.5: Palladium-catalyzed enantioselective α-arylation of fluorinated ketones.

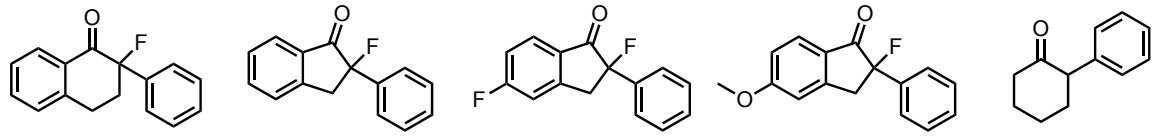

4.5 **4.6** **4.7** **4.8** **4.9**

Figure 4.1: Various α -chiral ketones synthesized from palladium-catalyzed enantioselective α-arylation of fluorinated ketones (**4.5-4.8**) and the control ketone (**4.9**).

4.4 PRELIMINARY RESULTS AND FUTURE WORK

4.4.1 Design of Sensing Assembly

The original assembly that was developed for *ee* determination of chiral amine can also be used for chiral sensing of α-chiral ketones. The condensation product from the ketones and hydrazine produces imines (**4.4**), which is the same final analyte that was produced from aldehydes and chiral amines.

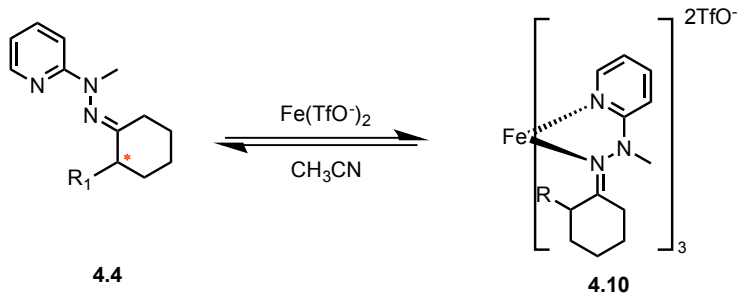

4.4 **4.10**

Scheme 4.6: Complexation of the condensation product of imine (**4.4**) with Fe(II) to form **4.10**.

However, in order to enhance the CD signals induced from the twists of the assembled complex, we have come up with two different bidentate ligands that will assemble with Fe(II). These two ligands were designed based on CPK model examinations (Figure 4.2).

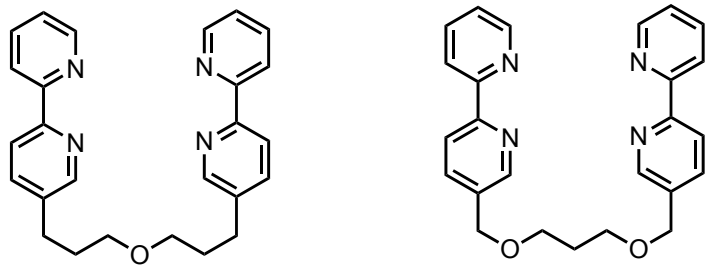

4.11 **4.12**

Figure 4.2: Two proposed bidentate ligands to complex with Fe(II) and imine (**4.4**)

The ligands will bind Fe(II), filling four coordination sites, while a hydrazine condensation product with the Hartwig chiral ketones, which will give a hydrazine, will fill the remaining two coordination sites in an octahedral geometry. The bipy-ligands are tethered together such that one equivalent of ligand induces only one equivalent of the hydrazone to bind, thereby controlling the stoichiometry of the final complex. The number of atoms linking the bipy's, the use of oxygen in the linker, and the meta

regiochemistry of linkage was proposed to lower the steric hindrance in the final complex and lower strain in the linker due to the gauche effect.

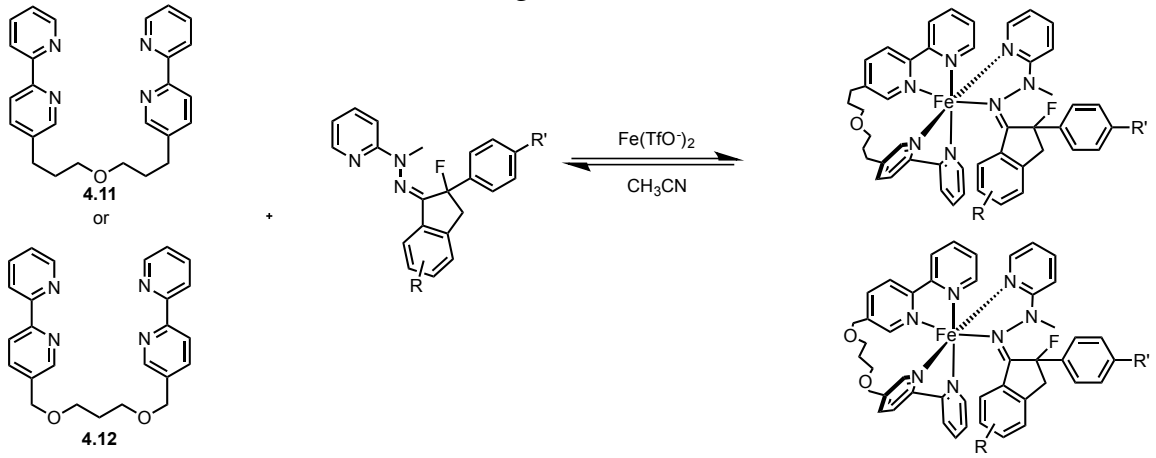

Scheme 4.7: Proposed ligand complexation with Fe(II) and Hartwig condensation product.

4.4.2 Synthesis of Ligands

The two synthetic routes of the ligands appear to be fairly straightforward (Scheme 4.6). The synthesis of the two candidate ligands occur by substituting bipy with 1,3-propanediol or brominated ether. The exact compounds have not been synthesized, but similar ligands of varying length with this regiochemistry of heteroatom substitution have been reported. Synthetic routes for the substituted bipys are also shown in Scheme 4.7.

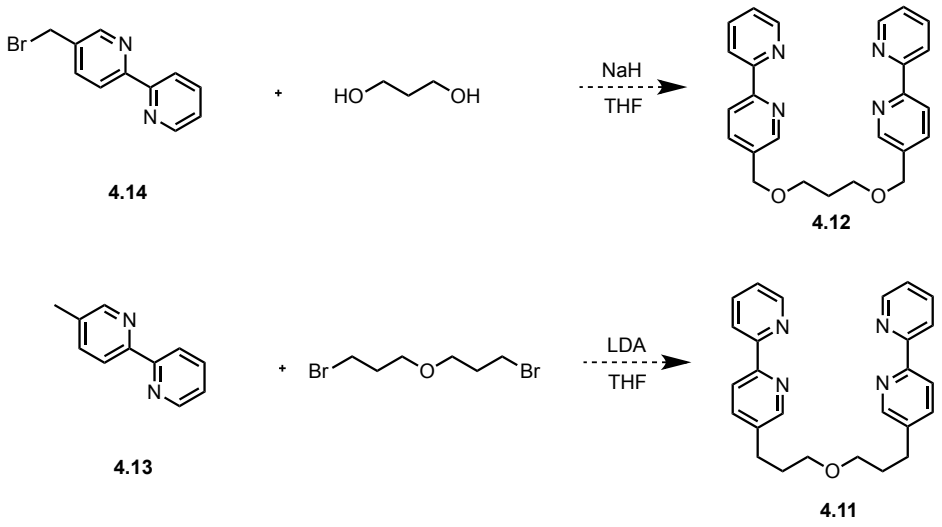

Scheme 4.8: Proposed synthetic route for the two bidentate ligands (**4.11**[7] and **4.12**)

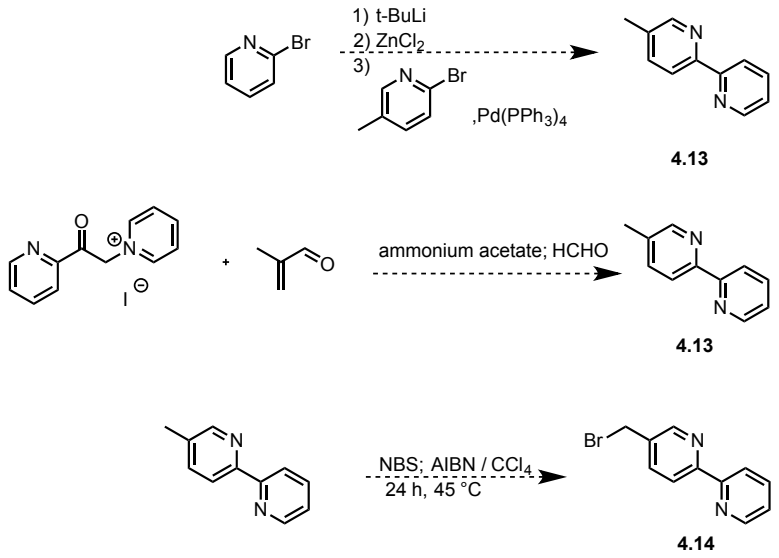

Scheme 4.9: Synthesis of substituted BIPY.[8,9]

4.4.3 *Ee* determination of α-chiral ketones

In the analysis, the binding of the hydrazone is predicted to induce a preference of the bipy ligands to adopt a M or P twist, which results in exciton coupled circular dichroism. Furthermore, the MLCT bands for the Fe(II) complexes (these structures are

likely violet or burgundy in color) will be in a chiral environment, and thus CD active. Any condensation of the hydrazine on a racemic mix of ketone reactants should be optically silent, as the M and P twists will cancel. Only an *ee* in the produce will lead to an optical signal.

4.4.4 Summary and Outlook

Our key end goal for this work will not only be limited to utilizing the sensing assembly for a rapid *ee* determination of the analyte, but also to employ the asymmetric synthesis that is developed from the varying methodology groups to be done in parallel.

4.5 EXPERIMENTALS

4.5.1 General Methods

NMR spectra were recorded on Agilent MR 400 at The University of Texas at Austin NMR facility. ESI-mass spectra were obtained on Agilent 6100 at The University of Texas at Austin mass spectrometry facility.

4.5.2 Synthetic Procedures and Spectroscopy

Synthesis of 1-methyl-1-(2-pyridyl) hydrazine (4. 3):

To a 50 mL 3-neck round bottom flask, 2-bromopyridine (3 mL, 31.5 mmol), and methylhydrazine (25 mL, 475 mmol) were added and refluxed for 6 h under Ar. After cooling, the excess methyl hydrazine was removed in vacuo. Then the residue was dissolved with EtOAc (250 mL) and extracted with 10% Na_2CO_3 aqueous (60 mL). The organic layer was then extracted with saturated aqueous NaCl (50 mL x 2). The organic layer was dried over Na_2SO_4 and the solvent was removed in vacuo to afford 3 (3.5 g, 90.0%) as a yellow-orange oil.

^{1}H NMR ($CDCN_3$, 400 MHz): δ 8.16 (ddd, J=5.0, 1.9, 0.9 Hz, 1H), 7.50 – 7.45 (m, 1H), 6.94 – 6.93 (m, 1H), 6.60 (ddd, J=7.1, 5.0, 0.9 Hz, 1H), 4.06 (bs, 2H), 3.27 (s, 3H).

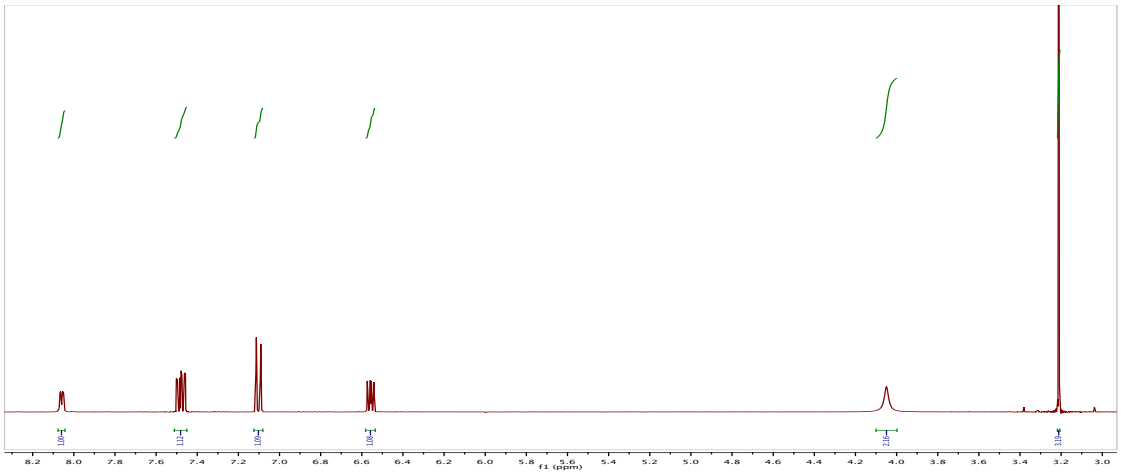

Synthesis of 5-Methyl-2,2´-bipyridine (4.13):

(2-Pyridacyl)pyridium iodide (10.0 g, 0.031 mmol), methacrolein (2.36 g, 0.034 mmol), and ammonium acetate (5.44 g, 0.071 mmol) were dissolved in formamide (95.5 mL). The reaction mixture was stirred at 75 °C for 6 h. After the addition of H_2O, the reaction mixture was extracted with Et_2O. The combined organic solution was washed with brine and dried ($MgSO_4$). The solvent was removed in vacuo, and the residue was subjected to column chromatography (SiO_2; CH_2Cl_2/MeOH, 20:1) to yield 5-methyl-2,2´-bipyridine (**4.13**) (3.26 g, 62%) as an orange oil.

^{1}H NMR (300 MHz,$CDCl_3$) δ 2.36 (s, 3H), 7.23-7.27 (m, 1H), 7.58-7.61 (m, 1H), 7.74-7.80 (m, 1H), 8.25 (d, J) 8.1 Hz, 1H), 8.31-8.35 (m, 1H), 8.48 (d, J) 1.8 Hz, 1H), 8.63, 8.65 (m, 1H); ^{13}C NMR (75 MHz, CDCl3) δ18.3, 120.6, 120.8, 123.4, 133.4, 136.9, 137.5, 149.1, 149.6, 153.6,156.3.

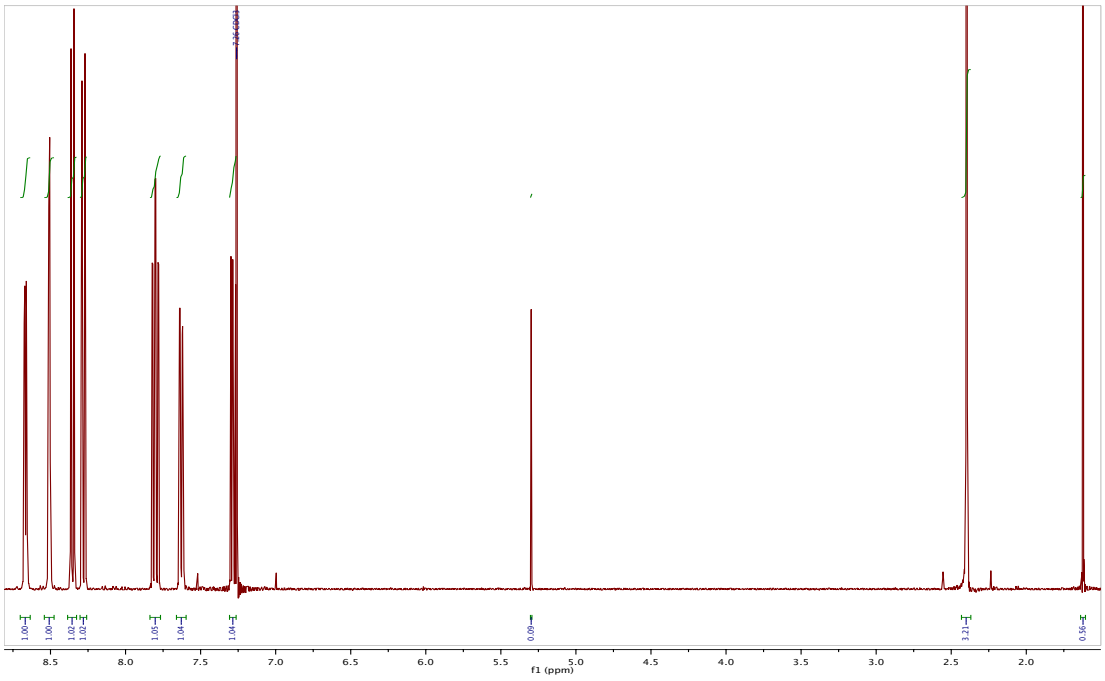

Synthesis of 5-Bromomethyl-2,2´-bipyridine (4.14).

5-Methyl-2,2´-bipyridine (**4.13**; 2.80 g, 16.4 mmol), NBS (2.93 g, 16.4 mmol), and AIBN(673 mg, 4.1 mmol) were refluxed in dry CCl_4 (250 mL) for 8 h. After cooling, the suspension was filtered. The solvent was removed in vacuo and the residue was purified by column chromatography (SiO_2; $CHCl_3/Me_2CO$, 30:20) to yield 5-bromomethyl-2,2´-bipyridine (4.14) (835 mg, 39%) as a yellow solid.

^1H NMR ($CDCl_3$): δ = 8.68 (s, 1 H), 7.97 (m, 2H), 7.75 (m, 2 H), 7.45 (m, 3 H), 4.52 (s, 2 H) ppm.

$C_{12}H_{10}BrN$ (248.1) + 0.25 H_2O: calcd. C 57.05, H 4.19, N 5.54; found C 56.81,H 3.95, N 5.57. DCI MS (NH_3): m/z (%) = 248.1 (33), 250.1 (34)[MH]+.

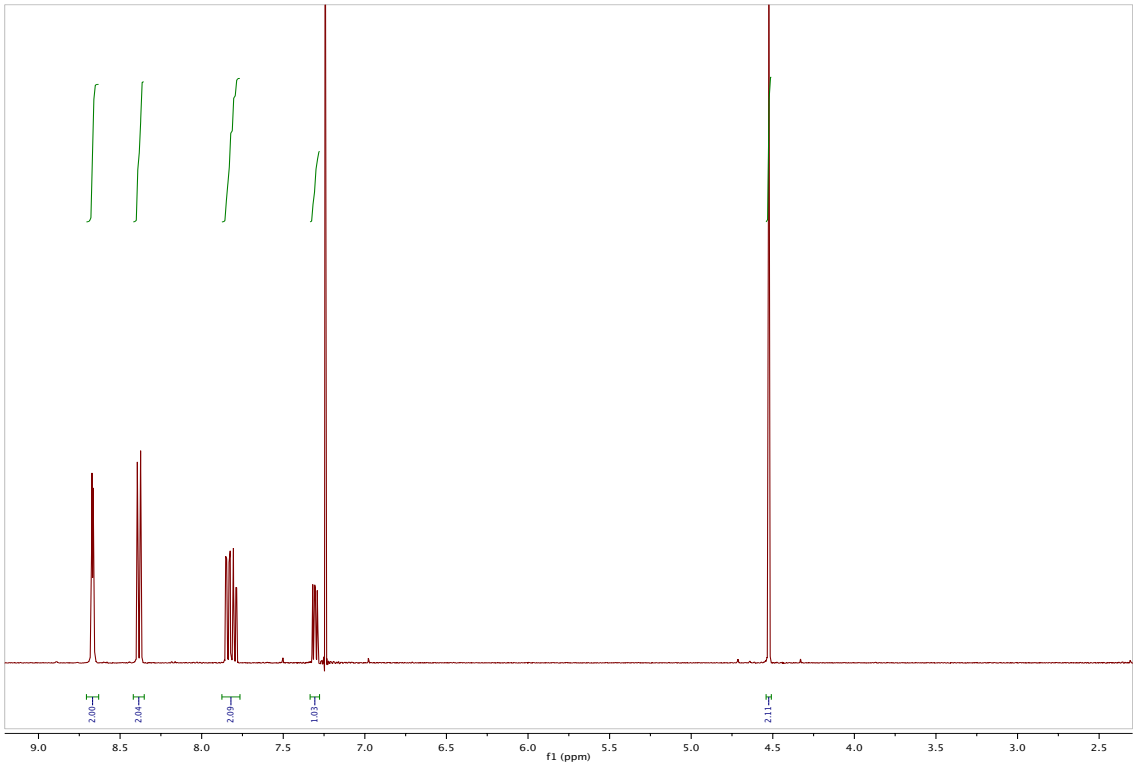

Synthesis of 5-Bromomethyl-2,2′-bipyridine (4.12).

A mixture of dry ethylene glycol (46.6 mg, 0.75 mmol) and NaH (157 mg, excess) in dry thf (23.5 mL) under N_2(g) was stirred for 40 minutes. 5-Bromomethyl-2,2-bipyridine (411 mg, 1.65 mmol) **4.14** was added and the reaction mixture was heated to reflux for 18 h. After cooling, MeOH was added to destroy residual NaH and the solvent was removed in vacuo. The crude mixture was loaded onto a silica column and eluted with 20% MeOH in CH_2Cl_2 to yield **4.12** as a pale yellow oil (0.27 g, 72%), which is hygroscopic.

^{1}H NMR ($CDCl_3$): δ 3.74 (s, 4 H, –OCH_2CH_2O–), 4.66 (s, 4 H, bpy-CH_2–), 7.30 (2 H, ddd), 7.87–7.76 (4 H, m), 8.42–8.35 (4 H, m), 8.72–8.65 (4 H, m).

EIMS: *m/z* 398 [M^+], 229 [M^+ bpy-CH_2].

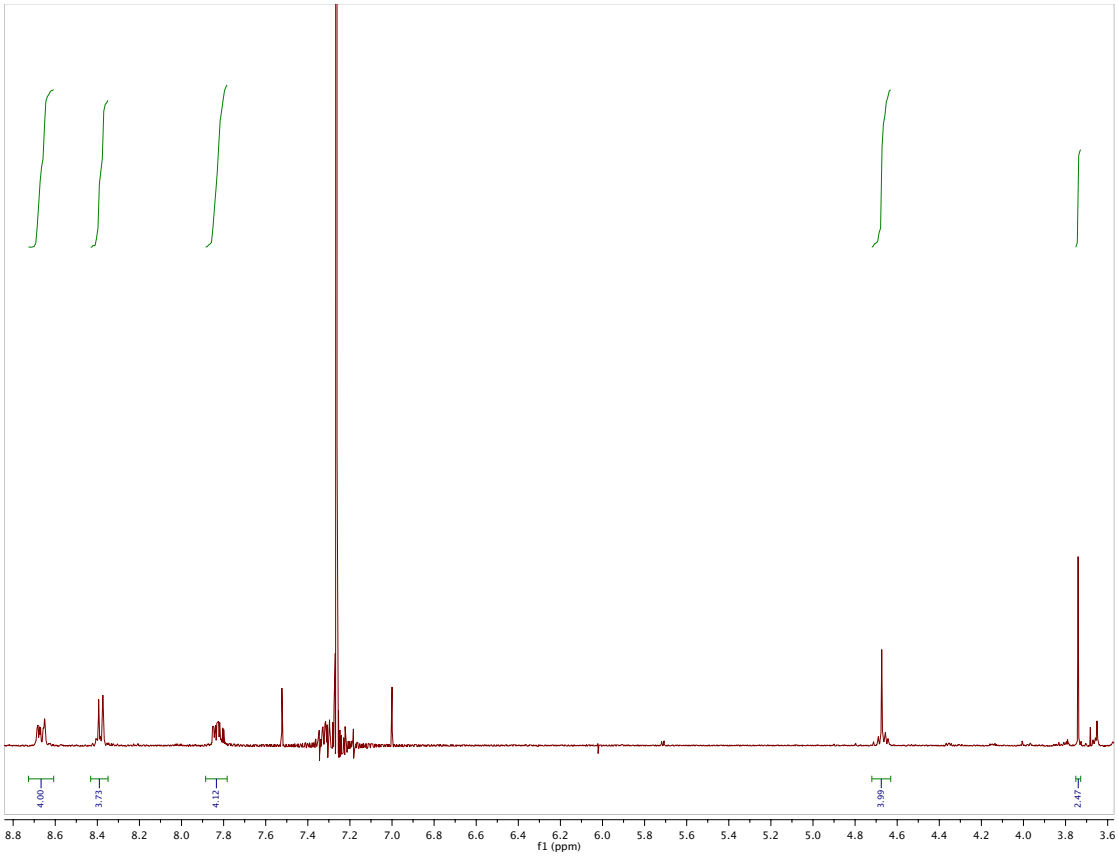

4.6 REFERENCES

1. Purser, S.; Moore, P. R.; Swallow, S.; Gouverneur, V. Fluorine in Medicinal Chemistry. *Chem. Soc. Rev.* **2008**, *37*, 320.

2. Wang, J.; Sanchez-Rosello, M.; Acena, J. L.; del Pozo, C.; Sorochinsky, A. E.; Fustero, S.; Soloshonok, V. A.; Liu, H. Fluorine in Pharmaceutical Industry: Fluorine-Containing Drugs Introduced to the Market in the Last Decade (2001–2011). *Chem. Rev.* **2014**, *114*, 2432.

3. Ge, S.; Chaładaj, W; Hartwig, J. F. Pd-Catalyzed α-Arylation of α,α-Difluoroketones with Aryl Bromides and Chlorides. A Route to Difluoromethylarenes. *J. Am. Chem. Soc.* **2014**, *136*, 4149–4152.

4. Ge, S.; Hartwig, J. F. Nickel-Catalyzed Asymmetric α-Arylation and Heteroarylation of Ketones with Chloroarenes: Effect of Halide on Selectivity, Oxidation State, and Room-Temperature Reactions. *J. Am. Chem. Soc.* **2011,** *133*, 16330–16333.

5. Leung, D.; Anslyn, E.V. Rapid determination of enantiomeric excess of α-chiral cyclohexanones using circular dichroism spectroscopy. *Org. Lett.* **2011**, *13*, 2298-2301.

6. Dragna, J.M.; Pescitelli, G.; Tran, L.; Lynch, V.M.; Anslyn, E.V. In situ assembly of octahedral Fe(II) complexes for the enantiomeric excess determination of chiral amines using circular dichroism spectroscopy. *J. Am. Chem. Soc.* **2012**, *134*, 4298-4407.

7. Simpson, N. R. M.; Ward, M. D.; Morales, A. F.; Barigelletti, F. Solvatochromism as a mechanism for controlling intercomponent photoinduced processes in a bichromophoric complex containing $[Ru(bpy)_3]^{2+}$ and $[Ru(bpy)(CN)_4]_2$ units. *J. Chem. Soc., Dalton Trans.,* **2002**, 2449–2454.

8. Ballardini, R.; Balzani,V.; Clemente-Leo´n, M.; Credi, A.; Gandolfi, M. T.; Ishow, E.; Perkins, J.; Stoddart, J. F.; Tseng, H-R.; Wenger, S. Photoinduced Electron Transfer in a Triad That Can Be Assembled/Disassembled by Two Different External Inputs. Toward Molecular-Level Electrical Extension Cables. . *J. Am. Chem. Soc.* **2002**, *124*, 12786-12795.

9. Labat, L.; Lamère, J-F.; Sasaki, I.; Lacroix, P. G.; Vendier, L.; Asselberghs, I.; Pérez-Moreno, J.; Clays, K. Synthesis, Crystal Structure, and Second-Order Nonlinear Optical Properties of Ruthenium(II) Complexes with Substituted Bipyridine and Phenylpyridine Ligands. *Eur. J. Inorg. Chem.* **2006**, 3105–3113.

Glossary

List of Abbreviations and Acronyms

ANN	Artificial Neural Network
BINAP	2,2’-Bis(diphenylphosphino)-1,1’-binaphthyl
BINOL	1,1’-Bi-2-naphthol
BIPHEP	Biphenylphosphine
BIPY (Bipy)	2,2’-Bipyridine
BPG	Bromopyrogallol Red
BQPA	Bis(quinolinylmethyl)amine
CD	Circular Dichroism
CE	Capillary Electrophoresis
CEA	Cyclohexylethanamine
CEI	(*E*)-2-(((1-cyclohexylethyl)imino)methyl)pyridin-3-ol
COD (cod)	1,5-Cycooctadiene
DIFLUORPHOS	5,5'-Bis(diphenylphosphino)-2,2,2',2'-tetrafluoro-4, 4'-bi-1,3-benzodioxole
d.r	Diastereomeric Ratio
ECCD	Exciton Coupled Circular Dichroism
ee	Enantiomeric Excess
eIDA	enantioselective Indicator Displacement Assay
GC	Gas Chromatography
FPBA	*o*-Formylphenyl boronic acid

HEPES	2-[4-(2-Hydroxyethyl)piperazin-1-yl]ethanesulfonic acid
HPA	2-Heptanamine
HPI	(*E*)-2-((Heptan-2-ylimino)methyl)pyridin-3-ol
HPLC	High Performance Liquid Chromatography
HTS	High-Throughput Screening
LC	Liquid Chromatography
LFER	Linear Free Energy Relationship
MBA	Methylbenzylamine
MBI	(*E*)-2-(((1-phenylethyl)imino)methyl)pyridin-3-ol
ML	4-Methylesculetin
MLCT	Metal Ligand Charge Transfer
MS	Mass Spectroscopy
NMR	Nuclear Magnetic Resonance
PCA	Principle Component Analysis
PV	Pyrocatechol Violet
RDS (rds)	Rate Determining Step
SEGPHOS	4,4'-Bi-1,3-benzodioxole-5,5'-diylbis(diphenylphosphane)
SYNPHOS	6,6'-Bis(diphenylphosphino)-2,2',3,3'-tetrahydro-5,5'-bi-1,4-benzodioxin
THF	Tetrahydrofuran
TMS	Tetramethylsilane
TLC	Thin Layer Chromatography
UV-Vis	Ultraviolet-visible spectroscopy

References

References for Chapter 1:

1. Jaroch, S.; Weinmann, H.; Zietler, K. Asymmetric Organocatalysis. *Chem. Med. Chem.* **2007**, *2*, 1261–1264.

2. Lin, G. Q.; Li, Y. M.; Chan, A. S. *Principles and Applications of Asymmetric Synthesis*; Wiley: New York, 2001.

3. Christmann, M.; Braese, S. *Asymmetric Synthesis: The Essentials, ed.*; Wiley: New York, 2008.

4. Tsukamoto, M.; Kagan, H. B. Recent Advances in the Measurement of Enantiomeric Excesses. *Adv. Synth. Catal.* **2002**, *344*, 453–463.

5. Finn, M. G. Emerging methods for the rapid determination of enantiomeric excess. *Chirality* **2002**, *14*, 534–540.

6. Welch, C. J.; Szczerba, T.; Perrin, S. R. Some recent high-performance liquid chromatography separations of the enantiomers of pharmaceuticals and other compounds using the Whelk-O 1 chiral stationary phase. *J. Chromatogr. A* **1997**, *758*, 93–98.

7. Welch, C. J.; Grau, B.; Moore, J.; Mathre, D. J. Use of Chiral HPLC-MS for Rapid Evaluation of the Yeast-Mediated Enantioselective Bioreduction of a Diaryl Ketone. *J. Org. Chem.* **2001**, *66*, 6836–6837.

8. Welch, C. J.; Fleitz, F.; Antia, F.; Yehl, P.; Waters, R.; Ikemoto, N.; Amstrong, I. J. D.; Mathre, D. Chromatography as an Enabling Technology in Pharmaceutical Process Development: Expedited Multikilogram Preparation of a Candidate HIV Protease Inhibitor. *Org. Process Res. Dev.* **2004**, *8*, 186– 191.

9. Sigman, M. S.; Jacobsen, E. N. Schiff Base Catalysts for the Asymmetric Strecker Reaction Identified and Optimized from Parallel Synthetic Libraries. *J. Am. Chem. Soc.* **1998**, *120*, 4901– 4902.

10. Wolf, C.; Hawes, P. A. A High-Throughput Screening Protocol for Fast Evaluation of Enantioselective Catalysts. *J. Org. Chem.* **2002**, *67*, 2727–2729.

11. Pu, L. Fluorescence of organic molecules in chiral recognition. *Chem. Rev.* **2004**, *104*,1687-1716.

12. Wolf, C.; Bentley, K. W. Chirality sensing using stereodynamic probes with distinct electronic circular dichroism output. *Chem. Soc. Rev.* **2013**, *42*, 5408-5424.

13. Bentley, K. W., Wolf, C. Stereodynamic Chemosensor with Selective Circular Dichroism and Fluorescence Readout for in Situ Determination of Absolute Configuration, Enantiomeric Excess, and Concentration of Chiral Compounds. *J. Am. Chem. Soc.* **2013**, *135*, 12200-12203

14. Zhu, L.; Anslyn, E. V. Facile Quantification of Enantiomeric Excess and Concentration with Indicator-Displacement Assays : An Example in the Analyses of α-Hydroxyacids. *J. Am. Chem. Soc.* **2004**, *126*, 3676.

15. Zhu, L.; Zhong, Z.; Anslyn, E. V. Guidelines in implementing enantioselective indicator-displacement assays for α-hydroxycarboxylates and diols. *J. Am. Chem. Soc.* **2005**, *127*, 4260.

16. Zhu, L.; Shabbir, S. H.; Anslyn, E. V. Two methods for the determination of enantiomeric excess and concentration of a chiral sample with a single spectroscopic measurement. *Chem. Eur. J.* **2007**, *13*, 99.

17. Shabbir, S. H.; Joyce, L. A.; da Cruz, G. M.; Lynch, V. M.; Sorey, S.; Anslyn, E. V. Pattern-based recognition for the rapid determination of identity, concentration, and enantiomeric excess of subtly different threo diols. *J. Am. Chem. Soc.* **2009**, *131*, 13125.

18. Shabbir, S. H.; Anslyn, E. V. A general protocol for creating high-throughput screening assays for reaction yield and enantiomeric excess applied to hydrobenzoin. *Proc. Nat. Acad. Sci.* **2009**, *106*, 10487.

19. Folmer-Andersen, J. F.; Lynch, V. M.; Anslyn, E. V. Colorimetric enantiodiscrimination of α-amino acids in protic media. *J. Am. Chem. Soc.* **2005**, *127*, 7986.

20. Folmer-Andersen, J. F.; Kitamura, M.; Anslyn, E. V. Pattern-based discrimination of enantiomeric and structurally similar amino acids: an optical mimic of the mammalian taste response. *J. Am. Chem. Soc.* **2006**, *128*, 5652.

21. Leung, D.; Folmer-Andersen, J. F.; Lynch, V. M.; Anslyn, E. V. Using Enantioselective Indicator Displacement Assays To Determine the Enantiomeric Excess of α-Amino Acids. *J. Am. Chem. Soc.* **2008**, *130*, 12318.

22. Leung, D.; Anslyn, E. V. Transitioning enantioselective indicator displacement assays for α-amino acids to protocols amenable to high-throughput screening. *J. Am. Chem. Soc.* **2008**, *130*, 12328.

23. Coommans, D.; Massart, D.L.; Kaufman, L. Optimization by statistical linear discriminant analysis in analytical chemistry. *Anal. Chim. Acta.* **1979**, *112*, 97-122.

24. Li, Y.; Jiang, J.-H.; Chen, Z.-P.; Xu, C.-J.; Yu, R.-Q. Robust Linear Discriminant Analysis for Pattern Recognition, *J. Chemom.* **1999**, *13*, 3-13.

25. Ringner, M. What is Principal Component Analysis? *Nat. Biotechnol.* **2008**, 26, 303-304.

26. Nieto, S.; Lynch, V.M.; Anslyn, E.V.; Kim, H.; Chin, J. High-throughput Screening of Identity, Enantiomeric Excess, and Concentration using MLCT Transitions in CD Spectroscopy. *J. Am. Chem. Soc.* **2008**, *130*, 9232-9233.

27. Nieto, S.; Lynch, V.M.; Anslyn, E.V.; Kim, H.; Chin, J. Rapid Identification, Enantiomeric Excess and Concentration Determination Using Simple Racemic Metal Complexes. *Org. Lett.* **2008**, *10*, 5167-5170.

28. Dezhahang, Z.; Merten, C.; Poopari, R.M.; Xu, Y. Vibrational Circular Dichroism Spectroscopy of Two Chiral Binaphthyl Diphosphine ligands and their Palladium Complexes in Solution. *Dalton Trans.* **2012**, *41*, 10817.

29. Nieto, S.; Dragna, J.M.; Anslyn, E.V. A Facile Circular Dichroism Protocol for Rapid Determination of Enantiomeric Excess and Concentration of Chiral Primary Amines. *Chem. Eur. J.* **2010**, *16*, 227-232.

30. Leung, D.; Anslyn, E.V. Rapid determination of enantiomeric excess of α-chiral cyclohexanones using circular dichroism spectroscopy. *Org. Lett.* **2011**, *13*, 2298-2301.

31. Perez-Fuertes, Y.; Kelly, A.M.; Arimori, S.; Bull, S.D.; James, T.D. Simple protocol for NMR analysis of the enantiomeric purity of diols. *Org. Lett.* **2006**, *8*, 1971-1974.

32. Perez-Fuertes, Y.; Kelly, A.M.; Fossey, J.S.; Powell, S.D.; Bull, S.D.; James, T.D. Simple protocols for NMR analysis of the enantiomeric purity of chiral primary amines. *Nat. Protoc.* **2008**, *3*, 210-214.

33. Metola, P.; Anslyn, E.V.; James, T.D.; Bull, S.D. Circular dichroism of multi-component assemblies for chiral amine recognition and rapid ee determination. *Chem. Sci.* **2012**, *3*, 156-161.

34. Berova, N.; Di Bari, L.; Pescitelli, G. Application of electronic circular dichroism in configurational and conformational analysis of organic compounds. *Chem. Soc. Rev.* **2007**, *36*, 914-931.

35. Zahn. S.; Canary, J.W. Absolute Configurations of Primary Amines from Exciton-Coupled Circular Dichroism Spectra of Cu(II) Complexes of their N,N-Bisquinaldyl Derivatives. *Org. Lett.* **1999**, *1*, 861-864.

36. Zhang, J.; Holmes, A.E.; Sharma, A.; Brooks, N.R.; Rarig, R.S.; Zubieta, J.; Canary, J.W. Derivatization, Complexation and Absolute Configurational Assignment of Chiral Primary Amines: Application of Exciton-Coupled Circular Dichroism. *Chirality*. **2003**, *15*, 180-189.

37. Huang, X.; Nakanishi, K.; Berova, N. Porphyrins and Metalloporphyrins: Versatile Circular Dichroic Reporter Groups for Structural Studies. *Chirality*, **2000**, *12*, 237-255

38. Balaz, M.; De Napoli, M.; Holmes, A.E.; Mammana, A.; Nakanishi, K.; Berova, N.; Purrello, R. A cationic zinc porphyrin as a chiroptical sensor for Z-DNA. *Angew. Chem. Int. Ed.* **2005**, *44*, 4006-4009.

39. Matile, S.; Berova, N.; Nakanishi, K.; Novakova, S.; Philipova, I. Blagoev, B. Porphyrins: Powerful Chromophores for Structural Studies by Exciton-Coupled Circular Dichroism. *J. Am. Chem. Soc.* **1995**, *117*, 7021-7022.

40. Furusho, Y.; Kimura, T.; Mizuno, Y.; Aida, T. Chirality-Memory Molecule: A D2-Symmetric Fully Substituted Porphyrin as a Conceptually New Chirality Sensor. *J. Am. Chem. Soc.* **1997**, *119*, 5267-5268.

41. Tanasova, M.; Yang, Q.; Olmsted, C.C.; Vasileiou, C.; Li, X.; Anyika, M.; Borhan, B. An Unusual Conformation of α-Haloamides Due to Cooperative Binding with Zincated Porphyrins. *Eur. J. Org. Chem.* **2009**, 4242-4253.

42. Borovkov, V.V.; Lintuluoto, J.M.; Inoue, Y. Supramolecular Chirogenesis in Zinc Porphyrins: Mechanism, Role of Guest Structure, and Application for the Absolute Configuration Determination. *J. Am. Chem. Soc.* **2001**, *123*, 2979-2989.

43. Li, X.; Borhan, B. Prompt determination of absolute configuration for epoxy alcohols via exciton chirality protocol. *J. Am. Chem. Soc.* **2008**, *130*, 16126-16127.

44. Li, X.; Burrell, C.E.; Staples, R.J.; Borhan, B. Absolute Configuration for 1,n-Glycols: A Nonempirical Approach to Long-Range Stereochemical Determination. *J. Am. Chem. Soc.* **2012**, *134*, 9026-9029.

45. Dragna, J.M.; Pescitelli, G.; Tran, L.; Lynch, V.M.; Anslyn, E.V. In situ assembly of octahedral Fe(II) complexes for the enantiomeric excess determination of chiral amines using circular dichroism spectroscopy. *J. Am. Chem. Soc.* **2012**, *134*, 4298-4407.

46. Barman, S.; Anslyn, E.V. Rapid determination of enantiomeric excess of α-chiral aldehydes using circular dichroism spectroscopy. *Tetrahedron*. **2014**, *70*, 1357-1362.

47. Joyce, L.A.; Maynor, M.S.; Dragna, J.M.; Cruz, G.M.; Lynch, V.M.; Canary, J.W.; Anslyn, E.V. A simple method for the determination of enantiomeric excess and identity of chiral carboxylic acids. *J. Am. Chem. Soc.* **2011**, *133*, 13764-13752.

48. Joyce, L.A.; Canary, J.W.; Anslyn, E.V. Enantio- and chemoselective differentiation of protected α-amino acids and β-homoamino acids with a single copper(II) host. *Chem. Eur. J.* **2012**, *18*, 8064-8069.

49. You, L.; Berman, J.S.; Anslyn, E.V. Dynamic multi-component covalent assembly for the reversible binding of secondary alcohols and chirality sensing. *Nature. Chem.* **2011**, *3*, 943–948.

50. You, L.; Pescitelli, G.; Anslyn, E.V.; Di Bari, L. An exciton-coupled circular dichroism protocol for the determination of identity, chirality, and enantiomeric excess of chiral secondary alcohols. *J. Am. Chem. Soc.* **2012**, *134*, 7117-7125.

51. You, L.; Berman, J.S.; Lcuksanawichien, A.; Anslyn, E.V. Correlating Sterics Parameters and Diastereomeric Ratio Values for a Multicomponent Assembly To

Predict Exciton-Coupled Circular Dichroism Intensity and Thereby Enantiomeric Excess of Chiral Secondary Alcohols. *J. Am. Chem. Soc.* **2012**, *134*, 7126-7134.

52. Terrett, N.K.; Gardner, M.; Gordon, D.W.; Kobylecki, R. J.; Steele, J. Combinatorial synthesis-the design of compound libraries and their application to drug discovery. *Tetrahedron* **1995**, *51*, 8135.

53. Pescarmona, P. P.; Van der Waal, J. C.; Maxwell, I. E.; Maschmeyer, T. Combinatorial chemistry, high-speed screening and catalysis. *Catal. Lett.* **1999**, *63*, 1.

54. Guebitz, G.; Schmid, M. G. Chiral separation principles in chromatographic and electromigration techniques. *Mol. Biotechnol.* **2006**, *32*, 159.

55. Thompson, R. A practical guide to HPLC enantioseparations for pharmaceutical compounds. *J. Liq. Chromatogr. Relat. Technol.* **2005**, *28*, 1215

56. Zhang, Y.; Wu, D.-R.; Wang-Iverson, D. B.; Tymiak, A. A. Enantioselective chromatography in drug discovery. *Drug Discovery Today* **2005**, *10*, 571

57. Ahuja, S. A strategy for developing HPLC methods for chiral drugs. *LCGC North Am.* **2008**, 70.

58. Chen, L.; Zhao, Y.; Gao, F.; Garland, M. Determination of enantiomeric excess using the ultraviolet-circular dichroism and the high-performance liquid chromatography-circular dichroism methods. *Appl. Spectrosc.* **2003**, *57*, 797.

59. Traverse, J. F.; Snapper, M. L. High-throughput methods for the development of new catalytic asymmetric reactions. *Drug Discovery Today* **2002**, *7*, 1002.

60. Kuhr, W. G.; Monnig, C. A. Capillary electrophoresis. *Anal. Chem.* **1992**, *64*, 389.

References for Chapter 2:

1. Aitken A.; Kilényi, S. N. Asymmetric Synthesis. 1992.

2. Hadik, P.; Szabó, L.-P.; Nagy, E. D,L-lactic acid and D,L-alanine enantioseparation by membrane process. *Desalination*, 2002, **148**, 193–198.

3. Farina, V.; Reeves, J. T.; Senanayake, C. H.; Song, J. J. Asymmetric synthesis of active pharmaceutical ingredients. *Chem. Rev.*, 2006, **106**, 2734–2793.

4. C. A. Busacca, D. R. Fandrick, J. J. Song, and C. H. Senanayake, *Adv. Synth. Catal.*, 2011, **353**, 1825–1864.

5. Etayo, P.; Vidal-Ferran, A. Rhodium-catalysed asymmetric hydrogenation as a valuable synthetic tool for the preparation of chiral drugs. *Chem. Soc. Rev.*, 2013, **42**, 728–754.

6. Ager, D. J.; de Vries, A. H. M.; de Vries, J. G. Asymmetric homogeneous hydrogenations at scale. *Chem. Soc. Rev.*, 2012, **41**, 3340–3380.

7. Blaser, H.-U. The Chiral Switch of (S)-Metolachlor: A Personal Account of an Industrial Odyssey in Asymmetric Catalysis. *Adv. Synth. Catal.*, 2002, **344**, 17–31.

8. Blaser, H.-U.; Pugin, B.; Spindler, F.; Thommen, M. From a chiral switch to a ligand portfolio for asymmetric catalysis. *Acc. Chem. Res.*, 2007, **40**, 1240–1250.

9. Ketcham, J. M.; Shin, I.; Montgomery, T. P.; Krische, M. J. Catalytic enantioselective C-H functionalization of alcohols by redox-triggered carbonyl addition: borrowing hydrogen, returning carbon. *Angew. Chem. Int. Ed. Eng.*, 2014, **53**, 9142–9150.

10. Hassan A.; Krische, M. J. Unlocking Hydrogenation for C-C Bond Formation: A Brief Overview of Enantioselective Methods. *Org. Proc. Res. Dev.*, 2011, **15**, 1236–1242.

11. Kim, I. S.; Ngai, M.-Y.; Krische, M. J. Enantioselective iridium-catalyzed carbonyl allylation from the alcohol or aldehyde oxidation level using allyl acetate as an allyl metal surrogate. *J. Am. Chem. Soc.*, 2008, **130**, 6340–6341.

12. Kim, I. S.; Ngai, M.-Y.; Krische, M. J. Enantioselective iridium-catalyzed carbonyl allylation from the alcohol or aldehyde oxidation level via transfer hydrogenative coupling of allyl acetate: departure from chirally modified allyl metal reagents in carbonyl addition. *J. Am. Chem. Soc.*, 2008, **130**, 14891–14899.

13. Lu, Y.; Kim, I. S.; Hassan, A.; Del Valle, D. J.; Krische, M. J. 1,n-glycols as dialdehyde equivalents in iridium-catalyzed enantioselective carbonyl allylation and iterative two-directional assembly of 1,3-polyols. *Angew. Chem. Int. Ed. Eng.*, 2009, **48**, 5018–5021.

14. Schmitt, D. C.; Dechert-Schmitt, A.-M. R.; Krische, M. J. Iridium-catalyzed allylation of chiral β-stereogenic alcohols: bypassing discrete formation of epimerizable aldehydes. *Org Lett*, 2012, **14**, 6302–6305.

15. Dechert-Schmitt, A.-M. R.; Schmitt, D. C.; Krische, M. J. Protecting-group-free diastereoselective C-C coupling of 1,3-glycols and allyl acetate through site-selective primary alcohol dehydrogenation. *Angew. Chem. Int. Ed.*, 2013, **52**, 3195–3198.

16. Dechert-Schmitt, A.-M. R.; Schmitt, D. C.; Gao, X.; Itoh, T.; Krische, M. J. Polyketide construction via hydrohydroxyalkylation and related alcohol C-H functionalizations: reinventing the chemistry of carbonyl addition. *Nat Prod Rep*, 2014, **31**, 504–513.

17. Han, S. B.; Hassan, A.; Kim, I. S.; Krische, M. J. Total synthesis of (+)-roxaticin via C-C bond forming transfer hydrogenation: a departure from stoichiometric chiral reagents, auxiliaries, and premetalated nucleophiles in polyketide construction. *J. Am. Chem. Soc.*, 2010, **132**, 15559–15561.

18. Gao, X.; Woo, S. K.; Krische, M. J. Total synthesis of 6-deoxyerythronolide B via C-C bond-forming transfer hydrogenation. *J. Am. Chem. Soc.*, 2013, **135**, 4223–4226.

19. Lu, Y.; Woo, S. K.; Krische, M. J. Total synthesis of bryostatin 7 via C-C bond-forming hydrogenation. *J. Am. Chem. Soc.*, 2011, **133**, 13876–13879.

20. Willwacher J.; Fürstner, A. Catalysis-based total synthesis of putative mandelalide A. *Angew. Chem. Int. Ed. Eng.*, 2014, **53**, 4217–4221.

21. Feng, Y.; Jiang, X.; De Brabander, J. K. Studies toward the unique pederin family member psymberin: full structure elucidation, two alternative total syntheses, and analogs. *J. Am. Chem. Soc.*, 2012, **134**, 17083–17093.

22. Wan, S.; Wu, F.; Rech, J. C.; Green, M. E.; Balachandran, R.; Horne, W. S.; Day, B. W.; Floreancig, P. E. Total synthesis and biological evaluation of pederin, psymberin, and highly potent analogs. *J. Am. Chem. Soc.*, 2011, **133**, 16668–16679.

23. Kretschmer, M.; Dieckmann, M.; Li, P.; Rudolph, S.; Herkommer, D.; Troendlin, J. Menche, D. *Chem. Eur. J.*, 2013, **19**, 15993–16018.

24. Prévost, S.; Thai, K.; Schützenmeister, N.; Coulthard, G.; Erb, W.; Aggarwal, V. K. Synthesis of Prostaglandin Analogues, Latanoprost and Bimatoprost, Using Organocatalysis via a Key Bicyclic Enal Intermediate. *Org. Lett.*, 2015, **17**, 504–507.

25. Jo, H. H.; Lin, C.-Y.; Anslyn, E. V. Rapid optical methods for enantiomeric excess analysis: from enantioselective indicator displacement assays to exciton-coupled circular dichroism. *Acc. Chem. Res.*, 2014, **47**, 2212–2221.

26. Zhu, L.; Zhong, Z.; Anslyn, E. V. Guidelines in implementing enantioselective indicator-displacement assays for alpha-hydroxycarboxylates and diols. *J. Am. Chem. Soc.*, 2005, **127**, 4260–4269.

27. Leung, D.; Folmer-Andersen, J. F.; Lynch, V. M.; Anslyn, E. V. Using enantioselective indicator displacement assays to determine the enantiomeric excess of alpha-amino acids. *J. Am. Chem. Soc.*, 2008, **130**, 12318–12327.

28. Shabbir, S. H. ; Joyce, L. A.; da Cruz, G. M.; Lynch, V. M.; Sorey, S.; Anslyn, E. V. Pattern-based recognition for the rapid determination of identity, concentration, and enantiomeric excess of subtly different threo diols. *J. Am. Chem. Soc.*, 2009, **131**, 13125–13131.

29. Pu, L. Fluorescence of organic molecules in chiral recognition. *Chem. Rev.*, 2004, **104**, 1687–1716.

30. Hembury, G. A.; Borovkov, V. V.; Inoue, Y. Chirality-sensing supramolecular systems. *Chem. Rev.*, 2008, **108**, 1–73.

31. Berova, N.; Di Bari, L.; Pescitelli, G. Application of electronic circular dichroism in configurational and conformational analysis of organic compounds. *Chem. Soc. Rev.*, 2007, **36**, 914–931.

32. Wolf C.; Bentley, K. W. Chirality sensing using stereodynamic probes with distinct electronic circular dichroism output. *Chem. Soc. Rev.*, 2013, **42**, 5408–5424.

33. Nieto, S.; Dragna, J. M.; Anslyn, E. V. A facile circular dichroism protocol for rapid determination of enantiomeric excess and concentration of chiral primary amines. *Chem. Eur. J.*, 2010, **16**, 227–232.

34. You, L.; Berman, J. S; Anslyn, E. V. Dynamic multi-component covalent assembly for the reversible binding of secondary alcohols and chirality sensing *Nat. Chem.*, 2011, **3**, 943–948.

35. Joyce, L. A.; Maynor, M. S.; Dragna, J. M.; da Cruz, G. M.; Lynch, V. M.; Canary, J. W.; Anslyn, E. V. A simple method for the determination of enantiomeric excess and identity of chiral carboxylic acids. *J. Am. Chem. Soc.*, 2011, **133**, 13746–13752.

36. Leung D.; Anslyn, E. V. Rapid determination of enantiomeric excess of α-chiral cyclohexanones using circular dichroism spectroscopy. *Org. Lett.*, 2011, **13**, 2298–2301.

37. Fiedler, S.; Cole, L.; Keller, S. Automated Circular Dichroism Spectroscopy for Medium-Throughput Quantification of Protein Conformation. *Biophy. J.*, 2013, **104**, 20a.

38. Metola, P.; Nichols, S. M.; Kahr, B.; Anslyn, E. V. Well Plate Circular Dichroism Reader for the Rapid Determination of Enantiomeric Excess. *Chem. Sci.*, 2014, **5**, 4278–4282.

39. Zhao, Q.; Wen, J.; Tan, R.; Huang, K.; Metola, P.; Wang, R.; Anslyn, E. V.; Zhang X., Rhodium-catalyzed asymmetric hydrogenation of unprotected NH imines assisted by a thiourea. *Angew. Chem. Int. Ed.*, 2014, **53**, 8467–8470.

40. Giuliano, M. W.; Lin, C.-Y.;Romney, D. K.; Miller, S. J.; Anslyn, E. V. *Adv. Synth. Catal.* **2015**, *357*, *In Press*. DOI: 10.1002/adsc.201500230.

41. Yoon, H.; Lee, C.-H.; Jang, W.-D. Absolute stereochemical determination of chiral carboxylates using an achiral molecular tweezer. *Chem. Eur. J.*, 2012, **18**, 12479–12486.

42. Han, S. B.; Gao, X.; Krische, M. J. Iridium-catalyzed anti-diastereo- and enantioselective carbonyl (trimethylsilyl)allylation from the alcohol or aldehyde oxidation level. *J. Am. Chem. Soc.*, 2010, **132**, 9153–9156.

43. Han, S. B.; Han, H.; Krische, M. J. Diastereo- and enantioselective anti-alkoxyallylation employing allylic gem-dicarboxylates as allyl donors via iridium-catalyzed transfer hydrogenation. *J. Am. Chem. Soc.*, 2010, **132**, 1760–1761.

44. Gao, X.; Zhang, Y. J.; Krische, M. J. Iridium-catalyzed anti-diastereo- and enantioselective carbonyl (α-trifluoromethyl)allylation from the alcohol or aldehyde oxidation level. *Angew. Chem. Int. Ed.*, 2011, **50**, 4173–4175.

45. Jo, H. H.; Edupuganti, R.; You, L.; Dalby, K. N.; Anslyn, E. V. Mechanistic studies on covalent assemblies of metal-mediated hemi-aminal ethers. *Chem. Sci.*, 2015, **6**, 158–164.

46. You, L.; Berman, J. S.; Lucksanawichien, A.; Anslyn, E. V. *J. Am. Chem. Soc.*, 2012, **134**, 7126–7134.

47. Khedr A.; Sheha, M. Quantitative Thin-Layer Chromatographic Method of Analysis of Azithromycin in Pure and Capsule Forms *J. Chromatogr. Sci.*, 2003, **41**, 10–16.

48. Hess, A. V. I. Digitally Enhanced Thin-Layer Chromatography: An Inexpensive, New Technique for Qualitative and Quantitative Analysis. *J. Chem. Educ.*, 2007, **84**, 842.

49. Askal, H. F.; Khedr, A. S.; Darwish, I. A.; Mahmoud, R. M. Quantitative Thin-Layer Chromatographic Method for Determination of Amantadine Hydrochloride. *Int. J. Biomed. Sci.,* 2008, **4**, 155–160.

50. Hoeltz, M.; Welke, J. E.; Noll, I. B.; Dottori, H. A. Photometric procedure for quantitative analysis of Aflatoxin B1 in peanuts by thin-layer chromatography using charge coupled device detector *Quím. Nova.*, 2010, **33**, 43–47.

References for Chapter 3:

1. Jin, Y.; Yu, C.; Denman, R. J.; Zhang, W. Recent advances in dynamic covalent chemistry. *Chem. Soc. Rev.*, 2013, **42**, 6634-6654.

2. Gasparini, G.; Dal Molin, M.; Lovato A.; Prins, L. J. in *Supramolecular Chemistry*: *From Molecules to Nanomaterials*, ed. J. W. Steed and P. A. Gale, John Wiley & Sons, Ltd, 2012, DOI: 10.1002/9780470661345.

3. Miller, B. L. *Dynamic Combinatorial Chemistry*, John Wiley & Sons, 2009.

4. Corbett, P. T.; Leclaire, J.; Vial, L.; West, K. R.;. Wietor, J.-L; Sanders, J. K. M.; Otto, S. Dynamic combinatorial chemistry. *Chem. Rev.*, 2006, **106**, 3652–3711.

5. Lehn, J.-M. From supramolecular chemistry towards constitutional dynamic chemistry and adaptive chemistry. *Chem. Soc. Rev.*, 2007, **36**, 151–160.

6. Wojtecki, R. J.; Meador, M. A.; Rowan, S. J. Using the dynamic bond to access macroscopically responsive structurally dynamic polymers. *Nat. Mater.*, 2011, **10**, 14–27.

7. Wilson, A.; Gasparini, G.; Matile, S. *Chem. Soc. Rev.*, Functional systems with orthogonal dynamic covalent bonds. 2014, **43**, 1948–1962.

8. Jiang, X.; Lim, Y.-K.; Zhang, B. J.; Opsitnick, E. A.; Baik, M.-H.; Lee, D. Dendritic molecular switch: chiral folding and helicity inversion. *J. Am. Chem. Soc.*, 2008, **130**, 16812–16822.

9. Yang, Y.; Pei, X.-L.; Wang, Q.-M. Postclustering dynamic covalent modification for chirality control and chiral sensing. *J. Am. Chem. Soc.*, 2013, **135**, 16184–16191.

10. Vongvilai, P.; Ramström, O. Dynamic asymmetric multicomponent resolution: lipase-mediated amidation of a double dynamic covalent system. *J. Am. Chem. Soc.*, 2009, **131**, 14419–14425.

11. Rowan, S. J.; Cantrill, S. J.; Cousins, G. R. L.; Sanders, J. K. M.; Stoddart, J. F. Dynamic covalent chemistry. *Angew. Chem. Int. Ed. Engl.*, 2002, **41**, 898–952.

12. Herrmann, A. Dynamic combinatorial/covalent chemistry: a tool to read, generate and modulate the bioactivity of compounds and compound mixtures. *Chem. Soc. Rev.*, 2014, **43**, 1899–1933.

13. Lehn, J.-M. Constitutional dynamic chemistry: bridge from supramolecular chemistry to adaptive chemistry. *Top. Curr. Chem.*, 2012, **322**, 1–32.

14. Black, S. P.; Sanders, J. K. M.; Stefankiewicz, A. R. Disulfide exchange: exposing supramolecular reactivity through dynamic covalent chemistry. *Chem. Soc. Rev.*, 2014, **43**, 1861–1872.

15. Jin, Y.; Wang, Q.; Taynton, P.; Zhang, W. Dynamic covalent chemistry approaches toward macrocycles, molecular cages, and polymers. *Acc. Chem. Res.*, 2014, **47**, 1575–1586.

16. Aricó, F.; Chang, T.; Cantrill, S. J.; Khan, S. I.; Stoddart, J. F. Template-directed synthesis of multiply mechanically interlocked molecules under thermodynamic control. *Chem. Eur. J.*, 2005, **11**, 4655–4666.

17. Hadik, P.; Szabó, L.-P.; Nagy, E. D,L-lactic acid and D,L-alanine enantioseparation by membrane process. *Desalination*, 2002, **148**, 193–198.

18. Reetz, M. T.; Sell, T.; Meiswinkel, A.; MehlerK, G. A New Principle in Combinatorial Asymmetric Transition-Metal Catalysis: Mixtures of Chiral Monodentate P Ligands. *Angew. Chem. Int. Ed.,* 2003, **42**, 790-793.

19. Eelkema, R.; van Delden, R. A.; Feringa, B. L. Direct Visual Detection of the Stereoselectivity of a Catalytic Reaction. *Angew. Chem. Int. Ed.,* 2004, **43**, 5013-5016.

20. Long, J.; Hu, J.; Shen, X.; Ji, B.; Ding, K. Discovery of Exceptionally Efficient Catalysts for Solvent-Free Enantioselective Hetero-Diels–Alder Reaction*J. Am. Chem. Soc.*, 2002, **124**, 10-11.

21. You, L.; Berman, J. S.; Anslyn, E. V. Dynamic multi-component covalent assembly for the reversible binding of secondary alcohols and chirality sensing. *Nature. Chem.*, 2011, **3**, 943–948.

22. You, L.; Long, S. R.; Lynch, V. M.; Anslyn, E. V .Dynamic Multicomponent Hemiaminal Assembly. *Chem. Eur. J.*, 2011, **17**, 11017–11023.

23. You, L.; Pescitelli, G.; Anslyn, E. V.; Di Bari, L. An exciton-coupled circular dichroism protocol for the determination of identity, chirality, and enantiomeric excess of chiral secondary alcohols. *J. Am. Chem. Soc.*, 2012, **134**, 7117–7125.

24. You, L.; Berman, J. S.; Lucksanawichien, A.; Anslyn, E. V. Correlating sterics parameters and diastereomeric ratio values for a multicomponent assembly to predict exciton-coupled circular dichroism intensity and thereby enantiomeric excess of chiral secondary alcohols. *J. Am. Chem. Soc.*, 2012, **134**, 7126–7134.

25. Li, G.; Fronczek, F. R.; Antilla, J. C. Catalytic asymmetric addition of alcohols to imines: enantioselective preparation of chiral N,O-aminals. *J. Am. Chem. Soc.*, 2008, **130**, 12216–12217.

26. Star, A.; Goldberg, I.; Fuchs, B. Dioxadiazadecalin/Salen Tautomeric Macrocycles and Complexes: Prototypal Dynamic Combinatorial Virtual Libraries New Supramolecular Host Systems, Part 12. Part 11: ref. 1. We gratefully acknowledge support by a research grant from the Israel Science Foundation and by an Intel Scholarship (to A.S.), as well as the valuable assistance of Shimon Hauptman with mass spectrometry and Yuri Paskover as an undergraduate research student. *Angew. Chem. Int. Ed. Engl.*, 2000, **39**, 2685–2689.

27. Fuchs, B.; Nelson, A.; Star, A.; Stoddart, J. F.; Vidal, S. Amplification of dynamic chiral crown ether complexes during cyclic acetal formation. *Angew. Chem. Int. Ed. Engl.*, 2003, **42**, 4220–4224.

28. Mason J. P.; Block, H. W. Preparation and Polymerization of β-4-Morpholinoethyl Chloride. *J. Am. Chem. Soc.*, 1940, **62**, 1443.

29. Lakhdar, S.; Tokuyasu, T.; Mayr, H. Electrophilic Reactivities of α,β-Unsaturated Iminium Ions. *Angew. Chem. Int. Ed. Engl.*, 2008, **47**, 8723–8726.

30. Baldwin, J. E. *J. Chem. Soc.,* Rules for ring closure. *Chem. Commun.* 1976, 734-736

31. Baldwin, J. E.; Thomas, R. C.; Kruse, L.I.; Silberman, L. Rules for ring closure: ring formation by conjugate addition of oxygen nucleophiles*J. Org. Chem.*, 1977, **42**, 3846–3852

32. Eldin, S.; Jencks, W. P. Lifetimes of Iminium Ions in Aqueous Solution.*J. Am. Chem. Soc.*, 1995, **117**, 4851–4857.

33. Eldin, S.; Digits, J. A.; Huang, S-T.; Jencks, W. P. Lifetime of an Aliphatic Iminium Ion in Aqueous Solution. *J. Am. Chem. Soc.*, 1995, **117**, 6631–6632.

34. Eldin, S.; Jencks, W. P. Concerted Bimolecular Substitution Reactions of Anilino Thioethers. *J. Am. Chem. Soc.*, 1995, **117**, 9415–9418.

35. Dalby, K. N.; Jencks, W. P. Lifetimes of Imidinium Ions in Aqueous Solution*J. Am. Chem. Soc.*, 1997, **119**, 7271–7280.

36. Pearson, R. G.; Sobel, H. R.; Songstad, J. Nucleophilic reactivity constants toward methyl iodide and trans-dichlorodi(pyridine)platinum(II). *J. Am. Chem. Soc.*, 1968, **90**, 319–326.

37. Mendham, J.; Denney, R. C.; Barnes, J. D.; Thomas, M. J. K. *Vogel's Quantitative Chemical Analysis (6th Edition)*, Prentice Hall, 6th ed. 2000.

38. Ritchie C. D.; Sager, W. F. Progress in Physical Organic Chemistry. *Prog. Phys. Org. Chem.*, 1964, **2**, 323-400.

39. Chen, R.; Zhang, K.-C.; Liu, L.; Li, X.-S.; Guo, Q.-X. Substituent effects in X-C≡C-H···NH3 (or OH2, FH) hydrogen bonding. *Chem. Phy. Lett.*, 2001, **338**, 61–66.

References for Chapter 4:

1. Purser, S.; Moore, P. R.; Swallow, S.; Gouverneur, V. Fluorine in Medicinal Chemistry. *Chem. Soc. Rev.* **2008**, *37*, 320.

2. Wang, J.; Sanchez-Rosello, M.; Acena, J. L.; del Pozo, C.; Sorochinsky, A. E.; Fustero, S.; Soloshonok, V. A.; Liu, H. Fluorine in Pharmaceutical Industry: Fluorine-Containing Drugs Introduced to the Market in the Last Decade (2001–2011). *Chem. Rev.* **2014**, *114*, 2432.

3. Ge, S.; Chaładaj, W; Hartwig, J. F. Pd-Catalyzed α-Arylation of α,α-Difluoroketones with Aryl Bromides and Chlorides. A Route to Difluoromethylarenes. *J. Am. Chem. Soc.* **2014**, *136*, 4149–4152.

4. Ge, S.; Hartwig, J. F. Nickel-Catalyzed Asymmetric α-Arylation and Heteroarylation of Ketones with Chloroarenes: Effect of Halide on Selectivity, Oxidation State, and Room-Temperature Reactions. *J. Am. Chem. Soc.* **2011,** *133*, 16330–16333.

5. Leung, D.; Anslyn, E.V. Rapid determination of enantiomeric excess of α-chiral cyclohexanones using circular dichroism spectroscopy. *Org. Lett.* **2011**, *13*, 2298-2301.

6. Dragna, J.M.; Pescitelli, G.; Tran, L.; Lynch, V.M.; Anslyn, E.V. In situ assembly of octahedral Fe(II) complexes for the enantiomeric excess determination of chiral amines using circular dichroism spectroscopy. *J. Am. Chem. Soc.* **2012**, *134*, 4298-4407.

7. Simpson, N. R. M.; Ward, M. D.; Morales, A. F.; Barigelletti, F. Solvatochromism as a mechanism for controlling intercomponent photoinduced processes in a

bichromophoric complex containing $[Ru(bpy)_3]^{2+}$ and $[Ru(bpy)(CN)_4]_2$ units. *J. Chem. Soc., Dalton Trans.,* **2002**, 2449–2454.

8. Ballardini, R.; Balzani,V.; Clemente-Leo´n, M.; Credi, A.; Gandolfi, M. T.; Ishow, E.; Perkins, J.; Stoddart, J. F.; Tseng, H-R.; Wenger, S. Photoinduced Electron Transfer in a Triad That Can Be Assembled/Disassembled by Two Different External Inputs. Toward Molecular-Level Electrical Extension Cables. . *J. Am. Chem. Soc.* **2002**, *124*, 12786-12795.

9. Labat, L.; Lamère, J-F.; Sasaki, I.; Lacroix, P. G.; Vendier, L.; Asselberghs, I.; Pérez-Moreno, J.; Clays, K. Synthesis, Crystal Structure, and Second-Order Nonlinear Optical Properties of Ruthenium(II) Complexes with Substituted Bipyridine and Phenylpyridine Ligands. *Eur. J. Inorg. Chem.* **2006**, 3105–3113.

Vita

Hyun Hwa Jo aka Hannah was born and raised in Seoul, South Korea. In 2006, she came to the United States for her undergraduate degree, first attending Stony Brook University and eventually transferring to the University of California at Berkeley. During her time there, she performed research under the guidance of Dr. Gabor Somorjai on the synthesis of dendrimer encapsulated one nanometer Rh and Pt particles, for their catalytic activity for ethylene and pyrrole hydrogenation. After receiving her Bachelor of Science degree in Chemistry from UC Berkeley, she joined the graduate program at the University of Texas in Austin in 2010. There, Hannah went on to study dynamic covalent multi-component assembly for its applications under the supervision of Professor Eric V. Anslyn.

Permanent address (or email): hhjo@utexas.edu

This dissertation was typed by the author.